Faculty of Engineering – Department of Civil Engineering

Nottingham Engineering Transportation Centre

IMPROVING THE RHEOMETRY OF HETEROGENEOUS BITUMINOUS BINDERS THROUGH EXPERIMENTAL AND NUMERICAL PROCEDURES

Thesis submitted to the University of Nottingham for the degree of Doctor of Philosophy in Civil Engineering

by

Gaspare Giancontieri

BSc Eng., MSc Eng.

Supervised by

Dr Davide Lo Presti, Dr David Hargreaves

March 2020

Abstract

Nowadays, heterogeneous materials are widely used for an extensive range of engineering applications and rheological measurements are intensively adopted for their development and quality control. These materials are often mixtures with different densities that exhibit improved engineering performance as well as a reduced environmental impact thanks to the addition of special modifiers. The success of these family of materials is very much linked to the accurate control of their properties during production and storage. This is the case of Heterogeneous Bituminous Binders (HBBs), such as crumb rubber modified bitumens (CR-MBs), used for asphalt mixtures for road pavements. Asphalt technologists are used to monitoring, in the range of 100°C to 200°C, the rotational viscosity of HBBs during product development and quality control. This exercise is usually carried out in a laboratory using a rotational viscometer. Nevertheless, due to their complexity, the characterisation of these materials may be challenging as some common procedures used to characterise their properties may not be adequate. Indeed, during rotational viscosity testing the sample may undergo a number of changes, such as phase separation, sedimentation, agglomeration, viscoelastic effects etc., leading to the here-defined sample instability which in turn provides misleading results. This is the reason behind the necessity of efficient mixing during viscosity measurements of HBBs.

To overcome the above-mentioned issues, this study introduces a combined experimental-numerical approach aimed to improve the rheometry of HBBs. To do that, a computational fluid dynamics (CFD) model was developed to assess whether the CFD is a tool capable to reproduce the observations of a laboratory campaign on HBBs. Numerical simulations confirmed the experimental results and proved sample instability during rotational testing of heterogeneous materials, hence the need of a new device able to reduce the

level of heterogeneity within the sample. Based on the numerical remarks, a deep literature investigation on mixing devices efficiency was carried out and a new geometry identified: the dual helical ribbon (DHR). The novel device was designed and verified by means of numerical modelling then manufactured in stainless steel. Once the DHR was realised, the combined experimental-numerical approach was used to provide evidence of the above-mentioned phenomena. The experimental campaign was performed, by recording eventual differences in rotational viscosity readings of HBBs while using both a standard spindle (SC-27) and the DHR as impellers of the rotational viscometer. In parallel, a tailored numerical model provided advanced visual aids aimed to better understanding the fundamentals behind the instability phenomena. Finally, an improved laboratory application based upon the adoption of the DHR for real-time monitoring of HBBs' properties during manufacturing and hot storage is presented.

Results of this combined numerical and experimental approach proved first that the CFD is a powerful tool able to reproduce the laboratory observations but also to offer a deeper insight into the measuring chamber by providing useful information about the sample instability. Laboratory campaign offered a further evidence that when dealing with HBBs the standard setup for rotational viscosity measurements does not appear to be adequate. Sample instability has been understood as correlated to deficient mixing, hence the DHR has shown to be beneficial in resolving the issue. Additionally, the procedure to perform quality control of HBBs has provided a set of practical conclusions to optimise full-scale production with regards to the type of modifier and the storage temperature. Therefore, the adoption of this geometry is strongly recommended for high-temperature viscosity measurements of CR-MB and potentially for any other HBB.

Acknowledgment

During the development of this thesis I had the great opportunity to collaborate with amazing professionals. Firstly, I would like to thank my advisors: Prof David Hargreaves and Dr Davide Lo Presti. Without their guidance and continuous help, I would not have been able to submit this thesis, thanks again. A special thanks also to Prof Antonino La Rocca that gave to me really precious advises that helped me to address this work. Thanks to all the professors, colleagues, and technicians at NTEC for making easier this experience during the years. I also would like to acknowledge the University of Huelva (Spain), where I spent one month but really beneficial for the development of this thesis, in particular thanks to Prof Pedro Partal for his patience, support and help.

Although I spent lot of time around the university laboratories, I have met also good friends outside the academia. Thanks to all of you in Nottingham that made my family there. Thanks to Mo, Gianluca, Lorenzo, Michele, Lucio, Ana, Giacomo, Helena, Giulia, Gustavo, Diana, Laura, Domenico, hopefully I am not forgetting anynone.

Last but not least (of course), thanks to my family, always ready to listen, support and understand me, you are my strength.

To my mother

Declaration

I declare that the contents and the work described in this thesis were performed at the University of Nottingham, Faculty of Engineering from April 2015 to March 2019. I hereby certify that this thesis is my own and has not been submitted in whole or in part to any other university or any other educational association for a higher degree.

Gaspare Giancontieri
Nottingham, 2019

We declare that the contents and the work described in this thesis were performed at the University of Nottingham, Faculty of Engineering from April 2015 to March 2019 and under our supervision.

Dr Davide Lo Presti,
International Projects coordinator and Visiting academic,
Nottingham Transportation Engineering Centre, University of Nottingham
Assistant Professor,
Dipartimento di Ingegneria, Scuola Politecnica, Universitá degli studi di Palermo

Dr David Hargreaves
Associate Professor,
Faculty of Engineering

Table of Contents

Abstract 3
Acknowledgment 5
Declaration 7
Table of Contents 9
List of figures 12
List of tables 17
1. Introduction 21
1.1. Background of the thesis 21
1.2. The need for more reliable viscosity measurements of HBBs 25
1.3. Aims and objectives 27
1.4. Methodology 28
1.5. Outline of the thesis and declaration 31
2. Literature Review 36
2.1. Rheology, deformation and flow of Newtonian materials 36
2.1.1. Rheology of heterogeneous materials 39
2.1.2. Rheology of suspensions 43
2.2. HBBs in pavement engineering applications 48
2.2.1. Modification of bitumen 48
2.2.2. Bitumen modifiers 50
2.2.3. Crumb rubber modified bitumen (CR-MB) 55
Brief history of crumb rubber modified bitumen 55
Ambient grinding 57
Cryogenic grinding 58
Rubber-Bitumen iteration mechanism 59
Processing variables 61
Specifications 63
Limitations 64
2.3. Mixing Rheometry 67
2.3.1. Measuring viscosity using non-standard equipment 73
2.3.2. Literature studies on mixing devices optimisation 75
2.3.3. Numerical modelling of mixing devices designed for heterogenous materials 81

2.4. Calibration procedure of non-standard impeller 88
2.5. CFD modelling of Heterogenous Materials 90
3. CFD as a tool to monitoring and optimising the mixing process.... 97
3.1. Experimental programme 98
3.2. Numerical techniques to model and optimise the mixing process of heterogeneous materials 100
3.2.1. CAD creation and meshing 102
3.2.2. Materials 107
3.2.3. Viscous model 107
3.2.4. Multiphases model 108
3.2.5. Boundary conditions and solution method 111
3.2.6. Governing equations 112
3.3. Results 113
3.3.1. Experimental 113
3.3.2. CFD simulations 118
Validation (Single Phase) 118
Understanding the DHI mixing process (multiphase) 120
3.4. Summary of results 126
4. The DHR: an optimised impeller for mixing rheometry which ensures sample stability during rotational test 131
4.1. CFD simulations 134
4.1.1. CFD model set-up 134
4.1.2. Kinematic Similarity 136
4.1.3. Multiphase Simulations 139
4.2. Manufacturing process 143
4.3. DHR calibration 148
4.3.1. Materials 149
Rheological measurements - Parallel and plate 150
4.3.2. Rheological Viscometer test 151
4.3.3. Experimental validation 155
4.4. Summary of results 161

5. Improving the rheometry of HBBs by ensuring sample stability during rotational tests: experimental and numerical approach 166

5.1. Experimental-numerical programme 167

5.2. Results 170

5.2.1. Experimental campaign on HBBs 170

Measurements on neat bitumen 170

Measurements on modified bitumens: apparent viscosity vs time 171

Measurements on modified bitumens: apparent viscosity vs temperature 174

5.2.2. CFD simulations 175

Validation of the model 175

Velocity field distribution within the chamber 177

Apparent viscosity measurements distribution within the chamber 178

Evaluating the effect of time on sample stability 179

5.3. Summary of results 183

6. Quality control of CR-MBs via laboratory simulation of full-scale manufacturing and hot storage. 188

6.1. Experimental programme 190

6.1.1. Real-time monitoring of CR-MB's properties during manufacturing and hot storage 191

6.1.2. Qualitative assessment of the proposed procedure 194

6.2. Results 200

6.2.1. Investigating the correlation between storage temperatures and initial storage viscosity 202

6.2.2. Investigating the relation between storage temperatures and CRM size. 204

6.2.3. Investigating the relation between storage temperatures and CRM content and type 209

6.2.4. Investigating the relation between storage temperatures and dissolution rates 214

6.3. Summary of results 215

7. Conclusions and Recommendations for future researches 221

8. References 226

Appendix A 239

List of figures

Figure 1.1 Rheological measurement problems with practical oil-particles emulsions using different testing geometry, a dual helical impeller on the left, a cylindrical spindle in the centre and a vane spindle on the right. Initially, the sample contained in the tubes may be homogeneous. After some time, the sample may become quite stratified. 24
Figure 1.2 Equi-viscous temperature for design purpose of a HBB 25
Figure 1.3 Summary of the combined numerical-experimental approach 30
Figure 2.1 Flow and viscosity curves of two ideally viscous fluids adapted from (Mezger, 2014) 37
Figure 2.2 Flow curves (on the left) and Viscosity functions (on the right), overview: (1) ideally viscous, (2) shear-thinning and (3) shear-thickening behaviour, adapted from (Mezger, 2014) 38
Figure 2.3 The relationship between apparent viscosity and shear rate for a shear thinning fluid of the Carreau model adapted from (Mezger, 2014) 40
Figure 2.4 Comparison of several sets of experimental data and the Einstein equation, adapted from (Schramm, 2006) 44
Figure 2.5 Schematic representation of the volume fraction dependence of relative viscosity ηr according to the Einstein, Batchelor, Krieger–Dougherty, and Quemada models, adapted from (Quemada, 1977) 46
Figure 2.6 Temperature susceptibility of an ideal thermoplastic binder adapted from (Brûlé, 1996) 49
Figure 2.7 Shredded end life tyres (left) and crumb rubber (right) 55
Figure 2.8 SEM Micrographs of rubber granulate grains obtained at ambient temperature (A) and cryogenically (B) adopted from (Sienkiewicz et al., 2012) ... 57
Figure 2.9 Progression of bitumen-rubber interaction at elevated temperature: change in particle size over time at elevated temperature adapted from (Abdelrahman and Carpenter, 1999) 59
Figure 2.10 SEM micrographs of the finished rubberised bituminous binder adapted from (Pereira et al., 2008) 60
Figure 2.11 Typical changes in viscosity values for rubberised bitumen at different temperatures over time, adopted from (Sabita, 2016) 61
Figure 2.12 Asphalt-Rubber portable Blending Systems adapted from (Allbiz, 2019) 62
Figure 2.13 A rotational viscometer (Brookfield, 2015) 69
Figure 2.14 The cup and bob configuration used in the rotational viscometer 69
Figure 2.15 Visualisation of the phase separation during rotational viscosity measurements of crumb rubber suspensions for (left) the SC-27 spindle and (right) a vane spindle 70
Figure 2.16 Vane Spindles (left) and the T-Bar Spindles with the Helipath stand (right) adopted from (Brookfield, 2015) 71
Figure 2.17 The idea through comparison between the impellers and the generated flows during rotation adopted from (Lo Presti et al., 2014) 72

Figure 2.18: The drawings of the most investigated impellers. a) Gate type anchor impeller, b) multi-paddle, c) helical ribbon, d) screw in draught tube, e) combined ribbon screw agitators. Adopted from (Havas et al. 1977) 76
Figure 2.19 Sketch of helical ribbon agitator system, adapted from (Takahashi et al., 1982) 78
Figure 2.20 Geometrical variables for helical ribbons impellers, adapted from (Takahashi et al., 1982) 79
Figure 2.21 Schematics of (a) the illuminated zone and (b) the secondary flow in a Helical Ribbon Impeller (Takahashi, Sasaki, et al., 1982) 80
Figure 2.22: Design and the flow pattern of an helical ribbon with screw at 10 Rpm, adopted from (Tanguy et al., 1992) 81
Figure 2.23: The flow pattern of the three helical ribbons analysed in (De La Villéon et al., 1998) 82
Figure 2.24 : From left to right the single helical ribbon (SHR), the double helical ribbon (DHR.) and the SHR with a central screw (CSR). The SHR also shows the geometry of the outer tank, adopted from (Robinson et al., 2012) 83
Figure 2.25 Time sequence showing the transport of a sphere of fluid in the SHR (left), the DHR (centre) and the CSR (right).Only the surface of the fluid volume coloured with an arbitrary pattern is shown, adopted from (Robinson et al., 2012) 84
Figure 2.26 Effects of impeller pitch, blade and width on the circulation number Kq, adapted from (Tsui et al., 2011b) 85
Figure 2.27: The mixing index Δ, adapted from (Tsui et al., 2011b) 87
Figure 2.28 Radial–angular temperature profile of, solid-liquid food mixture due to compression to 400 MPa at different heights of, 12, 60, 150, 240, 261 and 276 mm from the bottom, respectively. The red arrow shown in the figure is just for a point in the computation process, adapted from (Abdul Ghani et al., 2007). 92
Figure 3.1 The standard spindle SC-27 (on the left), the dual helical impeller (on the centre) and the glass tube realised to allow the visualisation of the particles (on the right) 98
Figure 3.2 The Brookfield silicone viscosity standard fluids, adopted from (Brookfield, 2018) 99
Figure 3.3 DHI mesh details 102
Figure 3.4 on the left, a solid model of the DHI mixer; and on the right, the surface mesh on the mixer and outer wall. 103
Figure 3.5 The DHI mesh sensitive analysis 104
Figure 3.6 on the left, a solid model of the Brookfield SC-27 spindle; and on the right, the surface mesh of the spindle and outer wall. 105
Figure 3.7 The details of the mesh performed on the SC-27 spindle 106
Figure 3.8 The mark command used in Fluent to highlight the different regions 111
Figure 3.9 Images of the distribution of particles in the viscometer using the f100 fluid + 400 μm tyre rubber particles for the SC-27 spindle (top) and DHI (bottom) at the start of the test and after 10minutes for various rotational speeds. 114

Figure 3.10 Images of the distribution of particles in the viscometer using the f500 fluid + 400 μm tyre rubber particles for the SC-27 spindle (top) and DHI (bottom) at the start of the test and after 10minutes for various rotational speeds. 115
Figure 3.11 Apparent viscosity measurements over time of f100 fluid by using the SC-27 spindle and DHI at 10, 100 and 200 Rpm.....116
Figure 3.12 Apparent viscosity measurements over time of f500 fluid by using the SC-27 spindle and DHI at 10, nd 100 Rpm. 117
Figure 3.13: Plot of the Spindle Multiplier Constant (SMC) against mixing Reynolds number for the DHI impeller at different rotational speeds. 119
Figure 3.14 Contours of velocity magnitude for the (a) SC-27 spindle and (b) DHI (right) at 100 Rpm.....121
Figure 3.15 A close-up of the inner and outer helices of the DHI impeller, showing the flow vectors on the plane y = 0. Vectors are the same length, and the velocity magnitude is indicated by the colour (blue is zero, red is 0.061m/s). 122
Figure 3.16 Volume fractions from the CFD model (top) and experimental images (bottom) for the SC-27 spindle. The volume fractions range from 0 (blue) to 0.08 (red).....123
Figure 3.17 Volume fractions (top) and experimental images (bottom) for the DHI. The volume fractions range from 0 (blue) to 0.08 (red). 124
Figure 4.1 The dual helical ribbon (DHR) designed for this work 131
Figure 4.2 On the left, the surface mesh on the mixer and outer wall; and on the right, a solid model of the DHR. 135
Figure 4.3 The DHR mesh sensitive analysis 135
Figure 4.4 Plots of the non-dimensional w-component of velocity along a vertical centreline, from bottom to top, for the Newtonian fluids. 137
Figure 4.5 Plots of the non-dimensional w-component of velocity along a vertical centreline, from bottom to top, for the non-Newtonian fluids. 137
Figure 4.6 Plots of the non-dimensional u-component of velocity along a horizontal centreline for the Newtonian fluids.....138
Figure 4.7 Plots of the non-dimensional u-component of velocity along a horizontal centreline for the non-Newtonian fluids. 138
Figure 4.8 Plot of the mixing index, Δ, against mixing Reynolds number, Rem, for the f100 fluid with 5% rubber particles (both buoyant and neutrally buoyant). ...140
Figure 4.9 Plot of the mixing index, Δ, against mixing Reynolds number, Rem, for the f100 and f500 fluids with 5% rubber particles for the DHR and SC-27 impellers. 141
Figure 4.10 Numerical comparison of contours of (a) volume fraction and (b) velocity magnitude during rotational test on f100 + 5% particles at 20 Rpm.....142
Figure 4.11 The set of DHRs with different pitches 143
Figure 4.12 The Stratasys Dimension 1200es 3D printer used in this work.....144
Figure 4.13 The DHR prototyped by using the 3D printing technology.....145
Figure 4.14 Stainless steel DHRs set 147
Figure 4.15 The stainless steel DHR impeller for use in a Brookfield Viscometer. 148

Figure 4.16 Low shear mixer used in this work for the preparation of the samples 149
Figure 4.17 Plot of the flow behaviours for the Newtonian and non-Newtonian fluids investigated in this work. 151
Figure 4.18 Schematics of (a) Standard spindle SC-27, (b) Dual Helical Ribbon, each with an indication of the main flow patterns seen with each. 153
Figure 4.19: Variations of the Metzner Otto parameter Ks with the power-law index n for the SC-27 spindle. 154
Figure 4.20: Variations of the Metzner Otto parameter Ks with the power-law index n for the DHR spindle. 154
Figure 4.21 Photographs sequence of the SC-27 and DHR impellers with a mixture of f10 fluid +5% of rubber particles at the start (a), (c) and end (b), (d) of the tests 156
Figure 4.22 Viscosity measurements over time by using Brookfield viscometer on standard fluid f10 plus 5% of suspended solids. 158
Figure 4.23 Viscosity measurements over time by using Brookfield viscometer on standard fluid f100 plus 5% of suspended solids. 158
Figure 4.24 Viscosity measurements over time by using Brookfield viscometer on standard fluid f500 plus 5% of suspended solids. 159
Figure 4.25 Photographs of the DHR impeller showing the axial pumping force with a mixture of f10 fluid and rubber particles at the start (a), after few seconds(c) and at the end (c) 160
Figure 5.1 The effective shear rate Vs the rotational for DHR and SC-27 168
Figure 5.2 The rotational viscometer and Thermosel used in this investigation...169
Figure 5.3 Viscosity measurements at different rotational speeds by using LV viscometer on a 35/50 bitumen at T = 140 °C and 180 °C 170
Figure 5.4 Apparent viscosity measurements over time of an CR-MB at 180 °C at 20–100 Rpm 171
Figure 5.5 Apparent viscosity measurements over time of an SBS-MB at 180 °C at 20–100 Rpm 172
Figure 5.6 Apparent viscosity of RTR-MB (up) and SBS-MB (down) at 180 °C by at 20 Rpm. Percentages indicates the difference in terms of viscosity between the two geometries. 173
Figure 5.7 Apparent viscosity of CR-MB Vs Rpm at 180 °C obtained through laboratory campaign and numerical simulations 176
Figure 5.8 Numerical velocity field distribution of RTR-MB at 180 °C at 20 Rpm, Brookfield spindle SC-27 (left), DHR (right) 177
Figure 5.9 Numerical apparent viscosity distribution of RTR-MB at 180°C at 5-100 Rpm, on the top the SC-27 and on the bottom the DHR 178
Figure 5.10 Effect of time on particles distribution of RTR-MB at 180 °C by numerical model, rotational speed 20 Rpm 181
Figure 5.11 Sample stability of RTR-MB at 180°C over time, by numerical model and with no geometry within the sample 182
Figure 6.1 An asphalt Rubber Reaction Tanks mounting a helical screw to promote the bitumen-rubber interaction adopted from (D&H Equipment, 2019) 188

Figure 6.2 Experimental programme 190
Figure 6.3 The laboratory set-up comprising the Brookfield viscometer and thermosel used to real-time monitoring the CRM binders 193
Figure 6.4 Real-time monitoring of the manufacturing stage (177.5 °C, 50 Rpm 18% ambient 125-800 µm CRM). 195
Figure 6.5 Qualitative comparison of testing samples poured after low shear mixing production using different geometries 198
Figure 6.6 SEM images (x50) of the samples processed with SC-27 and DHR, respectively. 199
Figure 6.7 Swelling extent for ambient and cryogenic CRM. 202
Figure 6.8 Initial storage Viscosity vs storage temperature, 10% CRM 203
Figure 6.9 Initial storage Viscosity vs storage temperature, 18% CRM 203
Figure 6.10 Viscosity evolution at different storage temperatures. 18% ambient CRM 125- 800 µm 205
Figure 6.11. Viscosity evolution at different storage temperatures. 18% ambient CRM 125- 250 µm 206
Figure 6.12. Viscosity evolution at different storage temperatures. 10% ambient CRM 125- 800 µm 207
Figure 6.13. Viscosity evolution at different storage temperatures. 10% ambient CRM 125- 250 µm 208
Figure 6.14 Evolution of viscosity at different concentration of ambient CRM 125-800 µm. 210
Figure 6.15 Evolution of viscosity at different concentration of ambient CRM 125-250 µm. 211
Figure 6.16 Evolution of viscosity at different storage temperature using cryogenic CRM 125- 800 µm. 212
Figure 6.17 Evolution of viscosity at different storage temperature using cryogenic CRM 125- 250 µm. 213
Figure 6.18 Dissolution rates vs storage temperature, 10% CRM. 214
Figure 6.19 Dissolution rates vs storage temperature, 18% CRM. 215

List of tables

Table 1.1 applications of HBBs 22
Table 1.2 Most common used geometries and respective applications for rotational test (Brookfield, 2015) 23
Table 2.1 Examples of additives used to modify bitumen (Yildirim, 2007; Zhu and Kringos, 2014) - A 53
Table 2.2 Specification for Rubberised bitumen (ASTM D6114) 63
Table 2.3 CR-MB gradation used for CR-MB, adapted from (TG1, 2015) 64
Table 2.4 Mixing time and circulation time data found in literature for various helical ribbon agitators. Symbols which appear in this table refer to experimental methods used to obtain these data, adopted from (Delaplace et al., 2000) 77
Table 3.1 Fluids and particle properties 100
Table 3.2 CFD simulations to assess phase separation phenomena during rotational tests, where ⋄ indicates cases where experimentally there was phase stratification, • where there was a good level of mixing. 120
Table 4.1 Ratios used into fluent to define the optimum dimensions based on the mixing index 133
Table 4.2 Fluids and particle properties 139
Table 4.3 Rotational test results comparison between different geometries, where (o) indicates cases where the geometry was able to keep the particles suspended within the sample , (x) not and (-) reports if the reading exceeds the lower or higher limits of the viscometer. 146
Table 4.4 Values of n and k for each system used in this study. 149
Table 4.5 Parameters used during parallel and plate tests 150
Table 4.6 Comparison of the SMC values found in this study compared with those from Brookfield's literature. 152
Table 5.1 Characterisation of material's rheological properties 166
Table 5.2 Apparent viscosity from 120°C to 200°C of neat bitumen, CR-MB and SBS-MB by using HA viscometer at 20 Rpm 174
Table 5.3 Comparison of results from laboratory campaign and numerical simulations for CR-MB at 180 °C at 5-100 Rpm 175
Table 5.4 Numerical apparent viscosity distribution of CR-MB at 180°C at 5-100 Rpm 180
Table 6.1 Quantitative parameters associated with the interaction process. 197
Table 6.2 Quantitative assessment of the real-time monitoring exercise 201

CHAPTER 1. INTRODUCTION

1. Introduction

1.1. Background of the thesis

Thanks to their enhanced engineering proprieties as well as a reduced environmental impact many industrial processes (Table 1.1.) involve the flow of heterogeneous materials that are often mixtures in which two or more phase, coexist together. Nevertheless, to achieve the target properties a detailed rheological characterisation is of paramount importance for their development, performance and applications. Differently to conventional materials they exhibit a diverse and often significant deviation from simple Newtonian behaviour. In fact, heterogeneous materials are often characterised by an unusual mechanical response to applied stress or strain due to the variety of these structures. Newtonian fluids can be characterised by a single coefficient of viscosity, which varies only as a function of temperature. For heterogeneous systems instead, the viscosity may also vary with strain rate, making their rheological characterisation difficult. In addition, this scenario may be further complicated when the heterogeneous blend presents the phases having different densities.

Current available rheometry instruments are designed for homogeneous systems but continue to be used for a wide range of materials, no matter the complexity. In a laboratory, rotational viscometers are commonly used as a practical means of determining the viscosity and/or shear rate dependency of these systems, because such instruments allow the testing of a wide range of materials over a wide range of temperatures, more than other viscosity measurements systems. All viscometers are supplied with spindles suitable for most applications within the viscosity range of the instrument. There are, however, situations where specialized spindle geometries are necessary to obtain optimum results (Table 1.2).

Table 1.1 applications of HBBs

Field	*Application*	*Rheology properties*	*App. Outcome*	*Technical issues*
Civil engineering	Asphalt rubber Bituminous Emulsion Mastics (Hunter *et al.*, 2015)	Viscosity profile Shear stress Particle-size distribution	Asphalt workability Asphalt coating Process optimising Pumping requirements Suspension stability	Lack in rheology measurements. Phase separation. Sedimentation.
Mining engineering	Hydraulic slurry transport by pipeline (Schramm, 2006)	Viscosity profile Flow rate Yield Stress Particle-size distribution Zeta Potential	Pressure drop Pumping requirements Suspension stability Process optimising Pipes sizing	Sedimentation Abrasion Pipes cost
	Mineral Flotation (Dzuy, 1983; Farrokhpay, 2012; Rahman et al., 2012)	Viscosity profile Yield stress Flow rate Zeta potential Particle-size distribution	Degree of particles aggregation Degree of particles dispersion Process optimising Wettability	Lack in rheology measurements Sedimentation Aggregation
Petroleum industry applications	Fracturing fluids (Schramm, 2006; Bunger *et al.*, 2013; Petrowiki, 2015)	Viscosity profile	Fluid design Provide sufficient fracture Provide a desired net pressure Provide carrying capability Control fluid loss Pumpability Suspending power	Lack in rheology measurements Viscosity needed overestimated Fluid cost Treating pressure Weissenberg Effect Reduced fracture conductivity
	Drilling fluids (Petrowiki, 2015)	Viscosity profile Flow rate Particle-size distribution	Fluid design Carrying capacity Avoiding excessive wellbore pressures Fluid system conditioning	Extreme temperature and pressure requirements Cost of non-productive time
Manufacturing and materials science	India Ink (Schramm, 2006)	Viscosity profile Zeta potential	Ink coating Suspension stability Wettability	Pigment agglomeration
Food products	Ice cream Vegetable shortening (Schramm, 2006)	Viscosity profile Yield stress	Texture	Sedimentation Agglomeration

Table 1.2 Most common used geometries and respective applications for rotational test (Brookfield, 2015)

Geometry	*Applications*	*Benefits*	*Limits*
Vane Spindle	• Cosmetics • Foods • Gels • Paints • Paste-like materials • Pharmaceuticals • Sealants • Suspensions	• Minimal disruption of sample during spindle immersion • Keeps particles in suspension during testing cycle • Provides information on yield behaviour at low rotational speeds	• Develops tangential forces but not axial forces resulting in poor mixing performance during testing. • Does not guarantee the sample stability of heterogeneous materials.
Cylindrical Spindle	• Adhesive • Asphalt • Chemicals • Cosmetics • Dairy • Hot waxes • Inks • Oils • Suspensions	• Particularly valuable when measuring non-Newtonian fluids • Provides accurate viscosity measurements thanks to its geometry	• Develops tangential forces but not axial forces resulting in poor mixing performance during testing. • Does not guarantee the sample stability of heterogeneous materials.
Dual Helical Impeller (DHI)	• Asphalt • Emulsions • Oils • Polymer solutions • Rubber solutions • Suspensions	• Creates a convective like flow within the sample which allows reducing the sample heterogeneity • Provides more realistic viscosity measurements of HBBs	• When measuring suspensions particles may tend to agglomerate or stuck between the inner screw and outer helix. • Does not guarantee the sample stability of heterogeneous materials.
Helipath Stand	• Creams • Gelatine • Gels • Pastes • Putty • Wax	• Creates a helical path through the test sample thus eliminating the problem of "channelling" typical in thixotropic fluids	• Does not guarantee the sample stability of heterogeneous materials.

However, due to their complex structure, obtaining reliable rheological measurements on heterogenous materials using standard equipment remains a challenge for rheologists.

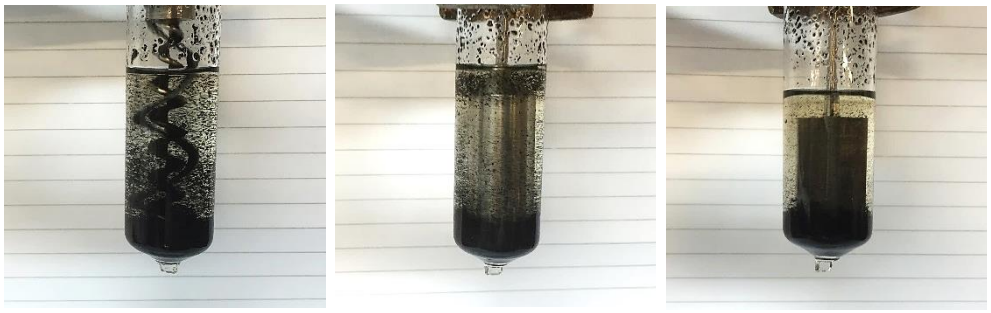

Figure 1.1 Rheological measurement problems with practical oil-particles emulsions using different testing geometry, a dual helical impeller on the left, a cylindrical spindle in the centre and a vane spindle on the right. Initially, the sample contained in the tubes may be homogeneous. After some time, the sample may become quite stratified.

In fact, a number of changes such as phase separation, sedimentation or agglomeration (Figure 1.1) may occur within the measuring chamber while the sample is tested. These phenomena may affect the sample stability, here defined as the ideal condition in which material's phases are well mixed within the sample during testing, that can lead to results that are not reproducible and representative of the original sample. These issues are reported for many materials such as adhesives, ceramic, chocolate, cosmetic detergent, bituminous binders, food, glazing, lubricants, inks paints, plastic, rubber, sealants (Dow, 1946; Lin et al., 1985; Gallegos et al., 1999; Tabilo-Munizaga et al., 2005; Malkin, 2009). Among these, one of crucial relevance for the pavement engineering applications are the heterogenous bituminous binders (HBBs). These materials, thanks to the addition of special modifiers to the base binder, are able to often enhance the performance of asphalt mixtures (e.g. stiffness, elasticity, rutting resistance and durability) (Huang, 2006; Widyatmoko et al., 2007; Peralta et al., 2010; Subhy et al., 2015; Visser et al., 2017; Zhang et al., 2018) and in the case of crumb rubber modifier (CR-MB) bitumens also to reduce the resource consuming, indeed the CR-MBs are usually produced from end life tyre (e.g. waste management, landfill reduction, noise emissions) (Lo Presti et al., 2013). CR-MB are HBB whose rheological characterisation still remains challenging.

1.2. The need for more reliable viscosity measurements of HBBs

As introduced in the previous section, HBBs are widely used in many applications for two main reasons, improving materials performance and reducing the environmental impact. Although it has been proved that they are more sustainable and resilient than conventional ones, their use is still limited due to a lack of engineering properties able to characterise them.

When dealing with HBBs such as CR-MBs, one of the key factors is the rotational/dynamic viscosity. Measuring properly the rotational viscosity of HBBs is crucial for different reasons:

- Bitumen technologists are used to monitoring the high-temperature rotational viscosity of HBBs (in the range 100 - 200°C) aimed to identify the equi-viscous temperature (Caltrans, 2011). This temperature is defined as the one at which a bitumen attains the proper viscosity for mixing as well as for ensuring pumpability and compactability of the mixtures. Manufacture's recommendations for HBBs are 0.17±0.002 Pa·S for mixing and 0.28±0.002 Pa·S for compaction (Figure 1.2).

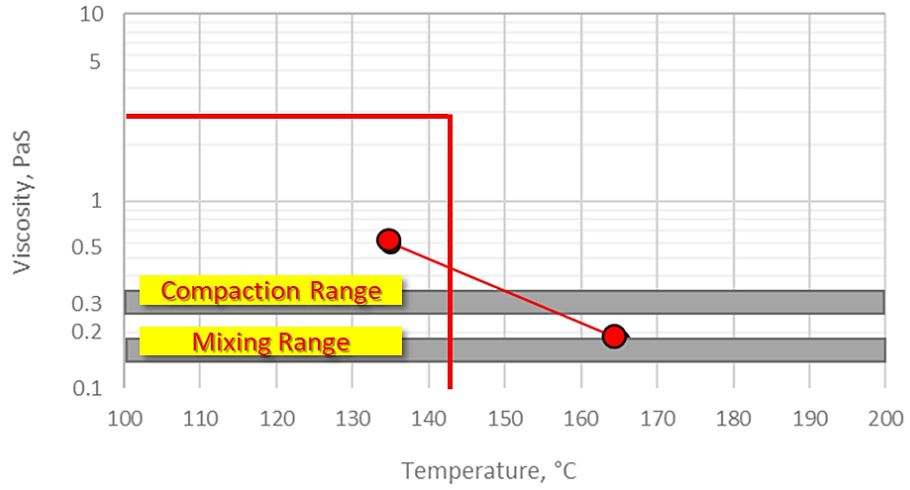

Figure 1.2 Equi-viscous temperature for design purpose of a HBB

- To assess weather adequate coating of the aggregate occurs. An increased binder viscosity allows thicker film thickness on aggregate and as a consequence a reduced oxidation, increased flexibility, and increased resistance to reflective cracking.

- To define the compaction viscosity and material classification, for example as mentioned in the ASTM D2170/D2170M, the 135 ºC measurement temperature is chosen to simulate the mixing and laydown typically encountered in hot mix asphalt (HMA) pavement construction. HBBs have a maximum rotational viscosity of 3000 Pa·S at 135 ºC.

- During product development to ensure that the binder guarantees the minimum performance requirements as well as monitoring the modification process.

Nevertheless, HBBs are multi-phase systems that can present internal structure behaving differently from the bitumen matrix. Material's heterogeneity is also enhanced by many parameters such as testing temperature, impeller speed and testing time. This is a practical issue that bitumen technologists have to cope during laboratory measurements if the difference between densities of modifier and bituminous matrix is significant. However, the same issue might be encountered within asphalt plant during hot storage where the modifier could separate, either to the top or bottom of the container. This could lead to significant mistakes in further steps such as choosing wrong temperatures to guarantee appropriate aggregate coating during mixing and/or ensuring good workability during compaction of asphalt concrete.

Furthermore, the needed of an improved mixing rheometry may be particularly beneficial for special laboratory applications such as the product development of HBBs with rotational viscometer used as a low shear mixer

offering a continuous monitoring of the viscosity (Celauro *et al.*, 2012; Subhy *et al.*, 2015). In fact, in this scenario the processing is made at high rotational speed and at a temperature where the bitumen viscosity is quite low (180°C) and the modifier tends to agglomerate in layers, mainly at the bottom of the tube. This lack of sample stability coupled with Non-Newtonian phenomena may produce significantly inconsistent data.

1.3. Aims and objectives

Within the contest described in sections 1.1 and 1.2, the main aim of this thesis is to improve the rheometry of HBBs by using a combined experimental-numerical approach and in turn to promote their use in pavement engineering applications. These coordinated operations will then allow obtaining new laboratory prototypes and associated procedures for rheological measurements of HBBs.

In this regard, the specific objectives of this thesis are:

- To assess whether a Computational Fluid Dynamics (CFD) model is able to reproduce the observations obtained from the laboratory investigation.

- To identify, design and calibrate by means of a combined numerical-experimental approach a novel testing geometry, that will allow performing rheological measurements of HBB while ensuring the sample stability.

- To evaluate, by comparing the novel geometry with the conventional coaxial cylinder setup for rotational viscometers, if currently available tests/procedures to measure the rotational viscosity of HBB are adequate.

- To develop an improved laboratory application for real-time monitoring of HBBs' rheological properties during manufacturing and hot storage aimed to produce binders with enhanced performance by governing the modification process and the processing conditions.

1.4. Methodology

The methodology of this thesis is divided into different steps/tasks related together as shown in Figure 1.3. This work introduces an innovative combined experimental-numerical approach aimed to improve the rheometry of heterogeneous bituminous binders for pavement engineering applications.

First, a computational model was developed, the overall objective of this stage was to assess whether the CFD would be able to simulate this complex scenario and to couple these outcomes with visual images to shed a light on the results obtained in a previous laboratory campaign (Lo Presti *et al.*, 2014), where a novel dual helical impeller (DHI) provided "more realistic" viscosity measurements when compared to the standard spindle. By doing this, it was also possible to highlight the benefits and limitations of using this geometry to perform rotational viscosity measurements of HBB, as well as using the model to validate the empirical calibration procedure. The CFD helped to clarify the results achieved during the previous experimental campaign but also showed that a further shape optimisation was required in order to reduce the level of heterogeneity of these materials.

Based on the above-mentioned observations, a literature studies on mixing geometries able to guarantee the sample stability was carried out and a new geometry identified, the dual helical ribbon (DHR) impeller. The new geometry was designed, tested, and verified by means of numerical modelling. First, to avoid expensive and time-consuming manufacturing procedures, a prototype was realised by using the 3D printing technology

showing outstanding results. Finally, the DHR was manufactured in stainless steel and then was calibrated by using a wide range of Newtonian and non-Newtonian materials.

Once the new geometry was identified and manufactured, the next step was to investigate if current procedures to measure the rotational viscosity of HBB are correct. The investigation was carried out with a combined approach of laboratory tests and numerical analyses. The laboratory tests were undertaken by using a coaxial cylinder configuration (SC-27) and the DHR to record eventual differences in viscosity measurements of a neat bitumen, an SBS-MB (polymer modified bitumen) and an RTR-MB (recycle tyre rubber modified bitumen). Parallel to the laboratory campaign, a bespoke CFD model reproducing the laboratory tests was defined. The computational platform provided a further support to evaluate and monitor the sample stability of these binders that otherwise would have been difficult to visualise during conventional laboratory test.

Finally, an improved product development and quality-control procedure by adapting the DHR to act as a low shear mixer is introduced. This configuration will allow engineers, while guarantee the sample stability, to constantly monitoring the rheology change of HBB during production and storage and develop superior, rubber-modified binders. The procedure allowed the practical investigation of a large number of variables while monitoring the viscosity in real-time. The effect of the processing temperature, rubber size, concentration and grinding technology has been investigated to evaluate the impact on the rotational viscosity during production and storage.

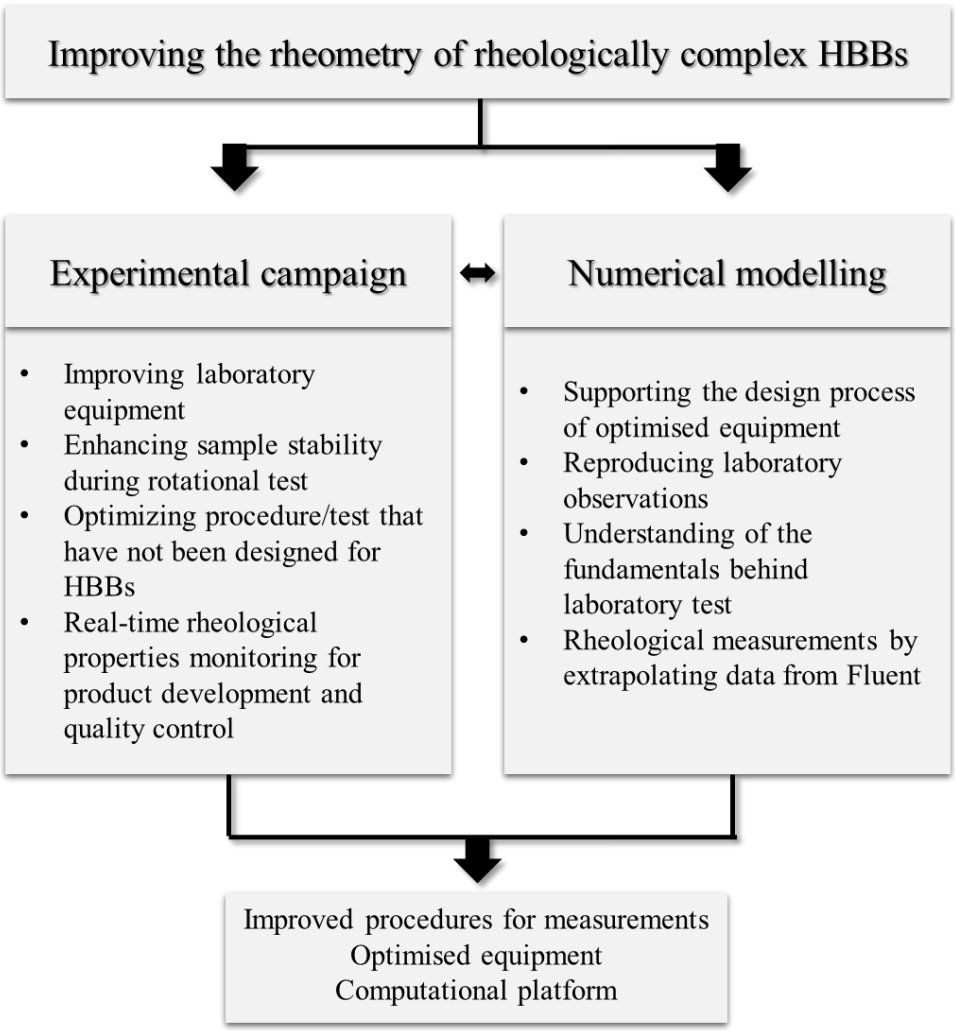

Figure 1.3 Summary of the combined numerical-experimental approach

1.5. Outline of the thesis and declaration

Based on the observations presented above, this thesis will be structured in a two-fold approach to improve the rheometry of heterogeneous materials, focusing on HBBs by using laboratory and numerical techniques. To this end, the thesis is divided in 7 chapters.

In **Chapter 1**, the scope, background, aim, objectives, and methodology of the thesis are explained.

Chapter 2 reviews the existing literature about the different topics addressed: rheology and rheometry of heterogeneous materials, focusing on rubberised bituminous binder, and computational fluid dynamics modelling.

Chapter 3 presents a preliminary study to assess whether the CFD platform could be able to reproduce this complex scenario and shed a light within the measuring chamber to investigate phenomena that otherwise would be difficult to understand but also to visualise during conventional laboratory test.

Chapter4 introduces a novel mixing device for heterogenous materials, designed, calibrated and validated by means of numerical modelling and laboratory test.

Following, **Chapter 5** shows an experimental campaign on HBBs aimed to provide an innovative insight by coupling laboratory and numerical procedures for measuring the rotational viscosity of modified binders.

In **Chapter 6** an improved quality control procedure to predict the rheological properties of crumb rubber modified bitumen during material manufacturing and storage is presented.

Finally, **Chapter 7** draws the conclusions of the work carried out and offers recommendations for further research.

Author's declaration: Some chapters of this thesis have been based on the following scientific publications:

1. D. Lo Presti, G. Giancontieri, D.M. Hargreaves (2016) *: Improving the rheometry of rubberized bitumen: experimental and computation fluid dynamics studies*, Construction and Building Materials, https://doi.org/10.1016/j.conbuildmat.2016.12.200.
2. G. Giancontieri, D. M. Hargreaves, D. Lo Presti (2018): *Are we correctly measuring the rotational viscosity of rubberised bituminous binder?* Proceedings of the rubberised asphalt/ Asphalt Rubber 2018 conference, ISBN: 978-989-20-8662-0
3. G. Giancontieri, D. M. Hargreaves, D. Lo Presti (2019): *Are we correctly measuring the rotational viscosity of heterogeneous bituminous binders?* Road Materials and Pavement Design https://doi.org/10.1080/14680629.2020.1724559.
4. J. Medina, G. Giancontieri, D. Lo Presti, (2019): *Quality control of crumb rubber modified binders via laboratory simulation of full-scale manufacturing and hot storage.* Construction and Building Materials. https://doi.org/10.1016/j.conbuildmat.2019.117351

CHAPTER 2. LITERATURE REVIEW

2. Literature Review

This section constitutes the starting point of the research and includes a review of pertinent literature. This literature review aims to achieve the objectives of this thesis by covering the following knowledge areas:

- Rheology principles: to gain a better understating of its importance and how it works but also to provide an overview about the different rheological behaviours and the models able to represent them.
- HBBs in pavement engineer; introducing the material, spacing from its development till its applications also showing limits and benefits of its use.
- Mixing rheometry; reviewing the actual procedures and devices to measuring the rotational viscosity of heterogeneous binders. Furthermore, this section provides a deeper literature investigation about mixing geometry aimed to identify the best shape able to guarantee the sample stability while performing rotational test.
- Computational fluid dynamics modelling of heterogeneous materials; going through the different numerical techniques suited to model their behaviour but also to optimise the mixing process.

2.1. Rheology, deformation, and flow of Newtonian materials

The rheology studies the internal response of materials to stresses. The word rheology is derived from the Greek and translates literally as rheos (flow) and logy (science); therefore, rheology means “the study of flow”. The term was coined in 1929 by Eugene C. Bingham, a professor that was researching the properties of materials that showed flow characteristics typical of liquids but also elastic properties like solids materials (Hunter *et al.*, 2015).

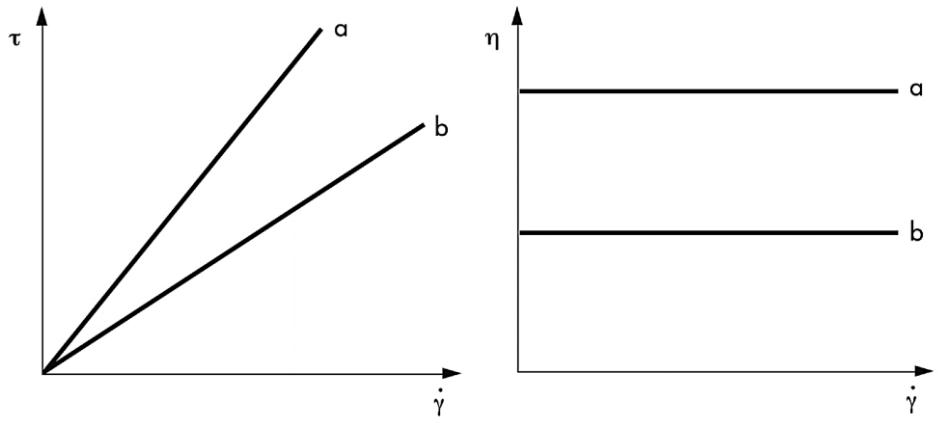

Figure 2.1 Flow and viscosity curves of two ideally viscous fluids adapted from (Mezger, 2014)

Therefore, rheology can be defined as the science that studies materials that exhibit both solid and liquid characteristics. A liquid or solid keeps its form at rest while under a certain load the material deforms. Once that the load is removed the deformation can be either elastic and then recoverable or viscous therefore irrecoverable. Simplifying, it can be said that ideal solids behave in an elastic manner and when the load is removed the deformation is recovered, whereas liquids act in a viscous manner and a permanent deformation is reported. In a real scenario, materials can exhibit what is linked to a viscoelastic behaviour, in which the response to an applied stress is partially elastic and partially viscous.

The aim of the rheologists' is to measure deformation and flow behaviour of a great variety of matters, to present the obtained results clearly and to explain it (Mezger, 2014). The concept of deformation and flow is of a crucial importance in rheology. Deformation is referred to a solid and can be defined as a change in the shape or size as a response to a load. Instead, flow is associated with liquids and describes a deformation that last as long as the load is applied.

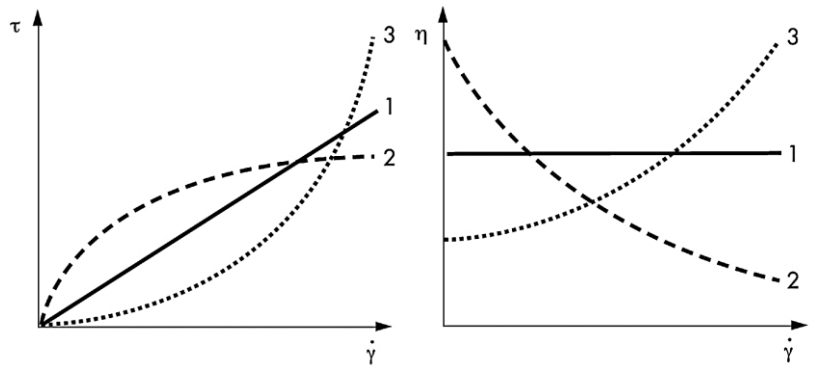

Figure 2.2 Flow curves (on the left) and Viscosity functions (on the right), overview: (1) ideally viscous, (2) shear-thinning and (3) shear-thickening behaviour, adapted from (Mezger, 2014)

The effects of loading time but also temperature during the measuring can lead to different behaviours and a material will show a range of behaviours in response to a force, based on the loading time and the temperature. These behaviours are illustrated graphically by fluid flow and viscosity curves (Figure 2.1). Flow curves are showing the interdependence of shear stress τ and shear rate $\dot{\gamma}$ while viscosity curves are derived from flow curves. The rheology of a material is characterised by its flow curve, which represents the relationship between shear stress and shear rate (Mezger, 2014). The ratio of shear stress to shear rate is the fluid viscosity and the SI unit is Pascal second (Pa·s).

$$\eta = \frac{\tau}{\dot{\gamma}} \qquad \textit{Equation 1}$$

Isaac Newton is often called the “father of classic physics”. He proposed, in a quite inaccurate form (Newton, 1687): The resistance to flow of liquids is proportional to the flow velocity. Based on later research on fluid dynamics by Daniel and Johann Bernoulli (Bernoulli, 1738), Leonhard Euler (Euler, 1749) and Georges Gabriel Stokes (Stokes, 1846) stated the accurate and modern form of Newton’s hypothesis.

Therefore, the viscosity law may be referred also as the "Newton/Stokes law". A Newtonian fluid is characterised by a linear flow curve, which passes through the origin, as shown in Figure 2.1. The viscosity of such fluid is constant and independent of shear rate. Examples of Newtonian behaviour include water, milk, and sugar solutions (Holdsworth, 1993).

2.1.1. Rheology of heterogeneous materials

In section 2.1, using Newton's law, the rheological background of materials showing ideally viscous flow behaviour was explained. This section investigates the mostly more complex, non-Newtonian flow behaviour of heterogeneous materials used in daily practice in industry.

In the process industries, due to performance limits, the use of materials with a Newtonian behaviour is decreasing. Instead, heterogeneous materials are encountered in a wide range of industrial applications, including most multi-phase mixtures (e.g. emulsions, suspensions, foams/froths, dispersions) (Metzner, 1985), high molecular weight systems and their solutions (e.g. polymers, proteins, gums) (Malkin, 2009), foods, pharmaceuticals, personal care products, agricultural chemicals, lubricants, and slurry fuels (Dow, 1946; Lin *et al.*, 1985; Bair *et al.*, 2003; Malkin, 2009).

As mentioned in section 2.1 if a fluid's internal flow resistance is independent of the external force - i.e. the shear rate - acting upon the fluid, it is ideally viscous. A viscosity function shows the viscosity over the shear rate and for a Newtonian liquid, this function is a straight line. This scenario drastically changes when dealing with highly heterogeneous materials, indeed, if its viscosity changes with the shear rate, a liquid is non-Newtonian and – for exact definition – one has to specify the apparent viscosity that means that viscosity depends on the shear rate.

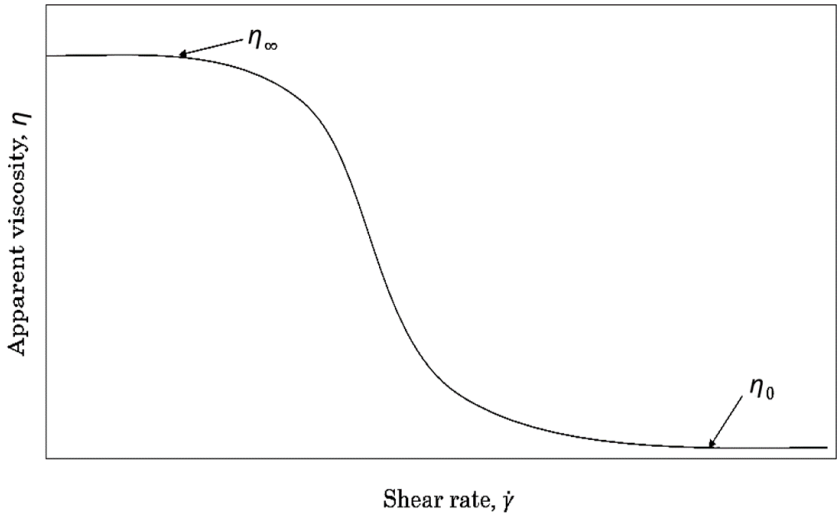

Figure 2.3 The relationship between apparent viscosity and shear rate for a shear thinning fluid of the Carreau model adapted from (Mezger, 2014)

Different shear-dependent fluids behave differently: typical non-Newtonian behaviours include shear thinning and shear thickening, Figure 2.2.

Shear thinning fluids, also known as pseudoplastic fluids, are characterised by an apparent viscosity, which decreases with increasing shear rate. This behaviour is typical of polymer melts and solutions (e.g. aqueous polyacrylamide solutions), protein concentrates, and cream (Holdsworth, 1993; Chhabra *et al.*, 1999). Most shear thinning fluids, however, exhibit a Newtonian behaviour at very low and very high shear rates, resulting in two limiting values of the apparent viscosity, a zero-shear viscosity, η_0, and an infinite shear viscosity, η_∞, respectively (Chhabra *et al.*, 1999). Figure 2.3 shows a qualitative logarithmic plot of apparent viscosity as a function of shear rate for a shear thinning fluid based on the Carreau model described below. At very low and very high shear rates the apparent viscosity is constant, thus, indicating Newtonian behaviour in this region, with a non-Newtonian regime in between where viscosity decreases with increasing shear rate.

The rate of this decrease and the shear rate values marking the upper and lower limits of this non-Newtonian regime vary from one material to another.

Non-Newtonian behaviours can be represented using different mathematical models, as described below:

(i) Power-law or Ostwald de Waele model

This model describes the relationship between shear stress and shear rate using a power-law expression of the form:

$$\tau = k\dot{\gamma}^n \qquad \textit{Equation 2}$$

where the constants *k* and *n* are known as the flow consistency index and flow behaviour index, respectively. The practical range of values that the flow behaviour index, *n*, may take is (0-1) for shear thinning fluids and $n > 1$ for shear thickening ones. The smaller the value of *n*, the greater the degree of shear thinning and, thus, the more pronounced the non-Newtonian behaviour of the fluid. For $n = 1$, the fluid reduces to a Newtonian one with a constant viscosity equal to *k* (Mezger, 2014).

One of the shortcomings of this model is that it can only be used to describe the shear-thinning regime of the flow curve, and therefore does not predict the zero and infinite shear viscosities at low and high shear rates, respectively. Furthermore, the empirically determined values of *k* and *n* depend on the range of shear rate considered (Chhabra *et al.*, 1999). Nevertheless, the power law model offers the simplest representation of shear thinning fluids, and due to its simplicity, it is perhaps, the most widely used model.

(ii) Sisko model

This is another three-parameter model, which is useful in describing flow in the Power law and upper Newtonian regions (Sisko, 1958). This model is of particular interest in this thesis framework since most the fluids investigated in this work are suspensions which behave in this way.

$$\eta = \eta_\infty + k\gamma^n \qquad \textit{Equation 3}$$

However, this model is not implemented in Ansys Fluent.

(iii) Carreau model

When the fluid experiences very low and very high shear rates, the power law model might not be adequate to describe the flow behaviour. The model proposed by Carreau, (1972) considers the limiting values of viscosity at such extremes of shear rate, and is given by:

$$\frac{\eta-\eta_\infty}{\eta_0-\eta_\infty} = [1 + (\lambda\dot{\gamma})^2]^{(n-1)/2} \qquad \textit{Equation 4}$$

where λ is a curve-fitting parameter, given in time units.

(iv) Ellis model

This model takes account of the zero-shear viscosity only. Unlike the power law and Carreau models, the Ellis model expresses apparent viscosity in terms of shear stress rather than shear rate, thus

$$\eta = \frac{\eta_0}{1+\left(\frac{\tau}{\tau_{1/2}}\right)^{\alpha-1}} \qquad \textit{Equation 5}$$

where $\tau_{1/2}$ is the shear stress at which the apparent viscosity has dropped to $\eta_0/2$, and α is a measure of the extent of shear thinning. Details of other shear thinning models can be found in the literature (see, for example, Holdsworth, 1993). In contrast with shear thinning fluids, shear thickening fluids, have an apparent viscosity which increases with increasing shear rate. This type of fluid is most widely observed in concentrated solid-liquid suspensions, such as china clay and corn flour in water (Chhabra *et al.*, 1999). However, shear thickening fluids are less used in the processing industries than shear thinning fluids. The mathematical representation of the shear thickening behaviour is described by the power law equations (Equation 2).

2.1.2. Rheology of suspensions

Materials investigated in this thesis are mainly liquid-solid systems. Therefore, a better understanding of the rheology of suspensions is required to investigate how the particles affect the rheological behaviour of the fluid. The dynamics of the particles in heterogeneous materials are an area of current research.

Many applications involve the flow of fluid systems containing suspensions, such as the processing of gelatinous foods and cosmetic items, the fabrication of high-performance materials in the ceramic and metallurgical industries, transportation in the petroleum industry, the preparation and handling of pigment slurries in the paint industry and the production and storage of HBBs for road pavement applications (Schramm, 2006; Rahman *et al.*, 2012b; Bunger *et al.*, 2013; Lo Presti, 2013). Nevertheless, adding particles does not simply improve the materials performance but it may further complicate the fluid flow scenario. Indeed, suspensions may resist to flow in particular situations or may make difficult to achieve the target properties. Furthermore, the terminal settling velocity defined by Stoke as inversely proportional to the viscosity of a suspension affects the sedimentation phenomena in several applications such as the HBBs manufacturing, treatment of wastewater, mineral fractionation, etc. (Schramm, 2006; Willenbacher *et al.*, 2013). In many cases, such complications do not allow to express the viscosity by a single value at constant pressure and temperature. Indeed, viscosity also depends upon whether the material is flowing, for these reasons it is a better practice to describe viscosity of suspensions in terms of the continuous phase (η_0) and the fraction of dispersed material (Schramm, 2006). Hence, the prediction and control of suspension rheology is crucial for the performance and development of these applications. A very large number of equations have been advanced for estimating suspension viscosities.

Most of these equations are derived from Einstein's equation for a dilute suspension of non-interacting spheres, that states that particles increase the viscosity of the dispersion medium as a linear function of the volume fraction φ according to the equation:

$$\eta = \eta_0(1 + 2.5\varphi) \qquad \textit{Equation 6}$$

where η_0 is medium viscosity and φ is the dispersed phase volume fraction (with a requirement that φ < 0. 1). Figure 2.4 shows several sets of experimental data compared with the Einstein's equation. Experimental results proved that when the volume fraction φ reaches values between 0.1 and 0.5, the viscosity increases drastically. At these values the fluid may exhibit a non-Newtonian behaviour due to particles "crowding" (Willenbacher *et al.*, 2013). The maximum volume fraction possible for the suspensions made up of uniform, incompressible spheres is 0.74 (Schramm, 2006).

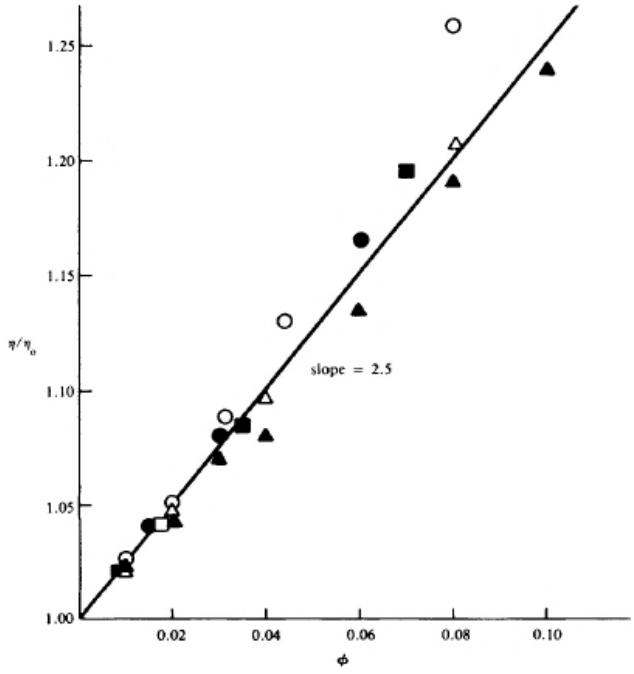

Figure 2.4 Comparison of several sets of experimental data and the Einstein equation, adapted from (Schramm, 2006)

At particles concentration higher than 0.1, the hydrodynamic interactions between particles become important and other equations have to be considered.

Einstein's equation does not take into account the interaction between particles. The effect of two-sphere hydrodynamic interactions on the suspension viscosity was calculated by Batchelor (Batchelor, 1977)

$$\eta_r = 1 + 2.5\varphi + 6.2\varphi^2 \qquad \textit{Equation 7}$$

Where η_r is the relative viscosity:

$$\eta_r = \eta/\eta_0 \qquad \textit{Equation 8}$$

As Einstein's equation also Batchelor's one is valid for volume fraction up to $\varphi < 0.1$.

When considering higher particle concentrations is mandatory to consider the particle interactions and an accurate model to predict the viscosity is still lacking. Many models have been realised aimed to find a correlation between viscosity of concentred suspensions and particles volume fraction. Krieger and Dougherty (1959) introduced a semi-empirical equation for the concentration dependence of the viscosity:

$$\eta_r = \left(1 - \frac{\varphi}{\phi_{max}}\right)^{-2.5\phi_{max}} \qquad \textit{Equation 9}$$

where ϕ_{max} is the maximum packing fraction or the volume fraction at which the zero-shear viscosity diverges. This equation reduces to the Einstein's one at low particle concentration. Quemada, (1977) suggested another phenomenological model to predict the $\eta_r(\phi)$ dependence:

$$\eta_r(\Phi) = \left(1 - \frac{\varphi}{\phi_{max}}\right)^{-2} \qquad \textit{Equation 10}$$

This model suits best as $\varphi \longrightarrow \phi_{max}$.

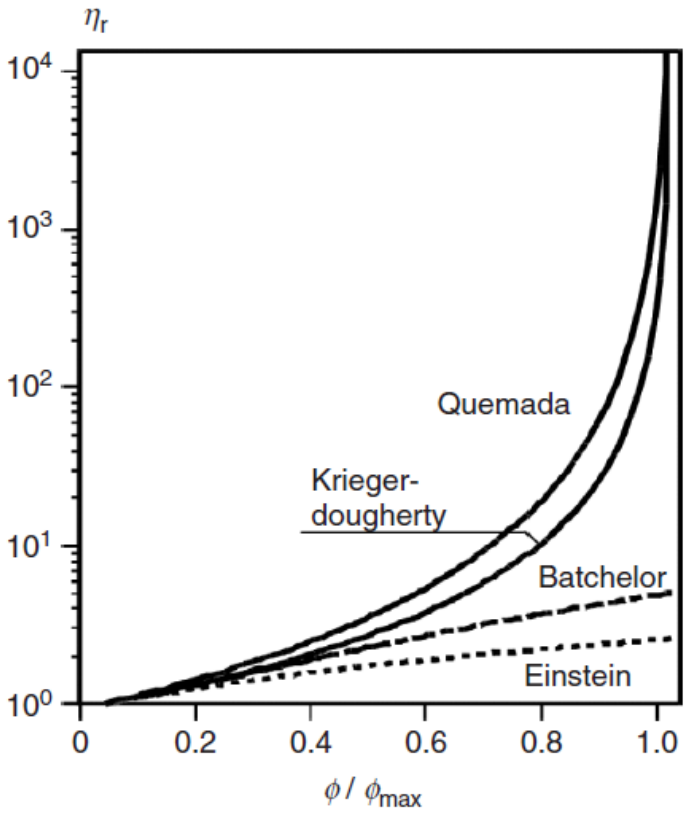

Figure 2.5 Schematic representation of the volume fraction dependence of relative viscosity η_r according to the Einstein, Batchelor, Krieger–Dougherty, and Quemada models, adapted from (Quemada, 1977)

Figure 2.5 compares the above introduced viscosity models by showing the volume fraction dependence of relative viscosity. The value for the maximum packing fraction ϕ_{max} is obtained by the packing geometry that is related to the particle shape and particle size distribution but not on particle size. The volume fraction at maximum packing has been calculated by theoretical models and different ϕ_{max}values have been found depending on the type of packing. The ϕ_{max}value for hard spheres is often taken as 0.64 (Buscall *et al.*, 1994), which is the value associated with random close packing. Many other analytical models of viscosity have been developed in the literature to calculate the effective viscosity, the most are summarised in a review carried out by Khanafer *et al.*(2011).

Furthermore, the transition from low shear to high shear plateau referred to as the shear-thinning region depends on the balance between Brownian and hydrodynamic forces. The Peclet number *Pe* expresses the relative importance of these two contributions (Willenbacher *et al.*, 2013):

$$Pe = \frac{6\pi a^3 \mu_0 \dot{\gamma}}{bT} \qquad \textit{Equation 11}$$

Where *b* is the Boltzmann constant, *T* the absolute temperature and *a* the particle radius.

Experiments show that viscosity becomes independent of Peclet number for Pe $\geq 10^3$ (Stickel *et al.*, 2005), as Brownian interactions are disrupted by hydrodynamic forces (Krieger, 1972). The impact of inertia is governed by the particle Reynolds number (Stickel *et al.*, 2005):

$$Re = \frac{\rho_0 a^2 \dot{\gamma}}{\eta_0} \qquad \textit{Equation 12}$$

where ρ_0 is the density of the suspending fluid. Stickel *et al.* (2005) links inertial effects, which become important at Re $\geq 10^3$, to the shear-thickening rheology which has been observed experimentally by several workers (*e.g.* Krieger, 1972; Barnes, Hutton and Walters, 1989).

Finally, the Stokes number indicates the coupling between the solid and fluid phases, variations in which may lead to non-Newtonian behaviour (Coussot *et al.*, 1999):

$$St = \frac{\rho_p a^3 \dot{\gamma}}{\lambda \mu_0} \qquad \textit{Equation 13}$$

where ρ_p is the particle density and λ the characteristic length of the particles. When *St* << 1, fluid–solid coupling is strong.

2.2. HBBs in pavement engineering applications

As mentioned in section 2.1.1 heterogenous materials cover a wide range of industrial applications, among the others, one that is of meaningful importance for pavement engineering applications is the modification of bitumen to enhance the material performance by adding special modifier.

Neat bitumen usually performs as a Newtonian material; however, this scenario drastically changes by adding a modifier to the base bitumen. Indeed, these materials show either a high level of heterogeneity either an unusual response to mechanical stresses making their rheological characterisation challenging. This thesis was carried out within the heterogenous materials framework focusing on HBBs particularly on CR-MB for pavement engineer applications.

The next sections introduce this material, from its development till its applications also showing limits and benefits of its use.

2.2.1. Modification of bitumen

The use of neat bitumen on asphalt mixes dates back the beginning of 1900 and it still performs well. Conventional bitumen grades possess satisfactory adhesion and mechanical properties for use in asphalt pavements for the vast majority of traffic and climatic conditions that are encountered. Nevertheless, with bitumen becoming the major binder for the paved highways and increasing demands made on pavement there was recognition that it could be modified to improve its durability and performance (Hunter *et al.*, 2015).

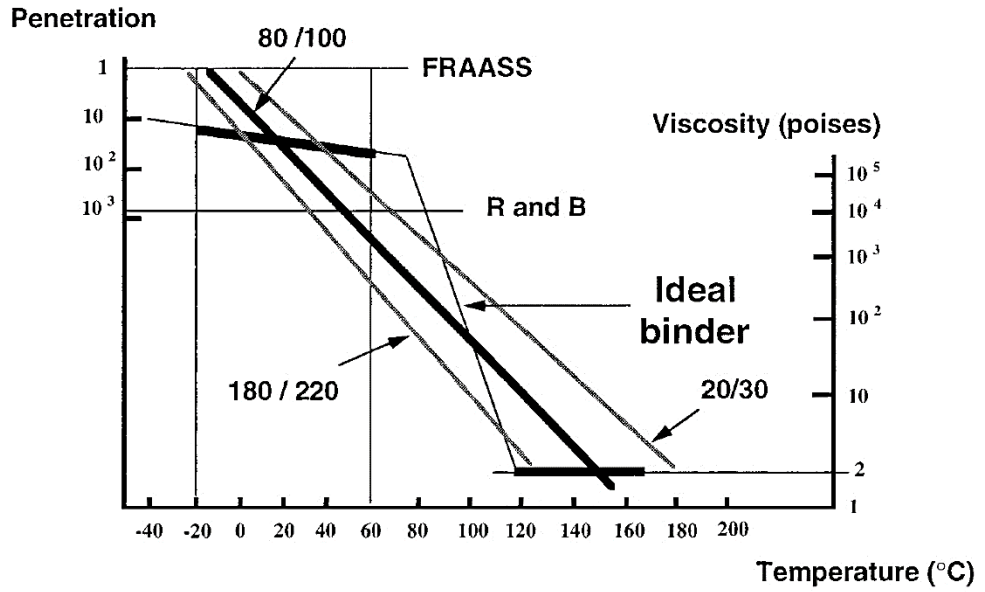

Figure 2.6 Temperature susceptibility of an ideal thermoplastic binder adapted from (Brûlé, 1996)

Indeed, the growth in the number of miles of roadways is tied to the growth in cars and it is well known that pavements suffer significant distresses due not only to temperatures but also to increasing traffic load (higher traffic levels, larger and heavier trucks, new axle designs and increased tyre pressure). Furthermore, since that key factors during pavement design are comfort, high standard of safety, maintenance frequency and service life, it is of main importance to enhance the properties of the binder.

Figure 2.6 shows the binder optimal characteristics, it should provide adequate coating and low temperature susceptibility throughout the range to which it will be used during service, while maintain a low viscosity at the usual placement temperatures. Its susceptibility to loading time should be low, whereas its permanent deformation resistance, fracture strength and fatigue characteristics should be high. Finally, its aging characteristics should be good, both for laying and in-service (Brûlé, 1996a).

Modifiers aim to improve the performance of conventional bitumen and consequentially of asphalt pavement by providing (Hunter *et al.*, 2015):

- Stiffer asphalt mixture at high service temperatures to minimise rutting
- Softer mixtures at low temperatures to minimise non-load associated thermal cracking
- Improved fatigue resistance
- Improved bitumen-aggregate bonding to reduce stripping or moisture susceptibility
- Improved abrasion resistance of asphalt mixture to reduce ravelling
- Improved workability of the asphalt during compaction
- Rejuvenating aged bitumen
- Permitting thicker bitumen films on aggregate for increased asphalt mixture durability
- Reduced flushing or bleeding
- Improved resistance to ageing or oxidation
- Reduced structural thickness of pavement layers

2.2.2. Bitumen modifiers

For many years, researchers have experimented modified bitumen by adding fillers, mineral fibres, plastomers, thermoplastic elastomers and rubbers aimed to improve the properties of the bituminous binder (Zhu *et al.*, 2014).

In point of fact, different substances can potentially give similar benefits to the bitumen, but for modifiers to be effective and for its use to be both practicable and economic, it must (Hunter *et al.*, 2015):

- Be readily available
- Resist degradation at asphalt mixing temperature

- Blend with bitumen
- Improve resistance to flow at high road temperature without making the bitumen too viscous at mixing and laying temperatures or too stiff or too brittle at low road temperatures
- Be cost effective

Moreover, when blended with bitumen the modifier should:

- Maintain its premium properties during storage, application and in service
- Be capable of being processed by conventional equipment
- Be physically and chemically stable during storage, application and in service
- Achieve a coating or spraying viscosity at normal application temperatures.

The above-mentioned characteristics cannot be achieved at the same time; indeed, modification technology depends on the specific applications and techniques (surface dressings, thin surface course systems, porous asphalt, surface courses for heavily trafficked roads, bases for heavily trafficked roads, anti-cracking membranes, bridge water proofing layers, etc.). The degree of improvement required, and hence the cost, will depend on the particular needs of the site where treatment is proposed. Table 2.1 shows the most assessed additives for modifying bitumen.

Among all of these, the most important are polymers, macromolecules having the same group of atoms repeated many times. Addition of natural or synthetic polymers to conventional bitumen is known to enhance service properties over a wide range of temperatures in road paving applications (Hunter *et al.*, 2015). Indeed, by adding polymers to the base bitumen it is possible to influence its rheological behaviour and thermal susceptibility which tends to incorporate the main characteristics of the modifier.

Several studies have been carried out to investigate the effect of these additives on the rheological properties of modified bitumens and performance (Brûlé, 1996; Airey, 2003; Yildirim, 2007): decreased thermal susceptibility and permanent deformation (rutting), increased fatigue, and low temperature cracking resistance.

Among all the HBBs one of particular interest for its pavement engineering applications and sustainability impact is the crumb rubber modified bitumen (CR-MB). The next section provides a brief description of the material's history, technologies, and specifications, but also showing its benefits and limitations.

Table 2.1 Examples of additives used to modify bitumen (Yildirim, 2007; Zhu and Kringos, 2014) - A

Type of modifier	**Examples**
Thermoplastic elastomers	Styrene–butadiene elastomer Styrene–butadiene–styrene elastomer Styrene–butadiene rubber Styrene–isoprene–styrene elastomer Styrene–ethylene–butadiene–styrene elastomer Ethylene–propylene–diene terpolymer Isobutene–isoprene random copolymer Polyisobutylene Polybutadiene Polyisoprene
Latex	Natural rubber
Thermoplastic polymers	Ethylene–vinyl acetate Ethylene–methyl acrylate Ethylene–butyl acrylate Atactic polypropylene Polyethylene Polypropylene Polyvinyl chloride Polystyrene
Thermosetting polymers	Epoxy resin Polyurethane resin Acrylic resin Phenolic resin
Chemical modifiers	Organometallic compounds Sulphur Phosphoric acid, polyphosphoric acid Sulfonic acid, sulfuric acid Carboxylic anhydrides or acid esters Dibenzoyl peroxide Silanes Organic or inorganic sulphides Urea

Examples of additives used to modify bitumen (Yildirim, 2007; Zhu and Kringos, 2014) – B

Recycled materials	Crumb rubber, plastics
Fibres	Lignin Cellulose Alumino-magnesium silicate Glass fibres Asbestos Polyester Polypropylene
Adhesion improvers	Organic amines Amides
Antioxidants	Phenols Organo-zinc or organo-lead compounds
Natural asphalts	Trinidad Lake Asphalt Gilsonite Rock asphalt
Fillers	Carbon black Hydrated lime Lime Fly ash
Reactive polymers	Random terpolymer of ethylene, acrylic ester and glycidyl methacrylate Maleic anhydride-grafted styrene–butadiene–styrene copolymer
Viscosity modifiers	Flux oils (aromatics, napthenics, parrafinics) Fischer–Tropsch waxes

2.2.3. Crumb rubber modified bitumen (CR-MB)

Brief history of crumb rubber modified bitumen

Rubber in asphalt pavements has been adopted about 180 years ago. The first experiment blending bitumen and natural rubber to modified the bitumen was performed in 1840s (Hoffman, 1974). Lately in the 1930s, both synthetic and natural rubber were used to produce a modified bitumen and the manufacturing process was progressively improved (Hanson *et al.*, 1994; Yildirim, 2007). Unfortunately, this technique at its early stage formulation provided little or no benefit, resulting in pavement that cost more and had a shorter service life than conventional asphalt.

In 1960, Charles H. MacDonald, that can be defined the father of asphalt rubber, discovered a successful formulation (McDonald, 1981). Indeed, while studying methods to fix potholes, MacDonald formulated a new material by adding ground tyre rubber to hot liquid bitumen. He found that after mixing crumb rubber with bitumen and allowing it to react for forty-five minutes to an hour, new material properties were obtained (Hoffman, 1974). The resulting material embraced the viscous (bitumen) and elastic (rubber) properties of base ingredients; he called it asphalt-rubber (McDonald, 1975).

Figure 2.7 Shredded end life tyres (left) and crumb rubber (right)

The difference compared to the previous attempts of modifying the bitumen by adding natural rubber is related to the different chemical structure of the rubbers. Natural rubber when not vulcanized returns a non-elastic response to deformation. The reason of that is related to the chemical structure of the rubber that is made of long polymer chains free to move independently between each other leading to a change in shape. Instead when vulcanized, cross-links are formed between the polymer chains avoiding them to move independently. Rubber as a result when stressed will deform but once realised the stress it will go back to its original shape. It was observed that the tyre rubber thanks to the vulcanisation process swells by means of absorbing the lower boiling constituents of the bitumen, thus alleviating serious defects in the bituminous surface. Additionally, incorporating vulcanized rubber in bitumen would provide a new use of some of 29.1 million tons of end-life tires (WBCSD & The Tire Industry Project, 2019).

The definition of asphalt-rubber, referred in this thesis as CR-MB, was introduced in a standard for the first time in 1988 (ASTM D 8, ASTM D6114-97). In the last decades, these materials have been used worldwide in many applications (asphalt binders, road pavement, roofing materials, stress absorbing lays, etc.) (Visser *et al.*, 2000; Lo Presti, 2013; Bueno *et al.*, 2014). The choice of using this modifier was a combination of environmental impact (landfill reduction, waste management and reduced noise emissions) and performance enhancement (increased skid resistance, improved stiffness and elasticity and durability). These binders provide significantly enhanced engineering properties over conventional paving grade bitumen (Terrel *et al.*, 1986; Lo Presti, 2013). As demonstrated by various researchers, at intermediate and high temperatures CR-MBs show properties different than those of neat bitumens. Indeed, increased stiffness and elasticity are reported.

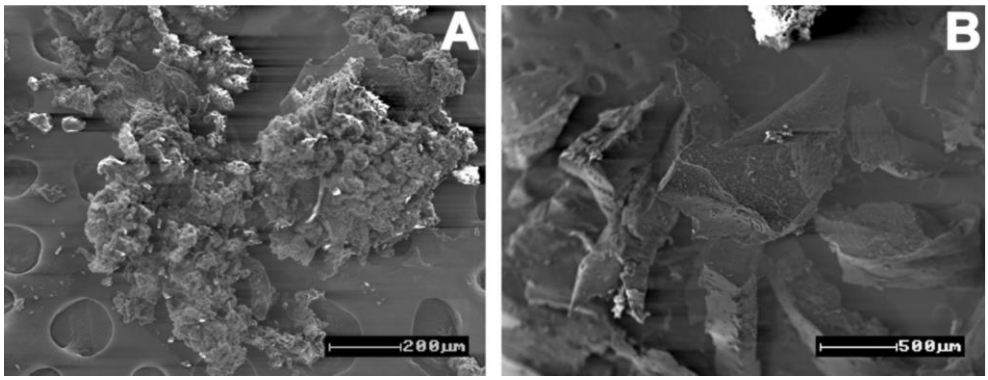

Figure 2.8 SEM Micrographs of rubber granulate grains obtained at ambient temperature (A) and cryogenically (B) adopted from (Sienkiewicz et al., 2012)

As a consequence, decreased pavement temperature susceptibility, improved resistance to permanent deformation (rutting) and fatigue with little effect on cold temperature properties are recorded (Kaloush *et al.*, 2003; Bertollo, 2004; Sousa, 2005). Furthermore, pavements using this technology required lower maintenance costs (Jung *et al.*, 2003) and showed lower noise production (Leung, 2006; Pasquini, 2009). Nowadays, the above described process is a highly controlled material, more complex than just grinding the tyres and adding the rubber to hot asphalt. The whole process from handling to shredding is carefully planned and monitored aimed to achieve the highest level of quality for the final product (Lo Presti, 2013).

There are different grinding technologies to produce crumb rubber modifier (CRM) from end life tyres, next sections introduce the most used.

Ambient grinding

This technology consists in grinding the rubber at ambient temperature by using mechanical rotating blades. After the milling process, the steel fibres are removed from the rubber. Usually particles size ranges from 0.3 mm to 5mm. The main characteristic of this method is that particles present an irregular shape with relative high surface area (Thodesen *et al*,.2009).

Usually rubber processed using this technology enhances the interaction with the base bitumen. To date, ambient grinding is the most used and cost-effective technology of processing end of life tyres (Lo Presti, 2013). Figure 2.8 shows scanning electron microscope (SEM) images taken at different magnifications of the individual rubber particles. The SEM images show that CR-MB produced by ambient grinding has irregular shapes and rough surface, properties which are desirable for rubber–bitumen interaction and hence better physical properties (Lee *et al.*, 2008).

Cryogenic grinding

The cryogenic technology, first, freezes the rubber by using nitrogen (between -87 ºC to -198 ºC) and then mills the frozen rubber into smooth particle by hammering (Thodesen *et al*,.2009). As a result of this process the particles present a reduced surface area compared to those produced by ambient grinding. However, the material performance enhances with the decrease of specific gravity and particle size and increase with the higher surface porosity of the granules. Particles with these characteristics provides a reduced rubber-bitumen reaction where the final mixture presents reduced elastic properties compared with those obtained by the ambient technology (Lo Presti, 2013). Thodesen *et al.*(2009) concluded that cryogenic crumb rubber exhibits a reduced level of bitumen modification by providing SEM images of bitumen modified with both ambient and cryogenic CRM particles.

To better understanding the impact of these technologies as well as other variables on the CR-MB it is essential to consider the rubber-bitumen interaction mechanisms, as they explain how the components and the parameters of the manufacturing procedure can determine the ultimate properties of the modified binder.

Rubber-Bitumen iteration mechanism

Different studies considered the interaction mechanism between the rubber and bitumen to be physical where the particles are swollen by the absorption of the oily compounds available in the bitumen (Heitzman, 1992; Ghavibazoo *et al.*, 2013). Nevertheless, other investigations show that the rise in binder viscosity cannot be explained only by the swelling of the particles (Bahia *et al.*, 1991). The rubber-bitumen interaction involve two parallel process, the absorption of aromatics oils from the bitumen to the rubber that lead to swelling and softening process (Lo Presti, 2013). The second is the digestion of the rubber into the bitumen (Chehovits *et al.*, 1982; Abdelrahman *et al.*, 1999). The swelling process requires high temperatures (140-220°C), during the process the binder develops a gel-like form by absorbing the oily fraction of the bitumen leading to an increase in the particle dimensions and a consequent reduced inter-particle distance. The swelling of the rubber particles can reach a ratio of 250% until saturation with the oily fractions of the bitumen with the consequent increase in viscosity up to a factor of 10 (Heitzman, 1992; Peralta *et al.*, 2010). The reaction of rubber with the base bitumen is a function of time and temperature. Indeed, if the temperature is too high or the time is too long, the swelling process will lead, , to the rubber depolymerisation/devulcanization which causes it dispersion into the bitumen (Lo Presti, 2013; Subhy *et al.*, 2016).

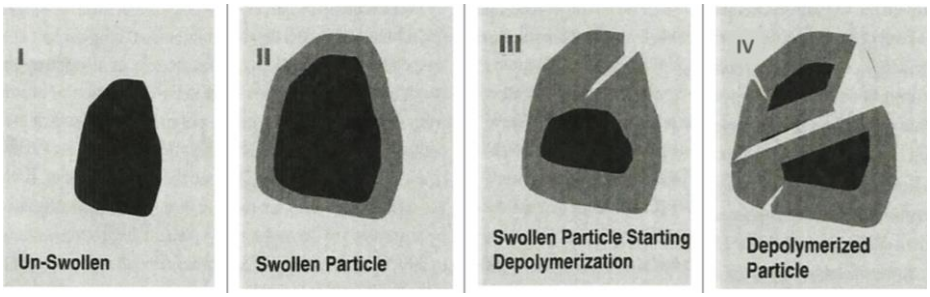

Figure 2.9 Progression of bitumen-rubber interaction at elevated temperature: change in particle size over time at elevated temperature adapted from (Abdelrahman and Carpenter, 1999)

During the depolymerisation the rubber starts releasing components back to the bitumen causing a decrease in the complex modulus (G^*), which affects the material stiffness, while the phase angle (δ), related to the elastic properties continue to modify (**Error! Reference source not found.**) (Subhy *et al.*, 2016). If the depolymerisation process is too extended it will continue causing more destruction of the binder networking and so δ modification is lost (Figure 2.9) (Abdelrahman et al., 1999). The rubber-bitumen interaction is material-specific and depends on several parameters, such as:

- Processing variables
- Base binder properties
- Rubber properties

These parameters have to be monitored during the CR-MBs production aimed to control the modification process.

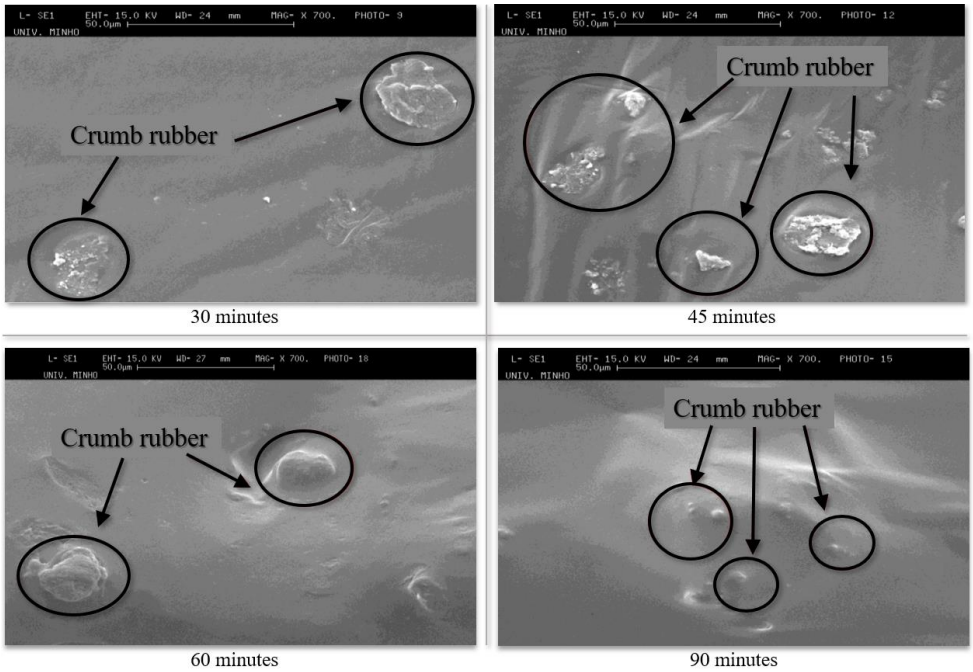

Figure 2.10 SEM micrographs of the finished rubberised bituminous binder adapted from (Pereira *et al.*, 2008)

Processing variables

Due to the high level of heterogeneity and variety of these materials, there are numerous issues relating to the design and material selection. The material's properties depend on several variables, not only the proportions and nature of the components (bitumen and rubber) but also the parameters of the manufacturing process (mixer type, mixing time and temperature), with substantial influence on the viscosity and the rheology of the final product (Chehovits *et al.*, 1982; Lo Presti *et al.*, 2013). These variables have a primary importance during the blending process. Among the others the temperature represents a key parameter during the modification process (Chung, 2000). Indeed, the final properties of CR-MB are strongly affected by the temperature. As previously introduced, the temperature is a crucial variable during the swelling process. Low temperatures (90 ºC -120 ºC) do not allow to break up the chemically crosslinked network (Navarro *et al.*, 2004;).

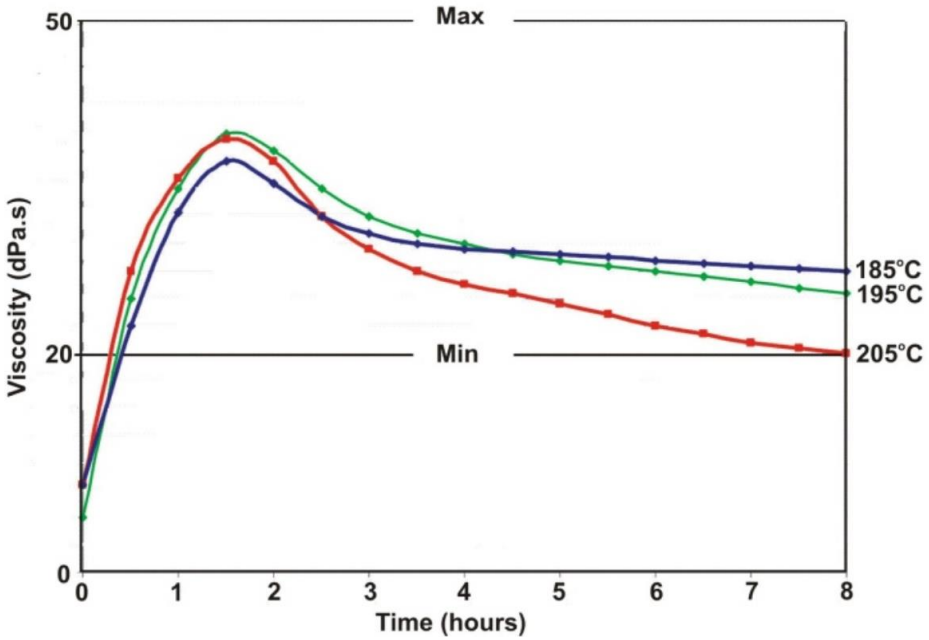

Figure 2.11 Typical changes in viscosity values for rubberised bitumen at different temperatures over time, adopted from (Sabita, 2016)

Instead, by increasing the temperature, the dissolution of the rubber into the bitumen is boosted due to an increased rate in breaking up the crosslinked network (Ghavibazoo *et al.*, 2013). The swelling process is enhanced in a temperature range between 140 ºC and 200ºC, at these temperatures the swelling rate is inversely proportional to the swelling extend. However, further increasing the temperature may lead to a downside effect. Figure 2.10 and Figure 2.11 highlight that the rubber-bitumen interaction is also time-temperature dependent. It can be observed that there are two phases during the CR-MB manufacturing, the first that lasts between 45 and 60 min where the swelling process takes place and a second where the modified binders' properties stabilise. Subhy *et al.* (2015) reported that a digestion time up to 2 hours over a temperature range of 180°C to 200°C improved the CR-MB properties.

Figure 2.12 Asphalt-Rubber portable Blending Systems adapted from (Allbiz, 2019)

As a general conclusion, it is possible to states that longer is the reaction time allowed for the digestion of the rubber than higher it will be the peak of viscosity reached by the binder.

However, various researchers proved that the depolymerisation process is directly proportional to the processing temperature and reported that extended digestion up to 24 hours have caused reduction in viscosity and elastic response due to the rubber devulcanization\depolymerisation (Oliver, 1980). Other parameters such as base binder and rubber properties have to be considered. Indeed, CR-MB in order to satisfy the specifications requirement must be accurately designed and produced and provide a final product that complies with the expected climate and traffic conditions (Lo Presti, 2013).

Specifications

According to Caltrans, (2011), a modified binder to be assessed as CR-MB needs to achieve a rotational viscosity of 1500 cP at 177.5 °C during the production. Physical requirements are shown in Table 2.2 according to ASTM D 6114. CR-MB is manufactured at high temperatures (177.5 °C) in low shear to favourite the rubber-bitumen interaction.

Table 2.2 Specification for Rubberised bitumen (ASTM D6114)

Binder Designation		***Type I***	***Type II***	***Type III***
Apparent Viscosity, 175°C	min	1500	1500	1500
Modified Test Method D 2196	max	5000	5000	5000
Penetration, 25°C	min	25	25	50
1⁄10 mm (Test Method D 5)	max	75	75	100
Penetration, 4°C 1⁄10 mm (Test Method D 5)	min	10	15	25
Softening Point: °C (Test Method D 36)	min	57.2	54.4	51.7
Resilience, 25°C : % (Test Method D 5329)	min	25	20	10
Flash Point: °C (Test Method D 93)	min	232.2	232.2	232.2
Thin-Film Oven Test Residue (Test Method D 1754)	…	…	…	…
Penetration Retention, 4°C	min	75	75	75

Table 2.3 CR-MB gradation used for CR-MB, adapted from (TG1, 2015)

Sieve #	Nominal size (mm)	% Passing
10	2.36	100
16	1.18	75-100
30	600 µm	25-100
50	300 µm	0-45
100	150 µm	0-10
300	75 µm	0

CR-MB manufactured at lower temperature may still achieve the minimum viscosity requirements but never the same characteristics as the laboratory design. Prior to being laid binders are usually tested in laboratory by using a rotational viscometer to assess if they comply with the specifications.

Table 2.3 shows the typical rubber gradation used to produce CR-MB, usually at least 15% of CRM is required to achieve the threshold viscosity. Therefore, the modified binders due to the presence of particles have to be constantly well mixed to avoid common phenomena such as phase separation, sedimentation or agglomeration. For these reasons, CR-MB are usually manufactured by using special blending equipment that provide continue agitation to keep the particles evenly dispersed within the tank (Figure 2.12).

Limitations

Although there are many benefits of using CR-MBs (Bahia *et al.*, 1991; Airey, 2003; Lee *et al.*, 2008), issues about the use of this technology that may limit its application still exist. These materials need to be properly selected, designed, manufactured to achieve the target performance. According to (Caltrans, 2011) limitations on the use of CR-MB include:

- CR-MB requires higher compaction temperatures compared to dense-graded HMA, that is due to the rubber stiffening the binders at high temperatures.

- CR-MB requires to be used within few hours the manufacturing process has been completed, otherwise the modified binder may not comply anymore with the specifications.
- CR-MB requires agitated tank for storage at high temperatures, otherwise phenomena like sedimentation may occur.
- Conventional laboratory procedure may not be adequate to characterise the rheological behaviour of CR-MB

Additionally, Caltrans, (2011) states that one of the main drawbacks of these family of binders is their lack in storage stability. The issue here is that rubber particles tend to settle down as a solid in a liquid phase (bitumen) with minor density. To overcome that, the tank has to be provided with a stirrer to guarantee the storage stability of the material. Several investigations have been performed to produce CR-MB with enhanced storage stability by reducing the size of the CRM particles (Navarro *et al.*, 2004), by adding sulphur (Ghaly, 2008) or particular polymers (Perez-Lepe *et al.*, 2007). But the problem has not been addressed yet, maintaining the stirring of the stored CR-MB necessary at industrial scale. Furthermore, the stirring in the tank for extended storage periods, beyond preventing the sedimentation of particles, it may promote the depolymerisation of the rubber leading to a loss of quality of the stored CR-MB. Researchers proposed to increase the viscosity by rising the temperature and the mixing time, nevertheless, it resulted valid only in some ranges of temperature and processing time (Hosseinnezhad *et al.*, 2014). In a further investigation, where experiments were extended for 8 hours, the increase of the viscosity reached a horizontal asymptote over the time (Jeong *et al.*, 2010). That could be explained, due the high mixing temperature, by the depolymerisation of the rubber in response to the hardening caused by the absorption of the oily fraction and the binder's ageing. Ragab *et al.*, (2018) proved that increasing the mixer speed from 10 to 50 Hz in the production

process, during a storage time of 8 hours, leads to a decreased separation index. These observations could be interpreted as the proof of the depolymerisation process along the time when interaction parameters increase. As a consequence, it could be stated that due to the depolymerisation the rubber particles are dissolved and that reduces the sedimentation issue. This lack of storage stability of HBB and particularly CR-MB is an issue that rheologists have to cope in asphalt plants. Nevertheless, the same scenario might also happen in a laboratory during rotational viscosity measurements that could lead to mistakes during the design or testing phase.

Therefore, based on the above observations it may be beneficial to develop a laboratory application aimed to govern the modification process and to estimate the conditions for the storage period to avoid or reduce the loss of viscosity of the CR-MB during storage. Researchers tried to develop a laboratory real-time procedure for monitoring the rotational viscosity of heterogeneous binders. Celauro (*et al.*, 2012) adapted a Brookfield rotational viscometer to act as a low shear mixer by using a standard coaxial cylinder spindle (SC-27). Nevertheless, the authors concluded that due to the spindle geometry the procedure was affected by the sedimentation of the crumb rubber particles during the rotational test.

The next section presents the rheometry, focusing on the mixing rheometry, that is the science that refers to the experimental techniques used to determine the rheological properties of materials. An overview about the actual procedures/test to measure the rotational viscosity of heterogenous binders is introduced.

2.3. Mixing Rheometry

The experimental characterization of a material's rheological properties is of fundamental importance during the design process but also for its development, performance, and applications. The rheometry is the measuring technology used to determine the rheological data. The emphasis here is on measuring systems, instruments, and test and analysis methods. This thesis refers to mixing rheometry, as the measuring technique that involves the mixing of heterogenous blends while performing rotational test measurements. Both liquids and solids can be investigated using rotational and oscillatory rheometers. Various types of viscometers and rheometers are used to determine the flow behaviour under different conditions. Rotational tests are performed to characterize viscous behaviour while in order to evaluate viscoelastic behaviour, creep tests relaxation tests and oscillatory tests are performed. This thesis focuses within the rotational test framework.

For pavement engineering applications, the rotational viscometer is used to ensure that the viscosity of the bitumen at normal applications temperatures is capable of being pumped, to coating the aggregate and to enable satisfactory compaction of the asphalt (Hunter *et al.*, 2015). Rheologists are used to control the high-temperature rotational viscosity of bituminous binders for product development and quality control purposes (Caltrans, 2011). Usually, this exercise is carried out in the field with hand-held viscometers or more typically in a laboratory by using a rotational viscometer with coaxial cylinders testing geometries (Figure 2.13 and Figure 2.14). The dynamic/rotational viscosity is therefore a key engineering parameter that asphalt technologists needs to carefully control and target.

In recent years several investigations introduced the concept of adapting the rotational viscometer to act as a low shear mixer (Celauro *et al.*, 2012; Lo Presti *et al.*, 2014; Subhy *et al*. 2015). Indeed, a real-time procedure for

monitoring HBBs' properties as a function of processing time and temperature may provide asphalt technologists with a better understanding of the actual physical change throughout the processing of the material and overall higher confidence during product development and quality-control. On this regard, Celauro *et al.* (2012) and Lo Presti *et al.* (2014) have successfully demonstrated the concept of adapting a rotational viscometer as a low shear mixer for CR-MBs. In all of these studies, viscosity measurements were carried out according to international standards on viscosity measurements of CR-MBs (ASTM D4402, ASTM D7741M), but they all presented specific peculiarities: Celauro *et al.* (2012) proposed a procedure where the real-time monitoring was undertaken by using conventional spindles, Lo Presti *et al*., (2014) introduced the use of improved testing geometry (Dual Helical Impeller), while Subhy *et al*. (2015) suggested the use of specific parameters to monitor the viscosity change over-time.

Nevertheless, these studies came to a common conclusion, that standard equipment used to perform rotational testing on HBBs may not be adequate due to the poor mixing performance provided.

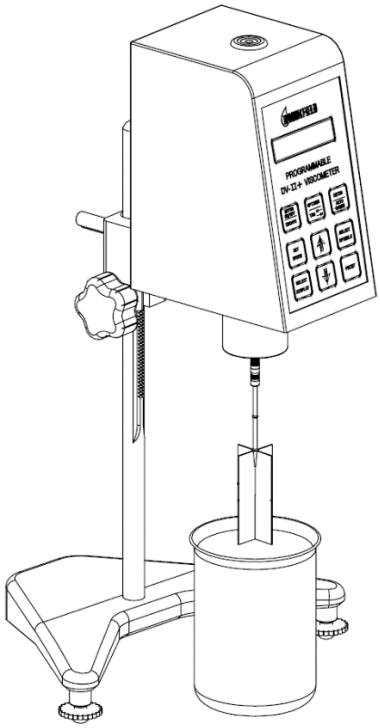

Figure 2.13 A rotational viscometer (Brookfield, 2015)

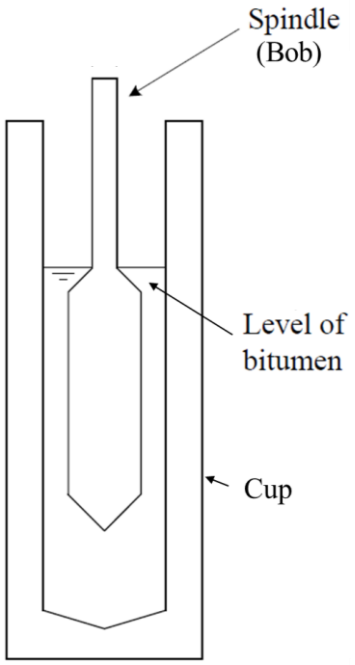

Figure 2.14 The cup and bob configuration used in the rotational viscometer

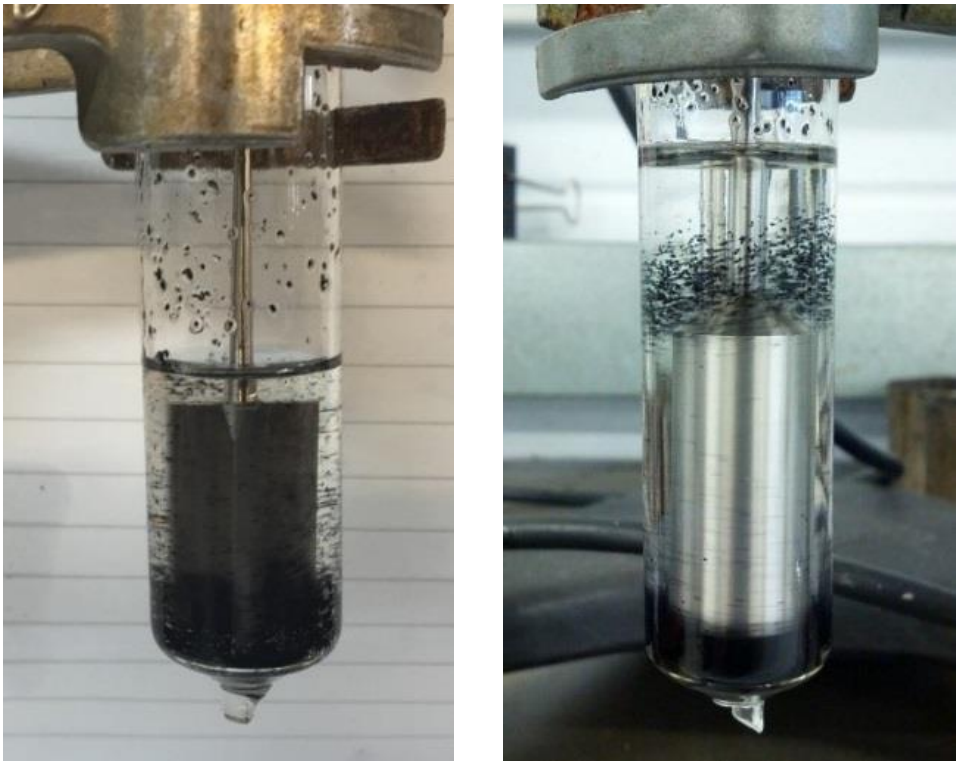

Figure 2.15 Visualisation of the phase separation during rotational viscosity measurements of crumb rubber suspensions for (left) the SC-27 spindle and (right) a vane spindle.

Indeed, due to the high level of heterogeneity showed by heterogenous binders, obtaining reliable rheological measurements remains a challenge. Several changes may occur in the sample while is tested in the measuring chamber. For example, Figure 2.15 shows the behaviour of a particulate suspension with both the SC-27 and a vane impeller. The figure shows clearly the settling and migration of the particulates away from the cylindrical gap. These phenomena (e.g. phase separation, sedimentation, agglomeration etc.), may affect the sample stability and can lead to results that are not reproducible and representative of the original sample.

Rotational viscometers are equipped with supplementary impellers designed to help rheologists for some of these scenarios.

Figure 2.16 Vane Spindles (left) and the T-Bar Spindles with the Helipath stand (right) adopted from (Brookfield, 2015)

For instance, the vane spindle seen in Figure 2.15 (right) and Figure 2.16 is designed for making measurements with paste-like materials, gels, and fluids where suspended solids migrate away from the measurement surface of standard spindles. The Brookfield Helipath Stand (Figure 2.16) is designed to slowly lower or raise a Brookfield T-bar spindle so that it describes a helical path through the test sample. These accessories are all fit for purpose although they are not designed to guarantee the sample stability of heterogeneity systems such as materials having the tendency to stratify during rotational tests due to phase density differences, as can be seen in Figure 2.15 (right).

In a first attempt to address this issue, Lo Presti (*et al.*, 2014) designed, manufactured and tested a prototype of a Dual Helical Impeller (DHI) for Brookfield Rotational Viscometers (Figure 2.17). Experimental studies were carried out to evaluate whether the DHI was able to improve the degree of homogenization of highly viscous fluids and in turn producing more consistent viscosity measurements. In comparison to the Brookfield standard cylindrical geometry (spindle SC-27), the DHI always predicted a different" apparent" viscosity. Here, apparent requires some explanation.

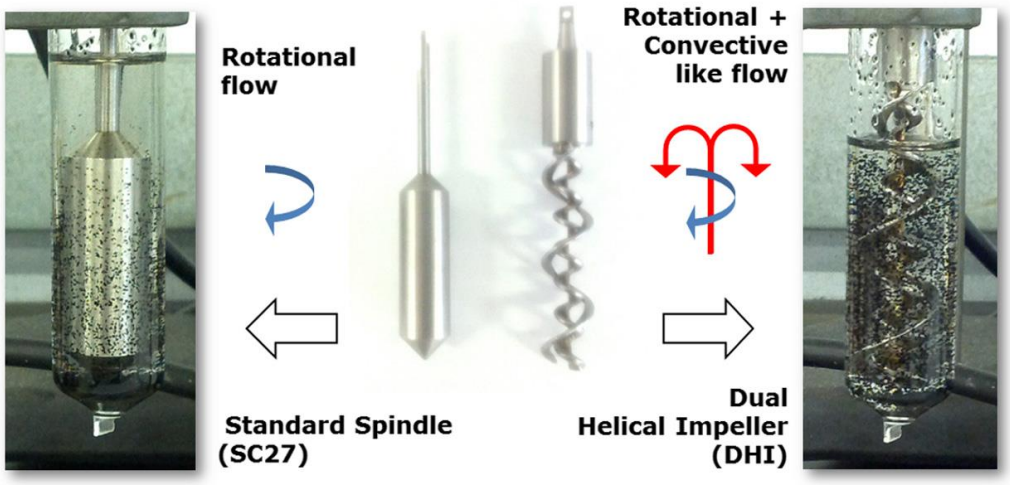

Figure 2.17 The idea through comparison between the impellers and the generated flows during rotation adopted from (Lo Presti et al., 2014)

For a cylindrical viscometer, the viscosity can be related to simple theory because the flow between the cylinders can be described analytically. With a complex impeller such as the DHI, a series of tests using standard fluids of known viscosity must be conducted to produce a library of torque versus viscosity curves. Thus, the absolute viscosity is not being measured when using the DHI. The more consistent behaviour of the DHI was explained by its capability to create convective-like flows as opposed to the axisymmetric swirling flow induced by the standard SC-27 spindle. The DHI generally produced good mixing but due to a small gap between the inner and outer helix, it failed to work well with all the suspensions tested. Therefore, when dealing with heterogenous materials, there is still the need to improve the impeller design and the interpretation of the results which will consequentially improve the meaningfulness of the viscosity measurements.

In order to provide the reader with further information for the interpretation of the presented results and conclusions, the following subsections will provide a brief review of measuring viscosity by means of a rotational viscometer.

2.3.1. Measuring viscosity using non-standard equipment

For rheological measurements of materials by means of rotational viscometer and coaxial cylinders, there is a theoretical basis for the calculation of the viscosity. Consider a cylinder of radius R_s and length, L, rotating at an angular velocity, ω, inside a stationary cylinder of radius, R_c (Mezger, 2014). The shear rate at the surface of the spindle,$\dot{\gamma}$, is

$$\dot{\gamma} = \frac{2\omega R_C^2}{R_C^2 - R_S^2} \qquad \textit{Equation 14}$$

and the shear stress, τ, is

$$\tau = \frac{T}{2\tau R_S^2 L} \qquad \textit{Equation 15}$$

where T is the torque input by the machine. The viscosity,η is

$$\mu = \frac{\tau}{\dot{\gamma}} = \frac{T(R_C^2 - R_S^2)}{4\pi\omega R_C^2 R_S^2 L} \qquad \textit{Equation 16}$$

So, since all the variables on the right-hand-side of Equation 16 are measurable, the viscosity can easily be determined. Now, when a non-cylindrical impeller is used in the viscometer, there are no tractable equations for the shear rate or shear stress akin to Equation 14 and Equation 15. This presents a challenge since, while the impellers may be good at mixing, there is no simple way of deriving the viscosity of the mixture. The only quantities that can be measured directly are the torque, T, and the angular velocity, ω. In this case, the only way to proceed is to use the impeller design in a range of single and multi-phase fluids of known viscosity, which have been measured with the standard spindle viscometer. Then, the viscosity becomes a function of these two measurable variables

$$\eta = \eta(T, \omega) \qquad \textit{Equation 17}$$

There is no information about the shear rate or the shear stress that can be derived because the complex 3D nature of the flow precludes that. After testing a wide range of fluids of different viscosities, a surface fit could be made and then for a given T and ω, the viscosity of an unknown fluid could be calculated. The situation is further complicated in that the calibration procedure would then have to be done for each class of fluid (Newtonian, shear thinning, shear thickening, etc.) and a judgement would have to be made by the user as to which class of fluid they had in the viscometer

A different approach is that promoted by Brookfield and utilized, for example, in Celauro *et al.*, (2012). Each different spindle geometry provided by Brookfield for use in their viscometers is ascribed a Spindle Multiplier (SMC) value. For example, the SC-27 has an SMC of 25. Further, each viscometer model, here we are using the LVDV-E, has a Torque Constant, *TK*, which allows the apparent viscosity to be found from

$$\eta = \frac{0.1}{N} \cdot TK \cdot SMC \cdot T\% \qquad \textit{Equation } 18$$

where N is the rotational speed (Rpm) and $T\%$ is percentage of the maximum spring torque that the viscometer can deliver. In addition, the Shear Rate Constant (SRC) is defined as

$$\dot{\gamma} = SRC \cdot \dot{N} = SRC \cdot \left(\frac{60}{2\pi}\right)\omega \qquad \textit{Equation 19}$$

Lo Presti *et al.*, (2014) attempted, with some success, to match the behaviour of the DHI to the range of SC-XX spindles offered by Brookfield. The SC-XX range are of the cylindrical type and each has unique SRC and SMC values. The Brookfield viscometer allows only the selection of a spindle code, which has associated SRC and SMC values, thus limiting fine adjustment to a discrete set of values. The authors were nevertheless able to find a spindle code that matched closely the DHI and did this by testing the DHI against a

number of standard liquids of known viscosity. The SC4-28 spindle was found to match the DHI most closely with values of SRC of 0.28 and SMC of 50. The validity of this approach is open to question because of the radically differing spindle geometries of the SC4-28 and DHI. However, for a design such as a DHI, this is a simplification but one which can produce values of apparent viscosity that are of practical use. Nevertheless, further studies are necessary to gain a better understanding of the nature of the convective like flow created by the DHI and to optimise its shape concerning different viscosities range. Results obtained in Lo Presti *et al.*, (2014) showed that an impeller with a dual helical shape could leads to more realistic viscosity measurements of any fluids with suspended particles.

Therefore, the first step aiming to improve the rheometry of heterogenous material was to identify a geometry able to guarantee the stability of the sample. The next section presents a literature review focused on mixing process optimisation and identification of a mixing geometry able to provide sample stability during rotational test.

2.3.2. Literature studies on mixing devices optimisation

A literature study was carried out aimed to identify which type of impeller geometry can promote homogenization within the measuring chamber of a rotational viscometer. The blending of high viscous multiphase fluids, whether it be solid/liquid or liquid/gas or combination thereof, are widely encountered in the production of asphalt blends, coatings, mineral, food, pharmaceutical, polymer, metallurgical, biochemical, and other industrial processes (Paul et al., 2004). Many impellers were proposed by researchers (Figure 2.18), based either on using large impeller diameter or close-clearance designs like anchors and helical ribbons (Havas *et al.*, 1977; Delaplace *et al.*, 2000, 2005; Tsui *et al.*, 2011; Robinson *et al.*, 2012).

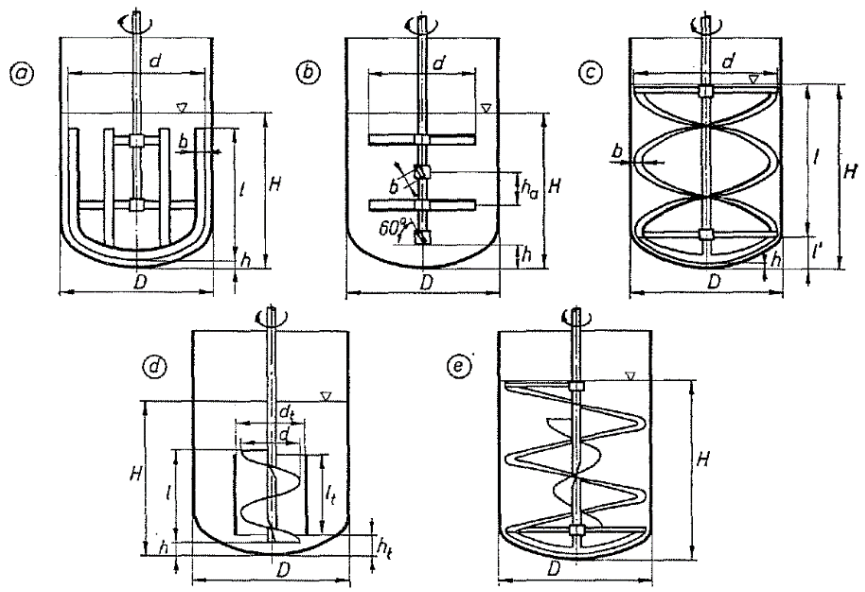

Figure 2.18: The drawings of the most investigated impellers. a) Gate type anchor impeller, b) multi-paddle, c) helical ribbon, d) screw in draught tube, e) combined ribbon screw agitators. Adopted from (Havas et al. 1977)

This operation is generally carried out in stirred vessels and it has been reported that the so-called helical ribbon impellers are most appropriate for efficient mixing of high viscosity Newtonian (Patterson *et al.*, 1979) and non-Newtonian fluids (Yap *et al.*, 1979),(Figure 2.19).

Before the development of numerical simulations, mixers were normally evaluated experimentally using various measures:

- power consumption (Takahashi, Arai, *et al.*, 1982; Takahashi *et al.*, 1984; Tanguy *et al.*, 1992; Cordobes *et al.*, 1998)
- mixing time (Takahashi *et al.*, 1979; Takahashi, Sasaki, *et al.*, 1982),
- circulation time (Delaplace *et al.*, 2000).

Table 2.4 shows a review of the mixing and circulation times obtained from various mixing systems equipped with helical ribbon agitators using different fluids.

Table 2.4 Mixing time and circulation time data found in literature for various helical ribbon agitators. Symbols which appear in this table refer to experimental methods used to obtain these data, adopted from (Delaplace et al., 2000)

Authors	Geometry	d (m)	t/d	w/d	s/d	l/d	H_L/d	K_s	N_r	Kp	Nt_m	Nt_c
Havas et al. (1978)	Ha-1	0.202	1.053	0.105	1.00	1.00	1.22	–	2	330.0	75.0[1a]	–
	Ha-1′	0.376	1.053	0.105	1.00	1.00	1.22	–	2	330.0	75.0[1a]	–
	Ha-2	0.191	1.111	0.108	1.00	1.06	1.29	–	2	247.0	52.0[1a]	–
	Ha-2′	0.356	1.111	0.108	1.00	1.06	1.29	–	2	247.0	52.0[1a]	–
	Ha-3	0.337	1.176	0.104	1.00	1.10	1.36	–	2	205.0	–	–
Takahashi et al.(1982a)	SH1	0.096	1.040	0.104	0.937	0.94	1.04	–	1	–	∞ [4a]	–
Ks parameters are	SH2	0.088	1.138	0.114	1.025	1.02	1.14	–	1	–	∞ [4a]	–
those obtained by	SH3	0.082	1.222	0.122	1.101	1.10	1.22	–	1	–	∞ [4a]	–
Takahashi et al.	DH1	0.096	1.040	0.104	0.937	0.94	1.04	37.9	2	–	239.0[4a]	8.2[i]
(1984). Note that the	DH2	0.089	1.126	0.113	1.015	1.01	1.13	24.7	2	–	53.8[4a]	10.0[i]
dimensions of the	DH3	0.083	1.209	0.121	1.089	1.09	1.21	19.3	2	–	∞ [4a]	11.3[i]
mixing sytems (DH1	DH4	0.090	1.110	0.111	0.665	1.00	1.11	32.7	2	–	56.4[4a]	14.7[i]
to DH7) are slightly	DH5	0.090	1.115	0.111	0.502	1.00	1.11	37.7	2	–	68.5[4a]	15.4[i]
different from those	DH6	0.089	1.126	0.113	1.351	1.01	1.13	28.2	2	–	245[4a]	9.9[i]
of the apparatus used	DH7	0.088	1.136	0.114	2.045	1.02	1.14	24.3	2	–	∞ [4a]	9.6[i]
for the determination	DH8	0.090	1.115	0.084	1.004	1.00	1.11	–	2	–	106.0[4a]	10.5[i]
of Ks parameters, but	DH9	0.090	1.114	0.140	1.003	1.00	1.11	–	2	–	42.3[4a]	7.2[i]
geometrical ratios	DH10	0.090	1.109	0.169	0.999	1.00	1.11	–	2	–	33.0[4a]	5.8[i]
are almost the same	DH11	0.091	1.098	0.220	0.989	0.99	1.10	–	2	–	56.2[4a]	7.6[i]
(see Takahashi et al. (1984))												
Takahashi et al. (1989)	Ta-DH1	0.122	1.049	0.106	0.959	0.94	1.05	37.9	2	351.1	239.0[4a]	8.7[i]
Kp and Ks parameters	Ta-DH2	0.112	1.143	0.117	1.104	1.03	1.14	24.7	2	290.6	53.8[4a]	9.2[i]
are found respectively	Ta-DH3	0.103	1.243	0.127	1.188	1.12	1.24	19.3	2	275.3	∞ [4a]	12.0[i]
in Takahashi et al.	Ta-DH4	0.113	1.133	0.116	0.728	1.02	1.13	32.7	2	356.6	56.4[4a]	12.0[i]
(1982b) and (1984).	Ta-DH5	0.115	1.113	0.114	0.503	1.00	1.11	37.7	2	425.1	68.5[4a]	18.2[i]
Values of Nt_c are	Ta-DH10	0.117	1.094	0.167	1.020	0.98	1.09	31.5	2	339.4	33.0[4a]	9.5[i]
those obtained with	Ta-DH11	0.116	1.103	0.224	1.009	0.99	1.10	30.5	2	372.4	56.2[4a]	8.8[i]
weak pseudoplastic fluids (n = 0.79–0.83 and K = 0.69–1.6 Pa s^n)												
Brito de la Fuente et al.	HR1B	0.185	1.135	0.162	1.000	1.00	1.14	23.0	1	137.1	55[iv]	22.9[iv]
(1990a) and Leuliet	HRS1B	0.185	1.135	0.162	1.00	1.00	1.14	23.0	1	132.5	–	–
et al. (1991) t_{50}	HRS2B	0.185	1.135	0.162	0.50	1.00	1.14	36.7	1	222.7	–	–
HRS refers to Helical	HRS2A	0.1850	1.135	0.108	0.500	1.000	1.14	34.6	1	206.4	–	–
Ribbon + Screw	HRS1A	0.1850	1.135	0.108	1.000	1.000	1.14	22.0	1	131.2	–	–
impellers												
Takahashi et al. (1994)	Ta-D′H10	0.117	1.094	0.167	1.020	0.98	1.09	31.50	2	339.4	38.4[1a]	8.4[i]

Mixing time- [1)]Decolorization by fast chemical reactions (oxydo/reduction or acid/basic neutralization): [1a)]visual observation. [1b)]followed by photoelectric measurements. [1c)]followed by video analysis, [2)]Colour addition/visual observation, [3)]Chemical decolourisation using a dye and decolorizing agent, t_{90}, [4)]Video vizualisation of flow lines of tracer liquids: [4a)]Liquid cristals method: this method is based on the change of colours of liquid crystals depending on their environmental temperature. [4b)]fluorescent markers. [5)]Conductivity method
Circulation time-[i)]Flow visualisation of a suspended particle, [ii)]Conductivity method, [iii)]Calculated from axial velocity measurements, [iv)]Thermal method.

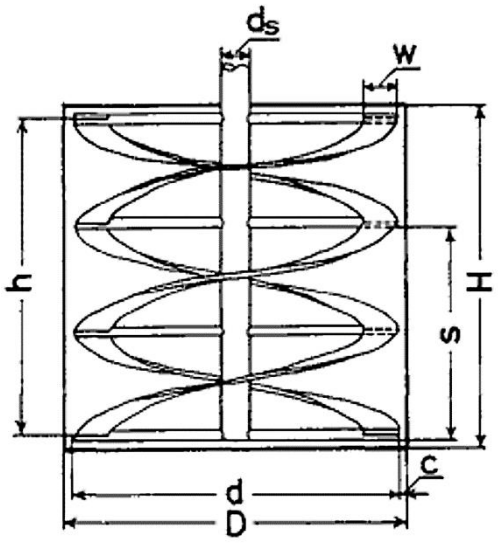

Figure 2.19 Sketch of helical ribbon agitator system, adapted from (Takahashi et al., 1982)

Helical ribbon performances are more suitable to mix highly viscous liquids thanks to two fundamental mechanisms:

1) The amount of shear deformation imparted by the impeller to the fluid, in the gap between the blade and the vessel wall, that causes the mixture to become more homogeneous as the deformation is increased.
2) The axial flow caused by the pumping action of the impeller; this mechanism enables the renewal of the fluid in the gap.

The first mechanism causes the mixture to become more homogeneous as the deformation is increased. The second enables the renewal of the fluid in the impeller-wall gap. If axial convection does not exist or is not enabled to renew the fluid in the gap where high shear rates are produced, there is no fluid exchange between the high shear region (located between the blade and the vessel wall) and the weak shear region (situated inside the inner edge of the blade).

Geometry No.	n_p [—]	n_a [—]	d [mm]	c/D [—]	s/D [—]	L [mm]	w [mm]
SH1	1	3	96.2	0.0190	0.901	315.0	10.0
SH2	1	3	87.9	0.0606	0.901	290.1	10.0
SH3	1	3	81.8	0.0910	0.901	272.0	10.0
DH1	2	3	96.2	0.0191	0.901	315.0	10.0
DH2	2	3	88.8	0.0558	0.901	293.0	10.0
DH3	2	3	82.7	0.0865	0.901	274.7	10.0
DH4	2	4	90.1	0.0496	0.599	434.8	10.0
DH5	2	5	89.7	0.0515	0.450	570.2	10.0
DH6	2	3	88.8	0.0559	1.20	227.7	10.0
DH7	2	3	88.0	0.0598	1.80	165.1	10.0
DH8	2	3	89.7	0.0507	0.901	296.0	7.50
DH9	2	3	89.8	0.0508	0.901	296.0	12.6
DH10	2	3	90.2	0.0489	0.901	297.1	15.2
DH11	2	3	91.1	0.0447	0.901	299.6	20.0

$D=H=100.0$ [mm] $h=90.0$ [mm] $d_s/D=0.10$ [—]

Figure 2.20 Geometrical variables for helical ribbons impellers, adapted from (Takahashi et al., 1982)

This is particularly true in the case of vane and cylindrical spindles for example. Although the amount of deformation produced by those spindles would be of the same order of magnitude as that of a helical ribbon impeller of same diameter, it has been proved that their performances are inferior. This is because the flow produced is only tangential and no pumping action of the fluid is created in the vessel. A interesting study about shape optimisation was carried out by Takahashi *et al.* (1982). The author introduced the use of a double helical ribbon and provided the optimum geometrical variables for the mixing process. Mixing patterns were observed using a tracer liquid containing small capsules of liquid crystal, called the liquid crystal method. The geometrical configuration of the helical ribbon impeller is shown in Figure 2.19 and details of impeller geometries are summarized in Figure 2.20.

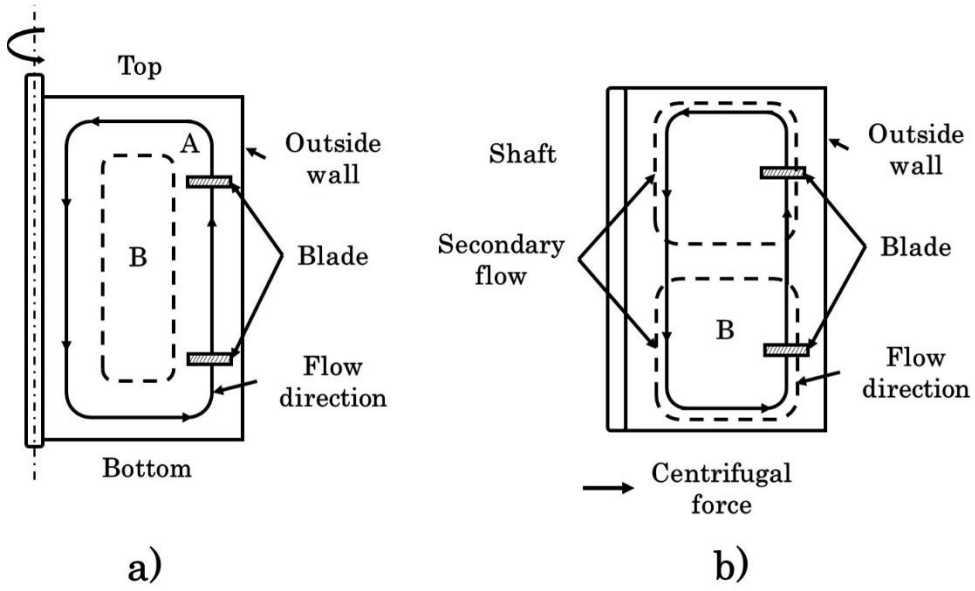

Figure 2.21 Schematics of (a) the illuminated zone and (b) the secondary flow in a Helical Ribbon Impeller (Takahashi, Sasaki, et al., 1982)

Figure 2.22 on the left shows a cross-section view of the primary circulation flow in the illuminated vertical plane. Namely, as observed in Carreau et al., (1976) the shear mixing proceeds mainly in the clearance between blades and vessel wall, and the well-mixed liquid flowing out of the clearance is easily distributed to the circulation path between the blades by the primary flow. This well-mixed zone is denoted by A in Figure 2.22**.** With an impeller of narrowest clearance, an unmixed zone can still be observed in region B. On the other hand, with the impeller of widest clearance, stagnant zones are detected at both top and bottom corners in region A. These phenomena may be explained by the difference in the effect of secondary flow on primary flow. As shown in Figure 2.21 (b), the same kind of secondary flow as observed in Smith (1970) in an anchor agitator, must also be created in a helical ribbon agitator, due to the change of centrifugal force in the axial direction.

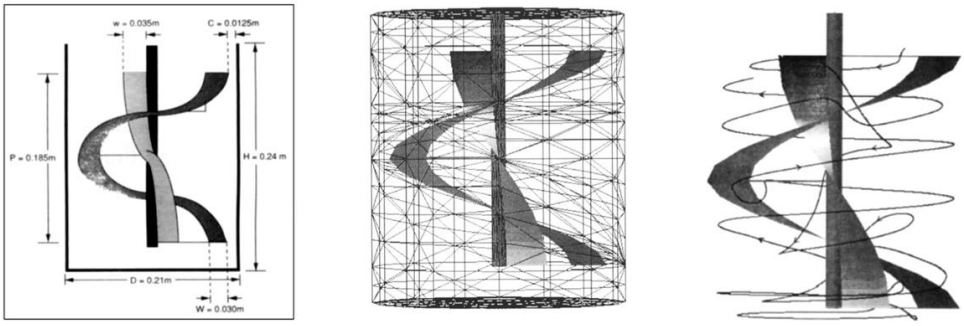

Figure 2.22: Design and the flow pattern of an helical ribbon with screw at 10 Rpm, adopted from (Tanguy et al., 1992)

This secondary flow will deform the primary flow to enhance the exchange flow between regions A and B. On the other hand, the presence of the side wall will depress the secondary flow, an effect that decreases as the clearance becomes wider. With the impeller of narrowest clearance, the flow pattern is not so much affected by the secondary flow and thus the liquid in region A exchanges only gradually with the liquid in region B. With the medium-clearance impeller, moderate deformation of the flow stream in both the top and the bottom regions seems to accelerate the exchange flow between regions A and B. With the impeller of widest clearance, stable secondary flow dominates in the top and bottom corners and closed loops develop.

2.3.3. Numerical modelling of mixing devices designed for heterogenous materials

While experimental studies provide useful, real-world information, they are unable to provide an understanding of the spatial variation of the phases or the nature of the transport processes, making the understanding and hence the efficient optimisation of the mixer designs difficult. Numerical simulations by means of Computational Fluid Dynamics (CFD) offer a greater flexibility in analysing and visualising the mixing.

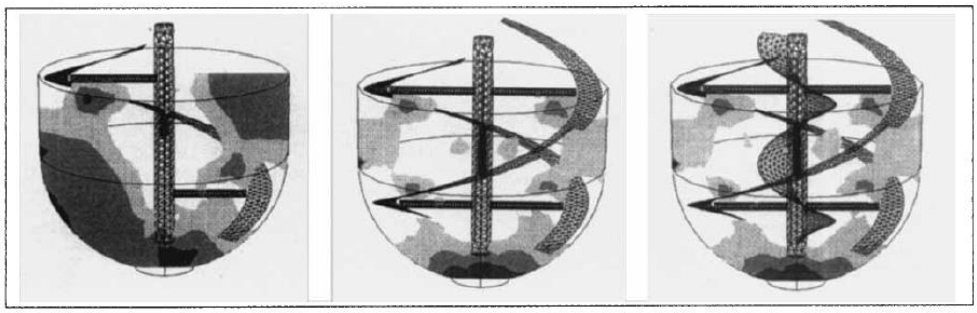

Figure 2.23: The flow pattern of the three helical ribbons analysed in (De La Villéon *et al.*, 1998)

In recent years, the simulation of mixing vessels has been used to optimize mixer geometries and get better insights of the complex flow patterns generated by the impeller-vessel wall interaction (Tsui *et al.*, 2011; Robinson *et al.*, 2012). From the perspective of numerical analysis, one of the pioneering works focused on the mixing performance of helical ribbon impellers in cylindrical vessels is the contribution made by Tanguy *et al.* (1992). He developed a three-dimensional model which was validated experimentally, based on the finite-element method for the analysis of a Helical Ribbon-screw impeller (Figure 2.22). The author reported good liquid circulation at low impeller speeds (10 Rpm) and showed evidence of poor pumping in the vessel bottom. He noticed that the segregation increased upon increasing the impeller speed. De la Villéon *et al.* (1998) following the study of Tanguy compared three helical ribbon impellers with different geometry. Different mixing criteria were used to study the stirring efficiency of three helical ribbon impellers mounted in an industrial batch tank (Figure 2.23). These criteria all led to the same conclusion that, at least for the shear-thinning polymer considered, the double helical ribbon impellers are more efficient and that adding a central screw does not enhance mixing significantly. Results proved that the CFD is a tool able to provide insights into the measuring chamber that otherwise it would be impossible to obtain.

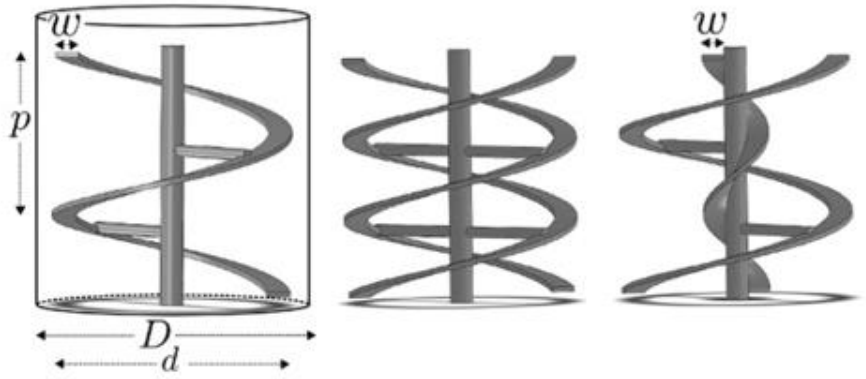

Figure 2.24 : From left to right the single helical ribbon (SHR), the double helical ribbon (DHR.) and the SHR with a central screw (CSR). The SHR also shows the geometry of the outer tank, adopted from (Robinson et al., 2012)

Modelling of the complex flow in the presence of a rotating impeller is a computational challenge because of the complex geometry of rotating impeller and the nature of the flow in stirred tanks. Robinson *et al.* (2012) studied the mixing flow within three variants of the helical ribbon mixers (Figure 2.24), consisting of a single helical ribbon impellor (SHR), a double helical ribbon (DHR) and a single helical ribbon combined with a central screw (CSR). In this study, the effect of impeller design on the mixing in a helical ribbon mixer was investigated. The horizontal bar supporting the ribbon generate strong circumferential mixing, but this is only within a narrow horizontal plane with thickness comparable with the bar diameter. The addition of an extra ribbon, 180 degrees out of phase (DHR) doubles the number of smaller circulation cells while decreasing their efficiency in mixing the fluid between the inner and outer regions of the tank (Figure 2.25). The mixing rate is improved over the other ribbon geometries. The addition of a central screw (CSR) creates a zone of low mixing immediately surrounding the screw. The mixing processes surrounding the helical ribbon are qualitatively identical to the SHR, but the overall mixing rate is slightly increased. Overall, the double helical ribbon recorded the best mixing performance among the three geometries.

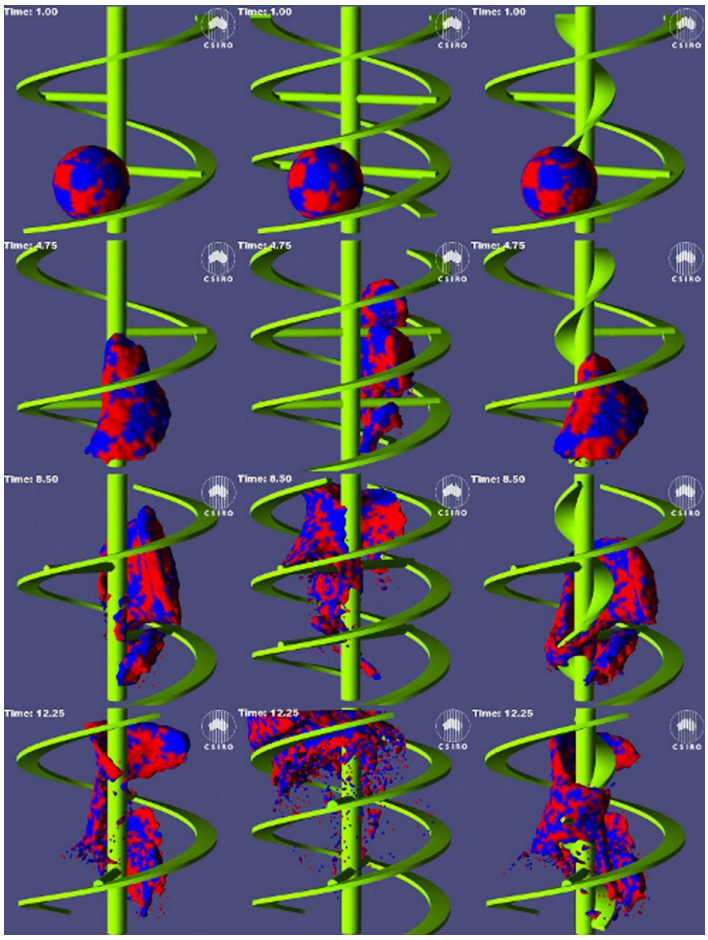

Figure 2.25 Time sequence showing the transport of a sphere of fluid in the SHR (left), the DHR (centre) and the CSR (right).Only the surface of the fluid volume coloured with an arbitrary pattern is shown, adopted from (Robinson et al., 2012)

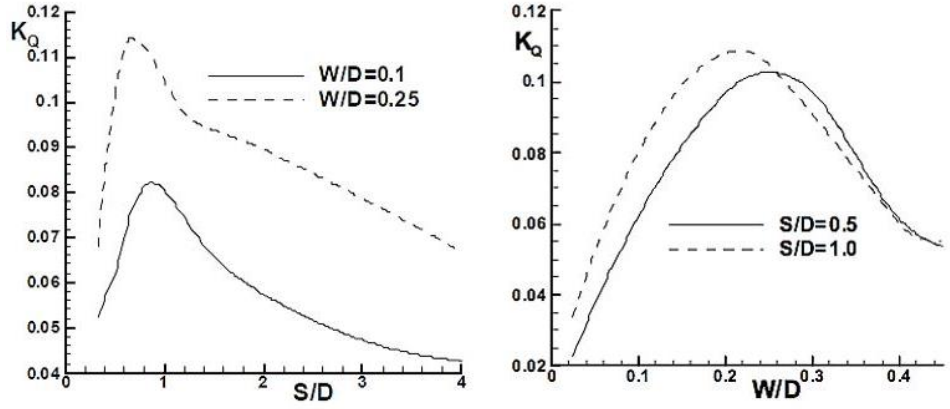

Figure 2.26 Effects of impeller pitch, blade and width on the circulation number Kq, adapted from (Tsui *et al.*, 2011b)

The numerical modelling of mixing in a stirred tank has attracted a great deal of attention and a review of the state-of-the-art in CFD simulations of stirred vessels can be found in Sommerfeld *et al.*(2004).

CFD studies were also carried out to optimize the shape of the helical impeller, finding some critical ratio that must be taken in consideration in the design of a mixer with such configuration. Tsui *et al.* (2011) investigated the flow mixing generated by a single helical ribbon impeller in a highly viscous fluid and provided a range of optimized parameters. He identifies that in the design of a helical mixer impeller the parameters that have to be considered in order to properly project a mixing device are (Figure 2.19):

- The clearance between the vessel wall and the impeller blades, *c*
- The impeller pitch, *S*
- The impeller diameter, *d*
- The blade width, *W*

with D being the diameter of the vessel.

The circulation time t_c is employed as a criterion for evaluation of the mixing performance.

It is the time for a fluid element to complete a vertical circulating loop in the vessel during the mixing process. It is directly related to the pumping capability of the impeller.

The discharge rate of the impeller can be estimated by:

$$Q_d = \frac{v_{tot}}{t_c}, \qquad \textit{Equation 20}$$

where v_{tot} is the total fluid volume of the vessel. A circulation number K_Q can be defined in terms of Q_d as:

$$K_q = \frac{Q_d}{ND^3} \qquad \textit{Equation 21}$$

The influence of the impeller pitch is shown in the Figure 2.27. There is a peak value of K_Q at S/D = 0.9 for the present configuration. The location of peak K_Q is affected by the arrangement of the geometry. For example, when the blade width, W, is enlarged from 0.1D in the benchmark case to 0.25D, the peak location is shifted to S/D = 0.7, as shown in the figure. It can also be seen that the circulation number becomes higher. Therefore, to have a better design the pitch needs to be optimized. For the configurations considered this value falls in the range S = 0.7D to D. The variation of the circulation number (Figure 2.26) reveals that the circulating flow induced by the impeller is strongly affected by width of the blade. For low values the circulation number is extremely sensitive to changes in W, while when the width of the blade becomes greater than 0.26D, the flow rate starts to decline. This is ascribed to the open space in the central region of the vessel being reduced severely and, thus, the returning flow in this open space extends into the channel region.

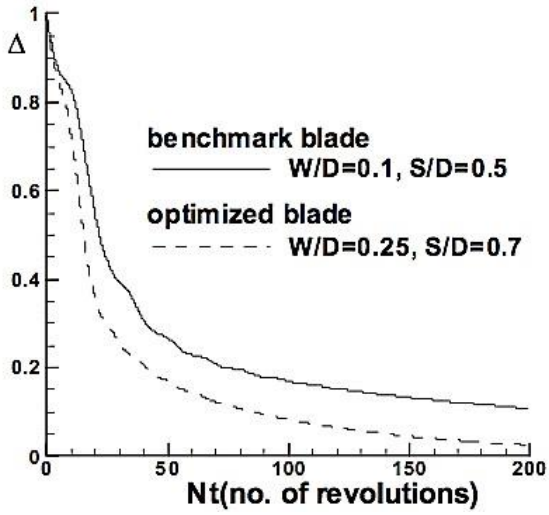

Figure 2.27: The mixing index Δ, adapted from (Tsui *et al.*, 2011b)

In the case studied by Tsui *et al.*(2011), the impeller pitch is set at *S/D* = 0.5. It can be seen in Figure 2.26 that when the pitch is increased to *S/D* = 1, the location of maximum K_Q is decreased to *W/D* = 0.21. A better blade width in the case of a helical ribbon impeller is in the range *W* = 0.2D to 0.26*D*.

Finally, the performances of two blade configurations are compared (Figure 2.27). The first is the benchmark one with pitch S/D = 0.5 and width W/D = 0.1 and the second is an optimized one with S/D = 0.7 and W/D = 0.25. The mixing index Δ stands for deviation of the mixing away from uniform distribution of the two fluids. Its value is 1 initially and becomes 0 when the mixing is complete. It indicates the level of homogeneity within the sample. A high value indicates a poorly mixed system.

$$\Delta = \frac{P_{VOF} - \bar{C}}{\bar{C}} \qquad \textit{Equation 22}$$

here P_{VOF} is the particles volume fraction and $\bar{C}$ the mean concentration.

2.4. Calibration procedure of non-standard impeller

As widely introduced in the previous section, helical ribbon impellers are considered the most efficient geometries to homogenise heterogenous materials. These impellers like others mixing solutions are designed based on empirical or experimental correlations. In industrial applications, one of the most critical parameters during the design stage is the power consumption (Yap *et al.*, 1979; Brito-De La Fuente *et al.*, 1997; Cordobes *et al.*, 1998). When mixing Newtonian fluids several studies (Novak *et al.*, 1969; Rieger *et al.*, 1973) have shown that the correlation between the power consumption and the Reynolds number *Re* in the laminar flow is expressed as:

$$N_p Re = K_p \qquad \textit{Equation 23}$$

where N_P is the power number proportional to power consumption P and K_p is the power constant, related to the impeller geometry. In Newtonian fluids *Re* can be calculated depending on the fluid properties and the rotational speed of the impeller, then N_p can be derived from the power curve (Zhang *et al.*, 2008). However, for non-Newtonian fluids, the viscosity changes with the shear rate. Metzner and Otto (1957) extended this correlation for non-Newtonian fluids, since then their work is considered the classical approach for close-clearance impellers in industrial applications to estimate shear rates when mixing non-Newtonian fluids. They defined the Reynolds number based on an apparent viscosity η.

$$Re_a = \frac{\rho N d^2}{\eta} \qquad \textit{Equation 24}$$

Where the apparent viscosity, η, is linked to an effective shear rate $\dot{\gamma}_{eff}$, that was assumed to be proportional to the rotational speed N as:

$$\dot{\gamma}_{eff} = K_s N \qquad \textit{Equation 25}$$

where the K_s, referred as the Metzner constant, is a function of the geometry and the flow index. For non-Newtonian fluids the apparent viscosity η is written as:

$$\eta = k\dot{\gamma}_{eff}^{n-1} \qquad \textit{Equation 26}$$

where k is the consistency index (a measure of the average viscosity of the fluid) and n is the flow behaviour index, which is an indication of the deviation from Newtonian behaviour. Tanguy *et al.*, (1992) demonstrated a good correlation between the power curve of non-Newtonian fluids using the Metzner-Otto method and that of Newtonian fluids confirming the reasons why this approach is well recognised to design impellers for non-Newtonian fluids.

K_s can be obtained experimentally by using either the Metzner-Otto method or the Rieger-Novak method (Rieger *et al.*, 1973; Thakur *et al.*, 2004). Following the Metzner method values of Re_n and Kp_n can be expressed by:

$$K_{pn} = N_p Re_n = K_p K_s^{n-1} \qquad \textit{Equation 27}$$

where K_{pn}, defined as the power constant for non-Newtonian fluids, is a function of n (Brito-De La Fuente *et al.*, 1997):

$$K_s = \left(\frac{K_{pn}}{K_p}\right)^{\frac{1}{n-1}} \qquad \textit{Equation 28}$$

Another approach is the Rieger-Novak method, where the value of K_s can be calculated from the slope of the following equation:

$$\ln K_{pn} = \ln K_p - (1-n)\ln K_s \qquad \textit{Equation 29}$$

The approaches here introduced are founded on the Metzner and Otto concept and both allow to obtain K_s by measuring the power input of mixing device. The reasons of doing that lays in the fact that these concepts can be translated to any torque measurement device, such as a rotational viscometer.

Although both of the method described are valid, due to its simplicity in this investigation the Metzner and Otto method is used to calibrate the mixing geometry.

2.5. CFD modelling of Heterogenous Materials

Computational fluid dynamics (CFD) has been a powerful tool in modelling heterogeneous flows. Despite the current capabilities of CFD in investigating complex multiphase flows, experimental data are still needed for the development of any numerical or computational model. As frequently noted in the literature, there is a lack of experimental data in many areas about heterogeneous materials, particularly solid-liquid flows. Moreover, such data, when available, tends to be specific and apply only for the conditions under which they were obtained. Numerical modelling and experimental approaches are complementary of each other; since experimental data are indispensable for the development and validation of numerical models while numerical models can provide more comprehensive data than experiments.

The use of CFD in modelling these systems has been notably limited. As noted by Van Wachem *et al.*, (2003), this is due to three factors:

(i) the complexity of the physical phenomenon of the flow, reflected in the wide range of flow types and regimes encountered in such flows.

(ii) the complex mathematical treatment of such flows remains still undeveloped.

(iii) the numerical effort required to solve governing equations is extremely high.

Nevertheless, substantial effort has been directed at the development of CFD models for heterogenous materials, and the application of these models in industry has been growing steadily. In fact, CFD models have reached such complex levels in their treatment that they sometimes outstrip the ability to obtain meaningful data.

Van Wachem *et al.*(2003) presented an overview of the CFD models used for complex flows. The authors derived the governing equations and closure models for multiphase flow and presented and compared different methods and formulations used for modelling such flows. It was concluded that the application of CFD in studying complex flow is promising but nonetheless requires further development.

With the rapid increase of computational power, the particle tracking Eulerian-Lagrangian approach has become feasible. This approach calculates the trajectories of particles in the flow. This method is computationally expensive and valid only for very dilute mixtures, i.e. < ~ 2% v/v (van Wachem *e t al.*, 2003).

Norton *et al.*(2006) conducted a state-of-the-art review of the applications of CFD in the food industry, including food sterilization. A steady increase has been observed in the number of studies relating to CFD applications in the food industry. For example, CFD has helped overcome some of the difficulties in relating heat transfer in food products to sterility and quality levels. CFD can assist the understanding of the physical mechanisms that govern the various properties of food products, including solid-liquid mixtures.

Krampa-Morlu *et al.*(2004) used CFD to predict the flow features of aqueous solid-liquid slurries in turbulent upward pipe flow. Among the investigated features was the velocity profile. Particles had a density of 2650 $kg \cdot m^{-3}$ and diameter of 0.47 or 1.7 mm at concentrations up to 30% v/v.

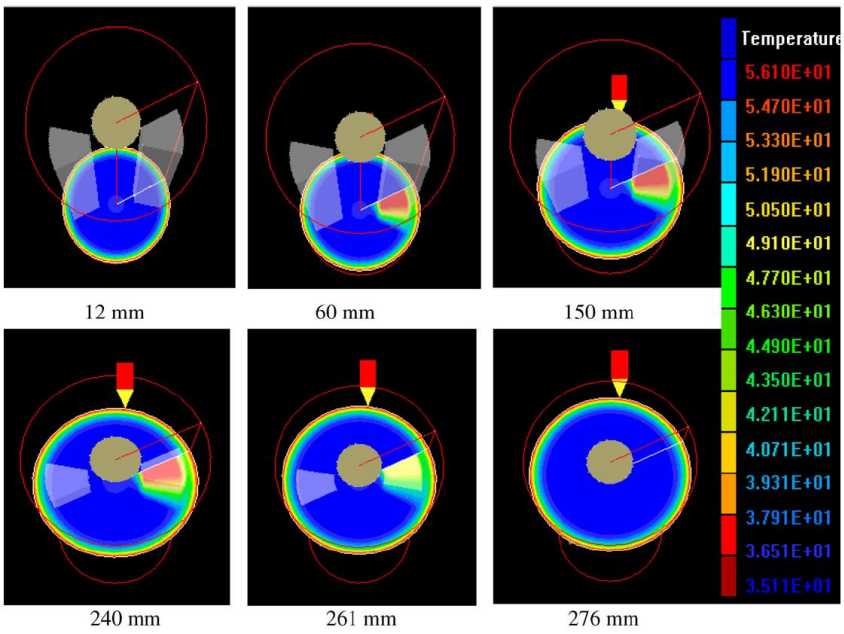

Figure 2.28 Radial–angular temperature profile of, solid-liquid food mixture due to compression to 400 MPa at different heights of, 12, 60, 150, 240, 261 and 276 mm from the bottom, respectively. The red arrow shown in the figure is just for a point in the computation process, adapted from (Abdul Ghani *et al.*, 2007).

The CFD model, formulated using the software CFX 4.4, was tested using the experimental results of Sumner *et al.* (1990). The agreement between CFD and experiment was generally good for the smaller particles but deteriorated for the 1.7 mm diameter particles. The authors concluded that the code failed to accurately predict important features of the flow using the default settings.

An example of the successful application of CFD in modelling solid-liquid food mixtures is the work of Abdul Ghani *et al.*, (2007) who used CFD to predict the temperature distribution and velocity and pressure profiles during high pressure compression of solid-liquid (beef-water) food mixtures within a 38 mm diameter cylinder (Figure 2.28). The CFD model, constructed using the commercial finite-volume code PHOENICS 3.5, was validated using experimental data reported in the literature, and a very close agreement was obtained.

The CFD results showed for the first time the effect of forced convection heat transfer on the temperature distribution of the solid and liquid phases. The temperature distribution at different stages of the high-pressure process was obtained.

Clearly, further work is needed to validate and utilize available CFD models in the study of heterogenous materials and highlight the developments needed for more accurate predictions of their flow behaviour. This, in turn, will result in an increased confidence in the capability of CFD in modelling such complex systems. The next chapter introduces a numerical model aimed to reproduce the findings of a previous experimental campaign where a novel mixing device was developed to reduce the level of heterogeneity of materials during rotational test.

CHAPTER 3. CFD AS A TOOL TO MONITORING AND OPTIMISING THE MIXING PROCESS

3. CFD as a tool to monitoring and optimising the mixing process

As introduced in section 2.4.3 HBBs are complex systems, where the neat bitumen is the fluid matrix, and the rubber particles are the swollen tyre rubber crumbs. These two components have a difference in densities and during rotational viscosity testing a number of changes (e.g. phase separation, agglomeration and sedimentation) may occur in the measuring chamber leading to unrealistic result.

An attempt to solve these issues was carried out in a previous investigation by Lo Presti *et al.* (2014) where experimental studies were carried out to design and calibrate a novel device, the dual helical impeller (DHI) (Figure 3.1). The novel impeller was specifically developed to solve these types of issues within low-shear development of CR-MB. Although the experimental campaign provided encouraging results, the mechanisms behind the enhanced mixing efficiency provided by the DHI and the actual level of enhancement were not clear.

This chapter presents a combined experimental-numerical investigation aimed to shed lights within the testing sample and to reproduce the observations obtained from the previous laboratory campaign by means of numerical modelling.

3.1. Experimental programme

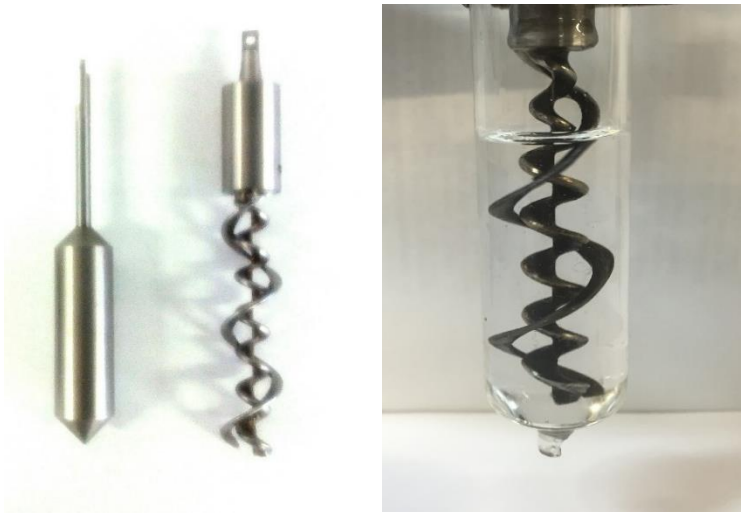

Figure 3.1 The standard spindle SC-27 (on the left), the dual helical impeller (on the centre) and the glass tube realised to allow the visualisation of the particles (on the right)

The experimental programme used multi-phase systems made-up of a range of silicone viscosity standard fluids (Figure 3.2) and tyre rubber particles. These fluids, provided by Brookfield, thanks to their known properties (e.g. viscosity, density etc.) are commonly used to verify the calibration of laboratory viscometers and are less temperature sensitive than mineral oils. Also, they are Newtonian fluids which are accurate to ±1% of viscosity value. Therefore, nine different materials were produced from the combination of different viscosity standard fluids and different particles diameter (Table 3.1). All fluids being tested at 10, 100 and 200 Rpm at ambient temperature (20 °C). The range of viscosity and particle diameters have been chosen in order to reproduce systems similar in terms of viscosity and physical composition to tyre rubber-bitumen blends at temperatures between 100 and 200°C. This is considered to be representative of the possible scenarios occurring during the low shear modification of bitumen with CRM (Lo Presti *et al.*, 2013).

Figure 3.2 The Brookfield silicone viscosity standard fluids, adopted from (Brookfield, 2018)

Table 3.1 Fluids and particle properties

	Fluid		Particles	
Name	Density (kg m^{-3})	Viscosity (Pa·S)	Diameter (μm)	Volume fraction
f100	960	0.1	400	5%
f500	970	0.5		

Furthermore, the rotational viscometer was customised with a glass outer cylinder, realised at the University of Nottingham, allowing the visualisation of the movement of particles in the system, (e.g. Figure 3.1). Due to the expected high torque, which would be close to the viscometer's limits, the tests with the high viscosity fluid (f500) were performed up to 100 Rpm to avoid damaging the equipment. Tests were conducted according to Subhy *et al.* (2015), which are based on international standards on viscosity measurements of a CR-MB (asphalt rubber) (ASTM a. D4402/D4402M and ASTM b. D7741/D7741M). These were undertaken for a duration of about 10 minutes, depending on how quickly the mixing was seen to reach a steady distribution. The rubber particles were added to the fluid and the blend was shaken to produce an even distribution of the particles. In these conditions, the impellers were quickly submerged in the blend and the viscometer was turned on to carry out the test, during which torque and angular velocity were measured and the viscosity calculated from Equation 19. Results were compared against those obtained with a standard spindle, SC-27 (Figure 3.1), to asses which device produced the highest degree of homogenisation and hence the more realistic, repeatable and reliable viscosity measurements.

3.2. Numerical techniques to model and optimise the mixing process of heterogeneous materials

In parallel with these experiments, a CFD analysis was carried out with the aim of qualitatively comparing the experimental and numerical results.

The CFD model helped to reproduce the laboratory scenario and to support the experimental observations.

Version 17 of Ansys Fluent, the commercially available CFD software, was used in this work (Ansys Inc., 2017). The software allows to solve a wide range of fluid flow problems. It includes several mathematical models for transport phenomena such as heat transfer and chemical reactions and is capable of modelling complex geometries. The computational fluid dynamics software permits to simulate applications such as laminar non-Newtonian flows in process equipment; conjugate heat transfer in turbomachinery and automotive engine components; pulverized coal combustion in utility boilers; external aerodynamics; flow through compressors, pumps, and fans; and multiphase flows in bubble columns and fluidized beds (Ansys Inc., 2017), to name but a few.

During the set-up of a numerical model, the main stages to define are:

- CAD creation
- Meshing
- Selection of a physical model
    - Viscous model
    - Multiphase model
- Materials
- Boundary conditions
- Solution

3.2.1. CAD creation and meshing

The DHI geometry was designed to create a convective like flow within the sample, which allows the uniform distribution of suspended solids within a viscous fluid. The idea is that the outer helix pumps the fluid downwards while the inner helix pumps it upwards. Based on the prototype design, Ansys-DesignModeler and Ansys-Meshing software were used to produce a CAD model of the DHI and then a mesh, which contained approximately 1.300.000 tetrahedral and triangular prism cells (Figure 3.3). The CAD model and associated surface mesh can be seen in Figure 3.4.

Sizing	
Use Advanced Size Function	On Curvature
Relevance Center	Medium
Smoothing	Medium
Transition	Slow
Span Angle Center	Fine
Curvature Normal Angle	24°
Min Size	1,48e-002 mm
Max Face Size	1,48 mm
Max Size	2,96 mm
Growth Rate	1.2

Inflation	
Use Inflaction	All Faces in a Name Selection
Named Selection	Wall-Outer
Inflation Option	Smooth Transition
Transition Ratio	0.272
Maximum Layers	5
Growth Rate	1.2

Statistics	
Nodes	241088
Elements	1285987

Figure 3.3 DHI mesh details

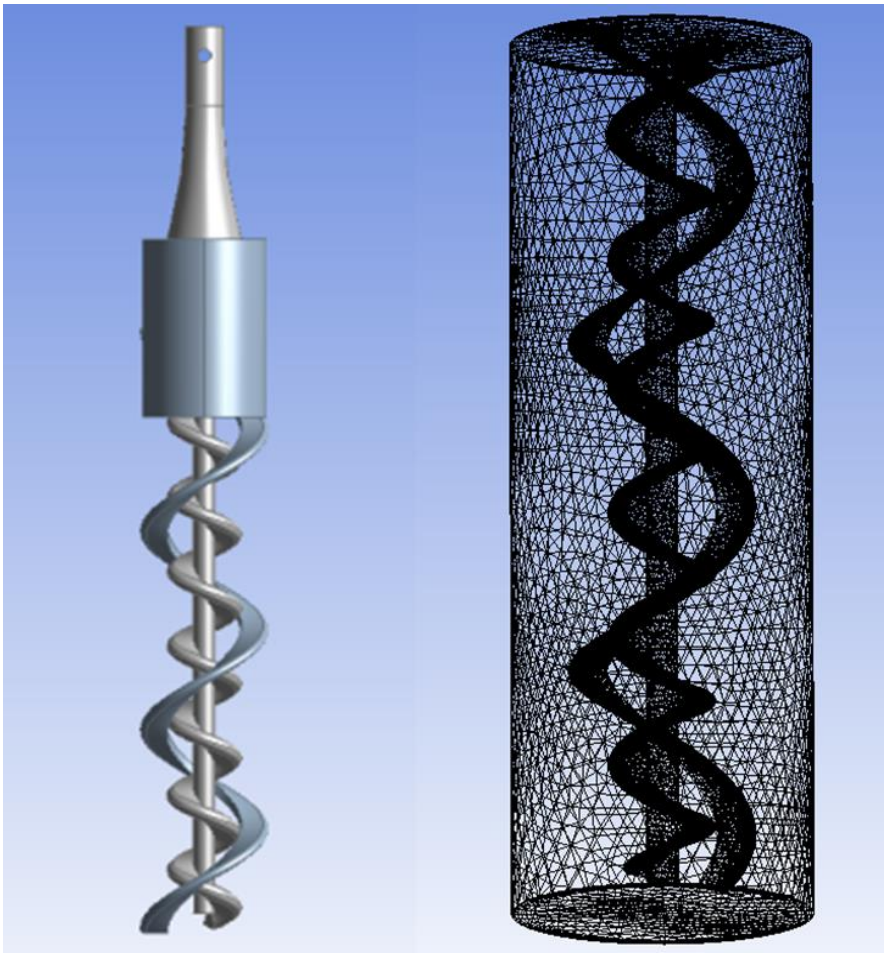

Figure 3.4 on the left, a solid model of the DHI mixer; and on the right, the surface mesh on the mixer and outer wall.

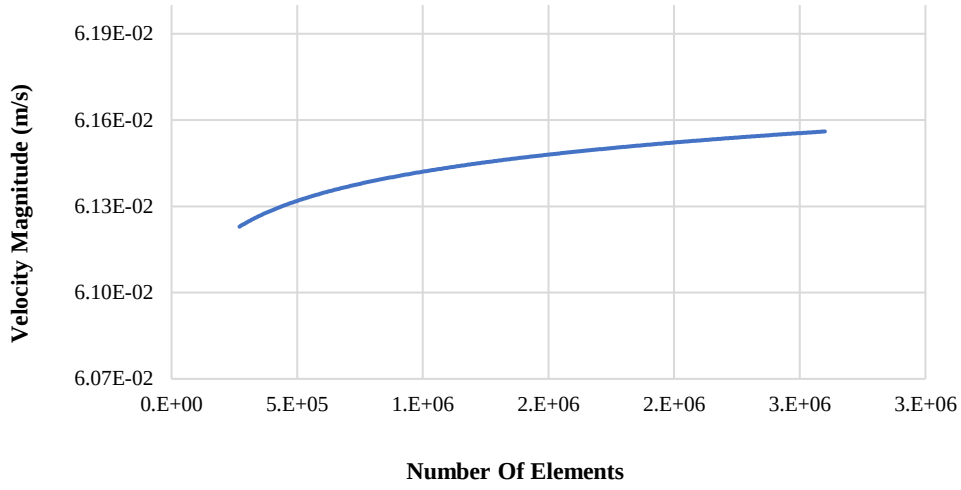

Figure 3.5 The DHI mesh sensitive analysis

To account for the high gradients in the flow variables, which usually exist near the container wall due to the no-slip condition, inflation layers near the wall were created. Using the inflation layers results in a more accurate prediction of the flow variables in this region.

To find the right compromise between computational effort and model accuracy a mesh-independence study was carried out for the DHI (Figure 3.5); this was done by performing a number of simulations with different mesh sizes, starting from a coarse mesh and refining it until results were no more dependent on the mesh size. The procedure used is the following: models of same geometry with different mesh elements are created and CFD analyses are conducted on them using same conditions until the solution converges. The analysis was carried out with a number of elements between 100,000 to 2,000,000. Analysis of the velocity field showed that the mesh with about 1.300.000 elements was sufficient for this analysis, since the meshes with more elements lead to a very similar result with the accompanying increased computational effort.

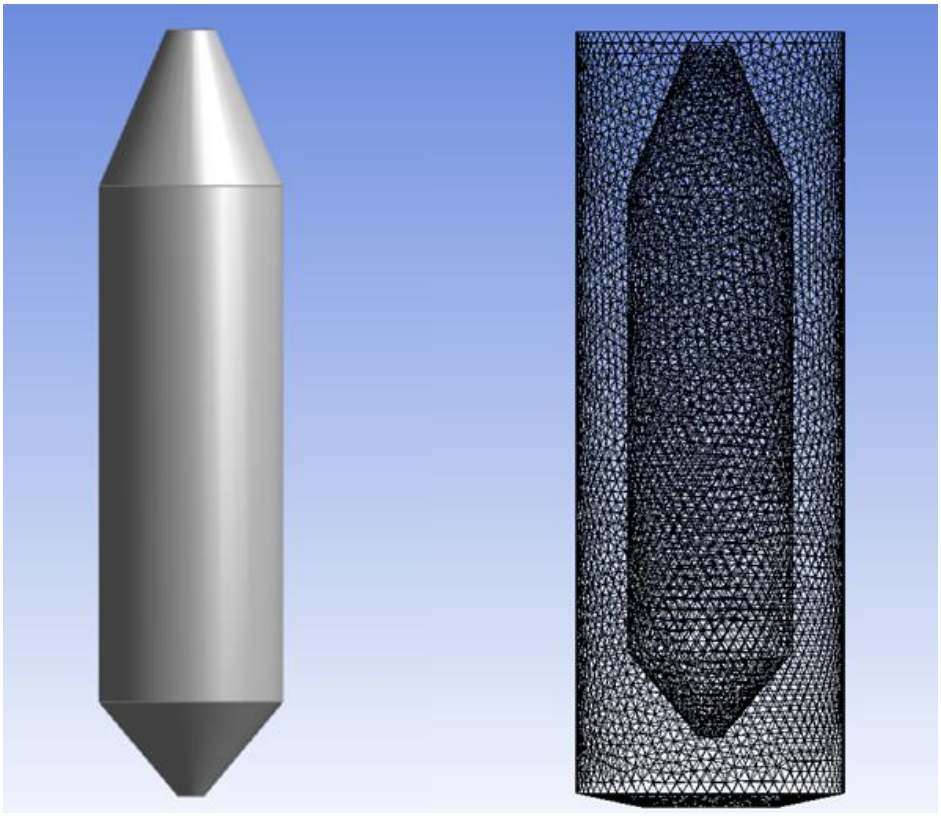

Figure 3.6 on the left, a solid model of the Brookfield SC-27 spindle; and on the right, the surface mesh of the spindle and outer wall.

Sizing	
Use Advanced Size Function	On Curvature
Relevance Center	Fine
Smoothing	Medium
Transition	Slow
Span Angle Center	Fine
Curvature Normal Angle	15°
Min Size	8,94,e-003 mm
Max Face Size	0,89 mm
Max Size	1,78 mm
Growth Rate	1.2
Inflation	
Use Inflaction	All Faces in a Name Selection
Named Selection	Wall-Outer
Inflation Option	Smooth Transition
Transition Ratio	0.272
Maximum Layers	5
Growth Rate	1.2
Statistics	
Nodes	46467
Elements	155035

Figure 3.7 The details of the mesh performed on the SC-27 spindle

A similar process was used to produce a mesh consisting of 155.000 tetrahedral and triangular prisms (in the inflation layers adjacent to walls) for the SC-27 spindle, (Figure 3.6 and Figure 3.7). However, in this case due to the simplistic geometry a mesh sensitive analysis was not necessary.

For both the geometries, a moving mesh approach was used, where the entire fluid domain was rotated about the vertical z-axis at the appropriate angular velocity, while the outer wall was held stationary relative to this zone. The reason for doing this, rather than simply moving the outer wall relative to a stationary fluid domain was so that animations, especially in the cases of the

DHI and after the DHR, could be produced with the helices being seen in motion. There was no computational overhead associated with the approach used.

3.2.2. Materials

Once the geometries were modelled and meshed the next step was to define the materials. The software itself provides a database of materials, in alternative is possible to create the ones that are not present in the software by defining density and viscosity.

Several options for the definition of the fluid viscosity are provided:

- constant viscosity
- temperature-dependent and/or composition-dependent viscosity
- kinetic theory
- non-Newtonian viscosity
- user-defined function

For the case shown in this chapter, considering the Newtonian nature of the fluids, both density and viscosity were constant. Therefore, visco-standard fluids were created based on the known properties listed in Table 3.1.

3.2.3. Viscous model

Fluent offers several accurate viscous models with a wide range of applicability, such as:

- Inviscid
- Laminar
- Spalart-Allmaras
- K-epsilon

- K-omega
- Reynolds stress
- Large eddy simulations

It is accepted practice in stirred or mixing vessels to use the mixing Reynolds number, Re_m to characterise the flow

$$Re_m = \frac{\rho D^2 N}{\mu} \qquad \textit{Equation 30}$$

where D is the diameter of the impeller and N is the number of revolutions per second. For $Re_m > 10000$, the flow is assumed to be fully turbulent. In the present study, with the least viscous fluid and the highest impeller speed, the mixing Reynolds number is approximately 100, which indicates all simulations are laminar, therefore the laminar model was selected.

3.2.4. Multiphases model

A further step in the CFD setup was to define the proper multiphase model able to reproduce with good accuracy the experimental tests. Several models are dedicated to simulating multiphase flows. These can be used to investigate gas-liquid, gas-solid, liquid-solid, and gas-liquid-solid flows.

For these types of problems, the software offers a wide range of model such as:

- Volume-of-fluid (VOF),
- Eulerian models,
- The discrete phase model (DPM),
- Mixture model.

Fallowing, a brief description of each model is introduced:

(i) The VOF Model

The VOF model is used in Ansys Fluent to a fixed Eulerian mesh and it consists in a surface-tracking technique. It is intended for fluids that cannot be mixed where the position of the boundary between the investigated fluids is of interest. Most common applications of the VOF model include stratified flows, free-surface flows, filling, sloshing, the motion of large bubbles in a liquid and the steady or transient tracking of any liquid-gas interface (Ansys Inc., 2017).

(ii) The Eulerian Model

The Eulerian model involves the solution of momentum and continuity equations for each phase. Coupling is accomplished by using the pressure and interphase exchange coefficients. For the above-mentioned reasons it is considered the most complex multiphase models in Ansys Fluent. Applications includes bubble columns, risers, particle suspension, and fluidized beds (Ansys Inc., 2017).

(iii) The Euler-Lagrange Approach

The fluid phase in this model is solved by calculating the Navier-Stokes equations. Instead the solution of the dispersed phase is achieved by tracking the particles.

The model well suits when particle-particle interactions can be ignored but also for low volume fraction. Common applications are spray dryers, coal and liquid fuel combustion but the model is unsuitable for applications where the volume fraction of the second phase cannot be ignored (Ansys Inc., 2017).

(iv) The Mixture Model

The mixture model is used for multiphases flow, either fluid or particulate. The different phases are considered as interpenetrating continua. It involves the solution of the mixture moment equation and specifies the relative velocities aimed to define the dispersed phases. Commonly used applications

with the mixture model comprise bubbly flows, sedimentation, and cyclone separators (Ansys Inc., 2017).

In this thesis, the mixture model has been selected to model the behaviour of HBBs that are described as mixtures in which two or more phases coexist together but also affected by sedimentation issues. It also provides a good compromise between simulations accuracy and computational effort. Indeed, it is a simplified multiphase model, a good substitute for the Eulerian multiphase model in several cases. A Eulerian multiphase model may not be feasible when there is a wide distribution of the particulate phase or when the interphase laws are unknown, or their reliability can be questioned (Ansys Inc., 2017).

In order to reduce the computational effort, the secondary phase (particles) was simulated in terms of volume fraction. When suspensions were added, particles were modelled by defining the diameter (400 µm) chosen to be representative of the particles size distribution of an HBB and the concentration (5%) in the Mixture model in Fluent. Thus, Newtonian behaviour is applied to the continuous phase (visco-standard fluid), and then rubber particles were added to simulate their motion within continuous phase.

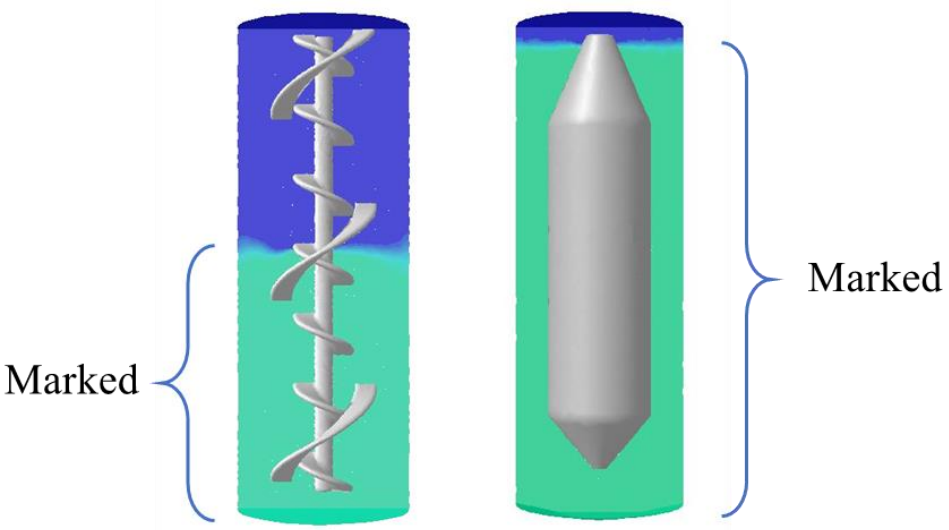

Figure 3.8 The mark command used in Fluent to highlight the different regions

Furthermore, to allow a better visualization of the mixing process within the measuring chamber the command Mark was enabled. Indeed, this command allows marking or refining cells inside the vessel based on the region defined and the in/out option. This command allowed to set the starting particles distribution within the testing sample (e.g. Figure 3.8). Then rotational speed was varied from 10 to 200 Rpm.

3.2.5. Boundary conditions and solution method

Every numerical model requires to define the boundary conditions that are a set of constraints to boundary value problem. For both the geometries, no slip wall boundary conditions were applied to the inner, outer, and bottom walls. The upper boundary was set as a symmetry plane as the shear between air and bitumen is insignificant. Standard solver settings were used throughout – for example, the SIMPLE algorithm was used for pressure velocity coupling. Least Squares Cell Based discretization for gradients and second-order schemes were used for the momentum and volume fraction equations.

Due to the use of a moving mesh, the solution was necessarily transient, and it was found that the simulations had to be run for up to 10 minutes of real time to achieve a stationary solution, where the mean velocity and volume fraction did not drift with time, as measured at a number of monitoring points. To simulate the movement of the DHI with accuracy, a maximum angular change of 2° was allowed per time-step. For example, at 100 Rpm this means 1 revolution every 0.6 seconds, 1 revolution is 360°, therefore the DHR needs 180-time steps per revolution to complete a revolution so it needs a time step of 0.6/180 = 0.00333 s.

3.2.6. Governing equations

The modelling involves the solution of the Navier-Stokes equations, which are based on the assumptions of conservation of mass and momentum within a moving fluid. In order to simulate the behaviour of the two-phase fluids in the present application, the mixture model was used. Here, the momentum and continuity equations are solved for the mixture, the volume fraction equations for the secondary phases, while algebraic expressions are used for the relative velocities and inter-phase drag. The mixture model lends itself to particle-laden flows with relatively low volume loading, which is the situation in the present work. First, the mixture continuity equation

$$\frac{\partial \rho_m}{\partial t} + \nabla \cdot (\rho_m \boldsymbol{u}_m) = 0 \qquad \textit{Equation 31}$$

where $\mathbf{u}_m$ is the velocity, $\boldsymbol{\rho}$ is the density and the subscript $_m$ indicates a quantity defined for the mixture. For example, the mixture velocity, $\mathbf{u}_m$ is a mass-weighted average of the *n* phases

$$\boldsymbol{u}_m = \frac{1}{\rho_m} \sum_{k=1}^{n} \alpha_k \rho_k \boldsymbol{u}_k \qquad \textit{Equation 32}$$

where α_k is the volume fraction and k refers to the k^{th} phase. The mixture density is

$$\rho_m = \sum_{k=1}^{n} \alpha_k \rho_k \qquad \textit{Equation 33}$$

The momentum equation is

$$\frac{\partial}{\partial t}(\rho_m \boldsymbol{u}_m) + \nabla(\rho_m \boldsymbol{u}_m \boldsymbol{u}_m) = \nabla p + \nabla[\mu_m(\nabla \boldsymbol{u}_m + \nabla \boldsymbol{u}_m^T)] + \rho_m \boldsymbol{g} + \nabla\left(\sum_{k=2}^{n} \alpha_k \rho_k \boldsymbol{u}_{dr,k} \boldsymbol{u}_{dr,k}\right) \qquad \textit{Equation 34}$$

where **g** is the gravitational acceleration and $\mathbf{u}_{dr,k}$ is the drift velocity for the secondary phase *k*,

$$\boldsymbol{u}_{dr,k} = \boldsymbol{u}_k - \boldsymbol{u}_m \qquad \textit{Equation 35}$$

The mixture model in Ansys Fluent uses an algebraic slip formulation, which is based on the work of Manninen et al. (1996). It uses the slip velocity, which is related on the drift velocity defined in Equation 34. The velocity of the k^{th} phase is calculated from algebraic expressions, rather than a separate momentum equation. So, the final term on the right-hand side of Equation 33 imparts a momentum source or sink to the mixture momentum equation, based on the relative motion of the primary and secondary phases.

3.3. Results

3.3.1. Experimental

In the manufacturing of rubberized bitumen, the process can take up to 2 h (Subhy *et al.*, 2015), at which point the particles have swollen to their maximum extent. However, in these experiments, in certain cases (i.e. for the f100 fluid with 400 μm particles) the particles were already settling after a few seconds.

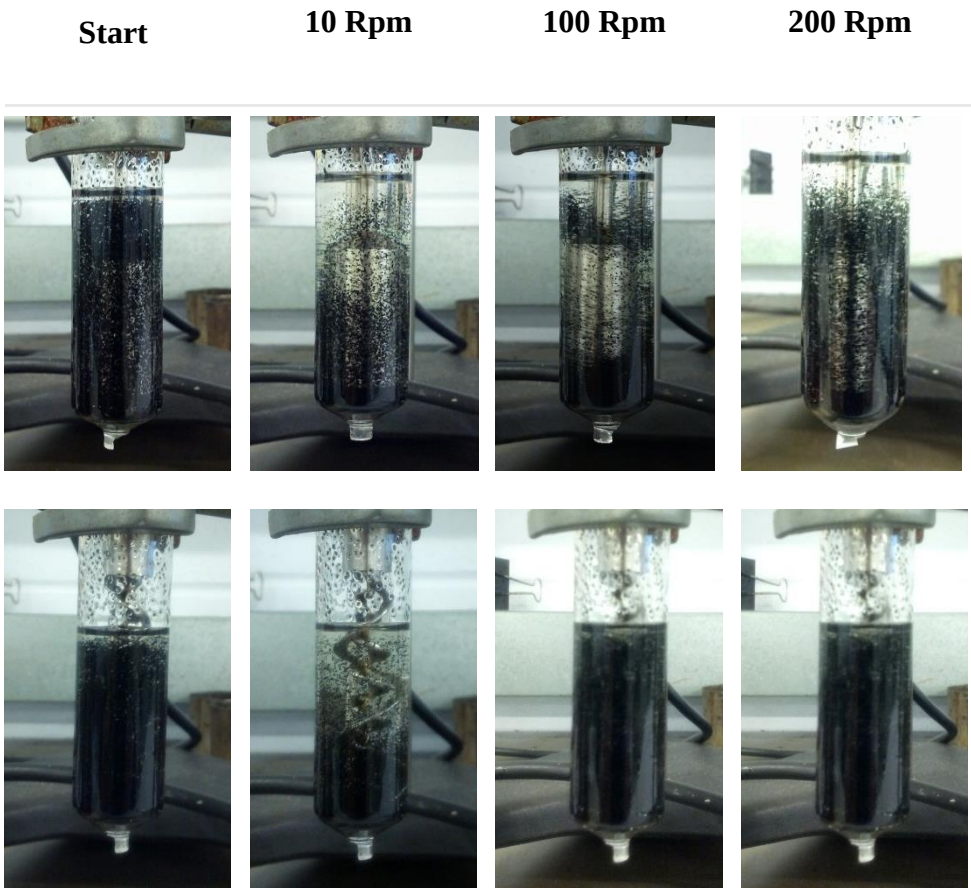

Figure 3.9 Images of the distribution of particles in the viscometer using the f100 fluid + 400 µm tyre rubber particles for the SC-27 spindle (top) and DHI (bottom) at the start of the test and after 10minutes for various rotational speeds.

It was decided that a testing period of 10 minutes was sufficient to resolve the settling process without the swelling of the particles compromising the results. Results presented in this section show the cases for the fluid f100 and f500 with 400µm tyre rubber particles. Figure 3.9 and Figure 3.10 show images of the particles distribution within the blend at the start of the tests and after 10 minutes of rotation for the f100 and f500 fluids respectively. These figures show that using the lower viscosity fluid, f100, at 10 Rpm both standard spindle and the DHI do not maintain particles in suspension.

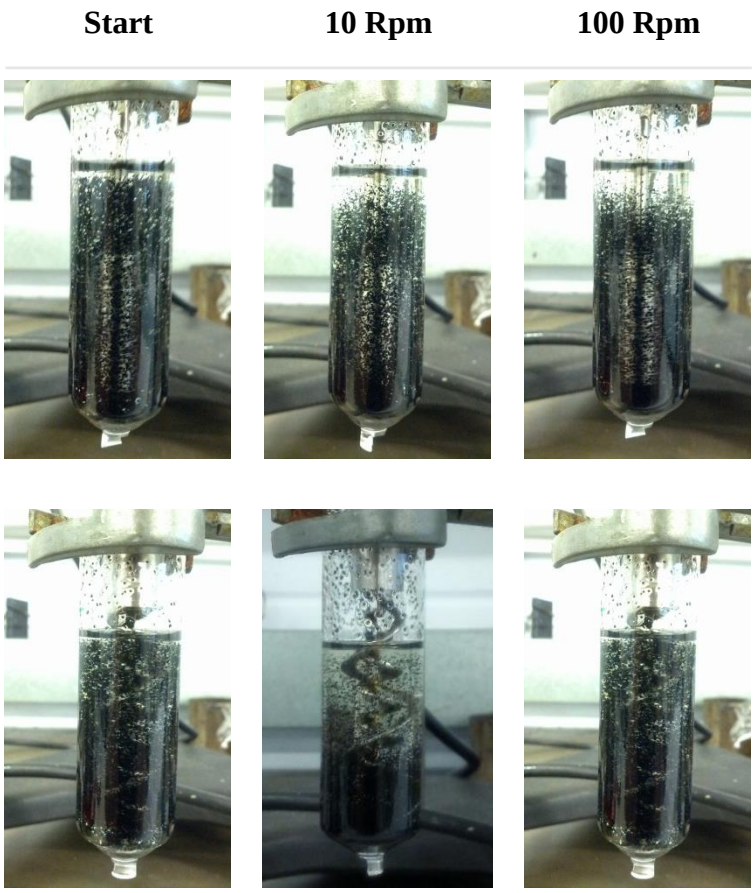

Figure 3.10 Images of the distribution of particles in the viscometer using the f500 fluid + 400 µm tyre rubber particles for the SC-27 spindle (top) and DHI (bottom) at the start of the test and after 10minutes for various rotational speeds.

At 100 and 200 Rpm it is interesting to note how, due to its shape, the standard impeller creates two layers of crumb rubber particles on top and bottom. In this case, the particles are forced to migrate from the narrow gap into regions where the swirl is less intense. However, at these higher rotation rates, the DHI creates a more even distribution of particles. Observations confirmed that this was a result of a combination of effects consisting in the inner spiral transporting the particles upwards while the outer thread moves the particles back down – confirming that the design was working as intended. As a result, particles are circulated throughout the container and phase separation is avoided for the whole duration of the experiment.

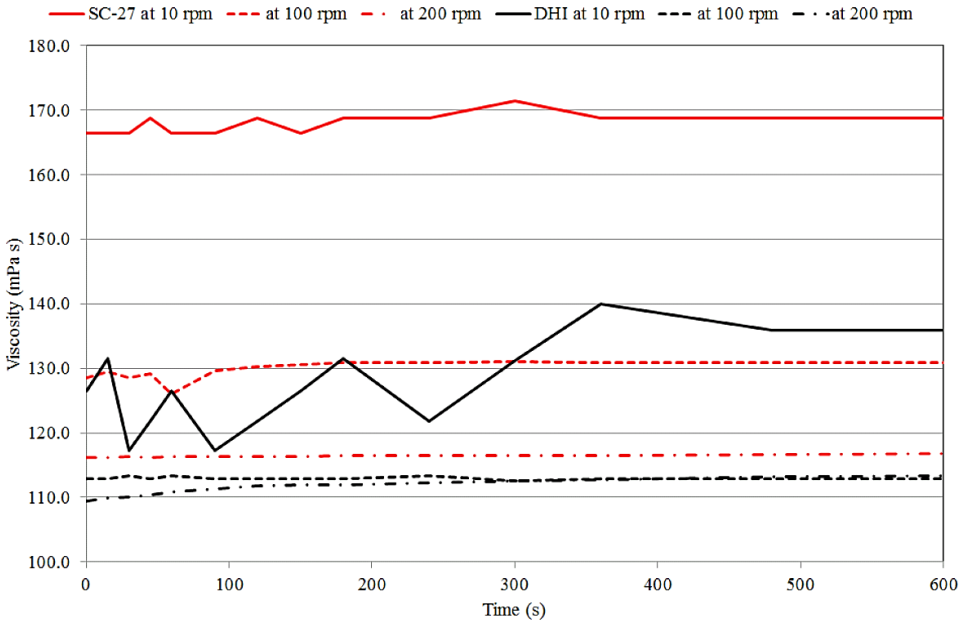

Figure 3.11 Apparent viscosity measurements over time of f100 fluid by using the SC-27 spindle and DHI at 10, 100 and 200 Rpm.

These results show that the rotational speed is of fundamental importance when considering the extent to which the sample is homogenised and plays a crucial role in determining the efficacy of the impeller. This, of course, has significant consequences on the viscosity readings, which are a function of testing geometry, rotational speed and applied torque.

Figure 3.11 shows that the apparent viscosity measurements are independent of the rotational speed for the DHI than the SC4-27 spindle (apart from at 10 Rpm). The fact that the curves for 100 and 200 Rpm are convergent for the DHI echoes the observations made about Figure 3.9, where the higher rotational speeds produce a less heterogeneous blend. At 10 Rpm, there is clearly some intermittency to the viscosity measurements as the particles do not reach a steady-state distribution. In any case, both viscosity values over time and shear dependency, play in favour of the DHI, which seems to provide more stable rheological information of this complex system.

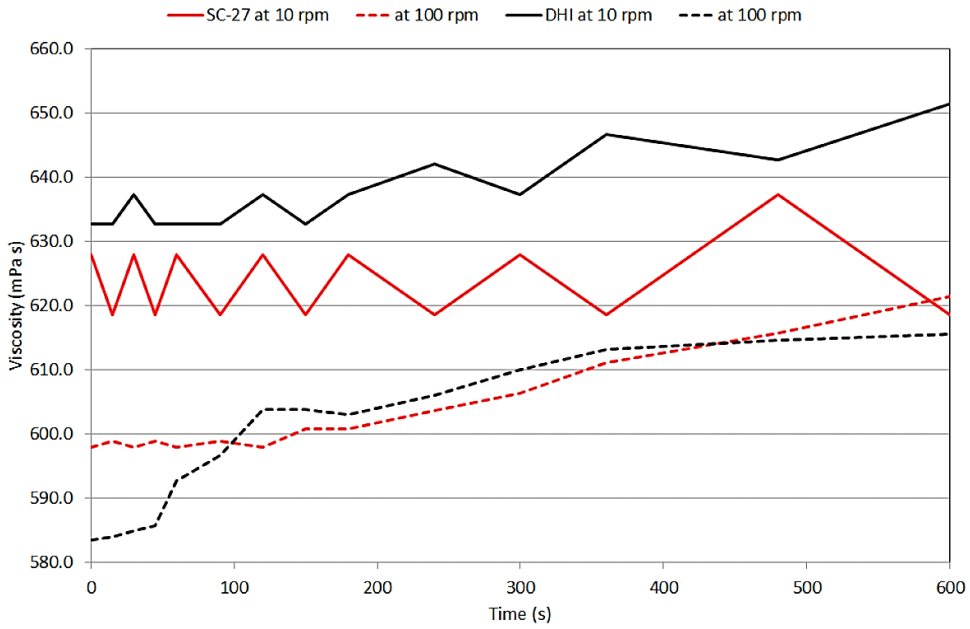

Figure 3.12 Apparent viscosity measurements over time of f500 fluid by using the SC-27 spindle and DHI at 10, nd 100 Rpm.

That is an indication of the better mixing efficiency over the timescale of the test. For the higher viscosity fluid, f500, over the same timescale, these observations are not so clear (Figure 3.12). In this test, all viscosity measurements are still increasing after 600s, suggesting that the particles were still undergoing redistribution or possibly the swelling process is starting, especially at the higher rotational speed. Indeed, the absence of a 200 Rpm result prevents the same conclusion being drawn for convergence of the viscosity results as the rotation speed is increased above 100 Rpm. After 20 minutes (1200s) the viscosity had still not settled down to a consistent value. Unfortunately, running the tests for a longer period meant that the temperature of the mixture would begin to drop, and viscosity measurements would then have a temperature component. Again, however, the viscosity trend with time still favours the DHI.

3.3.2. CFD simulations

Validation (Single Phase)

In an attempt to reproduce the single-phase experimental testing of a previous experimental campaign (Lo Presti *et al.*, 2014), a number of single phase simulations were performed. The rotational speed of the impeller was again varied as too was the viscosity of the fluid. Values of both the rotational speed and dynamic viscosity were matched to those used by (Lo Presti *et al.*, 2014) as closely as possible. The dynamic viscosity values used were 0.0094, 0.098, 0.488, 0.970 and 5.040 Pa·s, while rotational speeds of 10, 50, 100 and 200 Rpm were chosen. Thus, in total, 20 simulations were performed. In order to be able to compare across this range of viscosity and rotational speed, the mixing Reynolds number, Equation 30, was used with an equivalent diameter of 11.7 mm. The choice of the diameter is somewhat arbitrary and corresponds in this case to the diameter of the SC4-27 spindle, although it is a value roughly halfway between the inner and outer helices of the DHI. The SMC values are calculated from a re-arrangement of Equation 18, via a conversion of the torque that Fluent reported to an equivalent percentage torque, *T%*, reported by the Brookfield viscometer.

Figure 3.13 shows a clustering of the SMC values around a value of 50, across a 5-decade range of Reynolds numbers. Note that the value of SMC found for the DHI in the previous investigation was 50 and so there is quantitative agreement between the experiment and simulations. What the numerical modelling reveals, however, is that at a fixed rotational speed, there is a dependency on the Reynolds number, the extent of which is reduced at the highest rotational speed of 200 Rpm. Similarly, we see that for a fixed value of viscosity there is a marked increase in SMC as the rotational speed is increased.

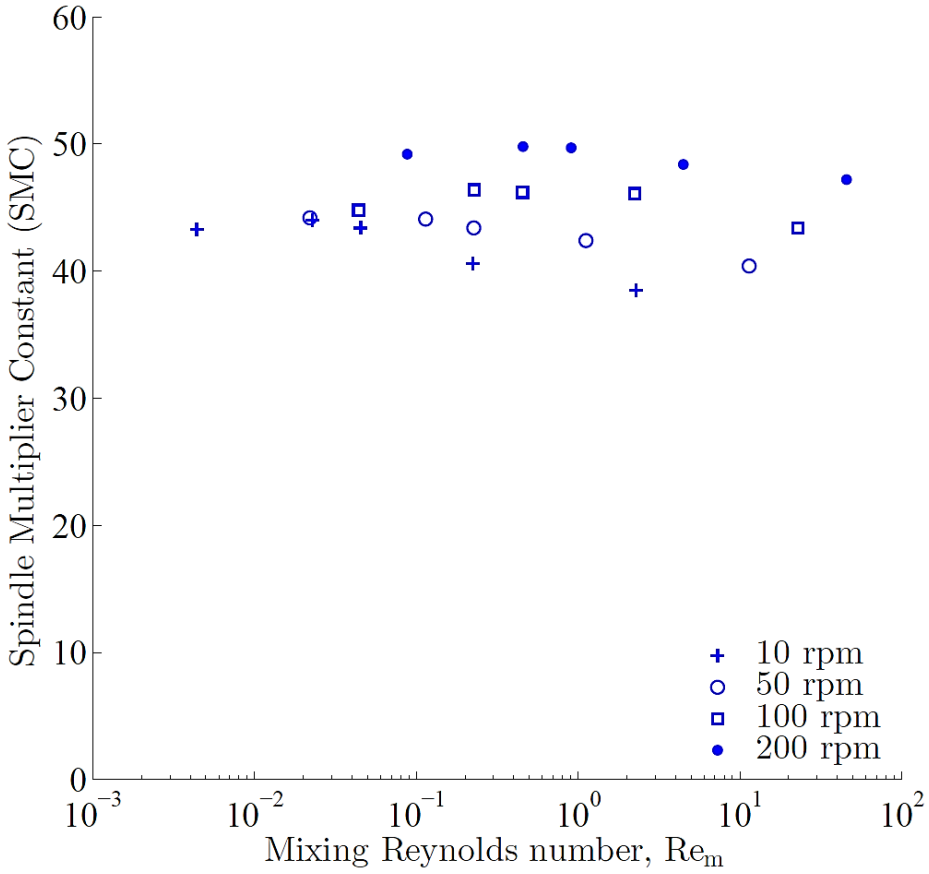

Figure 3.13: Plot of the Spindle Multiplier Constant (SMC) against mixing Reynolds number for the DHI impeller at different rotational speeds.

Table 3.2 CFD simulations to assess phase separation phenomena during rotational tests, where ◊ indicates cases where experimentally there was phase stratification, • where there was a good level of mixing.

	Sc-27			DHI		
Fluid	10 Rpm	100 Rpm	200 Rpm	10 Rpm	100 Rpm	200 Rpm
f100	◊	◊	◊	◊	•	•
f500	◊	•		◊	•	

This can be seen in the clustering of results in lines comprised of the four symbols from left to right. There are several explanations for this functional dependence of SMC on Re_m. First since the same mesh was used for all simulations, the local cell Reynolds numbers would differ from simulation to simulation, which may result in a numerical error being introduced. Second, from the physical perspective, it is thought that the variations are down to the flow patterns changing across the range of Reynolds numbers. There is some experimental evidence to back this up. With reference back to Figure 3.13, it can be seen that the DHI produces more consistent mixing at a rotational speed of greater than 100 Rpm. This may be attributed to the impeller producing a different flow field, a more efficient flow field from the mixing perspective, that at 10 Rpm. This difference may explain the function dependence of SMC on the mixing Reynolds number.

Understanding the DHI mixing process (multiphase)

When considering all the combinations of parameters in the experimental tests discussed in section 3.3.1, it became apparent that there were two distinct sets of cases: those with stratification of the particulate phase and those where homogeneous mixing was observed. Thus, the numerical modelling focused on the cases where these extremes were exhibited.

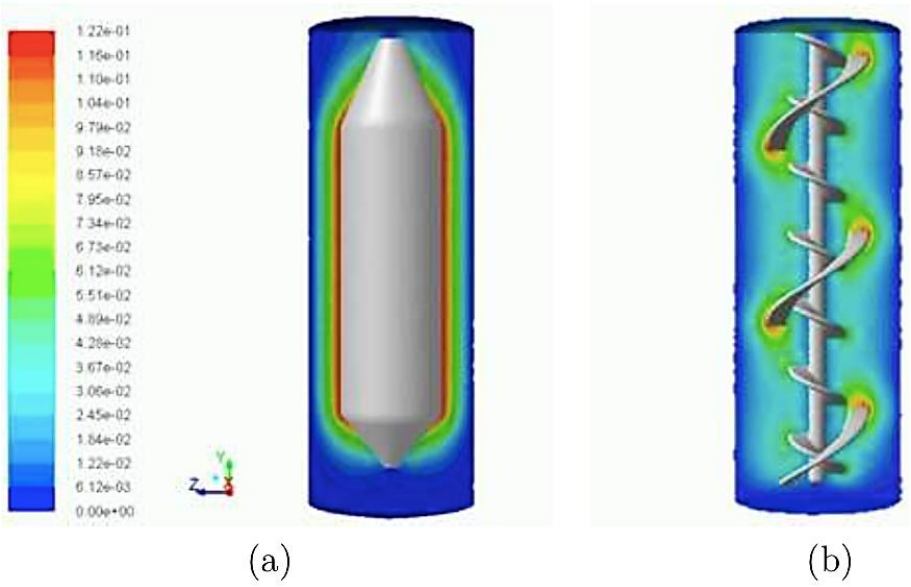

Figure 3.14 Contours of velocity magnitude for the (a) SC-27 spindle and (b) DHI (right) at 100 Rpm

Table 3.2 shows the range of simulations that were run with ⋄ indicating those cases where phase stratification was expected and • where a level of homogeneity in the secondary phase distribution was expected. The two gaps in the table are due to the high viscosity of the f500 preventing the viscometer from operating under those conditions. In all cases the volume fraction of the particulate phase was 5% and the diameter of the particles was 400 μm. Before considering the mixing efficiencies of the two designs, it is instructive to look at the velocity fields in both cases.

Figure 3.14 (a) shows contours of the steady-state velocity magnitude for the SC-27 spindle. The SC-27 creates a Taylor–Couette flow between the rotating spindle and the stationary wall. There is a large circumferential or swirling component to the flow but not a vertical component. As such, particulates in the flow are not driven vertically through the gap (in either direction) but rather tend to sink to the bottom under the effects of gravity.

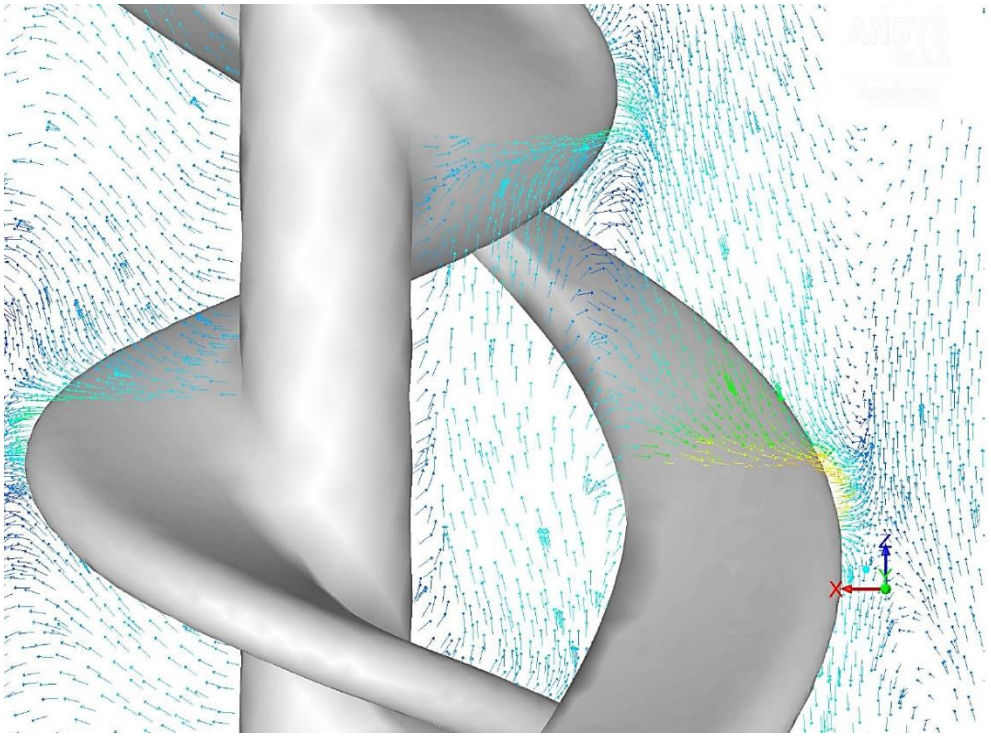

Figure 3.15 A close-up of the inner and outer helices of the DHI impeller, showing the flow vectors on the plane y = 0. Vectors are the same length, and the velocity magnitude is indicated by the colour (blue is zero, red is 0.061m/s).

On the other hand, the instantaneous velocity field for the DHI, Figure 3.14 (b), presents a far more complex picture. Here the plot is showing a snapshot of the velocity magnitude and what cannot be gleaned from this plot that the outer helix is moving fluid downwards, while the inner one is moving fluid upwards.

This becomes clear in Figure 3.15, in which the vector length is constant, but the colour represents the local velocity magnitude (blue is zero, red is 0.061 m/s). While the figure shows only the vectors on a vertical plane and the view focusses on the mid-height region, the flow is now entirely 3D in nature and the simple observations and theory associated with Taylor-Couette flow are no longer possible.

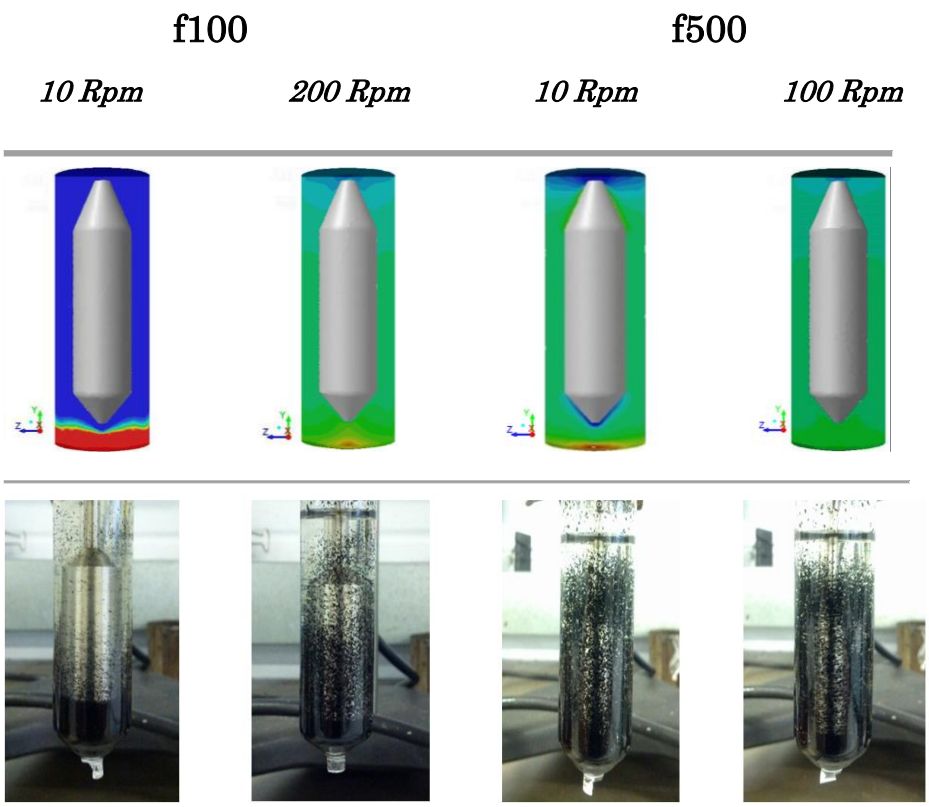

Figure 3.16 Volume fractions from the CFD model (top) and experimental images (bottom) for the SC-27 spindle. The volume fractions range from 0 (blue) to 0.08 (red).

To gain a better understanding of the degree of homogenisation, the volume fraction of the particulate phase was evaluated once the volume fraction for both types of spindle had reached a steady state. For the DHI, while the velocity is not steady, the distribution of particles does reach something very close to a steady state because of the very low settling velocity of the particles in the highly viscous fluids under consideration. Qualitatively, the results from the numerical simulations, compared very favourably with the experimental results.

Figure 3.16 shows the results achieved using the f100 and f500 fluids at different rotational speeds for both the CFD model and the experimental tests.

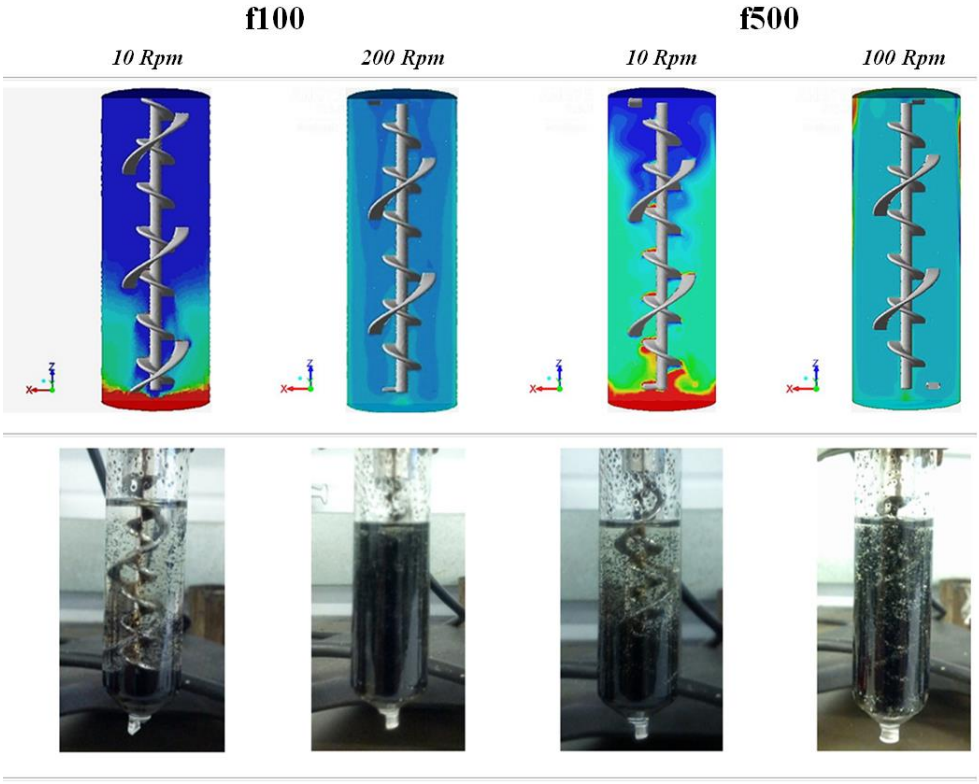

Figure 3.17 Volume fractions (top) and experimental images (bottom) for the DHI. The volume fractions range from 0 (blue) to 0.08 (red).

With reference to the figure, the contour plots of the volume fraction of the particulate phase do bear some similarity to the photographs from the experiments that are shown below them. The highly concentrated zone of particles near the bottom of the container (indicated by the red region, which corresponds to a volume fraction of 0.08) becomes less apparent when the angular velocity of the spindle and the viscosity of the fluids are increased. In fact, the contour range is clipped to a maximum of 0.08, so although the zone for the f100, 10 Rpm case looks small, it is in fact a very small region of very high concentrations. In this case, the suspended particles are able to sink to the bottom and concentrate on the central region where fluid motion is minimal – see Figure 3.14.

There is still some stratification of the secondary phase in all the plots in Figure 3.16, which is also apparent in the experimental results. Two effects are not captured by the CFD model, however. First, the floating scum of particles on the surface of the liquid are not seen because the top boundary of the CFD domain is a symmetry boundary – these particles are held there by surface tension effects, which are not included in the numerical model. Second, the CFD model does not show that some particles stay above the narrow Couette flow region, as well as falling below it. The gap between the spindle and the container wall seems to prevent the particles from settling out, at least on the time scales over which the experiments were run. The CFD model confirms that the main issue of using the standard spindle is that it causes phase separation between the particles and bitumen leading to misleading viscosity measurements. This is due to the absence of vertical components of velocity in what is essentially a flow regime with cylindrical symmetry. Increasing the fluid viscosity (f500) can also lead to a more homogeneous distribution of particles in the liquid and reduces the phenomenon of particles concentration on the bottom.

However, it is not clear that this enhanced mixing is not simply due to the lower terminal velocity of the particles in the more viscous fluid. A look at Figure 3.12 would indicate that the apparent viscosity for the f500, 100 Rpm case had not settled to a constant value and thus a longer test may have produced more stratification.

A very different picture generally emerges when considering the DHI impeller (Figure 3.17). There is qualitative agreement between the CFD and experimental data in this case. However, at 10 Rpm, the DHI still produces a noticeably stratified particulate phase. Again, due to the clipping of the volume fraction at 0.08, the fact that the red region (indicating volume fractions above 0.08) is larger than for the SC-27 cases, then there is some agitation of the fluid in this region.

This agitation is sufficient to keep the particles partially suspended above the base of the viscometer. Nonetheless, this level of mixing is not sufficient to render any apparent viscosity measurements reliable. At 100 Rpm, a level of homogeneity is seen in the particulate phase, which indicates that the impeller is performing its intended task, which is to mix the particulate phase throughout the device.

3.4. Summary of results

The experimental programme provided a clearer picture of the mixing enhancement provided by the DHI when measuring multiphase fluids composed of a liquid and a suspended particulate phase. Furthermore, the DHI geometry allows obtaining a steady apparent viscosity measurement and requires lower torques. This extends the range of measurable viscosity when compared to the standard spindle, SC-27.

CFD simulations clarified the mechanisms behind the previously assumed convective flow created by the DHI. In fact, the analysis of the velocity fields confirms that the central screw of the DHI drags up the complex system while the external screw transports the mixture downwards. Results also highlighted that with current design, the central screw of the DHI could be more effective at pumping the fluid vertically – this leads the way to enhancements in the design.

The single phase CFD simulations produced values of SMC that were in close agreement with the experiments Lo Presti *et al.* (2014). The computational platform helped to gain insights in the complex flow regimes and shows potential to be used as a platform to design new testing geometries for heterogenous fluids as well as for virtual rheology measurements.

The DHI showed to be a significant step forward from the testing geometries currently used for viscosity measurements of heterogenous fluids, especially within product development. Nevertheless, numerical, and experimental results showed that the DHI due to a small gap between the inner and outer helix, it failed to work well with all the suspensions tested. Therefore, when dealing with complex materials, there is still the need to improve the impeller design and the interpretation of the results which will consequentially improve the meaningfulness of the viscosity measurements.

Based on above mentioned observations, in the next chapter a new geometry aimed to overcome these issues is introduced.

CHAPTER 4. THE DHR: AN OPTIMISED IMPELLER FOR MIXING RHEOMETRY WHICH ENSURES SAMPLE STABILITY DURING ROTATIONAL TEST

4. The DHR: an optimised impeller for mixing rheometry which ensures sample stability during rotational test

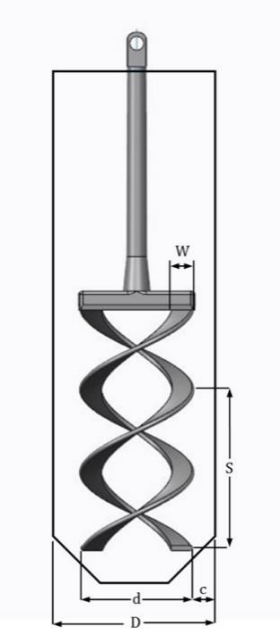

Figure 4.1 The dual helical ribbon (DHR) designed for this work

As highlighted in the previous chapter, when dealing with heterogenous binders such as CR-MBs the need of improving the mixing rheometry is a crucial step to characterise materials rheological behaviour. In a previous research, Lo Presti *et al.*, (2014), carried out an attempt to solve the issue by developing a dual helical impeller (DHI) to replace the conventional setup for rotational viscometer. Although the DHI performed well by improving the overall mixing performance compared to the cylindrical spindle, the CFD also highlighted the limits of this device. Indeed, numerical studies proved that the central screw does not work as expected but creates a low velocity field in the middle region that is not able to keep the particles suspended within the sample. In addition, the close gap between the inner screw and the outer helix may lead the particle to agglomerate.

Based on these observations an optimised testing geometry able to overcome the before-mentioned issues and in turn to provide more realistic rheological measurements of HBBs was required.

After a deep review about mixing devices (section 2.3.3), literature findings showed that the dual helical ribbon impeller was found to be the best solution of close-clearance impellers used for the mixing of highly heterogeneous fluids. This design reduces the heterogeneity of the testing sample by creating an axial flow that allows the continuous renewal of the fluid within the measuring chamber so leading to more stable and realistic viscosity measurements. Indeed, in a dual helical ribbon impeller, the mixing proceeds mainly in the clearance between blades and wall where the liquid is subjected to very high shearing. The overall mixing appears to be controlled by the flow pattern, which aids the renewal of the liquid in the clearance and distributes the liquid flowing out of the clearance region to the low-shear region of the vessel. The optimum geometrical ratios for the mixing process have been found to be:

$$c/D = 0.06,\ s/D = 0.9,\ w/D = 0.15,$$

where, c is the clearance between blades and wall, D the diameter of measuring chamber (19 mm), and d, s and w are respectively the diameter, the pitch and width of the impeller (Figure 4.1). These ratios have been selected first based on a literature investigation (Takahashi et al. 1982) aimed to narrow the case studies, then by using the numerical model through the use of the mixing index. Indeed, Fluent provides the option to perform calculations during a simulation by using the User-Defined Function (UDF) box. The mixing index Δ stands for deviation of the mixing away from uniform distribution of the two fluids. The index ranges from 0 to 1 where high values indicate a poorly mixed system.

$$\Delta = \frac{1}{\bar{\alpha}}\sqrt{\frac{1}{n}\sum(\alpha_i - \bar{\alpha})^2} \qquad \textit{Equation 36}$$

Table 4.1 Ratios used into fluent to define the optimum dimensions based on the mixing index

c/d	*s/D*	*w/D*	Mixing index Δ
0.05	0.9	0.15	0.14
0.06	0.9	0.15	0.08
0.07	0.9	0.15	0.10
0.06	0.8	0.15	0.09
0.06	1	0.15	0.12
0.06	0.9	0.14	0.15
0.06	0.9	0.16	0.11

Where $\bar{\alpha}$ is the mean volume fraction of rubber particles in the domain, n is the number of cells in the domain and α_i is the volume fraction in cell i. The numerical model was set up as described in section 4.1.1. and the mixing index compared (Table 4.1). That allowed to obtain a close-clearance impeller to be designed, aimed to enhance the mixing but also to guarantee enough room for the particles to freely circulate within the sample without being stuck.

Then the optimum DHR was modelled and validated by mean of numerical simulations then prototyped by using the 3D printing technology. That allowed to test the new impeller without incurring in expensive design mistake. Indeed, the 3D technology is cheaper than the stainless-steel manufacturing process. Just to make a quick comparison, a DHR realised by the 3D printing technology costs about 2 € while the same manufactured in stainless steel is about 600 €. Finally, the DHR was manufactured in stainless-steel and calibrated using a wide range of Newtonian and non-Newtonian materials.

The overall objective of this chapter is to demonstrate the ability of the DHR geometry to enhance the mixing within the sample by using numerical and experimental techniques. In the next section the design and validation of the DHR by means of numerical modelling is presented.

4.1. CFD simulations

A CFD analysis was carried out to design and validate the new geometry. Due to the high manufacturing cost the use of the computational platform helped to avoid a trial and error process that could had turn in a costly and time-consuming procedure. In fact, the numerical modelling provided useful evidence about the device performance that allowed to proceed to the manufacturing of the DHR with relatively confidence.

4.1.1. CFD model set-up

The modelling techniques used are broadly the same of section 3.2, DHR geometry was designed based on the ratios previously shown (Figure 4.1). Ansys-DesignModeler and Ansys-Meshing software were used to produce the CAD model and mesh of the DHR, which contained approximately 150,000 tetrahedral and triangular prism cells. Figure 4.2 shows the CAD model and associated surface mesh. A mesh-independence study was carried out using the same method as in section 3.2.1. It has to be noticed that compared to the DHI the DHR requires a lower number of elements due to the absence of the central screw. As a consequence, the computational effort is reduced.

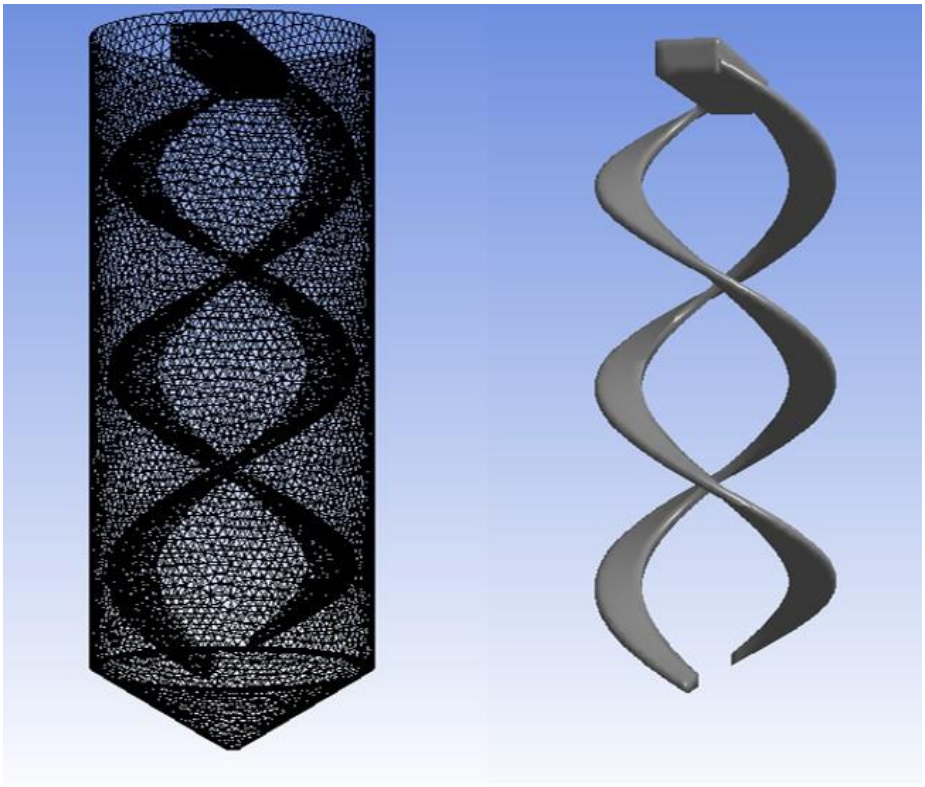

Figure 4.2 On the left, the surface mesh on the mixer and outer wall; and on the right, a solid model of the DHR.

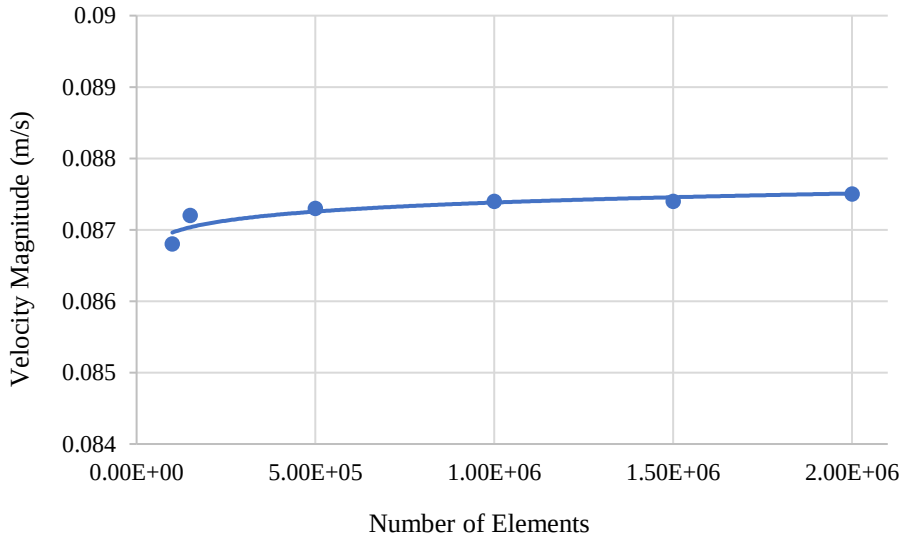

Figure 4.3 The DHR mesh sensitive analysis

4.1.2. Kinematic Similarity

Once that the CFD model was setup, an initial study was carried out to test the DHR design for kinematic similarity. In the field of fluid mechanics, kinematic similarity means, when the velocity at any point in the model flow is proportional by a constant scale factor to the velocity at the homologous point in the prototype flow, while considering it is maintaining the same flow streamline shape (Cengel *et al.*, 2006). The idea behind these tests was to prove that increasing the rotational speeds the flow pattern was not affected by the shear rate applied.

For both a Newtonian (ViscoFluidF100) and a non-Newtonian (Xantana 0.25 %) fluid, the model was run at 10, 50, 100 and 200 Rpm and components of the velocity were analysed along two lines through the domain – a vertical line going from the bottom to the top along the centre line of the vessel and a horizontal one in the middle of the sample. Using an appropriate non-dimensionalisation, Figure 4.4 and Figure 4.5 show the variation of the scaled w and u components of the velocity along these two lines for both the Newtonian and non-Newtonian fluids. What the two figures show is that, over a wide range of rotational speeds, the flow within the vessel displays kinematic similarity – the flow patterns seen are apparently independent of the shear rate and the properties of the fluid.

This gives us confidence that the DHR design can be used as a viscometer across a range of shear rates. If these velocity profiles differed over a range of shear rates, then the device would effectively have different flow patterns at different speeds and any extrapolation of results at one shear rate would be impossible.

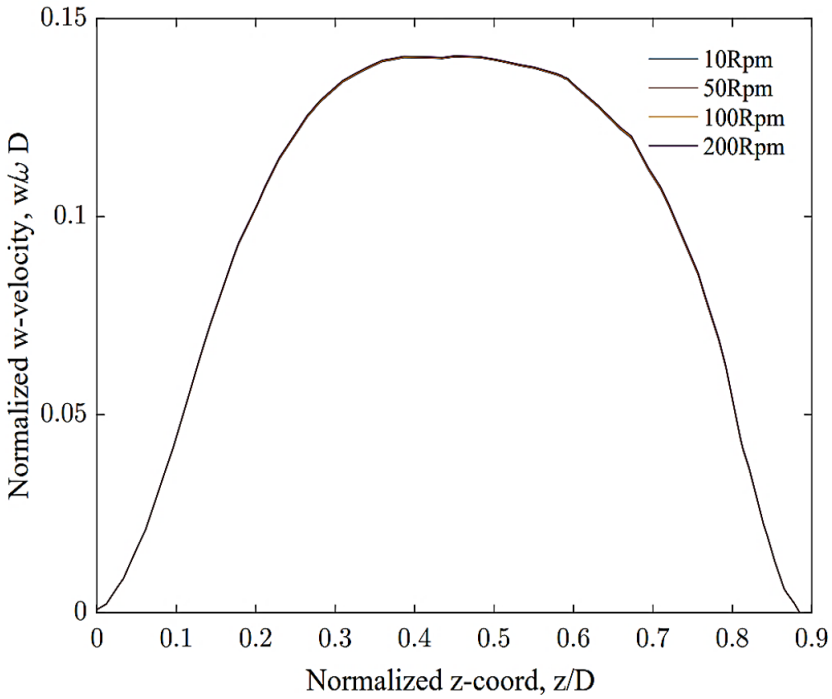

Figure 4.4 Plots of the non-dimensional w-component of velocity along a vertical centreline, from bottom to top, for the Newtonian fluids.

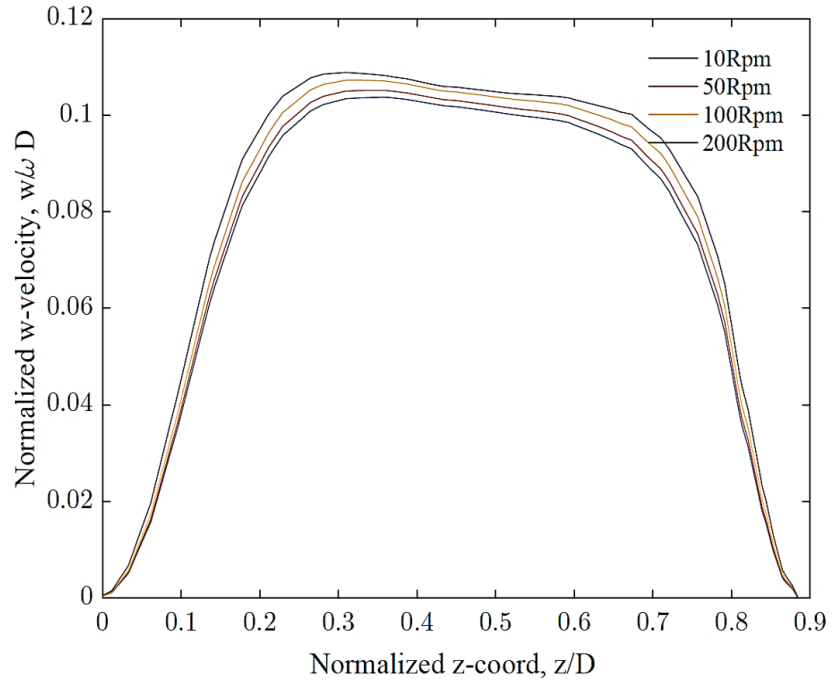

Figure 4.5 Plots of the non-dimensional w-component of velocity along a vertical centreline, from bottom to top, for the non-Newtonian fluids.

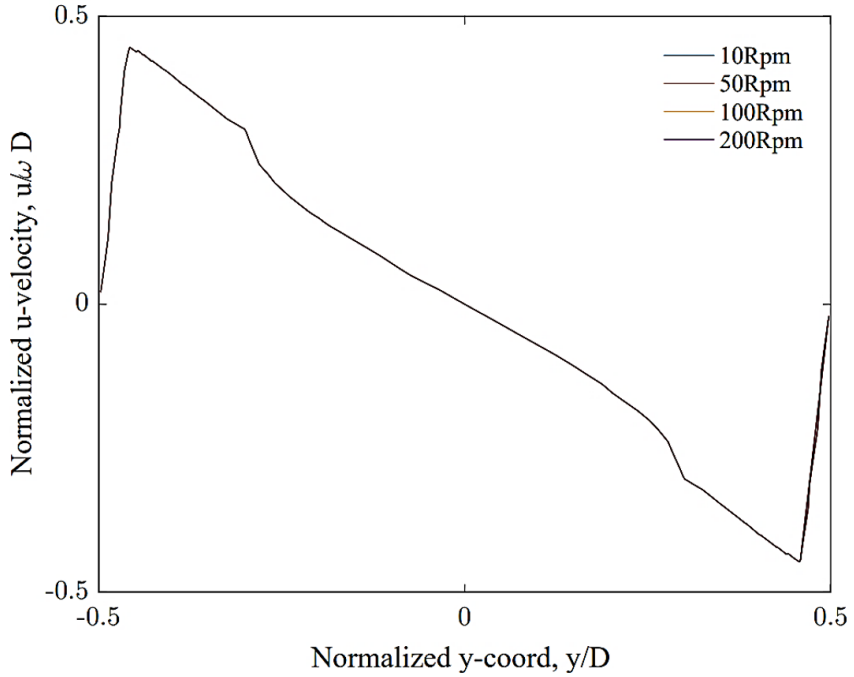

Figure 4.6 Plots of the non-dimensional u-component of velocity along a horizontal centreline for the Newtonian fluids.

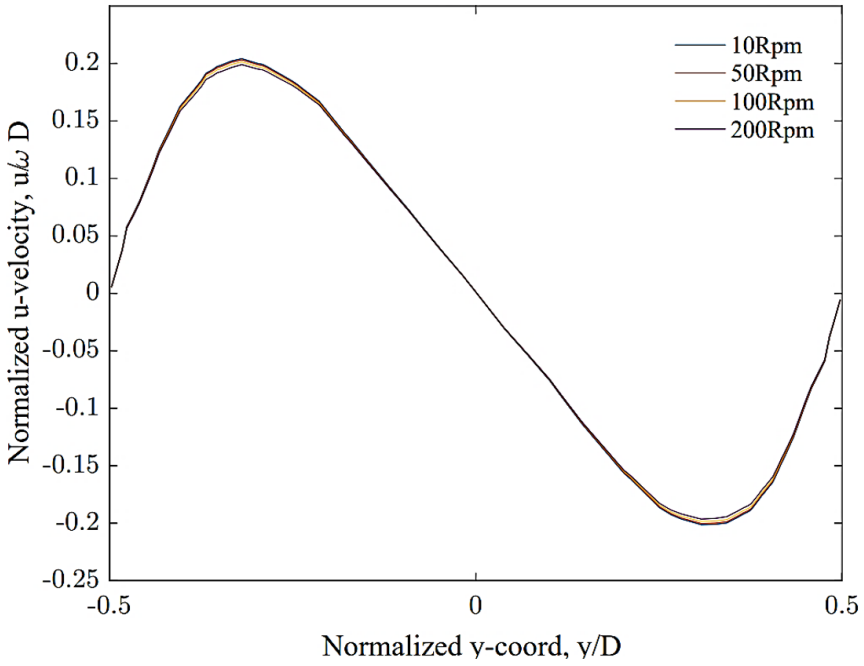

Figure 4.7 Plots of the non-dimensional u-component of velocity along a horizontal centreline for the non-Newtonian fluids.

4.1.3. Multiphase Simulations

With confidence in the kinematic similarity gained from the previous section, multiphase simulations, using the mixture model as described previously, were run to investigate the mixing of rubber particles in the DHR. Various Newtonian fluids were tested; 5% by volume of rubber particles were used with a diameter of 400 μm and density of 1050 kg/m^3; and various rotational speeds (10, 50, 100 and 200 Rpm) were used. In addition, several non-Buoyant cases were run where the density of the rubber particles exactly matched the density of the background Newtonian fluid as specified in Table 4.2.

Table 4.2 Fluids and particle properties

	Fluid		**Particles**		
Name	Density (kg/m^3)	Viscosity (Pa·S)	Diameter (μm)	Volume fraction	Density (kg/m^3)
f10	940	0.01			
f100	960	0.1	400	5%	1050
f500	970	0.5			

As mentioned in Section 2.3.3, a useful measure of the mixing within the vessel is the mixing index. Figure 4.8 shows the variation of the mixing index with the mixing Reynolds number for both buoyant and neutrally buoyant particles.

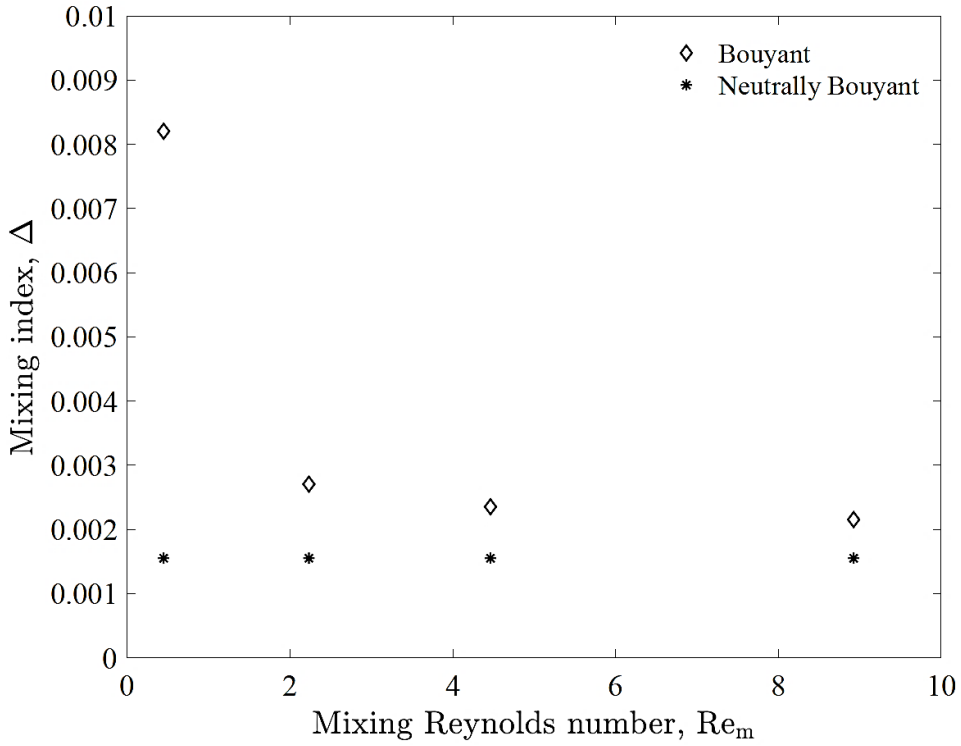

Figure 4.8 Plot of the mixing index, Δ, against mixing Reynolds number, R_{em}, for the f100 fluid with 5% rubber particles (both buoyant and neutrally buoyant).

We see that for the neutrally buoyant particles, the mixing index is independent of Re_m because the particles do not tend to settle out and the mixing is sufficient to keep them well mixed at any rotational speed. However, for the f100 fluid shown, there is a clear decrease in the mixing (as witness by an increase in the mixing index) for buoyant particles at the lowest rotational speed. For the higher two of the four speeds used, the mixing index becomes uniform, but at the lower speeds it increases. This has implications for the use of the DHR as a viscometer because of this dependence on the mixing Reynolds number. However, the deviation of volume fraction from the mean in all these cases is very small. Indeed, just how comparatively small the mixing index is for the DHR can be highlighted when the mixing capability of the DHR is compared with the SC-27 under identical conditions.

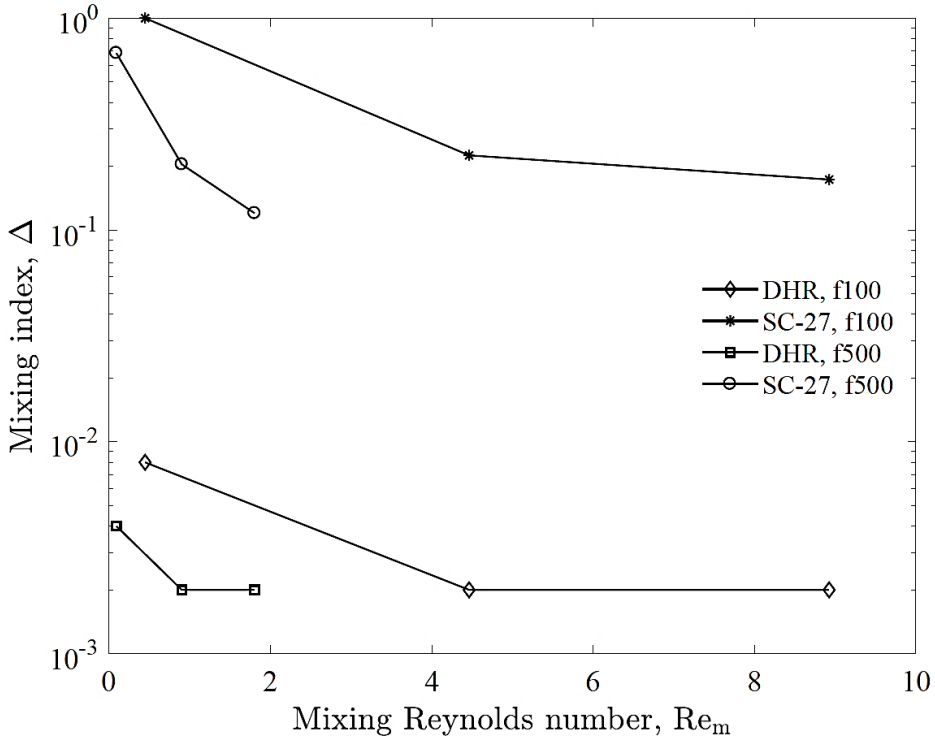

Figure 4.9 Plot of the mixing index, Δ, against mixing Reynolds number, R_{em}, for the f100 and f500 fluids with 5% rubber particles for the DHR and SC-27 impellers.

Figure 4.9 shows the variation in the mixing index with both rotational speed and fluid for both the SC-27 and DHR impellers. Noting that the y-axis is logarithmic, it can be seen that all devices produce more homogeneous mixtures at higher rotational speeds. However, the mixing index for the SC-27 under all conditions produced a highly stratified mixture, which the DHR clearly does not. This confirms findings from the experimental campaign (Figure 4.21) and is supported by Figure 4.10, which shows contours of particle volume fraction and velocity from both the SC-27 and DHR simulations. Clearly there is stratification of the particles in the SC-27 model, while the DHR displays a near-homogeneous value for the volume fraction.

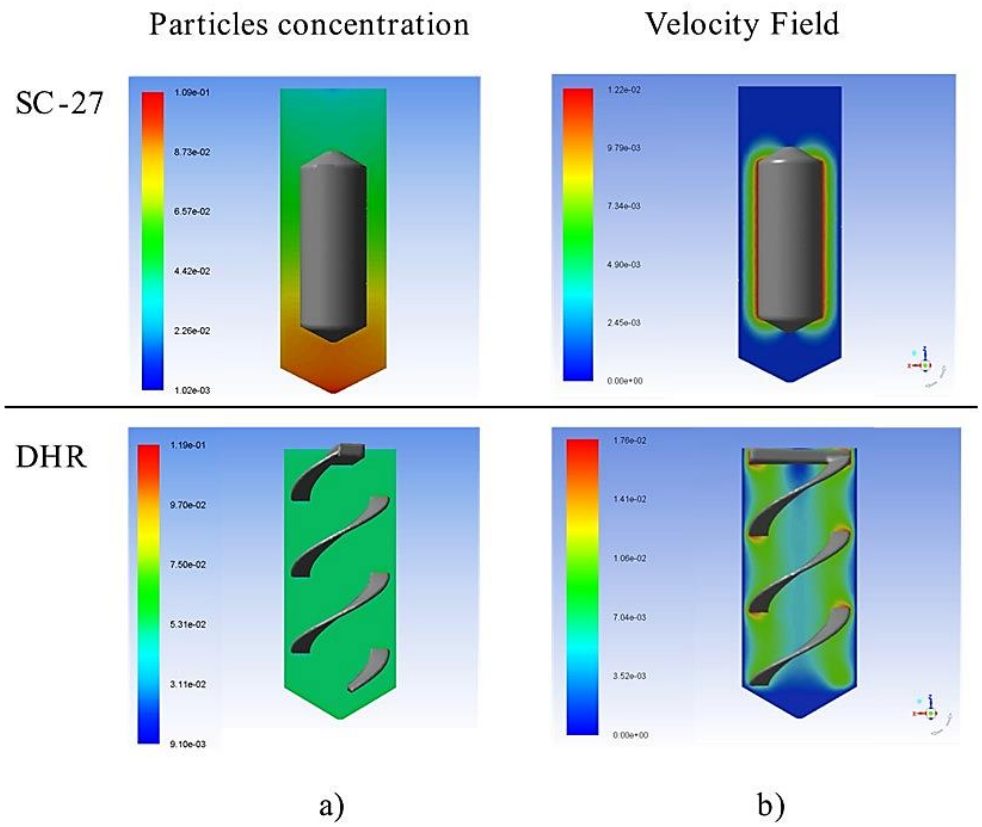

Figure 4.10 Numerical comparison of contours of (a) volume fraction and (b) velocity magnitude during rotational test on f100 + 5% particles at 20 Rpm.

The velocity magnitude plot for the SC-27 shows that once a particle has settled towards the bottom of the vessel, there is no mechanism for it to be re-entrained in the flow because of the low velocities outside of the zone between the two cylindrical surfaces. A similar zone would appear to exist towards the bottom of the DHR configuration, but closer inspection reveals that the upward flow of fluid is sufficient to re-entrain the particles in this region. As an aside, it might be sensible for the manufacturers to produce the vessels with a flat bottom, as opposed to the angled one used at present, to prevent this.

4.2. Manufacturing process

The numerical analysis proved that the DHR design worked as intended. However, before proceeding to manufacture the part in stainless steel, the DHR was realised by using the 3D printing technology. Thanks to this innovative technique it was possible to reduce manufacturing time and costs but also to make different prototypes in order to achieve the final geometry. The reason to do that lays in the fact that the standard for modified bitumens (ASTM D 6114-97) states that the apparatus measuring geometry should be selected so as to obtain dynamic viscosity readings under torsion torque values which are between 10% and 98 % of the maximum possible torsion torque of the spindle for the chosen test conditions. However, when measuring extremely low or high viscosity fluids may happen that these limits can be exceeded. To minimise this issue, a set of three DHRs was designed by applying different pitches Figure 4.11.

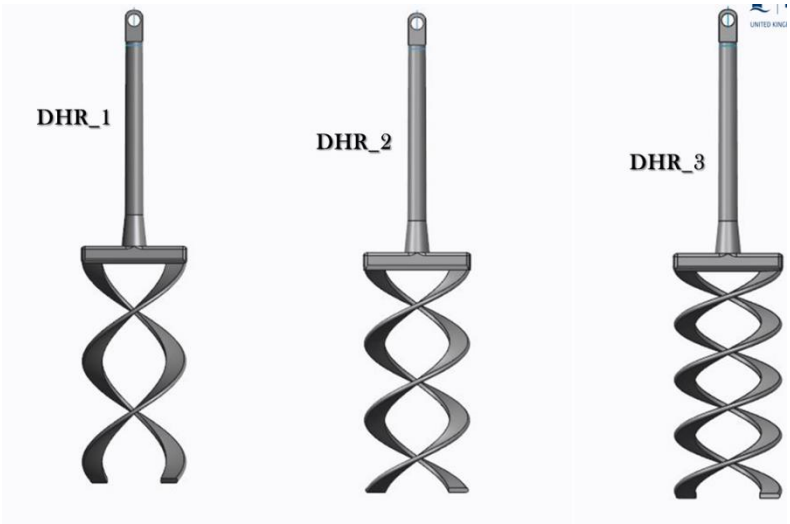

Figure 4.11 The set of DHRs with different pitches

Figure 4.12 The Stratasys Dimension 1200es 3D printer used in this work

Indeed, reducing the pitch of the DHR allows to increase the axial forces in the middle region of the DHR and it turn to develop higher values of torque that is crucial when measuring low viscosity fluids. On the other hand, increasing the pitch permits to cover lower values of torque and so to measure fluids with higher values of viscosity. A Stratasys Dimension 1200es powered by Fused Deposition Modelling (FDM) technology was used. The part was printed in real Acrylonitrile Butadiene Styrene (ABS) thermoplastic, material that during the tests showed to be affordable, but also durable. Finally, the set of DHRs was printed and adapted to a Brookfield rotational viscometer model LVDV-II+Pro EXTRA. At this stage, the author wanted to evaluate the mixing performance of the DHRs by visual assessment. To provide the reader with further details the validation process was performed by comparing the set of DHRs also with the DHI previously introduced.

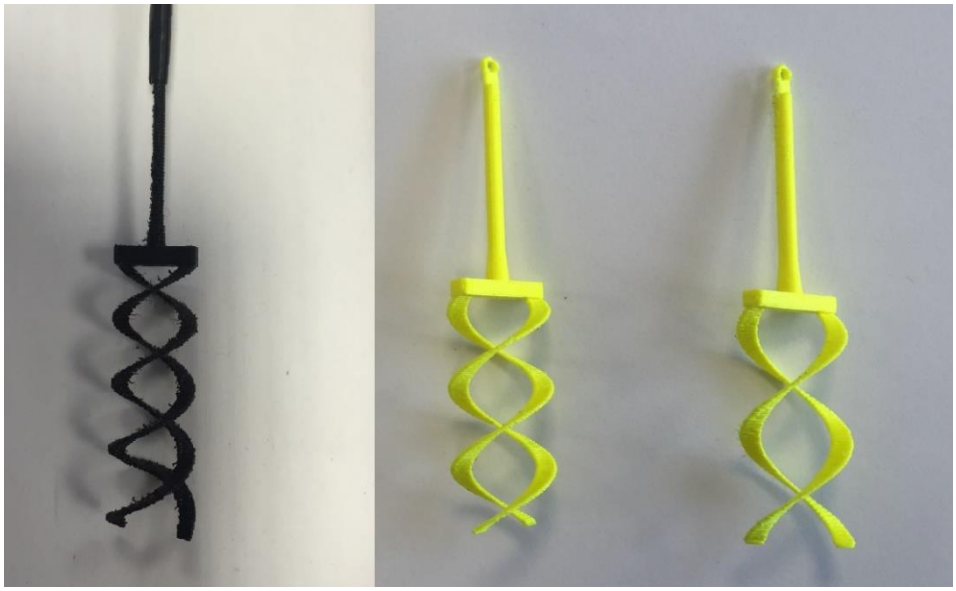

Figure 4.13 The DHR prototyped by using the 3D printing technology

Nine fluids made up from the combination of different fluids and crumb rubber particles concentrations (1, 3 and 5%) were tested. Three different fluids of known viscosity were used f10, f100 and f500 with a viscosity of 0.01 cP, 0.1 cP and 0.5 cP, respectively. All the test have been performed at 10, 50 and 100 Rpm. Tests were performed by adapting different geometries on the rotational viscometer. A glass tube (Figure 3.1.) in place of the conventional one allowed a visual investigation aimed to assess the mixing performance of each geometry. Indeed, thanks to the transparent fluid it was possible to visualise the mixing between the fluid (transparent) and the particles (black). Table 4.3 summarizes if the selected impeller is able to keep the particles suspended within the sample (O) or not (X). Furthermore, in the table the symbol (-) reports if the reading exceeds the lower or higher limits of the viscometer. over a wide range of fluids, and rotational speed. Findings proved that the set of DHRs extends the range of measurements while respecting the limits recommended by the ASTM standard. Now the stage is ready to proceed with the manufacturing of the DHRs in stainless-steel.

Table 4.3 Rotational test results comparison between different geometries, where (o) indicates cases where the geometry was able to keep the particles suspended within the sample , (x) not and (-) reports if the reading exceeds the lower or higher limits of the viscometer.

Fluids	Measurement with DHI			Measurement with DHR_1			Measurement with DHR_2			Measurement with DHR_3		
	10 Rpm	*50 Rpm*	*100 Rpm*	*10 Rpm*	*50 Rpm*	*100 Rpm*	*10 Rpm*	*50 Rpm*	*100 Rpm*	*10 Rpm*	*50 Rpm*	*100 Rpm*
f10 1% CRM	X	X	O	X	O	O	X	O	O	O	O	O
f10 3% CRM	X	X	O	X	O	O	X	O	O	O	O	O
f10 5% CRM	X	X	O	X	O	O	X	O	O	O	O	O
f100 1% CRM	O	O	-	O	O	O	O	O	O	O	O	O
f100 3% CRM	O	O	O	O	O	O	O	O	O	O	O	O
f100 5% CRM	X	O	O	O	O	O	O	O	O	O	O	O
f500 1% CRM	O	O	-	O	O	O	O	O	O	O	O	O
f500 3% CRM	O	O	-	O	O	O	O	O	O	O	O	O
f500 5% CRM	X	O	-	O	O	O	O	O	O	O	O	O

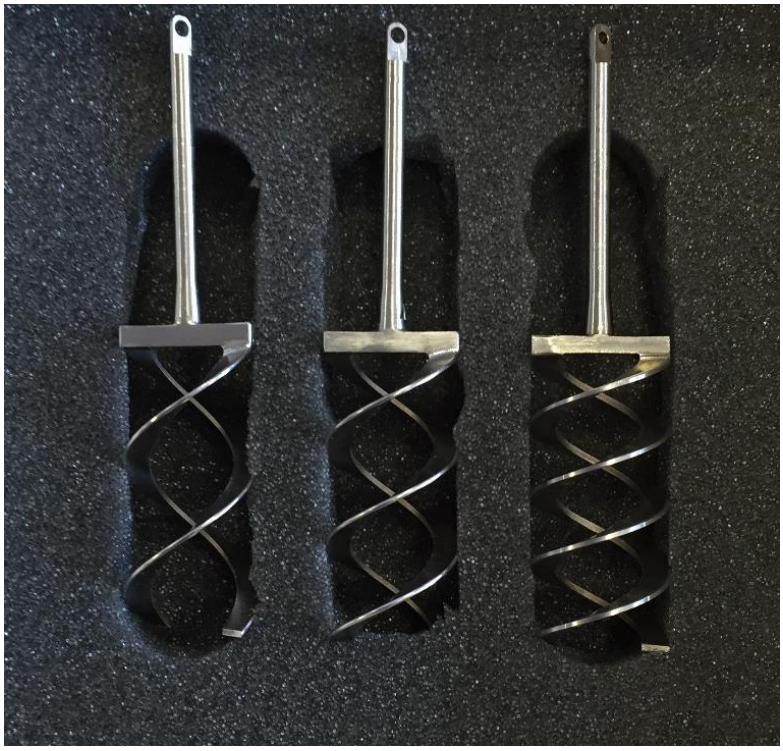

Figure 4.14 Stainless steel DHRs set

Finally, the devices were manufactured in stainless steel at the precision manufacturing centre based at the university of Nottingham (Figure 4.14) and then calibrated by using a wide range of Newtonian and non-Newtonian fluids.

The next section introduces the calibration procedure required to adapt the impeller to the rotational viscometer. The DHR then was compared with the standard SC-27 spindle while measuring multiphase fluids. The calibration of the DHR was carried out at the university of Huelva, laboratory of complex fluids.

4.3. DHR calibration

If the DHR (Figure 4.15) is to be used to measure the behaviour of heterogeneous materials, some of which may be non-Newtonian, it is important to calibrate the new design against a range of non-Newtonian fluids.

Figure 4.15 The stainless steel DHR impeller for use in a Brookfield Viscometer.

Here we use the Metzner-Otto method (Metzner *et al.*, 1957), introduced in section 2.4., for non-Newtonian fluids that uses the concept of apparent viscosity, η, which is linked to an effective shear rate $\dot{\gamma_{eff}}$. They suggested this effective shear rate to be proportional to the rotation frequency *N*. The idea behind the calibration procedure was to find a correlation between the *K*s and the flow index *n*.

4.3.1. Materials

The first steep of the calibration procedure was to prepare the materials necessary to carry out the experimental campaign. Five materials (Table 4.4) were selected to cover the wider range possible of flow index.

Table 4.4 Values of n and k for each system used in this study. (* CMS is carboxymethylcellulose sodium salt)

Fluid	Flow index	Consistency index
	n	*k*
1% Xanthan Gum	0.2	75.47
0.5% Xanthan Gum + 0.5% Guar Gum	0.3	15.041
0.25% Xanthan Gum	0.4	2.61
1.5% Xanthan Gum + 3% CMS*	0.69	9.366
Visco-fluid	0.99	4.4

A low shear mixer (Figure 4.16) was used to prepare the systems, to obtain stables mixtures the mixing time required was about 12 hours for each system.

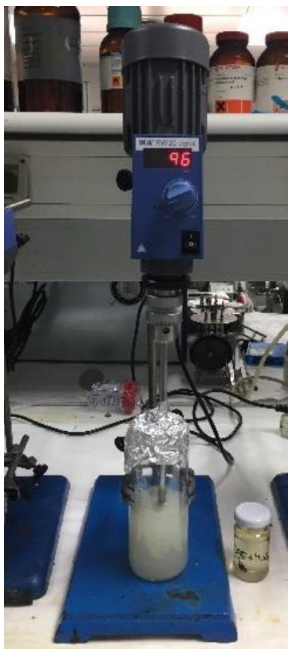

Figure 4.16 Low shear mixer used in this work for the preparation of the samples

Table 4.5 Parameters used during parallel and plate tests

Temperature	time	Shear rate	Geometry
30 °C	30 min	0.01 to 100 (1/s)	PP 35mm

Rheological measurements - Parallel and plate

Rheological tests (parallel and plate) were carried out by using a Malvern Kinexus PRO to obtain values of shear stress, τ, determined from the torque applied to the sample, at a number of shear rates, $\dot{\gamma}$, determined from the angular velocity of the plates. For the non-Newtonian materials, a power law was assumed according to Equation 26. Tests were performed for each material by using a parallel and plate configuration with a diameter of 35mm; operating parameters are showed in Table 4.5, to find out the consistency index k and the flow index n, which is an indication of the deviation from Newtonian behaviour. Indeed,

$$n \begin{cases} < 1 \; Shear \; thinning \; (pseudo \; plastics) \\ = \; 1 \; Newtonian \; fluid \\ > 1 \; Shear \; thickening \; (dilatant \; fluids) \end{cases}$$

Taking logarithms of both sides of equation 26 gives:

$$log_{10}\eta_{app} = (n-1)log_{10}\dot{\gamma} + log_{10}k \qquad \textit{Equation 37}$$

The results of utilizing Equation 37 are shown in Figure 4.17 for each of the five fluids tested in this way. The Newtonian visco-fluid has a flow behaviour index of close to unity, as expected, while all the other fluids have a value of less than unity, indicating that they are shear-thinning.

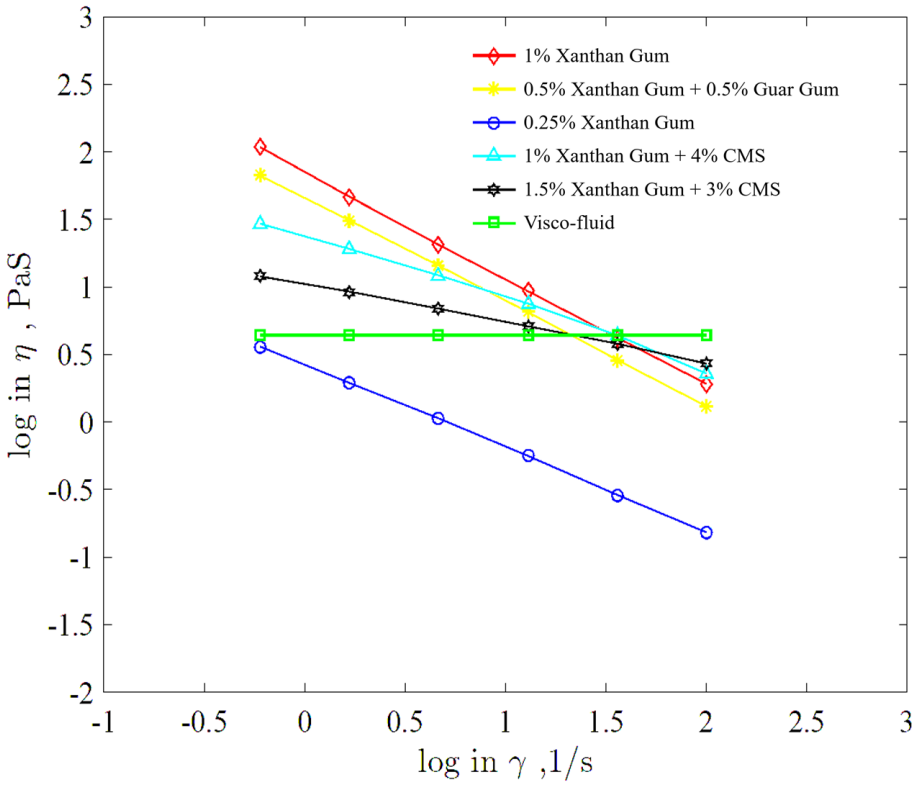

Figure 4.17 Plot of the flow behaviours for the Newtonian and non-Newtonian fluids investigated in this work.

It was key at this stage to have as large a range of values of *n* for subsequent testing of the DHR design. Each fluid showed a trend as in Figure 4.17, then it was assumed that every fluid was a power law fluid. The two key parameters *n* and *k* are respectively the slope and the intercept. Results proved that the flow index calculated covered a satisfactory range of the shear thinning behaviour fluids (*n* in the range 0.2–0.7).

4.3.2. Rheological Viscometer test

The DHR was adapted to a Brookfield LV-II pro viscometer, to record for each material the trend of the torque Vs the rotational speed (0 to 100 Rpm at 30°C for about 30 min). The reason for doing that was that Metzner-Otto also stated that

$$\frac{\eta_{nN}}{\eta_N} = \frac{M_{nN}}{M_N} \qquad \textit{Equation 38}$$

Where the η_{nN}/η_N is the ratio between the viscosity of a non-Newtonian fluid and a Newtonian one calculated by means of dynamic shear rheometer. M_{nN}/M_N is the ratio between the torque of a non-Newtonian fluid and a Newtonian calculated by means of rotational viscometer. In this phase of the experiments the torque as a function of rotational speed was recorded for all the geometries. From Equation 37 it was possible calculate the apparent shear rate of each systems using the Ostwald-de Waele power law relationship:

$$\dot{\gamma_{eff}} = \left(\frac{\eta_{nN}}{k}\right)^{\frac{1}{n-1}} \qquad \textit{Equation 39}$$

Two geometries were tested during the experimental procedure, the Brookfield SC27, the most widely-used spindles for multiphase applications and the DHR introduced in this work (Figure 4.18). For both the impellers, using a rotational viscometer the torque and angular velocity were recorded and used to calculate the non-Newtonian viscosity (using Equation 38, relative to the Newtonian fluid).

Table 4.6 Comparison of the SMC values found in this study compared with those from Brookfield's literature.

	SMC	
Geometry	**This work**	**Brookfield**
SC-27	25	25
DHR	11.5	-

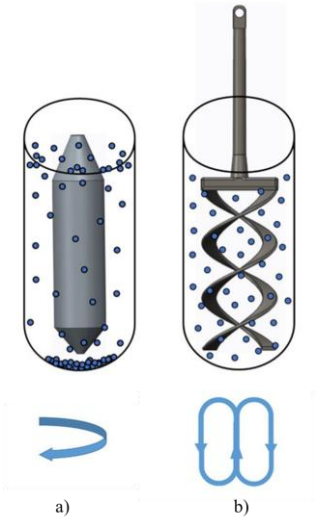

Figure 4.18 Schematics of (a) Standard spindle SC-27, (b) Dual Helical Ribbon, each with an indication of the main flow patterns seen with each.

The shear rate $\dot{\gamma}$ was calculated at every rotational speed and plotted versus the rotational speed, *N*. Finally, the variation of the Metzner-Otto parameter K_s with the power-law index, *n*, found for the various fluids, is shown in Figure 4.19 and Figure 4.20. For solutions of Xantana and Xantana and CMS, there is a correlation between K_s and *n*, the flow index. For lower values of the flow index, the fluid exhibits higher shear thinning characteristics, hence the expected lower value of K_s.

However, the combination of Xantana and Guar Gum does not follow this trend, which may be due to the particular interaction between this fluid and the DHR. For these reasons it was not possible find a unique correlation between the K_s and *n*, therefore it would be necessary calculate the value of *K*s for each material. Nevertheless, the unique constant, SMC, was calculated for both the geometries by combining Equation 18 and Equation 37. As can be seen from Table 4.6, the values of SMC found were in good agreement with those of the Brookfield literature for the SC-27 while the value of SMC for the DHR is the first measurement for this new design.

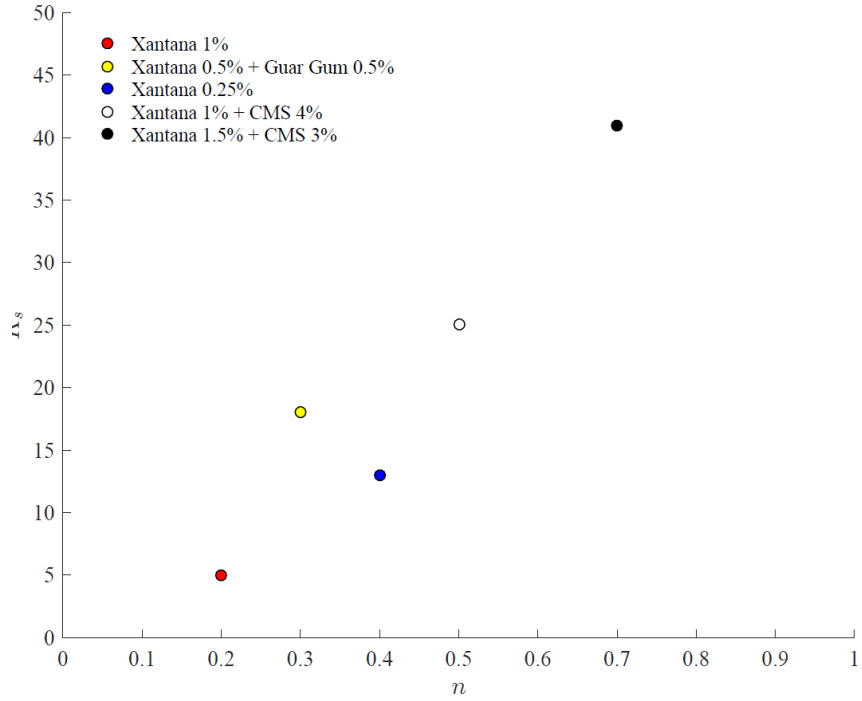

Figure 4.19: Variations of the Metzner Otto parameter Ks with the power-law index *n* for the SC-27 spindle.

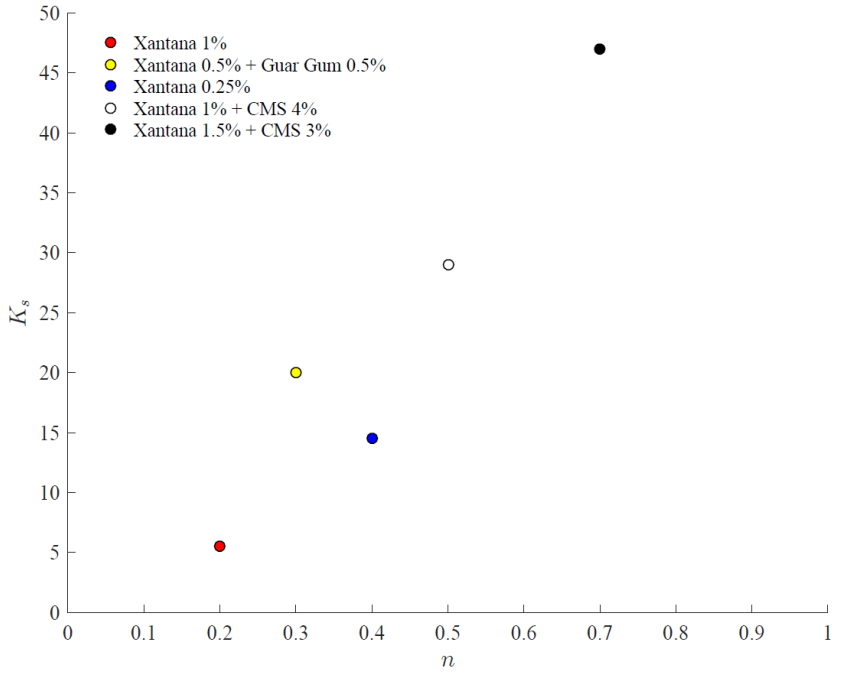

Figure 4.20: Variations of the Metzner Otto parameter Ks with the power-law index n for the DHR spindle.

4.3.3. Experimental validation

A number of multiphase fluids made up from a combination of different Newtonian fluids (Brookfield standard fluids) and crumb rubber particles were created (Table 4.2). The particles were added to the fluid and the blend was shaken to produce an even distribution of the particles. These were then tested in a Brookfield DV-II PRO Digital Viscometer using the SC-27 and DHR spindles. The impellers were quickly submerged in the blend and the viscometer was turned on to carry out the test, during which torque and viscosity were measured. These were tested at various rotational speeds up to a maximum of 100 Rpm at 25°C for period of 45 minutes. Each of the reported results is obtained as average of at least two repeats under the same experimental conditions. As shown in section 2.3 it is noted that the viscosity of a dilute suspension can be found from the Einstein equation (Equation 6). This equation is used as a benchmark to validate the experimental results.

To evaluate the response of the two geometries, tests were conducted at 10, 50 and 100 Rpm. Figure 4.21 shows the variation of viscosity with time for both the SC-27 and DHR impellors at 10 and 100 Rpm for a 5% mixture of rubber particles and the f10 fluid. Also shown on this and the subsequent two figures is the prediction of viscosity from Equation 6. For the SC-27 spindle, a high initial viscosity is seen at both speeds due to issues with accelerating the fluid and particles up to a constant speed. The viscosity then decreases gradually over the 45-minute testing period, falling below the Einstein viscosity in the process. This is due to the settling of the particles during the test, producing a fluid in the gap between the cylinders that is virtually free from particles (Figure 4.21 b). At 10 Rpm, the DHR provides produces more constant values of viscosity, which are also closer to the Einstein value. There is still a small decrease over the run time, but this appears to stabilize after 25 minutes.

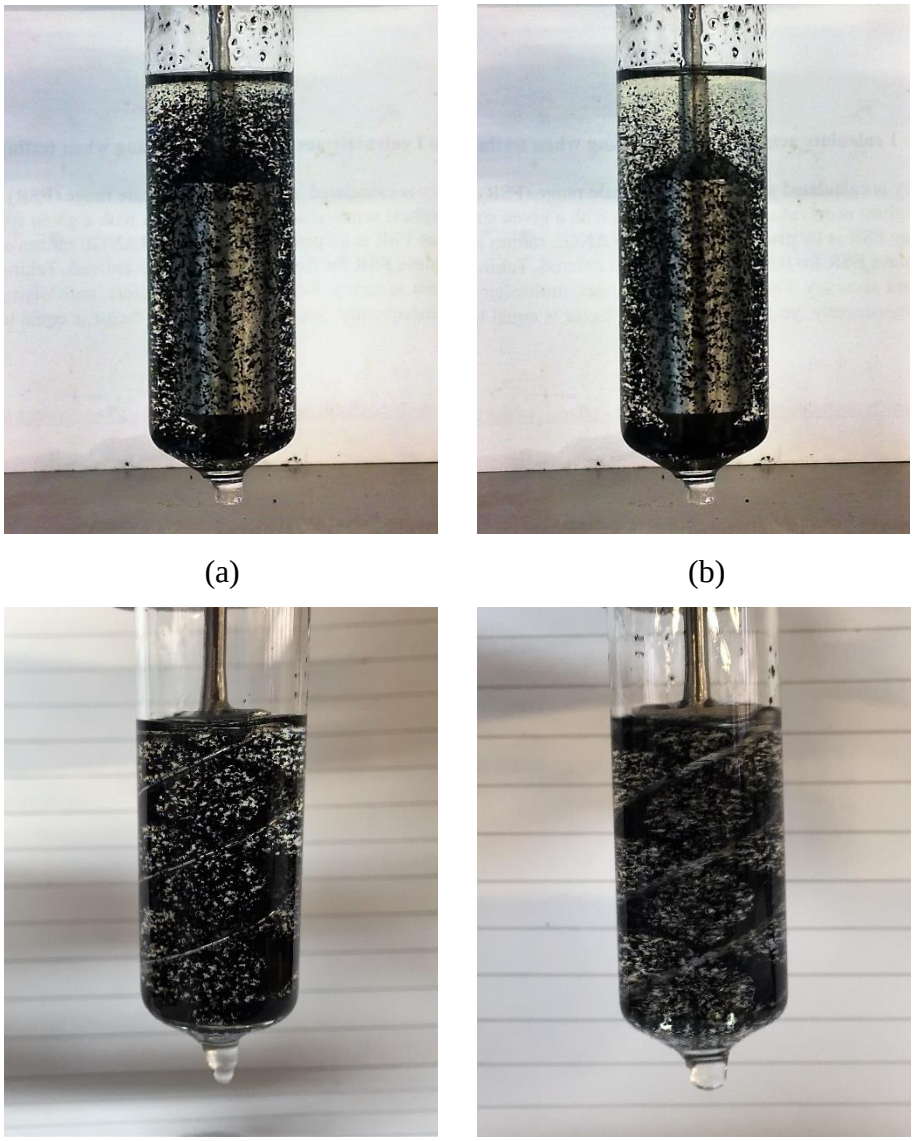

(a) (b)

(c) (d)

Figure 4.21 Photographs sequence of the SC-27 and DHR impellers with a mixture of f10 fluid +5% of rubber particles at the start (a), (c) and end (b), (d) of the tests

For the higher shear rate, the value of viscosity for the DHR is fairly constant during the test, only falling slightly towards the end. The value seen is very close to the Einstein prediction and is due to the particles remaining in suspension throughout (Figure 4.21 d). Increasing the rotational speed produces lower values of viscosity for both impeller due the shear-thinning behaviour of the fluid/particle mixture. At this point it is useful to consider the settling time, t_s , for a rubber particle in the background fluid

$$t_s = \frac{H}{v_t} \qquad \textit{Equation 40}$$

where H is the height of the Brookfield tube and v_t is the terminal velocity of the particles

$$v_t = \frac{(\rho_p - \rho_f) d^2{}_p g}{18\,\eta_f} \qquad \textit{Equation 41}$$

where ρ_p and ρ_f are the densities of the particles and fluid respectively, d_p is the diameter of the of the particles and η_f is the viscosity of the background fluid. For the f10 fluid, we find a settling time of the order of 1 minute, for f100, 10 minutes and 50 minutes for f500. These are rough values, assuming the fluid is stationary and the complete absence of other particles in the background fluid. With this in mind, Figure 4.23 and Figure 4.24 show the evolution of viscosity for the f100 and f500 background fluids respectively. It is clear that the SC-27 impeller in both cases shows the gradual decrease in time that was seen for the f10 fluid, albeit the decrease is slower (due to the increased settling times). For the DHR impeller, the values again decrease a little from their initial values, but the change is by no means as pronounced. Clearly with a settling time of the order of the length of the experiment for the f500 fluid, the values of viscosity for this experiment are by no means at their final value, those for the DHR show very little change over the period of measurement.

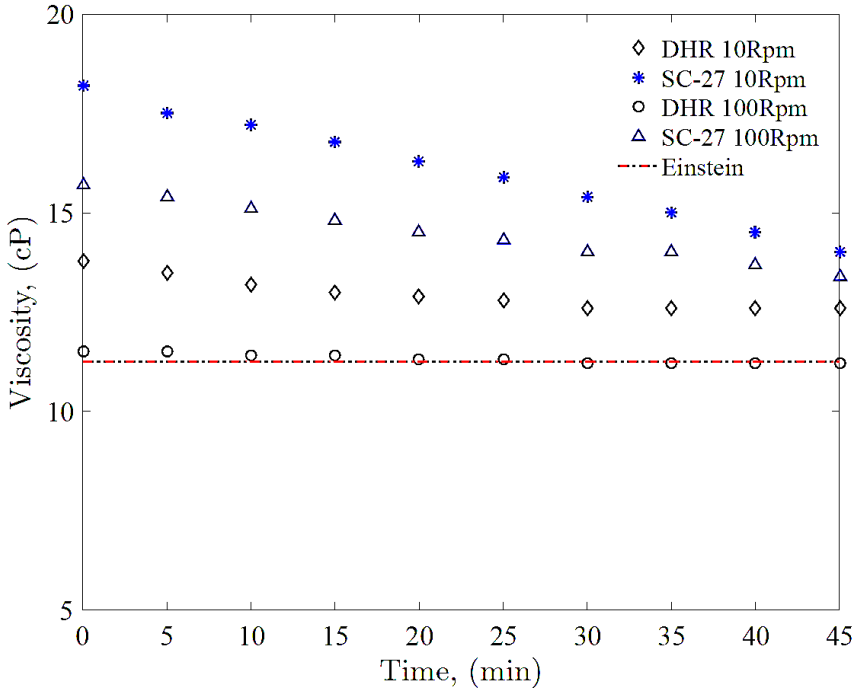

Figure 4.22 Viscosity measurements over time by using Brookfield viscometer on standard fluid f10 plus 5% of suspended solids.

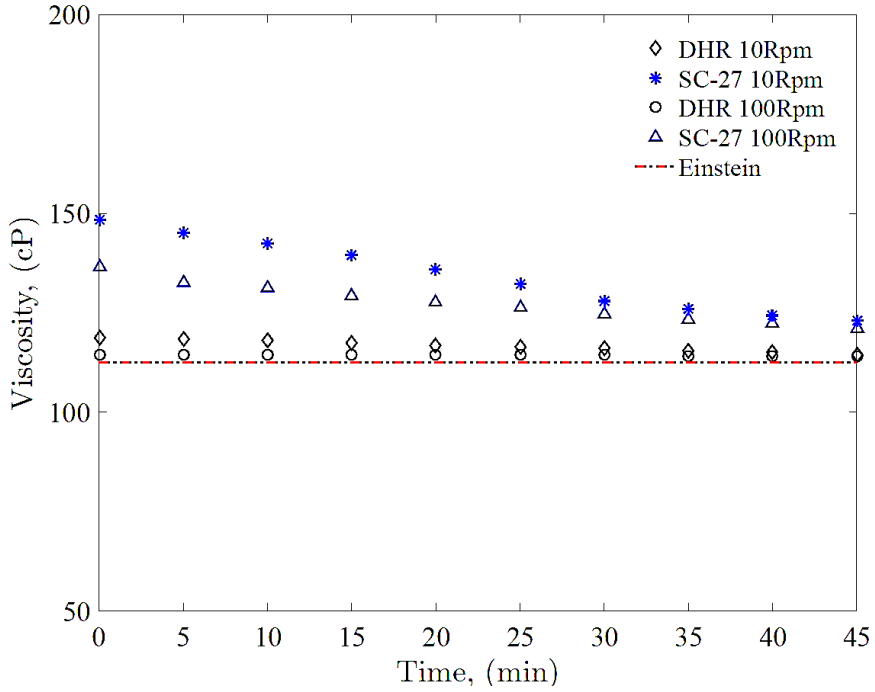

Figure 4.23 Viscosity measurements over time by using Brookfield viscometer on standard fluid f100 plus 5% of suspended solids.

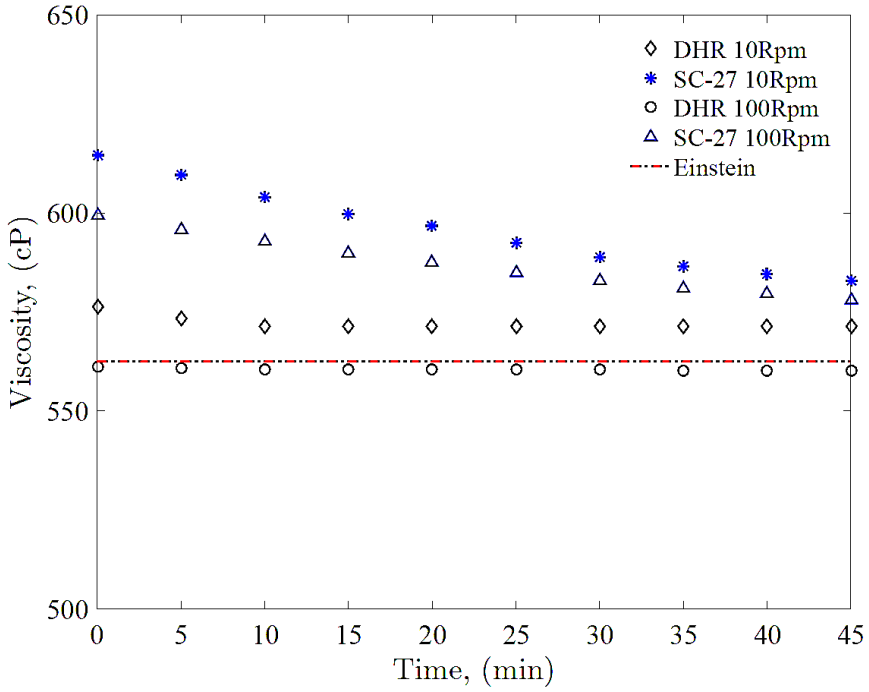

Figure 4.24 Viscosity measurements over time by using Brookfield viscometer on standard fluid f500 plus 5% of suspended solids.

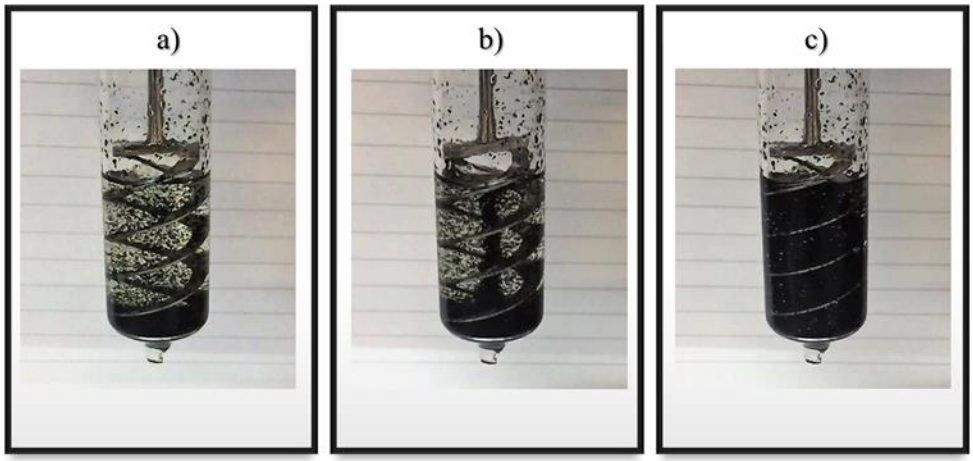

Figure 4.25 Photographs of the DHR impeller showing the axial pumping force with a mixture of f10 fluid and rubber particles at the start (a), after few seconds(c) and at the end (c).

A separate experiment where the particles were initially allowed to settle in the device before the DHR was rotated, reveal the mixing process clearly (Figure 4.25) In image (a) of this figure, the particles are clustered near the bottom, while shortly after the start of the mixing process, a clear plume of particles is observed spiralling upwards in the centre of the device, image (b). After some time, image (c), the particles are evenly distributed throughout the device, confirming our previous observations. As a result, particles are circulated throughout the container and phase separation is avoided for the remainder of this experiment.

These results show and confirm as mentioned earlier that the rotational speed is of fundamental importance when considering the extent to which the sample is homogenised and plays a crucial role in determining the efficacy of the impeller. This, of course, has significant consequences on the viscosity readings, which are a function of testing geometry, rotational speed and applied torque. Results show that the apparent viscosity measurements are less dependent on the rotational speed of the DHR than the SC-27.

The fact that results are convergent for the DHR confirm the observations made above, where the higher rotational speeds produce a less heterogeneous

blend. At 10 Rpm, there is clearly some intermittency to the viscosity measurements as the particles do not reach a steady-state distribution. In any case, both viscosity values over time and shear dependency, put the DHR in favourable light, which seems to provide more stable rheological information of this complex system.

4.4. Summary of results

This chapter presented a novel impeller for rheological measurements aimed at overcoming some of the well-known issues while testing heterogenous fluids (multiphase, non-Newtonian or a combination of both). For this purpose, after a literature study and a numerical validation a dual helical ribbon (DHR) was designed and tested with a view to being adopted as a rotational viscometer. This study also offers an innovative combined laboratory-based and computational approach. In fact, the CFD model was used as a support for the design and validation of the DHR but also helped to shed a light into the measuring chamber showing the limitations of the SC-27 and the benefit of the dual helical ribbon solution that otherwise it would have been impossible to visualize during laboratory tests.

The novel impeller was designed to reduce the heterogeneity of a complex system within the measuring chamber ensuring so the sample stability during the tests. The CFD investigation helped firstly in the design of the DHR and secondly to illustrate the fluid dynamics processes behind the improvement. Results showed that the sample stability was guaranteed using the DHR thanks to its ability to keep the system homogenized. In fact, the geometry was designed to create a vertical axial pumping within the sample with the idea that the outer helix pumps the fluid downwards while an inner helix pumps it upwards.

The experimental programme showed a clearer picture of the mixing enhancement provided by the DHR when measuring multiphase fluids composed of a liquid and a suspended particulate phase. The calibration procedure provided satisfactory results and allowed the DHR to be adopted as a rotational viscometer by using specific values of SRC and SMC.

Once particles were added to the standard fluids, the DHR compared to the SC-27 provided a stable trend of viscosity measurements and closer values to the Einstein equation for suspensions. The laboratory campaign reported evidence that heterogeneous fluids do not produce a stable value of measurements during the testing with SC-27. The final values of apparent viscosities can be significantly different from those obtained with the DHR, which instead provided stable readings already after few minutes. Finally, the CFD analysis, provided the additional opportunity to reveal the complex flow field inside the mixing vessel. Results that allowed to understand that using the SC-27 provides complex results which are mainly governed by the middle region. On the other hand, the viscosity results over the length of the tube are quite uniform when the DHR is used as impeller. Hence, as general conclusion can be stated that the DHR impeller offers a solution to ensure sample stability and considering its direct correlation with the resulting viscosity readings, it is recommended to consider this solution within rheological characterization of heterogenous materials.

Future recommendations can lie in exploring further use of CFD in the field of complex systems testing. In fact, based on these results the next chapter shows an experimental programme on HBBs using the optimised equipment and the numerical platform.

CHAPTER 5. IMPROVING THE RHEOMETRY OF HBBs BY ENSURING SAMPLE STABILITY DURING ROTATIONAL TESTS: EXPERIMENTAL AND NUMERICAL APPROACH

5. Improving the rheometry of HBBs by ensuring sample stability during rotational tests: experimental and numerical approach

This chapter aims to provide evidence that the standard setup for rotational viscosity measurements of bituminous binders might not be adequate, particularly when dealing with modified bituminous binders with high level of heterogeneity. In fact, as previously mentioned when using standard rheometry system for HBBs such as CR-MB, a number of phenomena may occur in the measuring chamber. These changes all contribute to undermine the here-defined sample stability that if altered could provide significantly misleading results.

Instability of the modified bitumens at the usual temperature for rotational tests (135 °C), can be minimal or none. This investigation, however, aims to prove that the sample stability is also compromised when equilibrium times are. This could lead to significant mistakes in further steps such as choosing wrong temperatures to guarantee appropriate aggregate coating during mixing and/or ensuring good workability during compaction of asphalt concrete. The investigation will offer a comparison of experimental and numerical results to highlight whether the DHR helps ensuring sample stability during rotational test of HBBs.

The experimental programme was tailored to allow a comparison between the DHR and the SC-27 systems by means of a combined laboratory-based and computational approach. The laboratory work will provide results of rotational viscosity tests on neat bitumen, an SBS-MB, and an CR-MB.

The numerical simulations will provide a qualitative insight into the measuring chamber, by means of velocity fields and distribution of volume fractions within the container. The outcomes of this combined approach will be used to understand whether lack of sample stability occurs and will also allow clarifying whether using the novel impeller ensures it as well the improving of rheological measurements.

5.1. Experimental-numerical programme

Three different binders were included in the experimental programme: a neat bitumen and two highly modified bitumen with different level and type of modifier (

). The crumb rubber modified bitumen (CR-MB) was produced by adding 15% of crumb rubber size 0,300mm in 35/50 grade bitumen, while the polymer modified bitumen (PMB) by adding 7.5 of SBS 30% rad in 180/240 grade bitumen. All fluids being tested at 5, 20 and 100 Rpm in a range of temperature between 120 to 200 °C for a total of about 45 minutes, where the first 15 min where allowed to reach the thermal equilibrium (0 Rpm). Then, impellers were quickly submerged in the blend and the viscometer was turned on to carry out the test, during which torque and angular velocity were measured and the viscosity calculated from Equation 18.

Table 5.1 Characterisation of material's rheological properties

No.	Material	Penetration	Rotational Viscosity @150°C [mPa.s]	Softening Point [°C]	*n*	K_s	
						DHR	***Sc-27***
1	Neat 35/50	40	170	51.4	-	-	-
2	CRM-MB	31	3000	63.2	0.8	45	41
3	PMB	76	2500	102.5	0.9	53	48

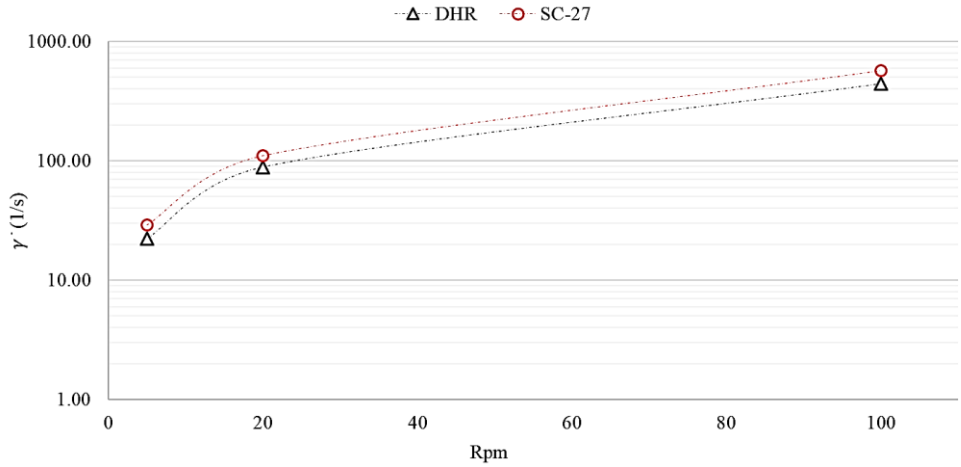

Figure 5.1 The effective shear rate Vs the rotational for DHR and SC-27

Tests were performed in coaxial cylinder setup with both the standard spindle SC-27 and the DHR as impellers. Each of the reported results is obtained as average of at three replicates. It has to be noted that, in this investigation, two Brookfield DV-II PRO Digital Viscometer were used: a low torque (LV model) and high torque (HA model). The two equipment differ mainly for the viscosity measurements range and as a consequence for the measurement's accuracy. In fact, torque measurement accuracy specified by manufacturer is 1% of the full-scale range. Furthermore, the difficulty with viscosity measurements of HBBs at elevated temperatures has been in maintaining accurate temperature control that is consistent from sample to sample so that meaningful data could be obtained. The Brookfield Thermosel solved this problem by providing a stable, precisely controlled sample environment with a control of sample temperature up to +300°C (Figure 5.2).

Tests were conducted according to Subhy (2016), which are based on international standards on viscosity measurements of rubberized bitumens (ASTM D4402, ASTM D6114).

Figure 5.2 The rotational viscometer and Thermosel used in this investigation

In parallel a numerical model was developed to support the experimental campaign. The idea was to reproduce the laboratory set-up and provide an insight within the testing chamber explaining the physic behind the tests. The CFD Model set up is the same showed in section 3.2 and 4.1. The viscosity model used is showed in section 4.1., here values n and of K_s (

) have been calculated for each material by dynamic shear rheometer using a similar procedure described in section 4.3.1. and used in Fluent. Then, the effective shear rate Vs the rotational speed for both SC-27 and DHR was calculated (Figure 5.1). Furthermore, a "cut-off viscosity" was defined in the power-law model to run the simulation, this viscosity arbitrarily given will be the highest viscosity predicted by the software when simulating at very low shear rates. This is necessary because as introduced in section 2.1.1 Ostwald-de Waele model gives an infinitive viscosity at shear rates close to zero.

5.2. Results

5.2.1. Experimental campaign on HBBs

Measurements on neat bitumen

A neat bitumen was analysed to provide the reader a comparison between the SC-27 and DHR when measuring conventional bitumen. Figure 5.3 and Table 5.2 shows viscosity measurements carried out on a 35/50 pen bitumen at 135 °C and 177.5 °C, by using both the SC-27 and the DHR impellers at different rotational speed. These two test temperatures were selected because typically used to measure rotational viscosity at elevated temperatures of neat bitumen (ASTM D4402) and CR-MB (ASTM D 6114-97). As a result, with a homogeneous material such as the neat bitumen DHR provides the same readings of the Sc-27.

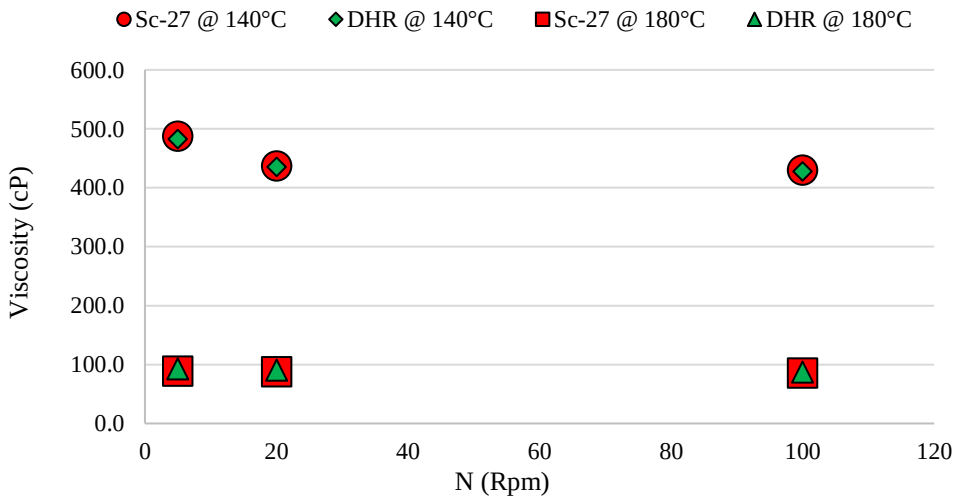

Figure 5.3 Viscosity measurements at different rotational speeds by using LV viscometer on a 35/50 bitumen at T = 140 °C and 180 °C

Measurements on modified bitumens: apparent viscosity vs time

After the positive tests performed on neat bitumen, the SC-27 and the DHR have been used to measure the apparent viscosity of CR-MB containing 15% (size 0.300 mm) and produced in high shear. Same tests were carried out for an SBS-MB produced by adding 7.5% of SBS 30% radial in 180/240 grade bitumen. Each test lasted 45 min, and in the first 15 mins the system was left reaching the thermal equilibrium (0 Rpm). Considering the shear thinning nature of the modified bitumen, to evaluate the response of the two geometries tests were conducted respectively at 5, 20, 100 Rpm.

Figure 5.4. and Figure 5.5 show the apparent viscosity measurement of the modified binders performed at 180 °C with a rotational speed of 20-100 Rpm. The difference in terms of viscosity between the two geometries at the end of the thermal equilibrium is due to the higher initial momentum required by the SC-27. Figure 5.6 instead shows the differences in terms of percentage between the two testing geometries at 1, 5 and 30 min.

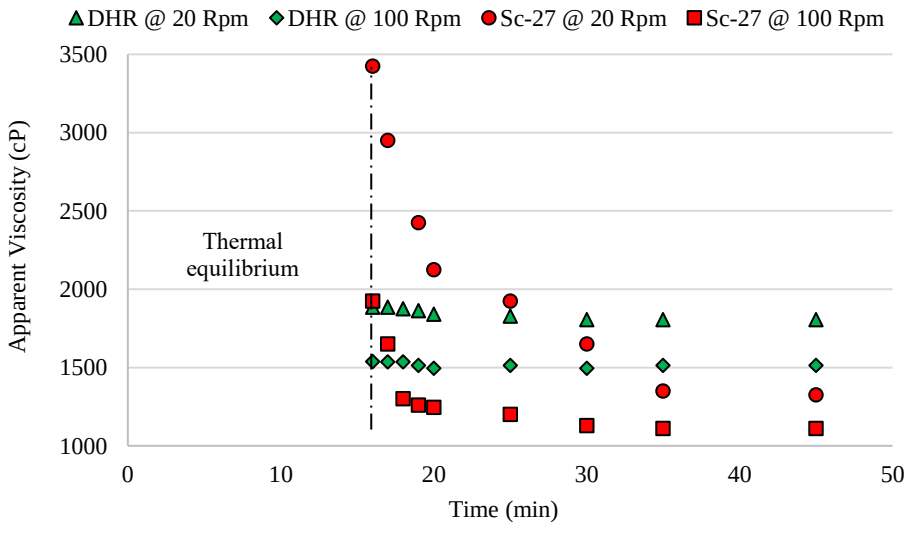

Figure 5.4 Apparent viscosity measurements over time of an CR-MB at 180 °C at 20–100 Rpm

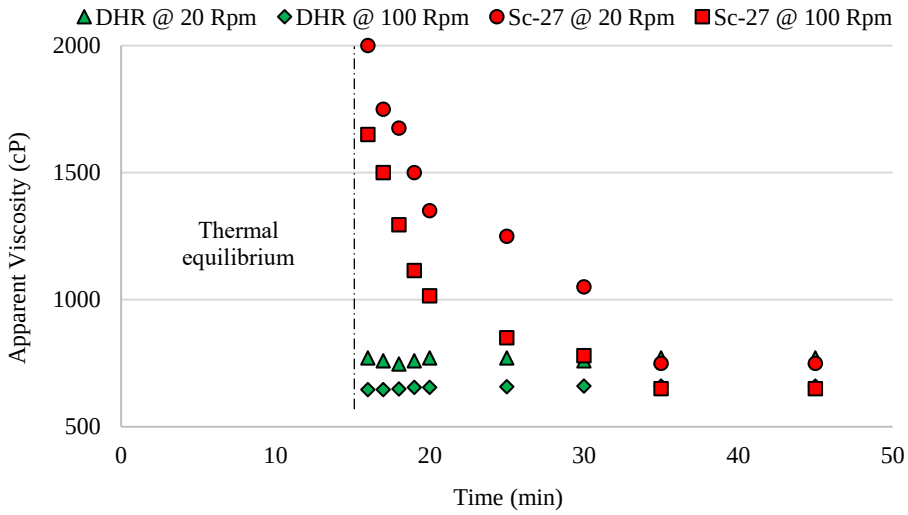

Figure 5.5 Apparent viscosity measurements over time of an SBS-MB at 180 °C at 20–100 Rpm

Considering that for both the materials similar trends were recorded at low Rpm (5 Rpm) for simplicity here only the graph at 20 and 100 Rpm are reported, the reader can find them in the annex. It can be observed that the SC-27 impeller provides measurements that pass through a wider transition period before achieving a stable measurement, while DHR allows obtaining measurements with a more stable trend. This is quite evident with both SBS-MB and CR-MB, however higher speeds (100 Rpm) seems diminishing the unstable trend showed from the SC-27. Moreover, during the whole campaign the SC-27 provided values of apparent viscosity (after 45 mins) that are always lower than the DHR. If compared with the measurements carried out on the neat bitumen, it seems that the modified bitumen is in some way affected during the measurements. Phenomena like phase separation and sedimentation may occur during the test leading to inconsistent results. Figure 5.4. and Figure 5.5 highlight how the DHR instead provides a stable trend of results, which seems not be affected with time.

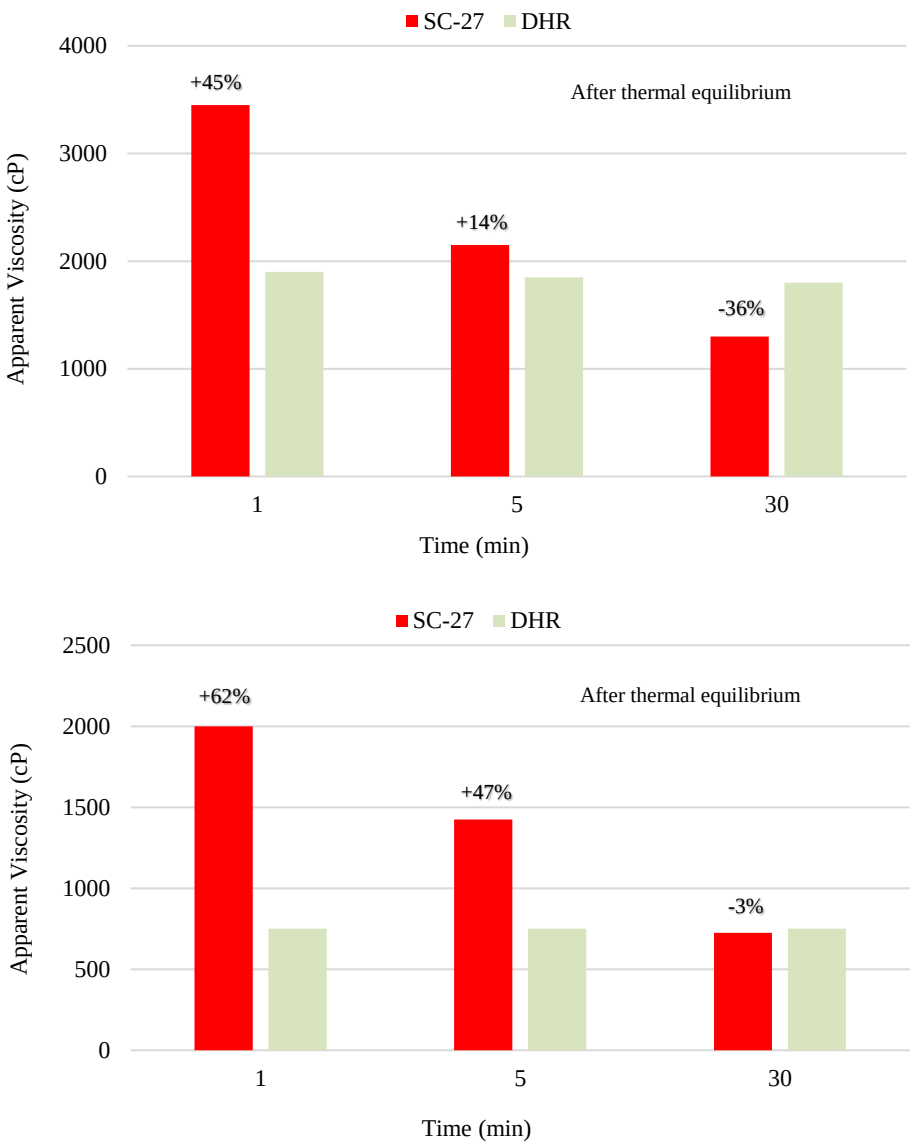

Figure 5.6 Apparent viscosity of RTR-MB (up) and SBS-MB (down) at 180 °C by at 20 Rpm. Percentages indicates the difference in terms of viscosity between the two geometries.

Table 5.2 Apparent viscosity from 120°C to 200°C of neat bitumen, CR-MB and SBS-MB by using HA viscometer at 20 Rpm

Material	Temperature ºC	SC-27 @ 20 Rpm Pa·s	DHR @ 20 Rpm Pa·s	Difference
Neat bitumen (pen 35/50)	120	1475	1564	-6.03%
	140	437	436	0.23%
	160	179	182	-1.68%
	180	88	90	-2.27%
	200	50	54	-8.00%
CR-MB	120	-	-	-
	140	7000	9591	-37.01%
	160	2625	3000	-14.29%
	180	1325	2040	-35.05%
	200	1000	1150	-15.00%
SBS-MB	120	9425	10833	-14.94%
	140	3050	3243	-6.33%
	160	1275	1414	-10.90%
	180	750	770	-2.67%
	200	375	396	-5.60%

Measurements on modified bitumens: apparent viscosity vs temperature

Table 5.2 provides a numerical assessment of the differences recorded between the reading obtained with both SC-27 and DHR. It has to be underlined that differences between the two measurements increases with the increase in heterogeneity of the materials: neat bitumen > SBS-MB > CR-MB.

In other words, using the SC-27 in standard conditions provides values of apparent viscosities that could be significantly different from those obtained with the DHR. With this investigation we are coupling the laboratory campaign with a numerical approach that could provide us with an insight of the phenomena happening inside the measuring chamber with the ambition of arriving to figure out the reasons behind this.

5.2.2. CFD simulations

Validation of the model

The CFD was configured to reproduce the whole laboratory campaign, although since both binders shows similar trend these simulations focused only on the most severe instability of the CR-MB scenario. The numerical simulations want to provide further insight of the sample instability phenomena by assessing the velocity fields, volume fraction and numerical measurements distribution within the measuring chamber. In order to use these simulations as a reliable source of information, at first a validation of the model was carried out. The validation consisted in comparing numerical measurements of the torque extrapolated from the software with those obtained from the laboratory test. Figure 5.7 and Table 5.3 show that the results obtained from the laboratory campaign and the numerical simulations. Indeed, the numerical software provides the option to plot the momentum along the impeller axis that can be easily compared with the one reported by the viscometer. Results are in good agreement, therefore validating the reliability of the numerical model.

Table 5.3 Comparison of results from laboratory campaign and numerical simulations for CR-MB at 180 °C at 5-100 Rpm

		Numerical			**Experimental**			
Device	*N (Rpm)*	*Torque (Nm)*	*Torque (%)*	*Viscosity (cP)*	*Torque (Nm)*	*Torque (%)*	*Viscosity (cP)*	*Error (%)*
Sc-27	5	3.14E-05	46.7	2189.8	2.74E-05	40.7	2007.4	8.3
	20	8.32E-05	5.8	1447.1	7.62E-05	5.3	1325	8.4
	100	2.88E-04	20.1	1040.9	3.19E-04	22.2	1110	-6.6
DHR	5	8.00E-05	5.6	2558.9	8.19E-05	5.7	2622	-2.5
	20	2.37E-04	16.5	1805.3	2.58E-04	18.0	2040	-8.7
	100	8.91E-04	62	1425.5	9.46E-04	65.8	1513.4	-6.2

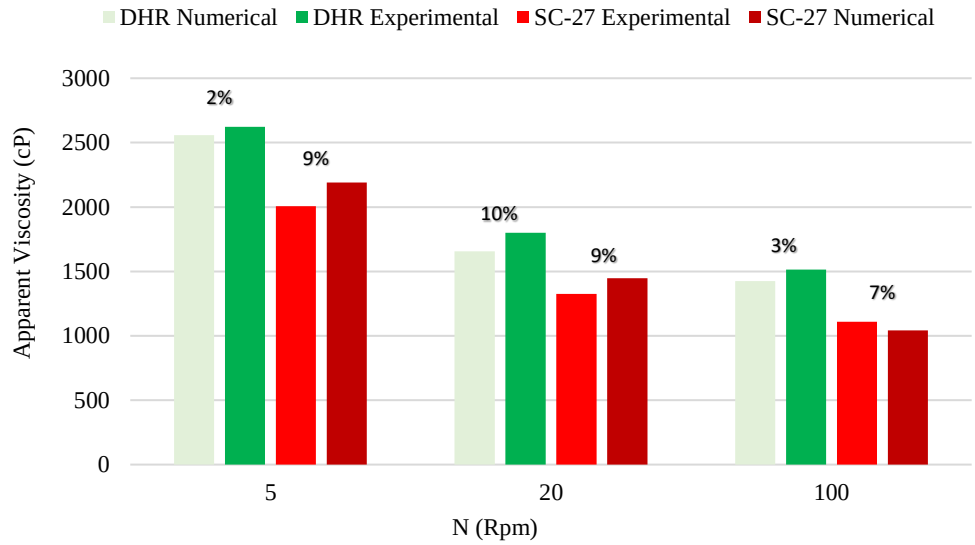

Figure 5.7 Apparent viscosity of CR-MB Vs Rpm at 180 °C obtained through laboratory campaign and numerical simulations

Indeed, the software allows to compute the moments about a specified centre, and the coordinates of the centre of pressure for selected wall zones making possible the comparison with the experimental results.

In support of this methodology, the reader should consider that rotational viscometers measure the viscosity by using a mechanical system to impose a controlled force or displacement onto a sample, hence the torque is the actual quantity directly measured during rotational tests. Once the model was considered able to reproduce the complex scenarios of rotational test even of complex binders, several investigations have been carried out. Each of them had the aim of providing a visual understanding of the phenomena happening within the measuring chamber while rotational measurements are performed. The next paragraphs offer the details of these simulations run only on the CR-MB at 180 °C at 20 Rpm, the binder with the highest level of heterogeneity.

Velocity field distribution within the chamber

A study of the velocity field distribution within the sample (Figure 5.8) highlighted that the DHR shape allows a better distribution of the velocity flow field thanks to the pumping effect induced by the axial force. Indeed, the inner blades push the fluid upwards while the outer push the fluid downward allowing a continuous recirculation of the flow. Instead, the standard concentric spindle due to its geometry creates low velocity field at the top and the bottom of the tube, while all the stresses are distributed around the vertical walls of the spindle. This confirms that the vertical film of sample sandwiched along the container and the spindle is the only portion tested during the measurements. Also, there is no axial pumping but only tangential forces that do not allow creating a convective flow. Phenomena like phase separation, sedimentation and agglomeration may occur due to those issues.

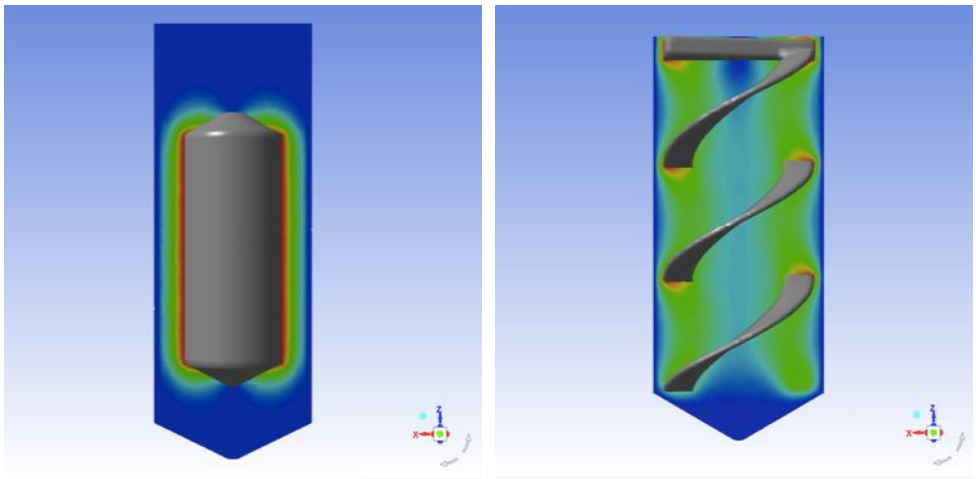

Figure 5.8 Numerical velocity field distribution of RTR-MB at 180 °C at 20 Rpm, Brookfield spindle SC-27 (left), DHR (right)

Apparent viscosity measurements distribution within the chamber

Complementary to the previous simulations, this section presents an analysis of the viscosity measurements made directly using the numerical model at different height of the container: top, middle and bottom thirds (Figure 5.9). Fluent allows to set a line or a point within the analysed domain and report the desired proprieties, viscosity in this case. The figure also provides the comparison with the experimental data obtained within the laboratory campaign (last column). As a result, for the SC-27 high values have been found in the top and the bottom region, while in the middle region due to the tangential forces the values of viscosity reported are lower. This is in line to what was shown in the previous section showing that velocity fields are concentrated in the middle section; hence the measured torque will strongly depend on the tangential forces in this section.

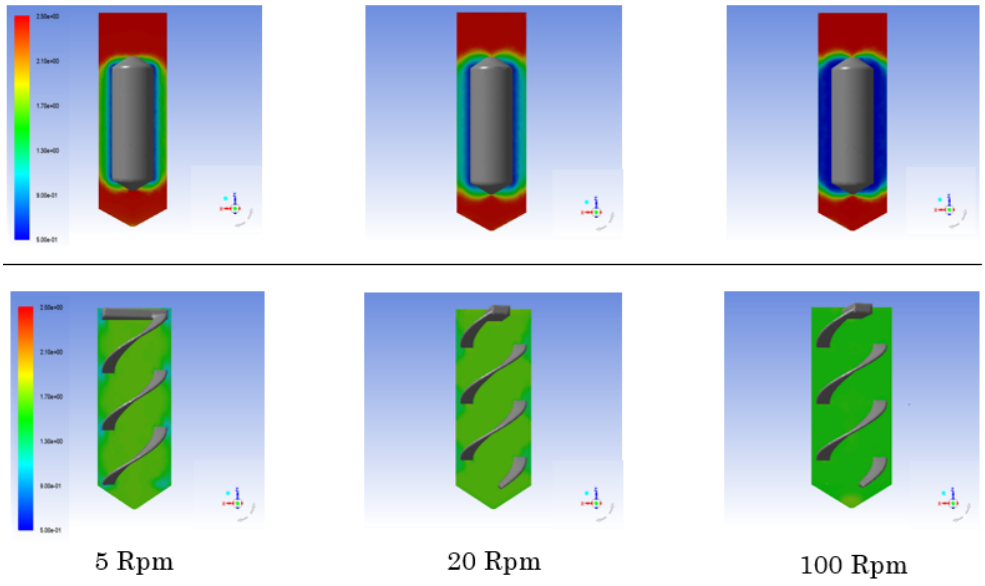

Figure 5.9 Numerical apparent viscosity distribution of RTR-MB at 180°C at 5-100 Rpm, on the top the SC-27 and on the bottom the DHR

In other words, as shown in Figure 5.9 and Table 5.4 , the values of viscosity reported by the instrument when the SC-27 is used, are related to the sample in the middle region. With the DHR the scenario is simplified. In fact, both Figure 5.8 and Figure 5.9 show that DHR is able to offer a better mixing of the sample, which in turns provide a more homogeneous distribution of the velocity fields and viscosity readings over the entire length of the container.

Evaluating the effect of time on sample stability

On the basis of the lesson learned in the previous section, the simulations in Figure 5.10 focused on understanding whether the viscosity measurements can be affected also by lack of sample stability over time.

The idea was to reproduce the same methodology used for the experimental campaign, but with the additional feature of obtaining visual data by plotting the volume fractions distribution within the container and over time. As a result, in both scenarios, seems evident that within the thermal equilibrium (from 0 to 15 min), the particles tend to settle down to the bottom due to the gravity force. From 15 to 45, min the viscometer motor is turned on and the impellers start rotating at 20 Rpm. In this phase, the SC-27 is not able to keep the particles evenly distributed within the tube leading to a high concentration of particles at the bottom. It is also important to observe that the fluid along the clearance between the wall and spindle - which as discussed seems to be the actual sample tested with the SC-27 - is heterogeneous for the entire length of the test. Instead, once the DHR starts rotating, it assures an evenly distribution of the particles within few minutes. For this reason, the value reported by the viscometer using a standard geometry cannot consider realistic. On the other hand, the DHR allows testing a well-distributed sample and this is surely contributing in guaranteeing a stable trend of results, as observed during the laboratory campaign.

Table 5.4 Numerical apparent viscosity distribution of CR-MB at 180°C at 5-100 Rpm

Device	*N (Rpm)*	*Viscosity Top (cP)*	*Viscosity Centre (cP)*	*Viscosity Bottom (cP)*	*Viscosity Exp (cP)*
Sc-27	5	2886	2046	3414	1907.4
	20	2737	1352	2836	1325
	100	1645	995	1666	1110
DHR	5	2537	2602	2649	2622
	20	1835	1803	1851	2040
	100	1419	1409	1437	1513.4

At last, simulations were run to understand whether the sample stability can be connected also the nature of the sample itself. In other words, simulations were run without the geometry in the tube for 45 min (Figure 5.11). Results showed that there is a high level of instability within the sample due to the particles settling down for the gravity. As a result, sample of RTR-MB lack of sample stability over time, hence misleading results can be obtained if no agitation is provided during rotational tests.

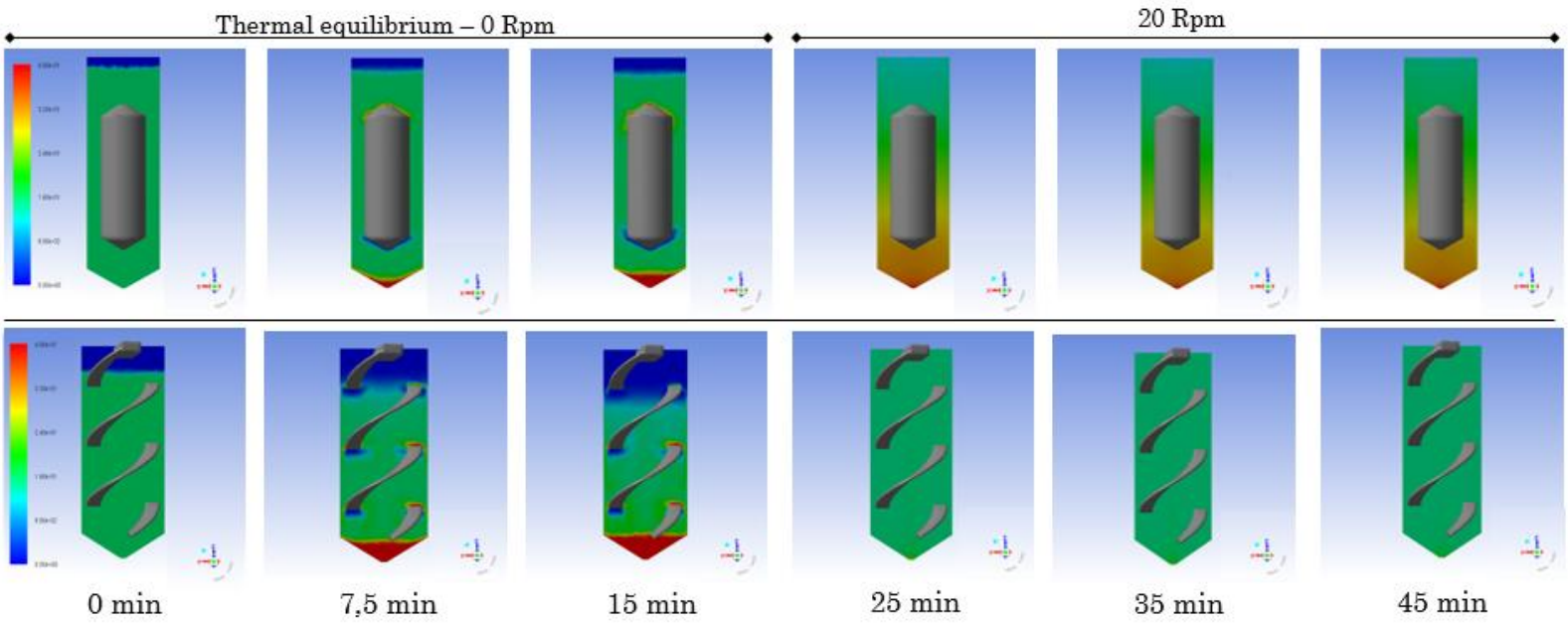

Figure 5.10 Effect of time on particles distribution of RTR-MB at 180 °C by numerical model, rotational speed 20 Rpm

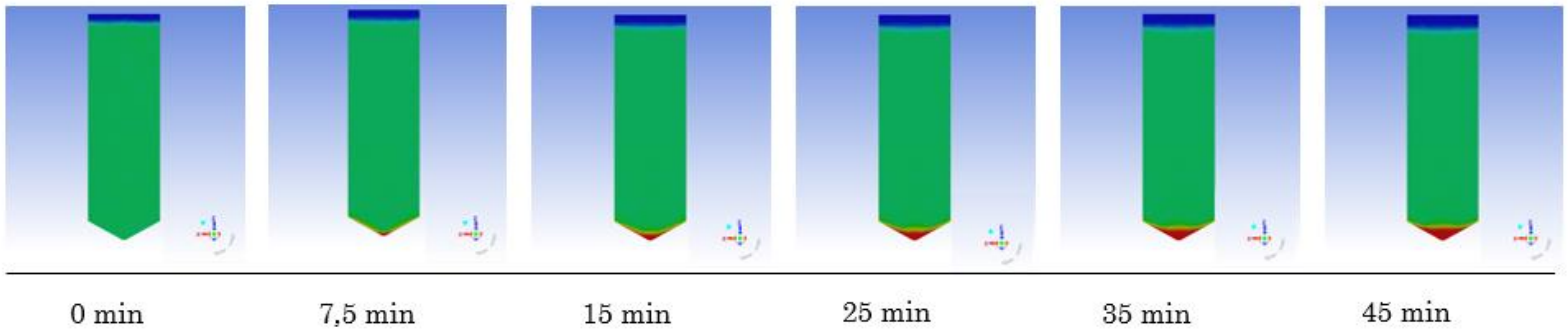

Figure 5.11 Sample stability of RTR-MB at 180°C over time, by numerical model and with no geometry within the sample

5.3. Summary of results

This investigation offers an innovative combined laboratory-based and computational approach aimed at understanding whether standard testing geometry for rotational tests are suitable for measuring high-temperature rotational viscosity of modified binders. The study also presents a solution to overcome some of the presented issues and this consists in changing the standard coaxial cylinder testing setup by substituting the standard spindle (SC-27) with the dual helical ribbon (DHR) developed within this thesis framework. After a careful analysis of the obtained results the following conclusions can be drawn

The laboratory campaign provided evidence that modified bitumens do provide an un-stable trend of measurements during the testing with SC-27. The final values of apparent viscosities can be significantly different from those obtained with the DHR, which instead provided stable readings already after few minutes.

The computational platform clarified that highly heterogeneous bituminous blends undergo sample instability already during thermal equilibrium and simply because they are stored at high temperatures in a vertical container. The lack of sample stability is not reversed when SC-27 is used at 20 Rpm. In this testing configuration, higher rotational speed (100 Rpm) might help decreasing but not eliminating the issue. The DHR instead is able to ensure sample stability even at low speed (5 Rpm). This is due to an axial pumping induced by the rotating impeller within the sample.

The laboratory campaign provided evidence that increasing the complexity of the bituminous blends is directly proportional to an increase in misleading readings of apparent viscosity of the blends, up to almost 40%.

This trend is mainly governed by the material type rather than the temperatures, despite the latter is directly linked to differential values of densities and viscosities of the blend's components.

The numerical analysis provided the additional opportunity to have readings over three thirds of the vertical container. Results, which authors judge sufficiently close to the experimental ones, allow understanding that using SC-27 provides complex results which are mainly governed by the middle region. On the other hand, the viscosity results over the length of the tube are quite uniform when the DHR is used as impeller.

Hence, as general conclusion can be stated that bitumen technologist should consider sample stability while performing high-temperature viscosity measurements of HBBs with the standard coaxial cylinder setup. The DHR impeller offers a solution to ensure sample stability and considering its direct correlation with the resulting viscosity readings, it is recommended to consider this solution within rheological characterization of HBBs at high-service temperatures.

Future recommendations can lie in using a similar approach to explore a wider range of modified binders and impellers. Also, this type of combined laboratory/computational approach provides new set of data and visual aids otherwise difficult to obtain, hence has great potential towards the definition of virtual laboratory testing protocols and should be further investigated possibly with another testing setup.

In the next chapter, an improved laboratory application to perform real-time monitoring of the rheological properties of CR-MBs during manufacturing and storage is presented.

CHAPTER 6. QUALITY CONTROL OF CM-MBs VIA LABORATORY SIMULATION OF FULL-SCALE MANUFACTURING AND HOT STORAGE

6. Quality control of CR-MBs via laboratory simulation of full-scale manufacturing and hot storage.

As widely introduced in section 2.2.3, crumb rubber modified bitumens (CR-MB) are studied by rheologists aimed to produce mixtures with enhanced properties compared to conventional ones. Although these materials are able to improve the performance of the asphalt pavements (e.g. resistance to cracking, noise reduction) their rheological characterisation is still challenging due to their complex structure. Indeed, during material manufacturing and hot storage bitumen technologist have to cope with several variables such as temperature, time, modifier, and storage stability that may affect the quality of the resultant product making their characterisation challenging.

This chapter aims to introduce an improved quality-control procedure for CR-MBs aiming at assessing their rheological properties development during a laboratory simulation of their manufacturing and hot storage. In fact, maintaining sample stability allows achieving the target viscosity for the CR-MBs after both manufacturing and storage. Thus, a laboratory procedure permitting to predict the viscosity changes during storage would allow evaluating the appropriate conditions during hot storage.

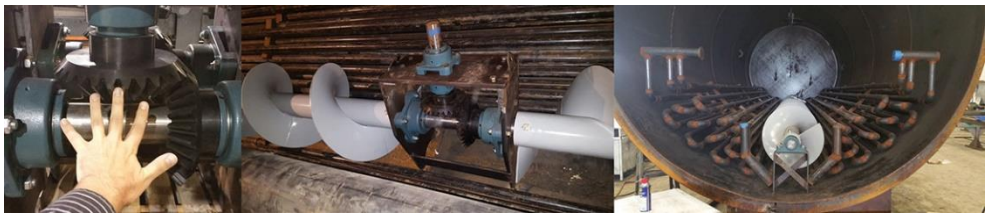

Figure 6.1 An asphalt Rubber Reaction Tanks mounting a helical screw to promote the bitumen-rubber interaction adopted from (D&H Equipment, 2019)

The procedure developed in this chapter consists in adapting a rotational viscometer to act as a low shear mixer with the DHR aiming to resemble an agitating tank (Figure 6.1). These tanks are usually needed in the production of CR-MB and many other rubber-modified asphalts products. After passing through a blending system, the product is stored and reacted inside the tank (typically for 30 minutes up to 1 hour). Aggressive agitation inside the tank promotes a uniform reaction, ensures the particles remains suspended, and produces a consistent blend. During this time, the rubber particles swell as they absorb some of the asphaltenes while simultaneously releasing some of their lighter oils into the asphalt – this reaction provides the many beneficial properties associated with these HBBs.

This investigation introduces a similar procedure but developed in a laboratory environment. The reason to doing that is to reproduce in a laboratory scale the set-up of a full-scale production and storage aiming to provide bitumen technologists with practical recommendations and advantages in terms of cost and time production.

As mentioned in section 2.3, researchers have been used this procedure to evaluate the change in material rheology by reducing the material and time consumption (Celauro *et al.*, 2012; Lo Presti *et al.*, 2014; Subhy *et al.*, 2015). However, the lack of a suitable mixing rheometry did not allowed to proper develop this procedure. The present investigation proposes a procedure with two further innovative elements:

1. It introduces the DHR, developed to increases mixing performance of impellers while guaranteeing reliable viscosity measurements.
2. It specifies a procedure allowing a real-time monitoring of the CRM binders viscosity during both manufacturing and hot storage phases.

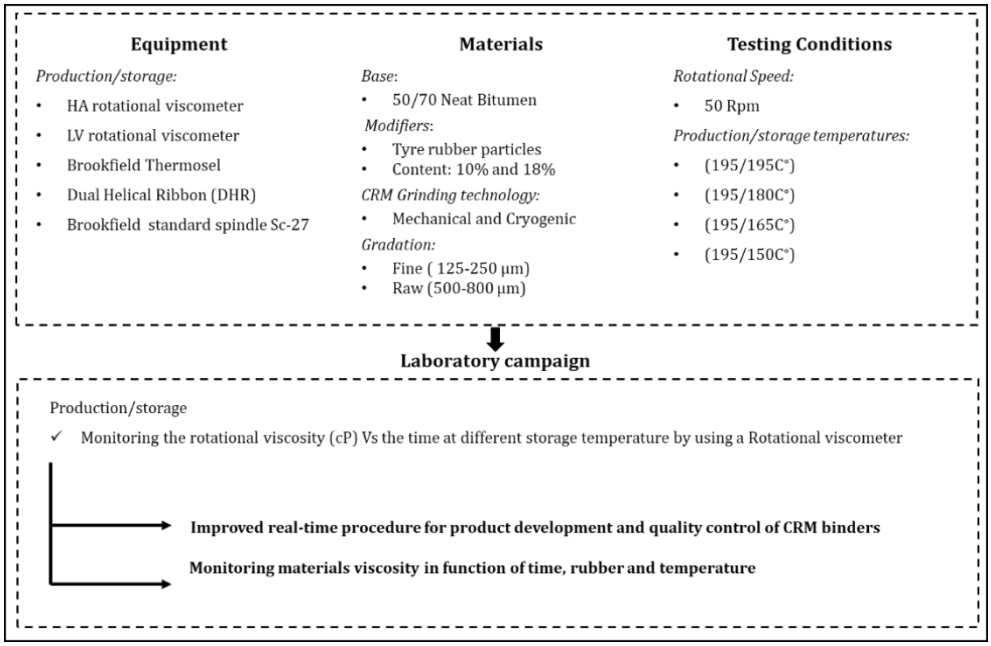

Figure 6.2 Experimental programme

The effect of the processing temperature, rubber size, concentration and grinding technology has been investigated to evaluate the impact on the rotational viscosity during production and storage. As outcomes, a set of practical conclusions regarding the influence of the type of rubber as well as the influence of temperature during storage, are provided to rheologists.

6.1. Experimental programme

The experimental programme presented in Figure 6.2 was designed to assess the processing variables that affect the CR-MBs rheology during the product development and hot storage. Eight different binders were included in the experimental programme made up from the combination of different crumb rubber contents, gradations and grinding technologies. Four modified binders were produced by adding 10% and 18% by bitumen weight of fine crumb rubber size (125-250µ) in 50/70 grade bitumen and four by adding 10 and 18% by bitumen weight of raw crumb rubber size (125-800µ).

The experimental programme was carried out by using both ambient and cryogenic crumb rubber modifier. The laboratory simulation for the manufacturing and agitated storage of CR-MBs was achieved by producing the blends at 195°C and simulating the storage at four temperature (195°C, 180°C, 165°C, 150°C). The reported results were obtained as average of three replicates each. Two Brookfield DV-II PRO Digital Viscometer were used: a low torque (LV model) and high torque (HA model). The two viscometers differ for the viscosity measurements range. The LV model is designed for low viscosity fluids (100% torque = 673.7 dyne cm), while the HA model is more appropriate for medium–high viscous fluid (100% torque = 14,374 dyne cm). Torque measurement accuracy specified by manufacturer is 1% of the full-scale range.

6.1.1. Real-time monitoring of CR-MB's properties during manufacturing and hot storage

Here is the laboratory procedures used in this study:

- The manufacturing process is simulated by using a viscometer with a cup and bob testing geometry and the Dual Helical Ribbon (DHR) in place of more conventional spindles (i.e. SC-27).
- Manufacturing of CR-MB is performed at 50 Rpm. This speed is not representative of in-field production and it was selected since it is adequate to ensures sample stability. The value is maintained constant to prevent potential complications due to the shear thinning nature of CR-MBs.
- Once that the viscosity reached his peak, the simulation of the hot storage is performed by changing temperature of the Thermosel, when required. This is accomplished under the assumption of storing the CR-MB in an agitated tank with a rotational speed of 50 Rpm

- The monitoring of the hot storage process is extended for a minimum of 8 hours. The test could be protracted to simulate longer storing period (i.e. 24h, 48h), but for laboratory reasons 8 hours were considered sufficient.
- The impact of storage temperatures can be studied by modifying the temperature setting of the Thermosel and monitoring the change in viscosity.
- This procedure can be used for any rotational viscometer equipped with a DHR.
- Through the real-time monitoring five parameters that can support technologists to optimise manufacturing and storage conditions are produced

These five parameters are:

1. The swelling extent, that expresses the time needed to achieve the maximum viscosity at the production temperature.
2. The swelling rate, which is defined as the rate of viscosity gain over the time and determined by the arithmetic average of tangents ($\partial v/\partial \tau$) of the viscosity progression curves from the start of the production up to the viscosity peak;
3. The maximum viscosity, which is the peak of the viscosity reported at the end of the production phase and/or at the beginning of the storage period, after the storage temperature has been reached.
4. The dissolution rate, which represents the decrease in viscosity over the time and is calculated by taking the slope of viscosity progression curves after reaching the peak viscosity. It offers information regarding the viscosity lost during the storage.
5. Final viscosity, which is the viscosity value at the end of the storage period.

Figure 6.3 The laboratory set-up comprising the Brookfield viscometer and thermosel used to real-time monitoring the CRM binders

The next section shows a qualitative evaluation of the mixing performance between the SC-27 and the DHR undertaken preliminary in order to show the importance of using the novel geometry for the suggested procedure, as well as providing an example of the results obtainable with a real-time monitoring of CR-MB manufacturing and storage.

6.1.2. Qualitative assessment of the proposed procedure

Figure 6.4 provides the viscosity trend of a laboratory simulation of CR-MB manufacturing produced by mixing a 50/70 pen base bitumen with 18% by bitumen weight of raw crumb rubber size. To complete the process a time of 360 min has been required. The parameters previously introduced in section 6.1.1 are shown in the trend viscosity-time, all these parameters characterize the evolution of a CR-MB during production. First, the binder was manufactured at 177.5°C, by using both the SC-27 and the DHR. Then, the manufacturing process was completed once the peak viscosity was achieved. After, viscosity measurements were recorded for 5 hours by performing a simulation of hot storage at the same temperature.

The crumb rubber modifier is progressively added within 5 min, only when using the SC-27, a rise in viscosity is followed by a drastic drop up to a more realistic trend of measurements. This is explained by the need of the operator to move up and down the spindle to guarantee an even dispersion of rubber particles within the bituminous matrix. After that the SC-27 reports a build-up of viscosity measurements characteristic of a swelling process.

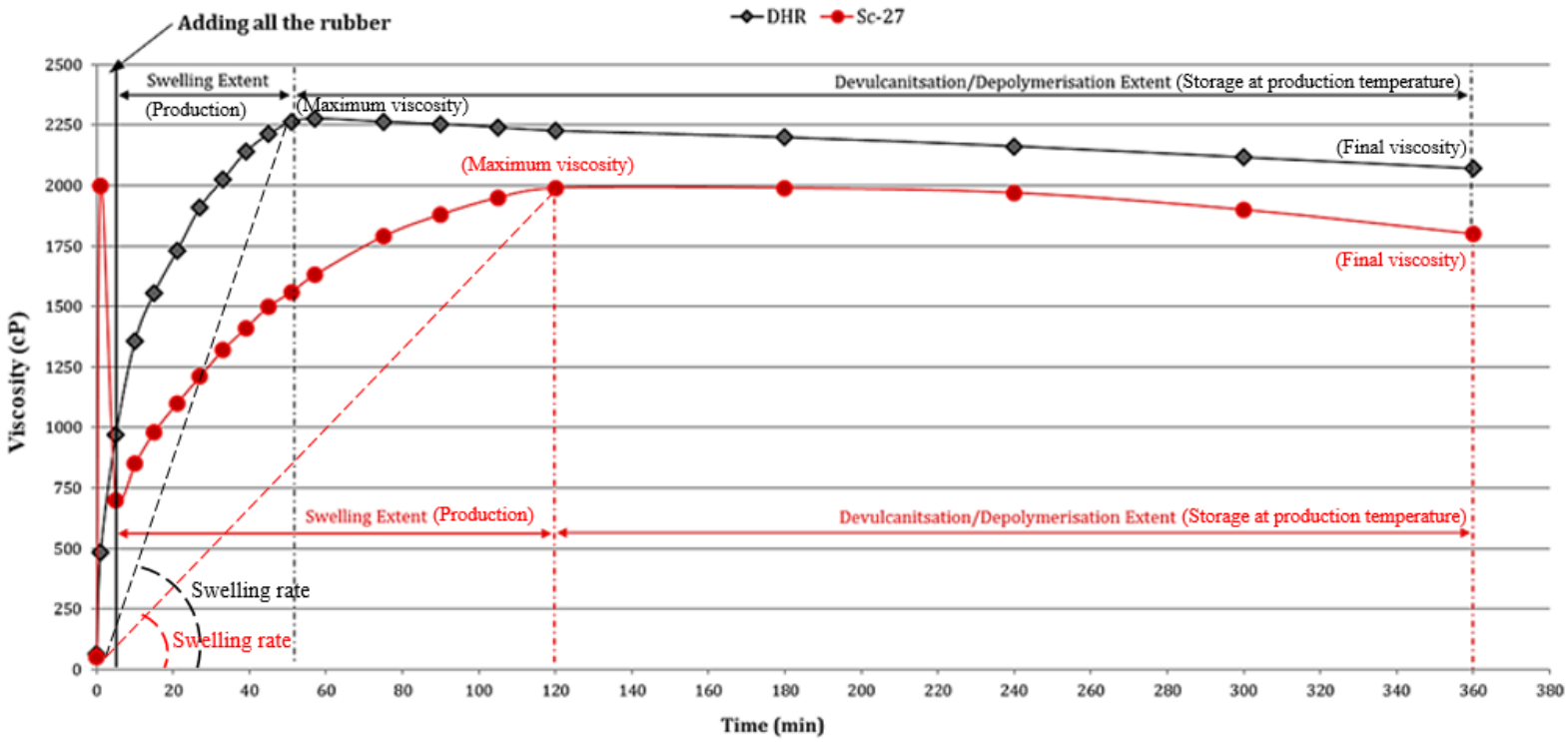

Figure 6.4 Real-time monitoring of the manufacturing stage (177.5 °C, 50 Rpm 18% ambient 125-800 µm CRM).

The increasing in viscosity is due to the rubber particles swelling which in turn results in a reduced distance between the rubber particles as well as stiffening of the binder by lowering the oily fractions of the bitumen (adsorbed by the rubber particles). At the end of the swelling process the rubber particles start to devulcanize/depolymerise leading to a decreasing in viscosity (Abdelrahman *et al.*, 1999; Subhy *et al.*, 2016).

The SC-27 recorded lower values of viscosity along the time, the reason behind that is due also to the spindle shape. Indeed, as proved in previous sections (section 3.3.2 and 5.2.2) the cylindrical geometry creates low velocity field at the top and the bottom of the tube, while all the stresses are distributed around the vertical walls of the spindle. Also, there is no axial pumping but only tangential forces that do not allow creating a convective flow leading to poor mix performance of the device. As a consequence, the sample stability is compromised, and the rubber-bitumen interaction is strongly affected.

Instead, using the DHR ensures proper mixing of the binder, allowing a smooth curve of viscosity readings during the swelling and does not require the involvement of the operator. Furthermore, the swelling process appears to perform faster and to reach a higher peak value that is an indication of an enhanced interaction between bitumen and the crumb rubber modifier. On this regard, Table 6.1 gives a quantitative evaluation of the parameters used to compare the simulation performed by using both SC-27 and DHR and shown in Figure 6.4.

Table 6.1 Quantitative parameters associated with the interaction process.

	DHR	***SC-27***
Swelling Extent (min)	51	120
Swelling Rate (cP/min)	46.9	18.5
Maximum Viscosity (cP)	2263	1990
Dissolution rate (cP/min)	0.8	1.1
Final Viscosity (cP)	2070	1800

Table 6.1 shows a quantitative comparison of the results displayed in Figure 6.4 between the SC-27 and the DHR.

Furthermore, to provide further evidence about the different interaction obtained by using the SC-27 and the DHR, at the end of the tests, the sample tubes were poured to allow a qualitative evaluation of the interaction rubber-bitumen by using the two different geometries (Figure 6.5).

Figure 6.5 provides a clear picture about the difference in terms of system heterogeneity. The binder produced by using the SC-27 shows particles agglomeration that certainly affects the viscometer measurements while the DHR provides a final binder where the rubber is visibly better dissolved, presenting an aspect comparable to that of industrial scale CR-MBs. Finally, Figure 6.6 shows SEM images (x50) of the binders ‘surface for both the samples. The binder manufactured by using the DHR shows a smother surface than the one manufactured with the SC-27, indicating that using the DHR promotes an enhanced interaction between rubber and bitumen.

Based on these observations, the DHR results to be well suited to perform quality-control of CR-MBs in laboratory.

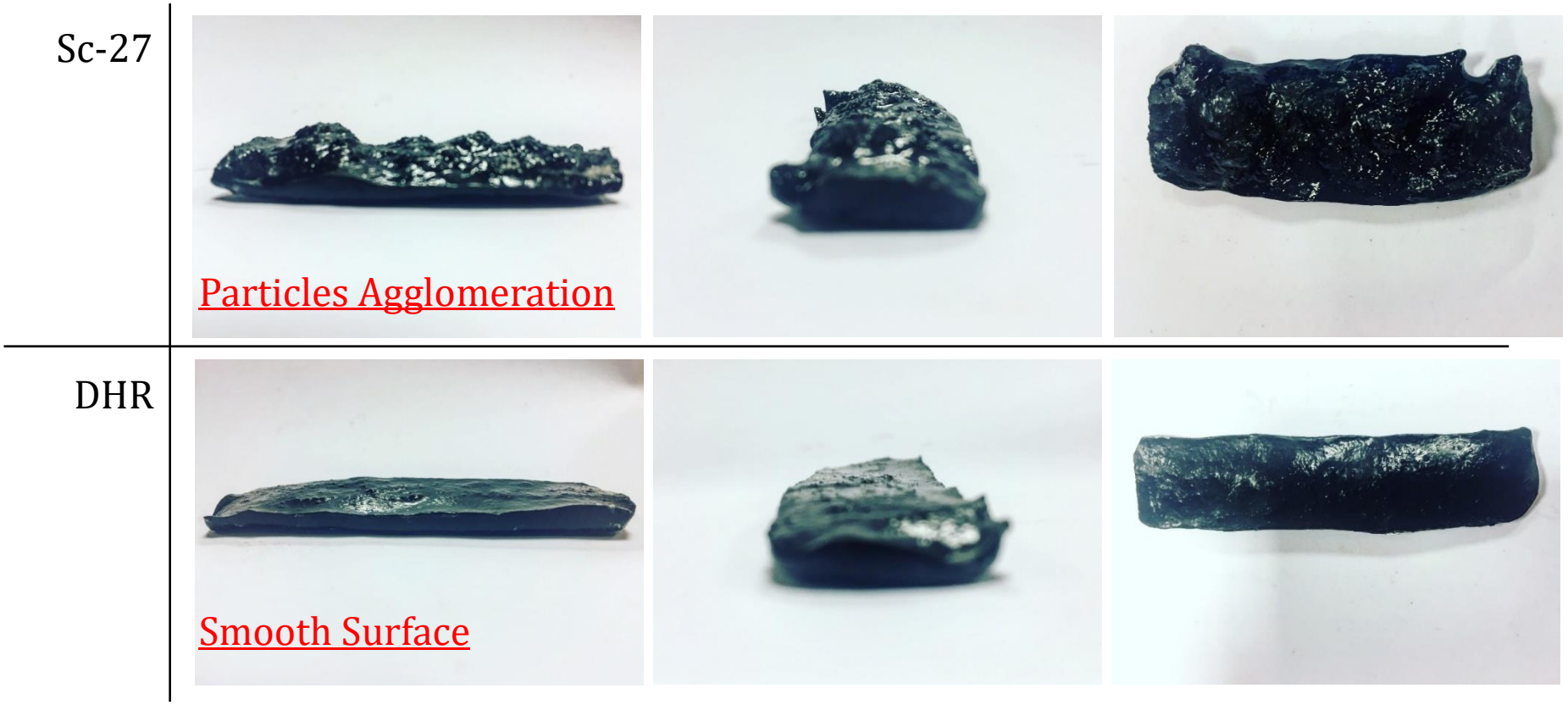

Figure 6.5 Qualitative comparison of testing samples poured after low shear mixing production using different geometries

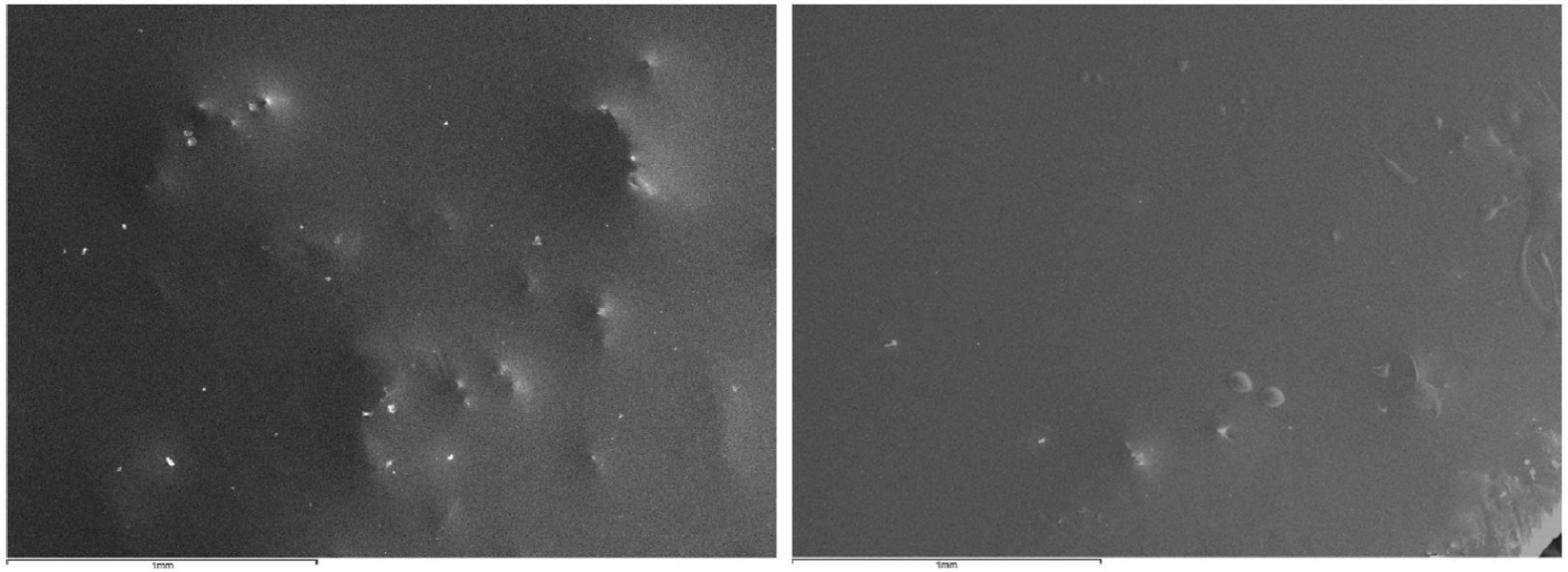

Figure 6.6 SEM images (x50) of the samples processed with SC-27 and DHR, respectively.

6.2. Results

The experimental programme was tailored to simulate the binder manufacturing as well as the storage stage under different temperatures. The aim of doing that was to evaluate the impact of different processing conditions on the viscosity trend.

Eight different materials were tested as a result of blending CR-MBs having different crumb rubber modified content (10-18%) size (raw 125-800 µm and fine 125-250 µm) and grinding technology (ambient and cryogenic) for a total time (production + storage) of 480 min (Figure 6.2). The real-time monitoring procedure was performed for both manufacturing and storage process as defined in section 6.2.1. First, binders were manufactured at 195°C with the DHR, then once the peak viscosity was achieved, the Thermosel temperature was decreased and the simulation of the hot storage phase at different storage temperatures performed.

To provide a comparative evaluation of the real-time monitoring of the CR-MB's storage stability, the results are recapitulated in Table 6.2. Therefore, to better study the trends observed, results are also plotted in Figure 6.7 to Figure 6.19 and examined in the next sections. As a preliminary result, from the manufacturing stage (Figure 6.7), it can be emphasised that it is clear that higher crumb rubber content needs further time to achieve the peak viscosity at production temperature of 195°C. Results provided a good agreement with the general rules usually applied at industrial scale where the time to complete the swelling process is 60 minutes for high crumb rubber content. The time decreases to 45 minutes when lower content of rubber is used.

Table 6.2 Quantitative assessment of the real-time monitoring exercise

Particle Content	*Grinding Tech*	*Particles size*	*Production Temp (ºC)*	*Swelling Extent (minutes)*	*Storage Temp (ºC)*	*Initial Storage Viscosity (cP)*	*Dissolution Rate (%)*	*Final Storage Viscosity (cP)*
10%	Ambient	Raw	195	45	195	276	33	184
					180	418	28	276
					165	662	13	602
					150	1002	9	910
		Fine	195	39	195	211	33	137
					180	349	25	262
					165	616	10	552
					150	818	10	740
	Cryogenic	Raw	195	39	195	179	13	156
					180	326	7	312
					165	547	4	529
					150	938	2	915
		Fine	195	33	195	151	12	133
					180	234	6	220
					165	427	5	404
					150	763	3	745
18%	Ambient	Raw	195	63	195	1159	36	740
					180	1734	35	1140
					165	2258	26	1665
					150	3215	11	2944
		Fine	195	60	195	1209	49	611
					180	1656	23	1274
					165	2208	24	1633
					150	2994	10	2668
	Cryogenic	Raw	195	51	195	1030	21	851
					180	1527	10	1370
					165	2231	7	2070
					150	2792	5	2645
		Fine	195	45	195	1071	18	878
					180	1527	8	1412
					165	1932	7	1826
					150	2589	8	2484

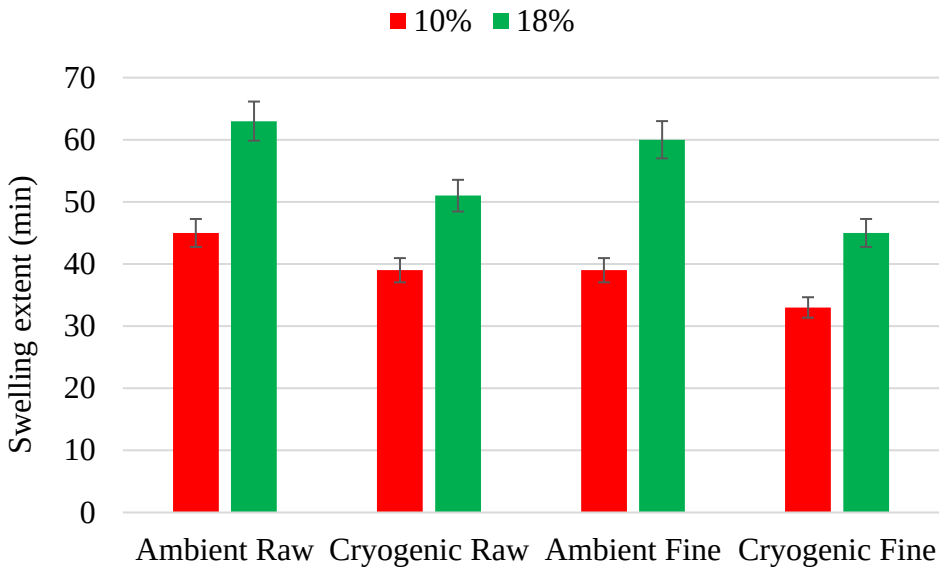

Figure 6.7 Swelling extent for ambient and cryogenic CRM.

6.2.1. Investigating the correlation between storage temperatures and initial storage viscosity

The experimental campaign considered also different grinding technology to evaluate the effect on the binder's viscosity. Considering the impact of the type of rubber on the initial storage viscosity, results shown in Figure 6.8 and Figure 6.9 confirm that CR-MBs produced using ambient rubber present higher viscosity values. The reason behind these results can be explained by the grinding technology adopted. The cryogenic technology produces smother particles with lower surface area compared to the ambient ones. As a consequence, the rubber-bitumen interaction is reduced when smoother particles are used, consequently the final mixture shows worse elastic properties compared to the ambient technology (Thodesen *et al.*, 2009). Therefore, the results presented in Figure 6.8 and Figure 6.9 can be explained by the larger specific surface of the ambient rubber that leads the rubber to absorb more oil and then to promote an enhanced swelling process.

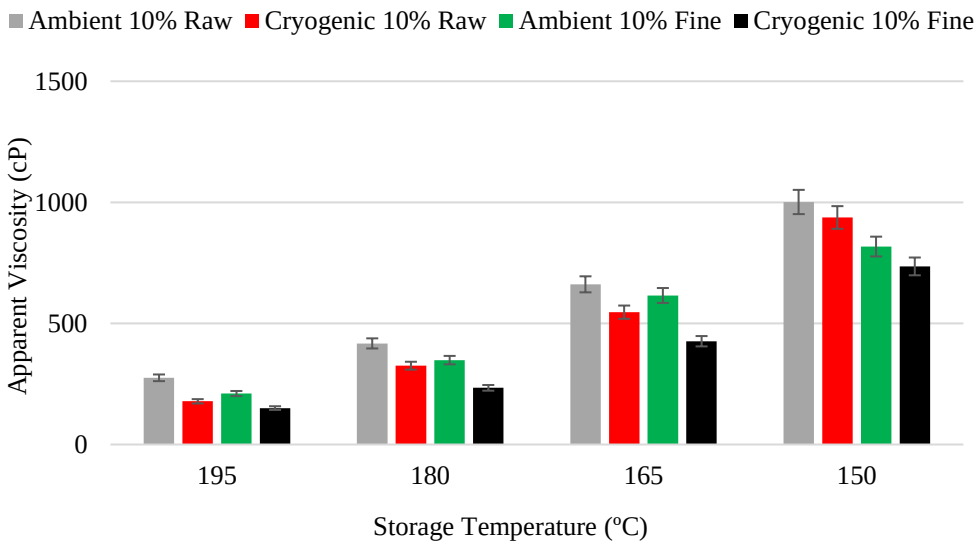

Figure 6.8 Initial storage Viscosity vs storage temperature, 10% CRM

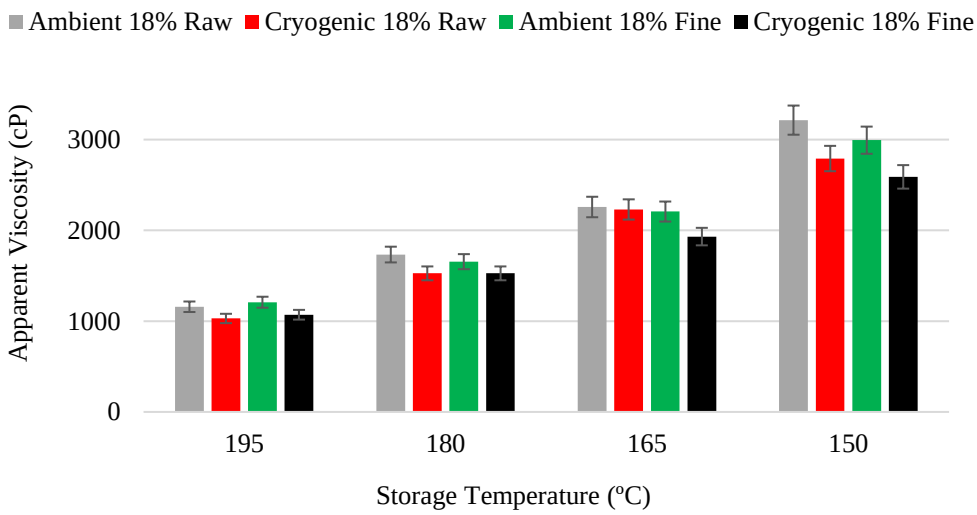

Figure 6.9 Initial storage Viscosity vs storage temperature, 18% CRM

As expected, CR-MBs with higher modifier content (18%) present higher viscosity values that when adding 10% of rubber. Nevertheless, the recorded trend of initial storage viscosity by modifying the storage temperature are similar for all the binders.

6.2.2. Investigating the relation between storage temperatures and CRM size.

This section presents a quantitative assessment (Table 6.2) of laboratory simulations performed by considering four storage temperatures (195°C, 180°C, 165°C and 150°C) and two different modifier content (10% and 18%) and size (raw and fine).

Viscosity trends over the time at different storage temperatures are shown in Figure 6.10 and Figure 6.11. The first shows the viscosity measurements of a binder produced with ambient raw crumb rubber modifier (125-800 µm), the second the viscosity trends of the blend with the fine rubber particles (125-250 µm). All the reported trends show a bump in the viscosity readings at approx. 60 minutes due to the change from the production temperature (195ºC) to the different storage temperatures.

Results show similar trend for all cases in terms of swelling extent and viscosity peak, it is evident that finer particles and lower content are easier to be digested/dissolute at 195ºC, as a consequence an increase of viscosity dissolution rate is recorded. Also, when increasing the storage temperature, the viscosity dissolution increases, while at lowest storage temperature (150°C) the material seems to be less temperature susceptible and a more stable viscosity values are recorded.

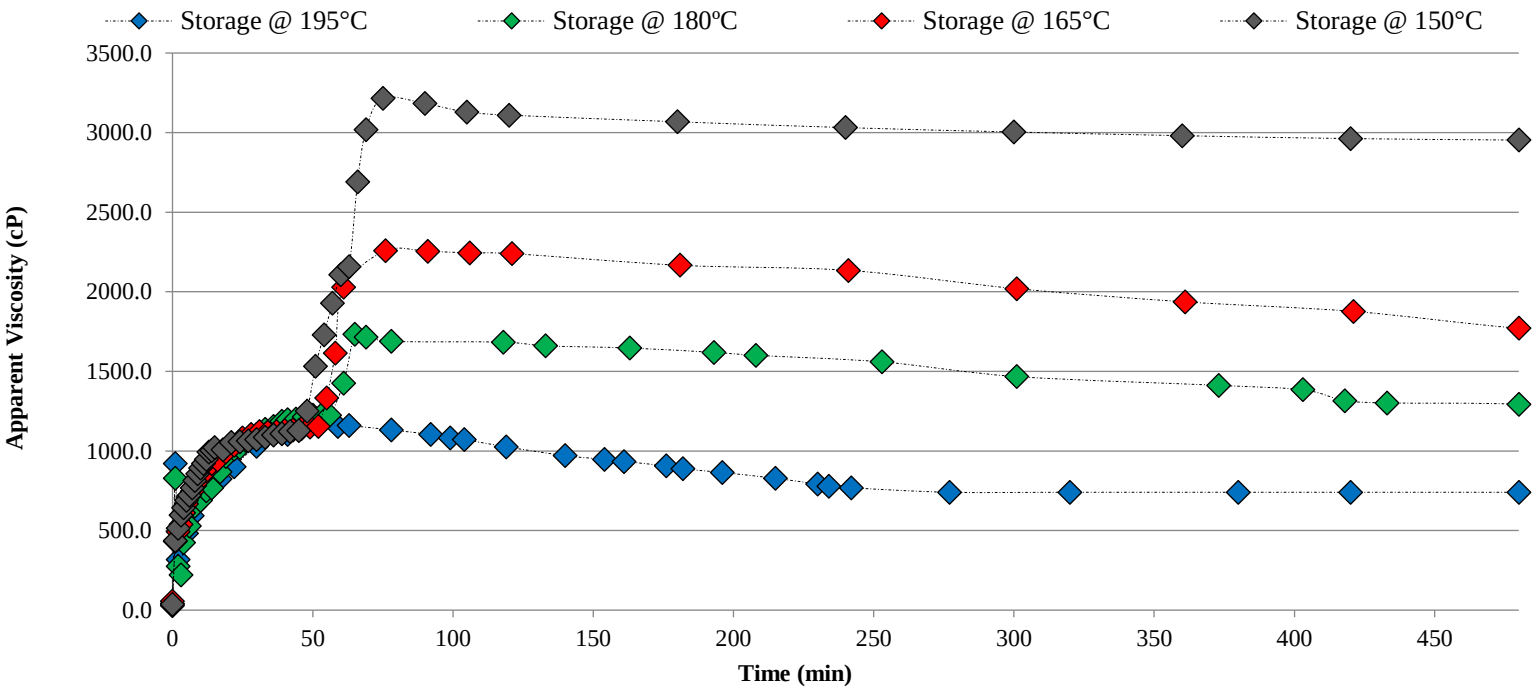

Particle Content (%)	*Grinding Tech*	*Particles size*	*Production Temp (°C)*	*Swelling Extent (min)*	*Storage Temp (°C)*	*Initial Storage Viscosity (cP)*	*Dissolution Rate (%)*	*Final Storage Viscosity (cP)*
18	Ambient	Raw	195	63	195	1159	36	740
					180	1734	35	1140
					165	2258	26	1665
					150	3215	11	2944

Figure 6.10 Viscosity evolution at different storage temperatures. 18% ambient CRM 125- 800 µm

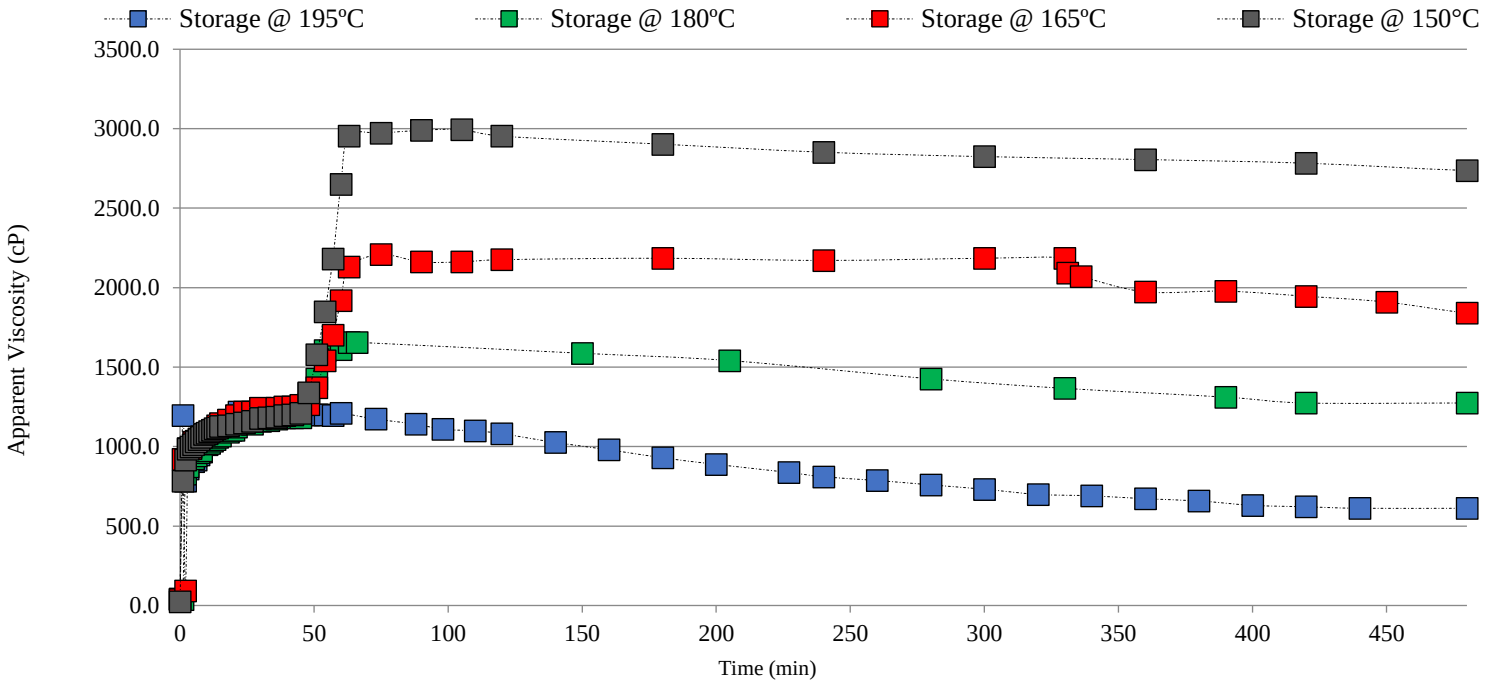

Particle Content (%)	*Grinding Tech*	*Particles size*	*Production Temp (°C)*	*Swelling Extent (min)*	*Storage Temp (°C)*	*Initial Storage Viscosity (cP)*	*Dissolution Rate (%)*	*Final Storage Viscosity (cP)*
18	Ambient	Fine	195	60	195	1209	49	611
					180	1656	23	1274
					165	2208	24	1633
					150	2994	10	2668

Figure 6.11. Viscosity evolution at different storage temperatures. 18% ambient CRM 125- 250 µm

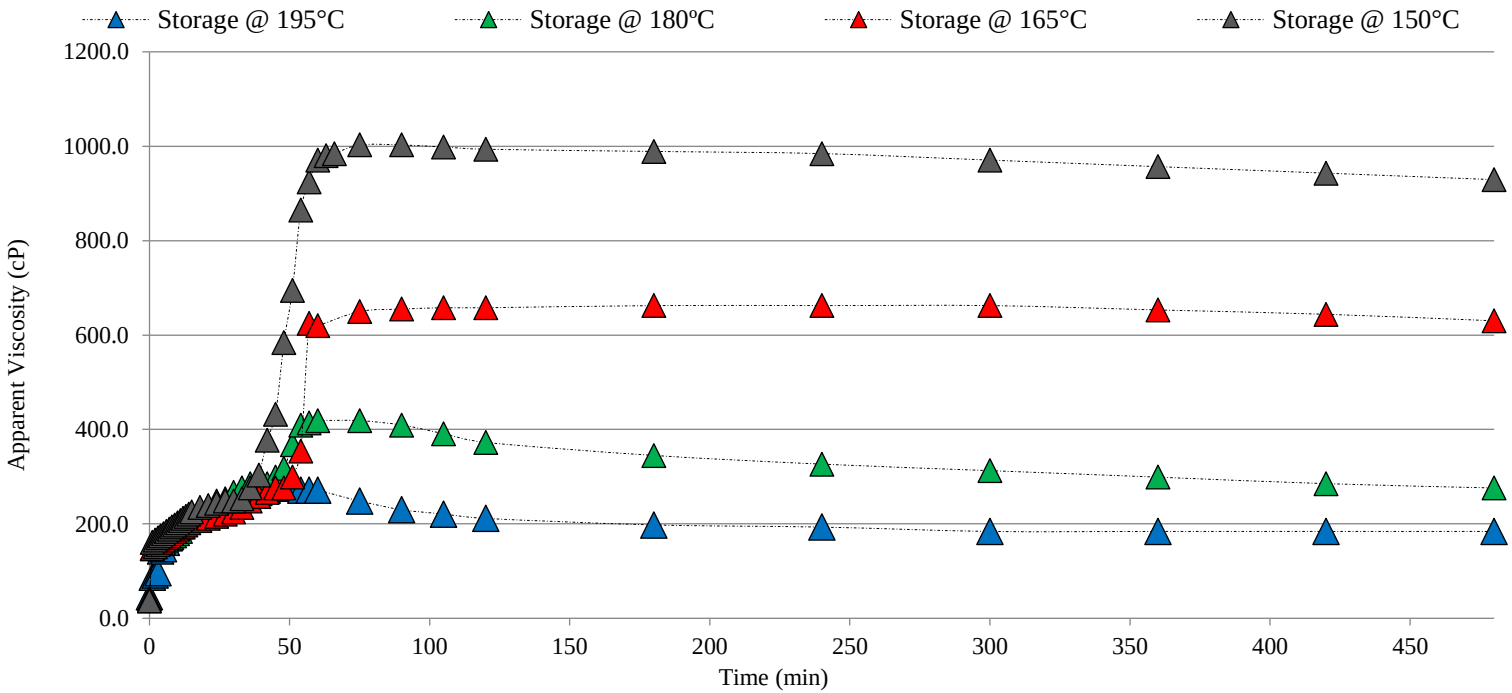

Particle Content (%)	*Grinding Tech*	*Particles size*	*Production Temp (°C)*	*Swelling Extent (minutes)*	*Storage Temp (°C)*	*Initial Storage Viscosity (cP)*	*Dissolution Rate (%)*	*Final Storage Viscosity (cP)*
10	Ambient	Raw	195	45	195	276	33	184
					180	418	28	276
					165	662	13	602
					150	1002	9	910

Figure 6.12. Viscosity evolution at different storage temperatures. 10% ambient CRM 125- 800 µm

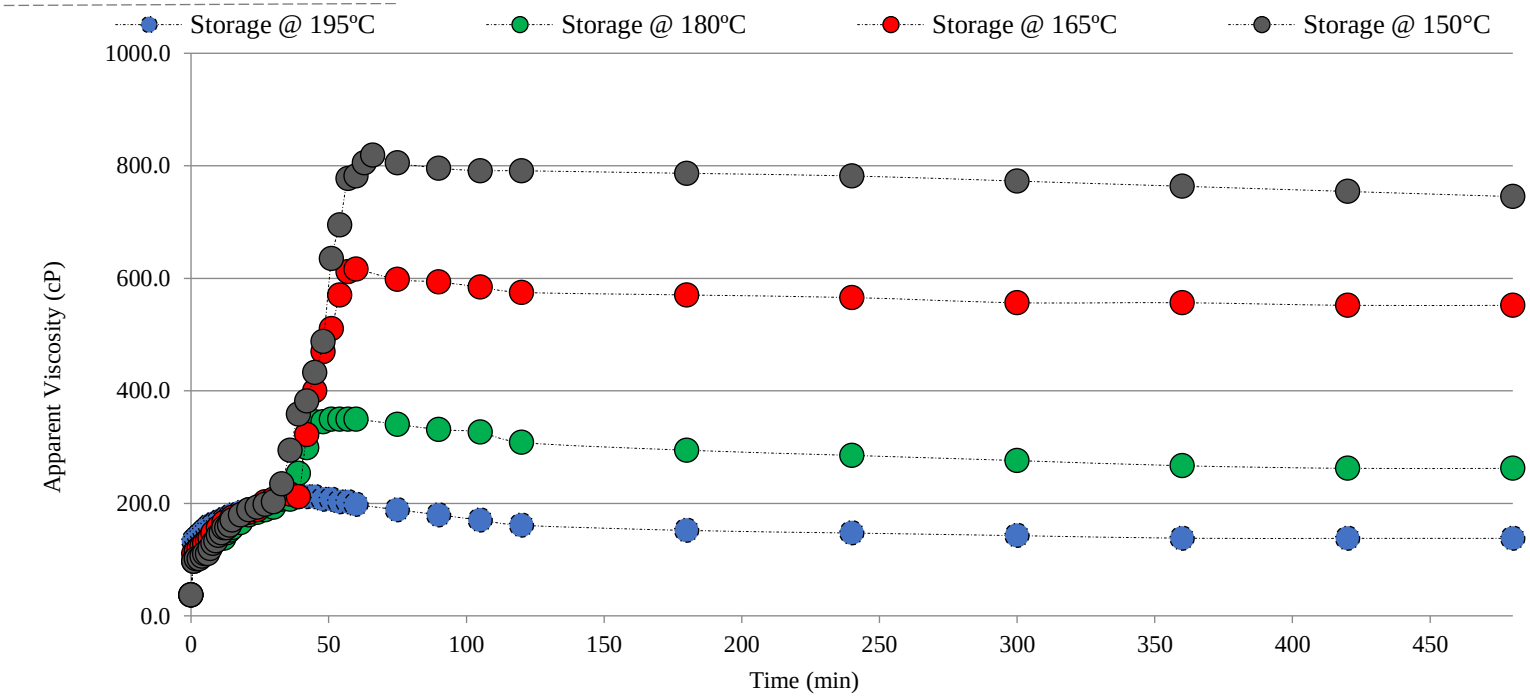

Particle Content (%)	*Grinding Tech*	*Particles size*	*Production Temp (°C)*	*Swelling Extent (minutes)*	*Storage Temp (°C)*	*Initial Storage Viscosity (cP)*	*Dissolution Rate (%)*	*Final Storage Viscosity (cP)*
10	Ambient	Fine	195	39	195	211	33	137
					180	349	25	262
					165	616	10	552
					150	818	10	740

Figure 6.13. Viscosity evolution at different storage temperatures. 10% ambient CRM 125- 250 µm

6.2.3. Investigating the relation between storage temperatures and CRM content and type

Figure 6.14 and Figure 6.15 provide a comparison of the storage stability of the blends obtained with different rubber content, respectively 10% and 18% for both raw and fine gradation. Higher modifier content (18%) leads to a higher viscosity peak at the end of the manufacturing process. Furthermore, as already mentioned in section 6.2.2, the viscosity dissolution is strongly affected by the storage temperature. Indeed, results (Table 6.2) show that the dissolution rates at 150 ºC are respectively 9 and 11% for the CR-MBs with 10 and 18% of content. Increasing the storage temperature to 180 ºC, the dissolution rates values increase to 28 (10% content) and 35% (18% content).

Regarding the grinding technology, Figure 6.16 shows that the binders produced with the cryogenic rubber present a reduced bitumen-rubber interaction. Indeed, the value of dissolution rate at 180 ºC for 18% content of cryogenic raw rubber is 10%, while with the binders produced by using the ambient rubber a value of 35% is achieved. A similar trend is recorded also at lower storage temperature, indicating once again that the rubber obtained by ambient grinding better reacts with the bitumen. For example, at a storage temperature of 150 ºC the values of dissolution rates are 5% and 11% for cryogenic and ambient, respectively. It can be said that CR-MBs manufactured with cryogenic rubber present reduced values of dissolution rates during the storage stage. Nevertheless, this section introduced few detailed examples aimed to show the method to analyse the results from the DHR. Furthermore, to provide the reader with more evidences, the next section plots all the values of dissolution rates achieved in this study to support general conclusions and recommendations aimed to preserve the quality of CR-MBs during the storage period.

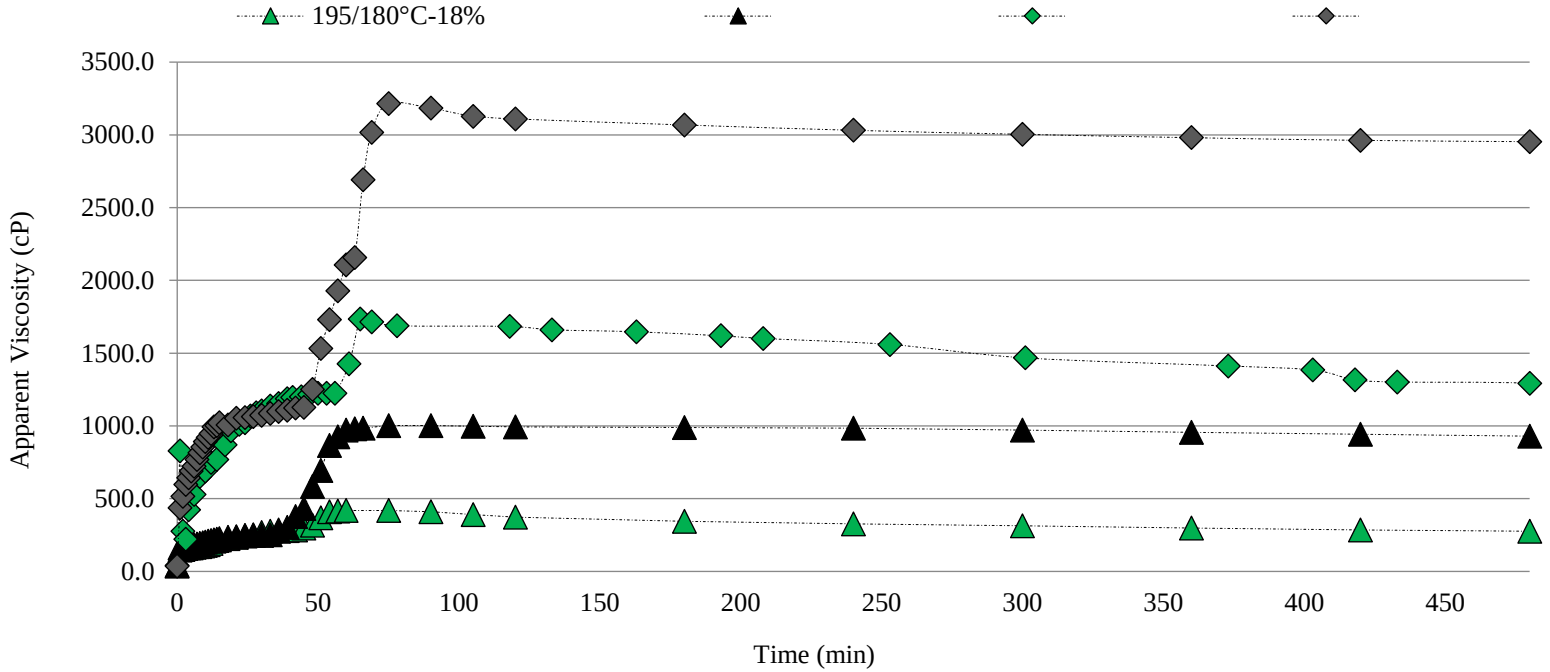

Grinding Tech	*Particles size*	*Production Temp (°C)*	*Particle Content (%)*	*Swelling Extent (min)*	*Storage Temp (°C)*	*Initial Storage Viscosity (cP)*	*Dissolution Rate (%)*	*Final Storage Viscosity (cP)*
Ambient	Raw	195	10	45	180	418	28	276
					150	1002	9	910
			18	63	180	1734	35	1140
					150	3215	11	2944

Figure 6.14 Evolution of viscosity at different concentration of ambient CRM 125-800 µm.

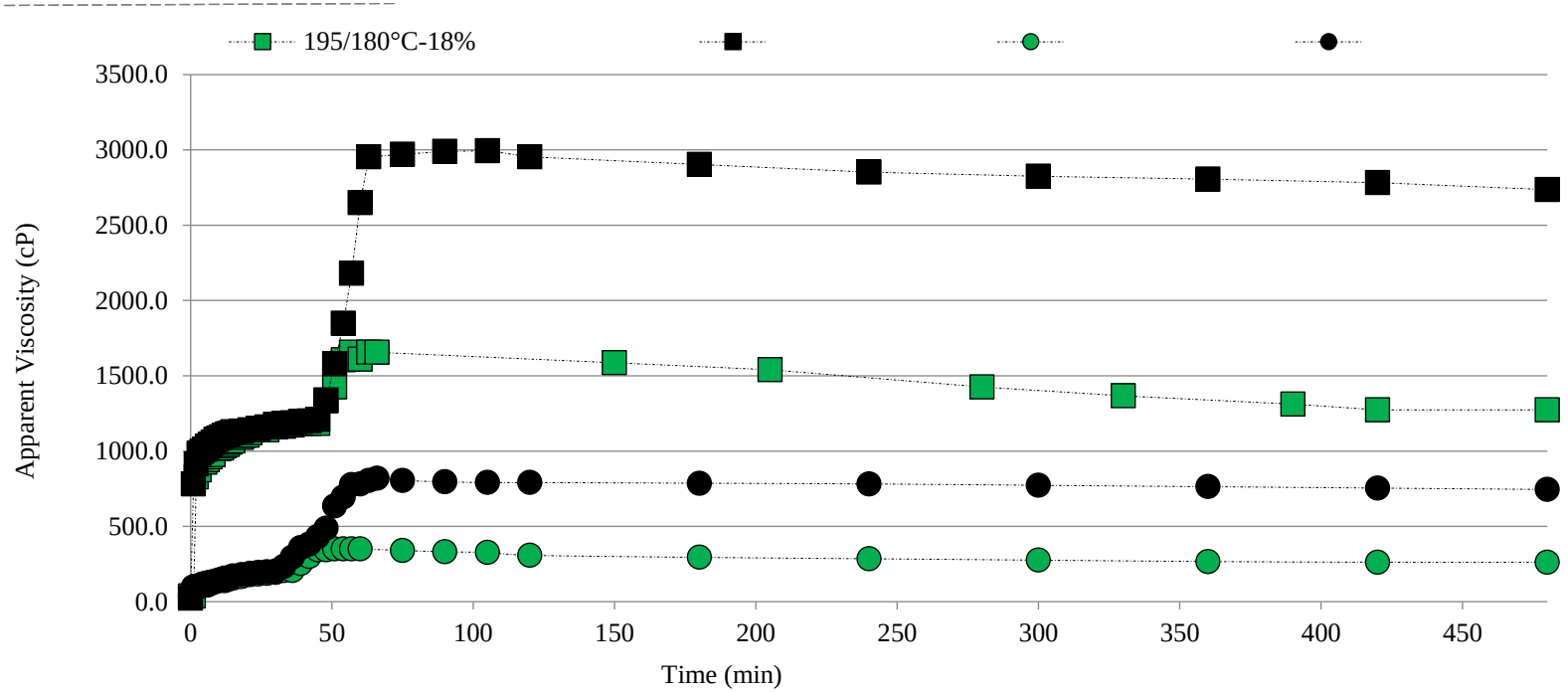

Grinding Tech	*Particles size*	*Production Temp (°C)*	*Particle Content (%)*	*Swelling Extent (minutes)*	*Storage Temp (°C)*	*Initial Storage Viscosity (cP)*	*Dissolution Rate (%)*	*Final Storage Viscosity (cP)*
Ambient	Fine	195	10	39	180	349	25	262
					150	818	10	740
			18	60	180	1656	23	1274
					150	2994	10	2668

Figure 6.15 Evolution of viscosity at different concentration of ambient CRM 125-250 µm.

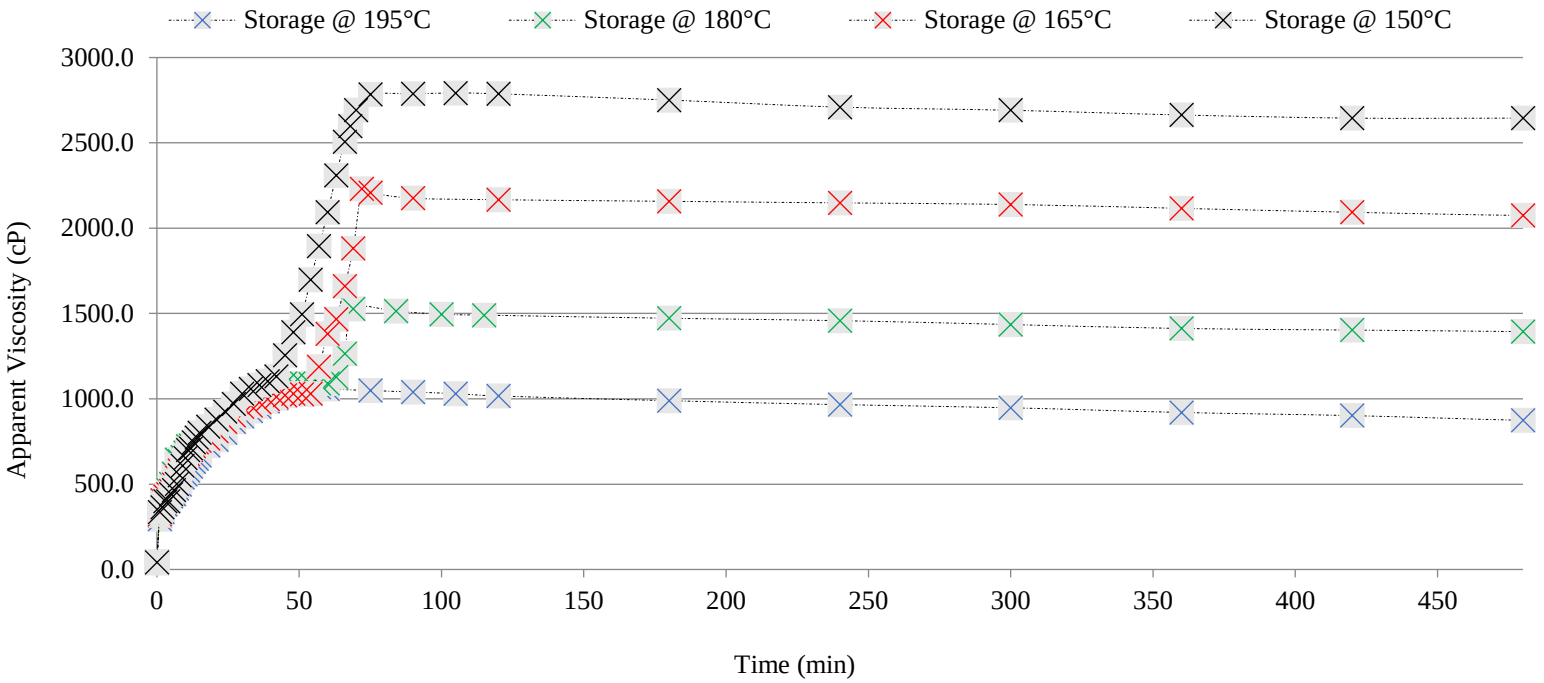

Particle Content (%)	*Grinding Tech*	*Particles size*	*Production Temp (°C)*	*Swelling Extent (minutes)*	*Storage Temp (°C)*	*Initial Storage Viscosity (cP)*	*Dissolution Rate (%)*	*Final Storage Viscosity (cP)*
18	Cryogenic	Raw	195	51	195	1030	21	851
					180	1527	10	1370
					165	2231	7	2070
					150	2792	5	2645

Figure 6.16 Evolution of viscosity at different storage temperature using cryogenic CRM 125- 800 µm.

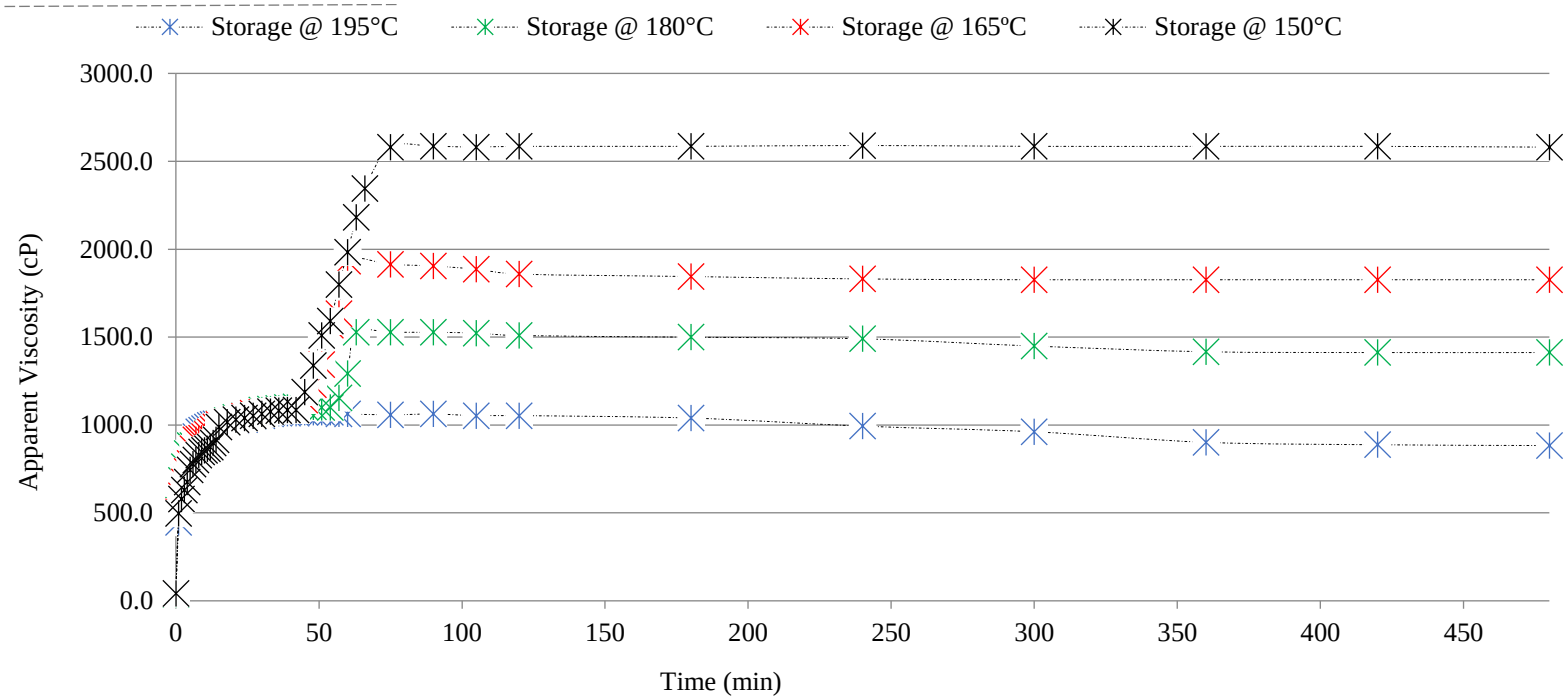

Particle Content (%)	*Grinding Tech*	*Particles size*	*Production Temp (°C)*	*Swelling Extent (minutes)*	*Storage Temp (°C)*	*Initial Storage Viscosity (cP)*	*Dissolution Rate (%)*	*Final Storage Viscosity (cP)*
18	Cryogenic	Fine	195	45	195	1071	18	878
					180	1527	8	1412
					165	1932	7	1826
					150	2589	8	2484

Figure 6.17 Evolution of viscosity at different storage temperature using cryogenic CRM 125- 250 µm.

6.2.4. Investigating the relation between storage temperatures and dissolution rates

During the storage period the binders lose part of their initial storage viscosity due to the high temperature. As introduced in 6.1.1, this phenomenon has been defined as the dissolution rate, which represents the amount of viscosity that has been lost from the beginning to the end of the storage period and it is expressed in percentage. Data in Table 6.2 and trends in Figure 6.18 and Figure 6.19, prove that binders manufactured by using ambient rubber always presents the highest dissolution rates thanks to the lower specific surface of the cryogenic rubber particles that slow the depolymerisation of the rubber.

Instead, the binders produced by using ambient rubber due to the higher specific surface, are more susceptible to the impact of temperature during storage, leading to higher dissolution rates.

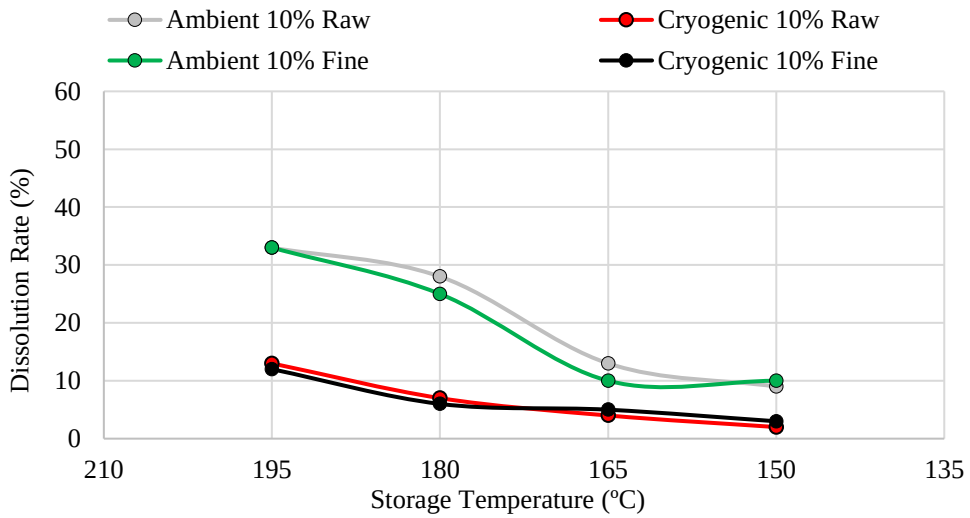

Figure 6.18 Dissolution rates vs storage temperature, 10% CRM.

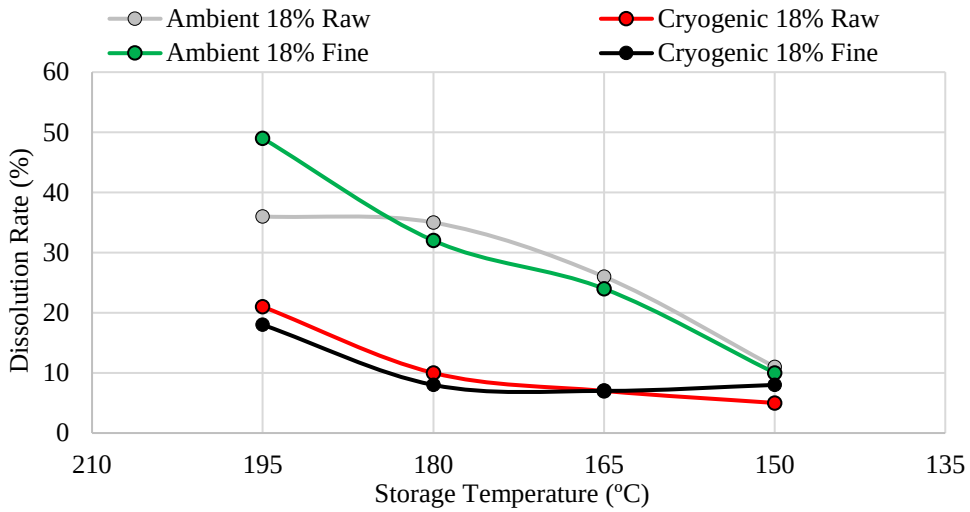

Figure 6.19 Dissolution rates vs storage temperature, 18% CRM.

Furthermore, the size of the rubber seems not to have a relevant impact on the dissolution rate, although has to be mentioned that finer particles are easier to be dissolved.

From these observations, it results that cryogenic rubber should be recommended in order to reduce the loss of viscosity during the storage of the CR-MB at the asphalt plant. Nevertheless, by lowering the storage temperature to 150ºC, the values of dissolution rate decrease significantly for both ambient and cryogenic rubber.

6.3. Summary of results

This investigation proved that using a rotational viscometer in an innovative setup by replacing the conventional spindle, such as the SC-27, with the DHR as impeller, provides bitumen technologists with a quality-control procedure for CR-MBs during full-scale production and hot storage.

Previous investigations have introduced the possibility of adapting a rotational viscometer to act as a low shear mixer and then to simulate the manufacturing of CR-MBs. Nevertheless, previous studies proved the

feasibility of the procedure as well as the need of a mixing rheometry device able to guarantee the sample stability.

This investigation wanted to extend the concept of controlling the modification process also to the hot storage phase. This was done by the introduction of the DHR, a device that not only allows to constantly monitor the viscosity of the sample, it also provides enhanced mixing performance which ensures the stability of the sample while performing the measurements.

To prove the potential of the presented procedure, several CR-MBs with different rubber content, size and type have been produced and tested at different storage temperatures. The binders were produced at 195°C, once reached the peak viscosity then the temperature was lowered to simulate different storage conditions. The DHR speed was set at 50 Rpm aimed to avoid sedimentation during manufacturing but also to maintain constant the shar rate aimed to allow a comparison among all the results achieved. Five parameters have been extrapolated from the real-time monitoring of the binders. These parameters allow a comparative analysis of the modification process during production and hot storage.

As a result, this investigation provided evidence to support the following conclusions:

- DHR allows a smooth real-time monitoring procedure which does not need the intervention of the operator which is typical when coaxial cylinders with spindles are used
- The proposed procedure includes the identification of five parameters that can help practitioners to establish targets for improved quality-control procedures.
- The percentage of viscosity lost during the simulation of the storage has been defined as dissolution rate. It has been noticed that the

dissolution rate of the CR-MBs is affected by the storage temperature and the grinding technology of the rubber.

- In terms of industrial production, the use of cryogenic rubber as a modifier will result in lower values of viscosity during the manufacturing of the CR-MBs, however cryogenic rubber is less affected during hot storage, leading to lower dissolution rates.
- Reducing the storage temperature at the asphalt plant to 150ºC will reduce the dissolution rates, which in turn will help preventing binder's drainage problems during the construction operations and pavement's rutting during the service life.

This study provides a procedure that can be used by practitioners to improve the design and quality control of CR-MBs. Further researches should look at assessing the procedure with a wider experimental programme which includes longer storage time. In fact, the dissolution rate looks to be a promising parameter to define the ideal storage stability conditions of HBBs, even beyond CR-MBs.

CHAPTER 7. CONCLUSIONS AND RECOMMENDATIONS FOR FUTURE RESEARCH

7. Conclusions and Recommendations for future research

The main objective of the work described in this thesis was to improve the rheometry of heterogenous bituminous binders for pavement engineering applications by using a combined experimental-numerical approach.

The work firstly focused on the development of a numerical model aimed to reproduce the laboratory observations of high temperature rotational test of HBBs. The numerical model successfully offered a deeper insight within the measuring chamber providing an explanation of the phenomena happening in the sample while is tested. The computational platform provided further evidence that heterogeneous binders suffer of sample instability due to a difference in densities between the phases. As a consequence, a number of changes, such as sedimentation, agglomeration and phase separation may occur in the sample while is tested leading to not representative results. Result from the numerical model also suggested that a shape optimisation was required to reduce the level of heterogeneity within the sample and in turn to provide a more stable and realistic trend of viscosity measurements. A deep literature study was performed to identify the best geometry able to address this issue. The dual helical ribbon was found to be the best solution to improve the mixing of HBBs. The new geometry was first designed, modelled and verified by means of numerical modelling then prototyped by using the 3D printing technology and finally manufactured in stainless steel. The combined experimental-numerical approach was used to assess if the actual procedure to measure the rotational viscosity of HBBs is correct. To achieve that, a comparison between the DHR and the SC-27 was carried out and both experimental and numerical results highlighted that using the conventional equipment such as the cylindrical spindle the sample may undergo sample instability while the DHR solves the issue.

Finally, the DHR was adapted to act as a low shear mixer with the aim to perform a real-time quality control procedure for product development and quality control of CR-MBs. The proposed procedure proved to be a practical laboratory application to estimate the conditions for the storage period and to avoid or reduce the loss of viscosity of the CR-MBs during extended storage times. Given the results obtained and considering the objectives of this thesis, the following conclusions can be drawn:

- The developed computational fluid dynamic model successfully reproduced the laboratory observations offering a clear picture of the mixing mechanism provided by different geometries. Indeed, Fluent allowed to investigate the differences between different geometries in terms of mixing performance by analysing the velocity fields and volume fraction. The CFD helped to gain a deeper insight in the complex flow regimes and showed potential to be used as a platform to design new testing geometries for heterogeneous binders. Numerical results confirmed the need of a mixing device able to reduce the level of heterogeneity within the sample and in turn to guarantee the sample stability during rotational test.

- A new shape (DHR) able to provide more reliable rotational viscosity measurements has been identified; first by conducting an accurate literature review on mixing devices then designed, calibrated and verified by means of numerical modelling and finally manufactured and tested. Numerical simulations proved that the CFD is a powerful tool to support and verify the design of new geometries such as the DHR and together with the laboratory campaign helped to shed lights into the measuring chamber showing both the limitations of using the conventional cylindrical spindle and the benefit of the dual helical ribbon solution. It can be stated that the DHR provides a solution to

overcome the sample instability phenomena and technologists are advised to consider this solution within rheological characterization of HBBs.

- This thesis also used the combined experimental-numerical approach to provide evidence that conventional cylindrical spindles are not suitable for measuring high temperature rotational viscosity of HBBs, while the DHR overcomes the issue by providing a more accurate trend of viscosity measurements while also ensuring the sample stability. Indeed, numerical and experimental results clarified that HBBs undergo sample instability because they are tested or stored at high temperature in vertical containers. These issues are directly proportional to the materials complexity and testing conditions, indeed by increasing the complexity it results in misleading measurements up to 40%.

- An improved laboratory application for real-time monitoring of CR-MBs rheological' properties during manufacturing and storage has been developed. The procedure consisted in adapting the DHR to act as a low shear mixer while performing rheological measurements in real-time. That allowed to govern the modification process by controlling several processing conditions and in turn to provide practical recommendations for full-scale production and storage of HBBs. In this thesis, the above-mentioned procedure was used to estimate the optimal conditions for the storage period to prevent the loss of viscosity of the CR-MB during the storage phase.

In the light of the results obtained in this thesis, the combined experimental-numerical approach can be considered to be a promising technique to investigate and improve actual procedure or tests that have not been designed for heterogenous materials.

The following points are recommended for future research work:

- The numerical model presented in this work has been used as a support for the design of a new geometry but also to gain a better insight of the phenomena happening within the sample. However, the CFD model showed to be a powerful tool that could provide more information. Hence, a possible next step would be to improve the numerical model with the aim to predict the laboratory results via numerical simulations.

- The DHR introduced in this thesis was specifically designed for rotational viscometer, however the same concept could be used for a dynamic shear rheometer widening the range of materials and applications.

- Heterogenous binders cover a wide range of materials used in many daily applications, such as cosmetic, pharmaceutic, food industry and many others. Here the spotlight is on HBBs, but next researches should focus on bitumen emulsions and highly modified PMBs. All these materials present similar issues to the ones investigated in this study.

- Regarding the real-time procedure introduced in this work, future investigations should study the relation between the shear rate produced by the DHR and the shear rate of full-scale mixers and

stirrers. That could help to adapt the speed of the DHR to the specific industrial equipment to be used for the manufacturing of the CR-BMs and to obtain more accurate predictions.

- Further studies should evaluate the real-time procedure for rotational viscosity measurements with an extensive experimental programme including longer storage periods.

8. References

ASTM. Standard test method for viscosity determination of asphalt at elevated temperatures using a rotational viscometer. American society for testing and materials, a. D4402/d4402m

ASTM. Standard test method for measurement of apparent viscosity of asphalt rubber or other asphalt binders by using a rotational hand-held viscometer. American society for testing and materials, b. D7741/d7741m.

ASTM D 8 – 02 (2002) Standard Terminology Relating to Materials for Roads and Pavements, American Society for Testing and Materials.

Abdelrahman, M. A. and Carpenter, S. H. (1999) 'Mechanism of Interaction of Asphalt Cement with Crumb Rubber Modifier', *Transportation Research Record*. SAGE Publications Inc, 1661(1), pp. 106–113. doi: 10.3141/1661-15.

Abdul Ghani, A. G. and Farid, M. M. (2007) 'Numerical simulation of solid-liquid food mixture in a high pressure processing unit using computational fluid dynamics', *Journal of Food Engineering*, 80(4), pp. 1031–1042. doi: 10.1016/j.jfoodeng.2006.08.018.

Airey, G. D. (2003) 'Rheological properties of styrene butadiene styrene polymer modified road bitumens', *Fuel*, 82(14), pp. 1709–1719. doi: 10.1016/S0016-2361(03)00146-7.

Allbiz (2019) *Asphalt-Rubber portable Blending Systems*. Available at: https://us.all.biz/asphalt-rubber-blending-systems-g18487.

Ansys Inc. (2017) *Fluent User's Guide*.

Bahia, H. U. and Davies, R. (1991) 'Research Associate and Assistant Professor of CEE and 2 Graduate Research Assistant, The Pennsylvania Transportation Institute, The Pennsylvania State University, University Park PA The oral presentation was made by Professor Bahia', pp. 414–438.

Bair, S. and Qureshi, F. (2003) 'The high pressure rheology of polymer-oil

solutions', *Tribology International*, 36, pp. 637–645. doi: 10.1016/S0301-679X(03)00008-2.

Barnes, Hutton and Walters (1989) *An Introduction to Rheology*, *Journal of Non-Newtonian Fluid Mechanics*. doi: 10.1016/0377-0257(89)85015-3.

Batchelor, G. K. (1977) 'The effect of Brownian motion on the bulk stress in a suspension of spherical particles', *Journal of Fluid Mechanics*, 83(01), p. 97. doi: 10.1017/S0022112077001062.

Bernoulli, D. (1738) 'Hydrodynamica, Sive Vivibus et Motimus Fluidorum Commentarii.', in *Hydrodynamica*. Dulsecker, Straßburg.

Bertollo, S. (2004) 'Mechanical properties of asphalt mixtures using recycled tyre rubber produced in Brazil – a laboratory evaluation', in *TRB Annual Meeting*.

Brito-De La Fuente, E., Choplin, L. and Tanguy, P. (1997) 'Mixing With Helical Ribbon Impellers', *Chemical Engineering Research and Design*, 75(1), pp. 45–52. doi: 10.1205/026387697523381.

Brookfield (2015) *Brookfield*. Available at: https://www.brookfieldengineering.com/products/viscometers.

Brookfield (2018) *General purpose Visco Fluid*. Available at: https://www.brookfieldengineering.com/products/viscometers.

Brûlé, B. (1996b) 'Polymer-Modified Asphalt Cements Used in the Road Construction Industry: Basic Principles', *Transportation Research Record: Journal of the Transportation Research Board*, 1535, pp. 48–53. doi: 10.3141/1535-07.

Bueno, M. *et al.* (2014) 'Noise Reduction Properties of an Experimental Bituminous Slurry with Crumb Rubber Incorporated by the Dry Process', *Coatings*, 4(3), pp. 602–613. doi: 10.3390/coatings4030602.

Bunger, A. P., McLennan, J. and Jeffrey, R. (2013) 'Effective and Sustainable Hydraulic Fracturing', *Effective and Sustainable Hydraulic Fracturing*, p. 1024. doi: DOI: 10.5772/45724.

Buscall, R., D'Haene, P. and Mewis, J. (1994) 'Maximum Density for Flow of

Dispersions of Near Monodisperse Spherical Particles', *Langmuir*, 10(5), pp. 1439–1441. doi: 10.1021/la00017a020.

Caltrans (2011) 'Quality Control Manual for Hot Mix Asphalt - State of California', *State of California, Department of Transportation, Division of Construction*, (June). Available at: http://www.dot.ca.gov/hq/construc/publications/qcqaman1.pdf.

Carreau, P. J. (1972) 'Rheological Equations from Molecular Network Theories', *Journal of Rheology*, 16(1972), p. 99. doi: 10.1122/1.549276.

Carreau, P. J., Patterson, W. I. and Yap, C. Y. (1976) 'Mixing of viscoelastic fluids with helical-ribbon agitators I- Mixing time and flow patterns.', *Can. J. Chem. Eng.*, 54(3), pp. 135–142.

Celauro, B. *et al.* (2012) 'Definition of a laboratory optimization protocol for road bitumen improved with recycled tire rubber', *Construction and Building Materials*. Elsevier Ltd, 37, pp. 562–572. doi: 10.1016/j.conbuildmat.2012.07.034.

Cengel, Y. and Cimbala, J. (2006) *Fluid mechanics: fundamentals and applications*. Edited by McGraw-Hill.

Chehovits, J. G., Dunning, R. L. and Morris, G. R. (1982) 'Characteristics of asphalt-rubber by the sliding plate microviscometer', in *Association of Asphalt Paving Technologists Proceedings*.

Chhabra, R. P. and Richardson, J. F. (1999) 'Non-Newtonian Flow in the Process Industries: Fundamentals and Engineering', p. 436.

Chung, C. I. (2000) *Extrusion of Polymers Theory & Practice*.

Cordobes, F., Brito de la fuente, E. and Gallegos, C. (1998) 'Effect of rheological properties on power input and effective shear rates when mixing with different impellers.', *Anales de química*. Springer, 94(4–5), pp. 274–278. Available at: http://cat.inist.fr/?aModele=afficheN&cpsidt=10064702 (Accessed: 20 April 2015).

Coussot, P. and Ancey, C. (1999) 'Rheophysical classification of concentrated suspensions and granular pastes', *Physical Review E*, 59(4), pp. 4445–4457. doi: 10.1103/PhysRevE.59.4445.

Cullen, P. J., Duffy, a P. and Callaghan, D. J. O. (2005) 'In situ rheological monitoring of viscous non-Newtonian fluids using a helical ribbon agitator'.

D&H Equipment (2019) *D&H Equipment - Asphalt plant*.

Delaplace, G., Leuliet, J. C. and Relandeau, V. (2000) 'Circulation and mixing times for helical ribbon impellers. Review and Experiments', *Experiments in Fluids*, 28(2), pp. 170–182. doi: 10.1007/s003480050022.

Dow, R. B. (1946) 'The rheology of lubricants', *Journal of Colloid Science*, pp. 81–91. doi: https://doi.org/10.1016/0095-8522(47)90011-1.

Dzuy, N. Q. & D. V. B. (1983) 'Yield Stress Measurement for Concentrated Suspensions', *Journal of Rheology*, 27(4), p. 321. doi: 10.1122/1.549709.

Euler, L. (1749) *Scientia navalis*.

Farrokhpay, S. (2012) 'The importance of rheology in mineral flotation: A review', *Minerals Engineering*. Elsevier Ltd, 36–38, pp. 272–278. doi: 10.1016/j.mineng.2012.05.009.

Gallegos, C. and Franco, J. M. (1999) 'Rheology of food, cosmetics and pharmaceuticals', *Current Opinion in Colloid and Interface Science*, 4(4), pp. 288–293. doi: 10.1016/S1359-0294(99)00003-5.

Ghaly, N. (2008) 'Effect of Sulfur on the Storage Stability of Tire Rubber Modified Asphalt', *World Journal of Chemistry*, 3(2), pp. 42–50.

Ghavibazoo, A. and Abdelrahman, M. (2013) *Composition analysis of crumb rubber during interaction with asphalt and effect on properties of binder*, *International Journal of Pavement Engineering*. doi: 10.1080/10298436.2012.721548.

Giancontieri, G., Hargreaves, D. M. and Lo Presti, D. (2018) 'Are we correctly measuring the rotational viscosity of rubberized bituminous binder ?', in *Proceedings of the Rubberised Asphalt - Asphalt Rubber 2018 Conference*. South Africa.

Hanson, D. I. *et al.* (1994) 'Evaluation and characterization of rubber-modified hot mix asphalt pavement', *Transportation Research Record*, 1436, pp. 98–107.

Havas, G., J.Sawinsky and Deak, A. (1977) ‘Investigation of homogenization efficency of the screw agitator, helical ribbon agitator, gate type anchor impeller and the multi-paddle agitator in the mixing of high-viscosity newtonian liquids’, *Periodica Polytechnica Chemical Engineering*, 22(4).

Heitzman, M. (1992) ‘Design and construction of asphalt paving materials with crumb rubber modifier’, *Transportation Research Record: Journal of the Transportation Research Board*, p. 132.

Hoffman, R. L. (1974) ‘Discontinuous and Dilatant Viscosity Behavior in Concentrated Suspensions .2. Theory and Experimental Tests’, *Journal of Colloid and Interface Science*, 46(3), pp. 491–506. doi: 10.1122/1.549250.

Holdsworth (1993) ‘Rheological models used for the prediction of the flow properties of food products: a literature review’, *Institution of Chemical Engineers*.

Hosseinnezhad, S., Holmes, D. and Fini, E. H. (2014) ‘Decoupling the Physical Filler Effect and the Time Dependent Dissolution Effect of Crumb Rubber on Asphalt Matrix Rheology’, *Transportation Research Board*.

Huang, S. C. (2006) ‘Rheological characteristics of crumb rubber-modified asphalts with long-term aging’, *Road Materials and Pavement Design*, 7(January 2015), pp. 37–56. doi: 10.1080/14680629.2006.9690057.

Hunter, R., Self, A. ; and Read, J. (2015) *The Shell Bitumen Handbook*. ICE.

Jeong, K. D. *et al.* (2010) ‘Interaction effects of crumb rubber modified asphalt binders’, *Construction and Building Materials*. Elsevier Ltd, 24(5), pp. 824–831. doi: 10.1016/j.conbuildmat.2009.10.024.

Jung, J., Kaloush, K. and Way, G. (2003) ‘Life cycle cost analysis: conventional versus asphalt rubber pavements’, *ements. s.l.: Rubber Pavement Association*.

Kaloush, K. E. *et al.* (2003) ‘Laboratory Evaluation of Asphalt Rubber Mixtures Using the Dynamic Modulus (E*) Test’, in *TRB Annual Meeting*.

Khanafer, K. and Vafai, K. (2011) ‘A critical synthesis of thermophysical characteristics of nanofluids’, *International Journal of Heat and Mass Transfer*.

Elsevier Ltd, 54(19–20), pp. 4410–4428. doi: 10.1016/j.ijheatmasstransfer.2011.04.048.

Krampa-Morlu, F. N. *et al.* (2004) 'Numerical Simulation of Dense Coarse Particle Slurry Flows in a Vertical Pipe', in *International Conference on Multiphase Flow*, p. 2004.

Krieger, I. M. (1959) 'A Mechanism for Non-Newtonian Flow in Suspensions of Rigid Spheres', *Journal of Rheology*, 3(1), p. 137. doi: 10.1122/1.548848.

Krieger, I. M. (1972) 'Rheology of monodisperse latices', *Advances in Colloid and Interface Science*, 3(2), pp. 111–136. doi: 10.1016/0001-8686(72)80001-0.

De La Villéon, J. *et al.* (1998) 'Numerical investigation of mixing efficiency of helical ribbons', *AIChE Journal*, 44(4), pp. 972–977. doi: 10.1002/aic.690440423.

Lee, S. J., Akisetty, C. K. and Amirkhanian, S. N. (2008) 'The effect of crumb rubber modifier (CRM) on the performance properties of rubberized binders in HMA pavements', *Construction and Building Materials*, 22(7), pp. 1368–1376. doi: 10.1016/j.conbuildmat.2007.04.010.

Leung, F. (2006) 'Noise Reducing Asphalt Pavements: a Canadian Case Study.', in *In: 10th International conference on asphalt pavements. Quebec City;*

Lin, S. and Brodkey, R. S. (1985) 'Rheological Properties of Slurry Fuels', *Journal of Rheology*, 29, p. 147. doi: 10.1122/1.549814.

Malkin, A. Y. (2009) 'The state of the art in the rheology of polymers: Achievements and challenges', *Polymer Science Series A*, 51(1), pp. 80–102. doi: 10.1134/S0965545X09010076.

Manninen, M. and Taivassalo, V. (1996) 'On the mixture model for multiphase flow', *Vtt Publications*, (VTT publications 288), pp. 1–67. Available at: http://www.vtt.fi/inf/pdf/publications/1996/P288.pdf.

McDonald, C. H. (1975) 'Elastomeric pavement repair composition for pavement failure and method of making the same'.

McDonald, C. H. (1981) 'National Seminar on Asphalt Rubber', *Recollections of*

Early Asphalt-Rubber History, (October).

Metzner, A. B. (1985) 'Rheology of Suspensions in Polymeric Liquids', *Journal of Rheology*, 29(6), p. 739. doi: 10.1122/1.549808.

Metzner, A. B. and Otto, R. E. (1957) 'Agitation of non-Newtonian fluids', *AIChE Journal*, 3(1), pp. 3–10. doi: 10.1002/aic.690030103.

Mezger, T. G. (2014) *The Rheology Handbook, 4th Edition*.

Navarro, F. J. *et al.* (2004) 'Thermo-rheological behaviour and storage stability of ground tire rubber-modified bitumens', *Fuel*, 83(14–15 SPEC. ISS.), pp. 2041–2049. doi: 10.1016/j.fuel.2004.04.003.

Newton, I. (1687) *Philosophiae naturalis principia mathematica ("Principia")*. London.

Norton, T. and Sun, D.-W. (2006) 'Computational fluid dynamics (CFD) – an effective and efficient design and analysis tool for the food industry: A review', *Trends in Food Science & Technology*, 17(11), pp. 600–620. doi: 10.1016/j.tifs.2006.05.004.

Novak, V. and Rieger, F. (1969) 'Homogenization with helical screw agitators', *Trans. Inst. Chem. Eng.*, 47.

Oliver, J. W. H. (1980) 'Modification of paving asphalts by digestion with scrap rubber', in *TRB Annual Meeting*.

Pasquini, E. (2009) *Advanced characterisation of innovative environmentally friendly bituminous mixtures*. s.l.: Università Politecnica delle Marche. PhD thesis;

Patterson, Carreau, P. J. and Yap, C. Y. (1979) 'Mixing with helical ribbon agitators: Newtonian fluid', *AICHE Journal*, 25(3), pp. 508–516.

Paul, E. L., Atiemo-obeng, V. a and Kresta, S. M. (2004) *Handook of industrial mixing*.

Peralta, J. *et al.* (2010) 'Changes in Rubber Due to its Interaction with Bitumen when Producing Asphalt Rubber', *Road Materials and Pavement Design*, 11(4), pp. 1009–

1031. doi: 10.1080/14680629.2010.9690317.

Pereira, P. and Pais, J. C. (2008) 'Laboratory optimization of continuous blend asphalt', *Materials Science*.

Perez-Lepe, Martı´nez-Boza and Gallegos (2007) 'High Temperature Stability of Different Polymer-Modified Bitumens: A Rheological Evaluation', *Journal of Applied Polymer Science*. doi: 10.1002/app.

Petrowiki (2015a) 'Drilling fluids'. Available at: http://petrowiki.org/Drilling_fluids.

Petrowiki (2015b) 'Fracturing fluids and additives'. Available at: http://petrowiki.org/Fracturing_fluids_and_additives.

Lo Presti, D. (2013) 'Recycled Tyre Rubber Modified Bitumens for road asphalt mixtures: A literature review', *Construction and Building Materials*. Elsevier Ltd, 49, pp. 863–881. doi: 10.1016/j.conbuildmat.2013.09.007.

Lo Presti, D. *et al.* (2014) 'Toward more realistic viscosity measurements of tyre rubber–bitumen blends', *Construction and Building Materials*. Elsevier Ltd, 67, Part B(0), pp. 270–278. doi: http://dx.doi.org/10.1016/j.conbuildmat.2014.03.038.

Lo Presti, D. and Airey, G. (2013) 'Tyre rubber-modified bitumens development : the effect of varying processing conditions', 0629(December). doi: 10.1080/14680629.2013.837837.

Quemada, D. (1977) 'Rheology of concentrated disperse systems and minimum energy dissipation principle - I. Viscosity-concentration relationship', *Rheologica Acta*, 16(1), pp. 82–94. doi: 10.1007/BF01516932.

Ragab, M. and Abdelrahman, M. (2018) 'Enhancing the crumb rubber modified asphalt's storage stability through the control of its internal network structure', *International Journal of Pavement Research and Technology*. Chinese Society of Pavement Engineering, 11(1), pp. 13–27. doi: 10.1016/j.ijprt.2017.08.003.

Rahman, R. M., Ata, S. and Jameson, G. J. (2012a) 'The effect of flotation variables on the recovery of different particle size fractions in the froth and the pulp',

International Journal of Mineral Processing. Elsevier B.V., 106–109, pp. 70–77. doi: 10.1016/j.minpro.2012.03.001.

Rahman, R. M., Ata, S. and Jameson, G. J. (2012b) 'The effect of flotation variables on the recovery of different particle size fractions in the froth and the pulp', *International Journal of Mineral Processing*. Elsevier B.V., 106–109, pp. 70–77. doi: 10.1016/j.minpro.2012.03.001.

Rieger, F. and Novak, V. (1973) 'Power consumption of agitators in highly viscous non-Newtonian liquids', *Trans. Inst. Chem. Eng.*, 51, pp. 105–11.

Robinson, M. and Cleary, P. W. (2012) 'Flow and mixing performance in helical ribbon mixers', *Chemical Engineering Science*. Elsevier, 84, pp. 382–398. doi: 10.1016/j.ces.2012.08.044.

Sabita (2016) *Guidelines for the design, manufacture and construction of bitumen-rubber asphalt wearing courses*.

Schramm, L. L. (2006) *Emulsions, Foams, and Suspensions: Fundamentals and Applications, Emulsions, Foams, and Suspensions: Fundamentals and Applications*. doi: 10.1002/3527606750.

Sienkiewicz, M. *et al.* (2012) 'Progress in used tyres management in the European Union: A review', *Waste Management*. Elsevier Ltd, 32(10), pp. 1742–1751. doi: 10.1016/j.wasman.2012.05.010.

Sisko, A. W. (1958) 'The Flow of Lubricating Greases', *Industrial & Engineering Chemistry*, 50(12), pp. 1789–1792. doi: 10.1021/ie50588a042.

Smith, J. . (1970) 'The Mixing of Newtonian and non- Newtonian fluids', *J. Soc. Cosmet. Chem*, 552, p. 242. Available at: https://books.google.com/books/about/The_Mixing_of_Rubber.html?id=NV7L3Jb1URwC&pgis=1.

Sommerfeld, M. and Decker, S. (2004) 'State of the art and future trends in CFD simulation of stirred vessel hydrodynamics', *Chemical Engineering and Technology*, 27(3), pp. 215–224. doi: 10.1002/ceat.200402007.

Sousa, J. (2005) ‘Experiences with use of reclaimed rubber in asphalt within Europe.’, *Rubber in Roads*.

Stickel, J. J. and Powell, R. L. (2005) ‘Fluid Mechanics and Rheology of Dense Suspensions’, *Annual Review of Fluid Mechanics*, 37(1), pp. 129–149. doi: 10.1146/annurev.fluid.36.050802.122132.

Stokes, G. G. (1846) *Report on the recent researches in hydrodynamics*.

Subhy, A., Lo Presti, D. and Airey, G. (2016) ‘Rubberised bitumen manufacturing assisted by rheological measurements’, *Road Materials and Pavement Design*, 17(2), pp. 290–310. doi: 10.1080/14680629.2015.1079549.

Tabilo-Munizaga, G., Barbosa-Cánovas, G. V and Tonir, S. (2005) ‘Rheology for the food industry’, *Journal of Food Engineering*, 67(1–2), pp. 147–156. doi: 10.1016/j.jfoodeng.2004.05.062.

Takahashi, K., Sasaki, M., *et al.* (1982) ‘Effects of Geometrical Variables of Helical Ribbon Impellers on Mixing of Highly Viscous Newtonian Liquids.’, *Journal of Chemical Engineering of Japan*, 15(3), pp. 217–224. doi: 10.1252/jcej.15.217.

Takahashi, K., Arai, K. and Shozaburo, S. (1982) ‘An extended power correlation for anchor and helical ribbon impellers’, *Journal of Chemical Engineering of Japan*, pp. 77–79.

Takahashi, K., Yokota, T. and Konno, H. (1979) ‘Mixing of pseudoplastic liquid in a vessel equipped with a variety of helical ribbon impellers’, *Journal of Chemical Engineering of Japan*, 45(1978), pp. 63–68.

Takahashi, K., Yokota, T. and Konno, H. (1984) ‘Power Consumption of Helical Ribbon Agitators in Highly Viscous Pseudoplastic Liquids.’, *Journal of Chemical Engineering of Japan*, 17(6), pp. 657–659. doi: 10.1252/jcej.17.657.

Tanguy, P. a *et al.* (1992) ‘Finite element analysis of viscous mixing with a helical ribbon-screw impeller’, *AICHE Journal*, 38(6), pp. 939–944. doi: 10.1002/aic.690380614.

Terrel, R. and Walter, J. (1986) ‘Modified asphalt materials – the European

Experience.', *In:s.l.: AAPT proceedings.* ., 55., pp. 482–518.

TG1 (2015) *Technical Guideline : The Use Of Modified Bituminous Binder In Road Construction*. Edited by Sabita.

Thakur, R. K. *et al.* (2004) 'Mixing of complex fluids with flat-bladed impellers: Effect of impeller geometry and highly shear-thinning behavior', *Chemical Engineering and Processing: Process Intensification*, 43(10), pp. 1211–1222. doi: 10.1016/j.cep.2003.11.005.

Thodesen, C., Shatanawi, K. and Amirkhanian, S. (2009) 'Effect of crumb rubber characteristics on crumb rubber modified (CRM) binder viscosity', *Construction and Building Materials*. Elsevier Ltd, 23(1), pp. 295–303. doi: 10.1016/j.conbuildmat.2007.12.007.

Tsui, Y. and Hu, Y. (2011) 'Flow Characteristics in Mixers Agitated', *Engineering Applications of Computational Fluid Mechanics Vol.*, 5(3), pp. 416–429.

Visser, A. T., Duhovny, G. S. and Sachkova, A. V. (2017) 'Comparison of bitumen–rubber use in extreme conditions in Russia and South Africa', *Road Materials and Pavement Design*, 18(5), pp. 1190–1199. doi: 10.1080/14680629.2016.1201524.

Visser, A. and Verhaege, B. (2000) 'Bitumen–rubber: lessons learned in South Africa.', *ISBN: 972-95240-9-2, 2000. Asphalt Rubber; 2000.*

van Wachem, B. G. M. and Almstedt, A. E. (2003) 'Methods for multiphase computational fluid dynamics', *Chemical Engineering Journal*, 96(1–3), pp. 81–98. doi: 10.1016/j.cej.2003.08.025.

WBCSD & The Tire Industry Project (2019) 'Global ELT Management-A global state of knowledge on regulation, management systems, impacts of recovery and technologies', (December).

Widyatmoko, I. and Elliot, R. (2007) 'A review of the use of crumb rubber modified asphalt worldwide. 2007.', *UK : Waste & Resources Action Programme (WRAP)*.

Willenbacher, N. *et al.* (2013) 'Rheology of Disperse Systems', *Product Design and Engineering: Formulation ofGels and Pastes, First Edition*, pp. 1–49. doi:

10.1002/9783527654741.ch1.

Yap, C. Y., Patterson, W. and Carreau, P. J. (1979) 'Mixing with helical ribbon agitators: Non- Newtonian Fluids', *AIChE Journal*, 25(3), pp. 516–521.

Yildirim, Y. (2007) 'Polymer modified asphalt binders', *Construction and Building Materials*, 21(1), pp. 66–72. doi: 10.1016/j.conbuildmat.2005.07.007.

Zhang, M. *et al.* (2008) 'Calculation of Metzner Constant for Double Helical Ribbon Impeller by Computational Fluid Dynamic Method', *Chinese Journal of Chemical Engineering*, 16(5), pp. 686–692. doi: 10.1016/S1004-9541(08)60141-X.

Zhang, Y. *et al.* (2018) 'Comparison of the partitioning of evapotranspiration – numerical modeling with different isotopic models using various kinetic fractionation coefficients', *Plant and Soil*. Plant and Soil, 430(1–2), pp. 307–328. doi: 10.1007/s11104-018-3737-z.

Zhu, J., Birgisson, B. and Kringos, N. (2014) 'Polymer modification of bitumen: Advances and challenges', *European Polymer Journal*, 54(1), pp. 18–38. doi: 10.1016/j.eurpolymj.2014.02.005.

Appendix A

Construction and Building Materials 136 (2017) 286–297

Contents lists available at ScienceDirect

Construction and Building Materials

journal homepage: www.elsevier.com/locate/conbuildmat

Improving the rheometry of rubberized bitumen: experimental and computation fluid dynamics studies

D. Lo Presti *, G. Giancontieri, D.M. Hargreaves

Faculty of Engineering, University of Nottingham, Nottingham NG7 2RD, UK

HIGHLIGHTS

- Background on viscosity measurements and CFD studies on mixing complex fluids.
- Laboratory tests provide visual proves of enhanced mixing efficiency with DHI.
- CFD models validated the empirical calibration with single phase fluids.
- CFD simulations compared well with experimental results.
- CFD clarifies reasons behind the improved rheometry of complex fluids with DHI.

ARTICLE INFO

Article history:
Received 17 May 2016
Received in revised form 1 December 2016
Accepted 29 December 2016
Available online 20 January 2017

Keywords:
Asphalt rubber
Rubberized bitumen
CFD
Rheometry
Complex fluids
Viscosity

ABSTRACT

Multi-phase materials are common in several fields of engineering and rheological measurements are intensively adopted for their development and quality control. Unfortunately, due to the complexity of these materials, accurate measurements can be challenging. This is the case of bitumen-rubber blends used in civil engineering as binders for several applications such as asphalt concrete for road pavements but recently also for roofing membranes. These materials can be considered as heterogeneous blends of fluid and particles with different densities. Due to this nature the two components tends to separate and this phenomenon can be enhanced with inappropriate design and mixing. This is the reason behind the need of efficient dispersion and distribution during their manufacturing and it also explains while real-time viscosity measurements could provide misleading results. To overcome this problem, in a previous research effort, a Dual Helical Impeller (DHI) for a Brookfield viscometer was specifically designed, calibrated and manufactured. The DHI showed to provide a more stable trend of measurements and these were identified as being "more realistic" when compared with those obtained with standard concentric cylinder testing geometries, over a wide range of viscosities. However, a fundamental understanding of the reasons behind this improvement is lacking and this paper aims at filling these gaps. Hence, in this study a tailored experimental programme resembling the bitumen-rubber system together with a bespoke Computational Fluid Dynamics (CFD) model are used to provide insights into DHI applicability to perform viscosity measurements with multi-phase fluids as well as to validate its empirical calibration procedure. A qualitative comparison between the laboratory results and CFD simulations proved encouraging and this was enhanced with quantitative estimations of the mixing efficiency of both systems. The results proved that CFD model is capable of simulating these systems and the obtained simulations gave insights into the flow fields created by the DHI. It is now clear that DHI uses its inner screw to create a vertical dragging of particles within a fluid of lower density, while the outer screw transports the suspended particles down. This induced flow helps keeping the test sample less heterogeneous and this in turns allows recording more stable viscosity measurements.

This work was supported by the Engineering and Physical Sciences Research Council (EPSRC) [grant number EP/M506588/1].

© 2017 The Authors. Published by Elsevier Ltd. This is an open access article under the CC BY license (http://creativecommons.org/licenses/by/4.0/).

1. Introduction

Rheological properties and their measurement are of paramount importance for the development, performance and applications of products across a wide range of industries. More

* Corresponding author.
E-mail addresses: davide.lopresti@nottingham.ac.uk (D. Lo Presti), Gaspare.Giancontieri@nottingham.ac.uk (G. Giancontieri), david.hargreaves@nottingham.ac.uk (D.M. Hargreaves).

http://dx.doi.org/10.1016/j.conbuildmat.2016.12.200
0950-0618/© 2017 The Authors. Published by Elsevier Ltd.
This is an open access article under the CC BY license (http://creativecommons.org/licenses/by/4.0/).

specifically, bitumen technologists are used to monitoring the high-temperature viscosity of these binders (in the range 100–200 °C) during manufacture, compaction and quality control [6]. Furthermore, the use of bituminous binders modified with polymers is a common practice used to enhance the performance of road pavements and roofing membranes. Nevertheless, measurements of their viscosity/rheology can be challenging due to the often heterogeneous structure of these complex systems, especially if these materials suffer from phase stratification within the time frame of typical viscosity measurements, as in the case of rubberized bitumen [7].

A common instrument used to perform these measurements is the rotational viscometer, typically by means of the coaxial cylinder testing geometry. This setup consists of a static outer cylindrical vessel into which is poured the test fluid and a concentric cylinder (spindle) which is inserted and then rotated at a given angular velocity so that the applied torque can be measured. A standard cylindrical spindle that can be used in the Brookfield viscometer is shown in Fig. 1(a). This arrangement, however, is incapable of providing reliable viscosity measurements of multiphase systems containing suspended particles with a density different to that of the continuous phase [19]. In fact, when standard cylindrical spindles are used to measure viscosity of fluids with suspended solid particles, if the two phases have very different densities the higher density component will tend to settle to the bottom during the measurement rendering the data acquired of very little use.

These type of scenarios are encountered in many type of complex systems such as: chocolate, plastic, rubber, ceramics, food, cosmetics, detergents, paints, glazings, lubricants, inks, adhesives and sealants [12,13,17,20,27]. Rotational viscometers (Brookfield in this case) are provided with supplementary spindle designs that help in some of these cases. For instance, a vane spindle allows performing measurements with paste-like materials, gels, and fluids where suspended solids migrate away from the measurement surface of standard spindles. Furthermore, the Brookfield Helipath Stand is designed to slowly lower or raise a Brookfield T-bar spindle so that it describes a helical path through the test sample. Nevertheless, these accessories are not designed to minimize the heterogeneity of multiphase blends, especially when that sample has the tendency to stratify due to phase density differences.

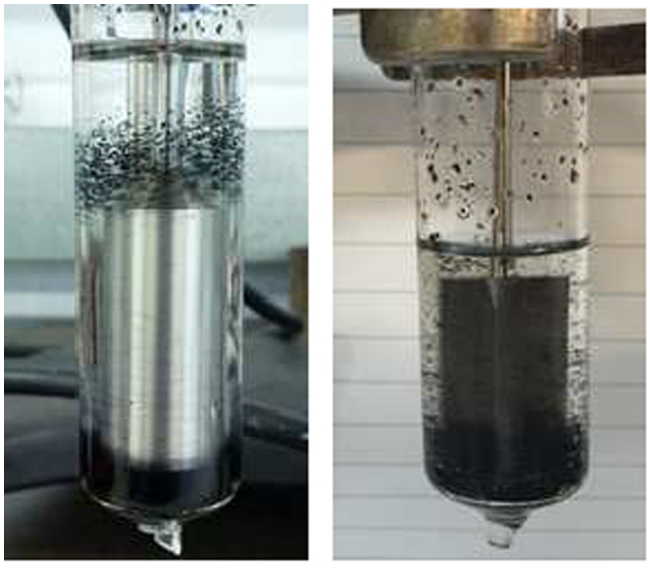

Fig. 1. Visualisation of the phase separation during viscosity measurements of suspensions for (a) the SC4-27 spindle and (b) a vane spindle.

Fig. 1(b) shows the inefficiency of the vane spindle when used for viscosity measurements of suspensions. In an effort to improve the rheometry of these scenarios by overcoming sample's phase separation issues, Lo Presti et al. [19] successfully designed, manufactured and tested a prototype of a Dual Helical Impeller (DHI) for Brookfield Rotational Viscometers (Fig. 2, right). Experimental studies were carried out to evaluate whether the DHI is able to improve the degree of homogenisation of high viscous fluids in order to obtain more realistic viscosity measurements of a blend of fluid with suspended particles. In comparison to the Brookfield standard, cylindrical geometry (spindle SC4-27), the DHI always predicted a different "apparent" viscosity (see Section 1.1 for definition). This result was explained by the capability of the DHI to create what have been likened to convective flows as opposed to the axisymmetric swirling flow induced by the standard SC4-27 spindle.

Rubberised bitumen is a complex system of the type described above, where the bitumen is the fluid matrix and the particles are the swollen tyre rubber crumbs. These two components have a moderate difference in densities and for this reason the phase separation could not possibly occur within standard rotational viscosity measurements at 135 °C. However if long equilibrium times are required, rather than high percentage of modifier, higher testing temperatures and high spindle speeds, the phase separation issue is very likely to occur, especially for a wet process-high viscosity binder. Furthermore, this issue is particularly relevant within the product development of rubberised binder with rotational viscometer used as a mixing device offering a continuous monitoring of the viscosity [7,26]. In fact, in this scenario the processing is made at high rotational speed and at a temperature where the bitumen viscosity is quite low (180 °C) and rubber particles are not swollen yet and tend to agglomerate in layers, mainly at the bottom of the tube. The DHI presented above was developed [19] specifically to solve this type of issue within low-shear development of rubberised bitumen. This research showed that carrying out measurements of rubberised bitumen with the DHI at 135 °C reduces the initial effort needed to accelerate a bitumen-rubber blend from a stationary position and provide more stable viscosity readings. This allowed the authors to declare that this type of measurements were "more realistic" (Fig. 3). However, despite these satisfying results, the mechanisms behind the enhanced mixing efficiency provided by the DHI and the actual level of enhancement were not clear and this present study aims to clarify.

In order to provide the reader with further information for the interpretation of the presented results and conclusions, the following sections will provide a background on measuring viscosity by means of a rotational viscometer and a brief review on the use of CFD for modelling mixing of complex fluids.

1.1. Background – Measuring viscosity by means of a rotational viscometer

For the rheological measurement of materials by means of a rotational viscometer with a coaxial cylindrical geometry, there is a theoretical basis for the calculation of the viscosity. Consider a cylinder of radius R_s and length, L_s, rotating at an angular velocity, ω, inside a stationary cylinder of radius, R_c. The shear rate at the surface of the spindle, $\dot{\gamma}$, is

$$\dot{\gamma} = \frac{2\omega R_c^2}{R_c^2 - R_s^2}, \tag{1}$$

and the shear stress, τ, is

$$\tau = \frac{T}{2\pi R_s^2 L}, \tag{2}$$

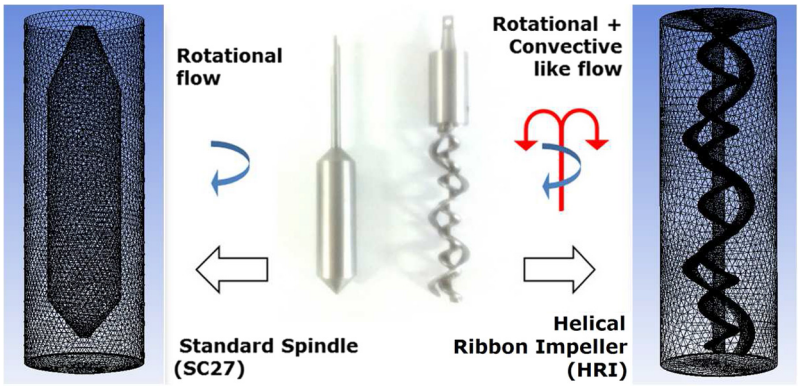

Fig. 2. On the left, the standard SC27 spindle and associated surface mesh; on the right, the Dual Helical Ribbon Impellor (DHRI) and mesh.

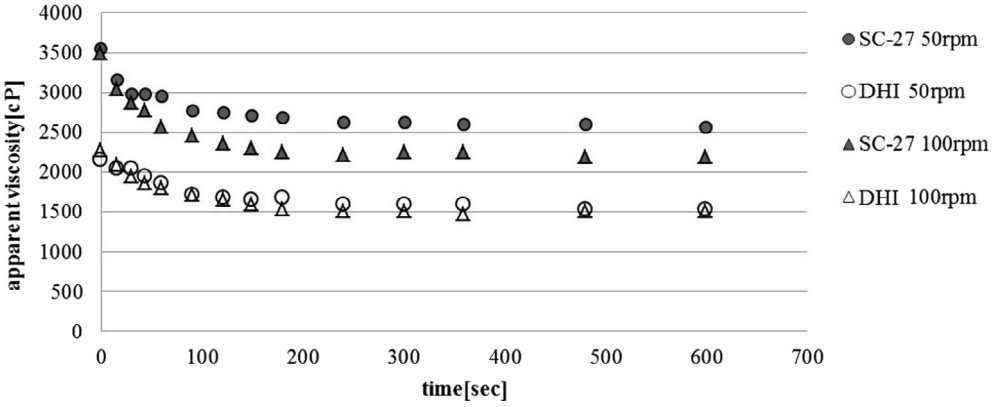

Fig. 3. Apparent viscosity of a TR-MB at 180 °C using a rotational viscometer at 50 to 100 rpm [19].

where T is the torque input by the machine. The viscosity, μ, is

$$\mu = \frac{\tau}{\dot{\gamma}} = \frac{T(R_c^2 - R_s^2)}{4\pi\omega R_c^2 R_s^2 L}. \tag{3}$$

So, since all the variables on the right-hand-side of Eq. (3) are measurable, the viscosity can easily and reliably be determined.

Now, when an non-cylindrical impeller is used in the viscometer, there are no tractable equations for the shear rate or shear stress akin to Eqs. (1) and (2). This presents a challenge since, while the impellers may be good at mixing, there is no simple way of analytically determining the viscosity of the mixture. The only quantities that can be measured directly are the torque, T, and the angular velocity, ω.

In this case, one way to proceed is to calibrate the impeller using a range of single and multi-phase fluids of known viscosity, which may have been measured with the standard spindle viscometer. Then, the viscosity becomes a function of the two measurable variables

$$\mu = \mu(T, \omega). \tag{4}$$

There is no information about the shear rate or the shear stress that can be derived because the complex 3D nature of the flow precludes that. After testing a wide range of fluids of different viscosities, a surface fit could be made and then for a given T and ω, the viscosity of an unknown fluid could be calculated. The situation is further complicated in that the calibration procedure would then have to be done for each class of fluid (Newtonian, shear thinning, shear thickening, etc.) and a judgement would have to be made by the user as to which class of fluid they had in the viscometer.

A different approach is that promoted by Brookfield and utilized, for example, in Lo Presti et al. [19]. Each different spindle geometry provided by Brookfield for use in their viscometers is ascribed a Spindle Multiplier Constant (SMC) value. For example, the SC4-27 has an SMC of 25. Further, each viscometer model, here we are using the LVDV-E, has a Torque Constant, TK, which allows the apparent viscosity to be found from

$$\mu = \frac{0.1}{N} \cdot \mathrm{TK} \cdot \mathrm{SMC} \cdot \mathrm{T\%}, \tag{5}$$

where N is the rotational speed (rpm) and T% is percentage of the maximum spring torque that the viscometer can deliver. In addition, the Strain Rate Constant (SRC) is defined as

$$\dot{\gamma} = \mathrm{SRC} \cdot N = \mathrm{SRC} \cdot \left(\frac{60}{2\pi}\right)\omega. \tag{6}$$

Equating (1) and (6) allows us to write

$$\mathrm{SRC} = \frac{\pi}{15}\frac{R_c^2}{R_c^2 - R_s^2}, \tag{7}$$

which, when the dimensions of the SC4-27 spindle and its container (Fig. 4) are considered, results in a value of 0.34, which tallies with that in Brookfield's literature [5].

For a design such as a DHI, this is a simplification but one which can produce values of apparent viscosity that are of practical use. Lo Presti et al. [19] attempted, with some success, to match the behaviour of the DHI to the range of SC-XX spindles offered by Brookfield. The SC4-XX range are of the cylindrical type and each has unique SRC and SMC values. The Brookfield viscometer allows only the selection of a spindle code, which has associated SRC and

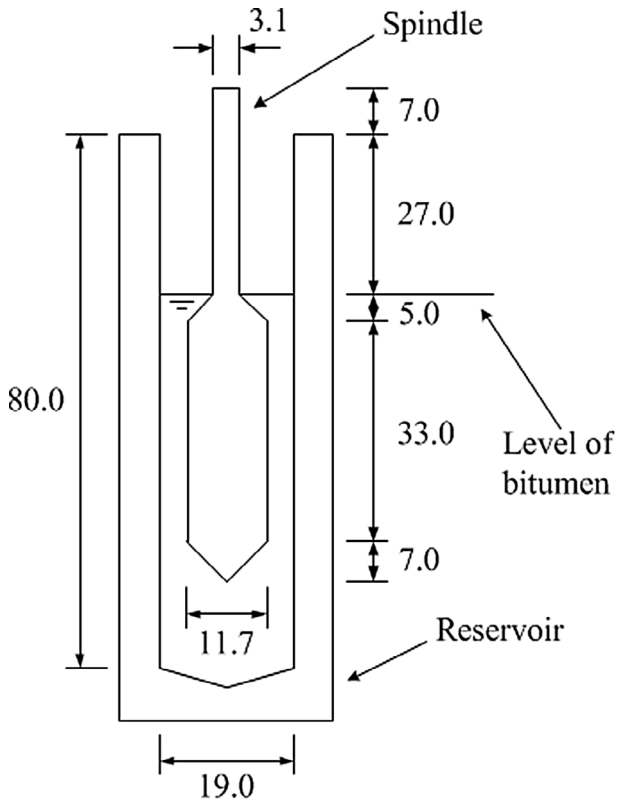

Fig. 4. A schematic of the Brookfield SC4-27 spindle.

SMC values, thus limiting fine adjustment to a discrete set of values. Lo Presti et al. [19] were nevertheless able to find a spindle code that matched closely the DHI and did this by testing the DHI against a number of standard liquids of known viscosity. The SC4-28 spindle was found to most closely match the DHI with values of SRC of 0.28 and SMC of 50. The validity of this approach is open to question because of the radically differing spindle geometries of the SC4-28 and DHI. Thus, computational fluid dynamics was seen as an alternative method of obtaining values of SRC and SMC for the DHI geometry.

1.2. Background – CFD modelling of the mixing of complex fluids

The mixing of two or more miscible phases, whether it be solid/liquid, gas/liquid or liquid/gas or combinations thereof, are widely encountered in mineral, food, pharmaceutical, polymer, metallurgical, biochemical, and other industrial processes [23]. The mixing of highly viscous fluids is often carried out in the laminar and transition regimes. Many impellers were proposed by researchers based either on using large impeller diameters or close-clearance designs like anchors and helical ribbons [9,14,8,30,24].

Generally, this mixing is carried out in stirred vessels and it has been reported that the so-called helical ribbon and helical screw impellers are most appropriate for efficient mixing of high viscosity Newtonian [22] and non-Newtonian liquids [33]. Before the development of numerical simulations, mixers were normally evaluated experimentally using various measures: power consumption (e.g. [29,27]); mixing time (e.g. [28,26]); and circulation time.

However, none of these measures give an understanding of the spatial variation of the phases or the nature of the transport processes, making the understanding and hence the efficient optimisation of the mixer design difficult. Numerical simulations offer a greater flexibility in analysing and visualising the mixing. In recent years, the simulation of mixing vessels is widely used to optimize mixer geometries and get better insights of the complex flow patterns generated by the impeller-vessel wall interaction [30,24]. From the perspective of numerical analysis, one of the pioneering CFD works focused on the mixing performance of helical ribbon impellers in cylindrical vessels is the contribution made by Tanguy et al. [29]. They developed a three-dimensional model, which was validated experimentally, based on the finite-element method for the analysis of a Helical Ribbon-screw impeller. The authors reported good liquid circulation at low impeller speeds (10 rpm) and showed evidence of poor pumping in the vessel bottom. They noticed that the segregation increased upon increasing the impeller speed. In subsequent work numerical models were developed for several helical ribbon geometries and fluids of rheological behaviours [4]. The numerical modelling of mixing in a stirred tank has attracted a great deal of attention and a review of the state-of- the-art in CFD simulations of stirred vessels can be found in Sommerfeld and Decker [25].

The rapid development of numerical techniques and computational power has unleashed the possibilities of Computational Fluid Dynamics (CFD) in this area. CFD is now an important tool for understanding the mixing in stirred tanks [31]. Nevertheless, modelling of the complex flow in the presence of a rotating impeller is a computational challenge because of the complex geometry of the impeller and the nature of the flow in stirred tanks. Although CFD codes have made remarkable steps towards the solution of such engineering problems over the last decade, it still remains a difficult task to use such codes to help the design and the analysis of stirred tanks. Iranshahi et al. [16] investigated the flow patterns and mixing progress in a vessel equipped with a Maxblend impeller in the case of Newtonian fluids. In that study, they found that the Maxblend impeller showed good performance when used with baffles in the transition and laminar regimes. In another study, a CFD characterization of the hydrodynamics of the Maxblend impeller with Newtonian and non-Newtonian inelastic fluids in the laminar and transition regimes was carried out by Devals et al. [11]. In that study, the effect of the impeller bottom clearance and the Reynolds number on the power characteristics, the distribution of shear rates and the overall flow condition in the vessel were investigated. Yao et al. [32] performed numerical analysis for the local and total dispersive mixing performance in a stirring tank with a standard type of Maxblend and double helical ribbon impellers. They showed that the double Helical Ribbon cannot be an efficient dispersive mixer – however, the results were not validated by experimental tests.

Iranshahi et al. [15] investigated the fluid flow in a vessel stirred with a Ekato Paravisc impeller in the laminar regime using CFD. The viscous mixing characteristics of the Ekato Paravisc were compared with those of an anchor and a double helical ribbon. They were able to show, through a number of experimentally validated criteria, that the Paravisc impeller was capable of producing homogeneous mixtures. Numerical modelling was carried out by Bertrand et al. [4] to predict a rise in power draw due to elasticity. They explained the numerical methodology and compared the results of the simulation with experimental tests in the case of a stirred tank with a helical ribbon. Barailler et al. [3] performed CFD modelling of a rotor–stator mixer in the laminar regime. In this study they investigated the characteristics of the rotor–stator mixing head in the case of viscous Newtonian fluids. Delaplace et al. [10] developed an approximate analytical model based on the Couette flow analogy to predict power consumption for the mixing of pseudoplastic fluids with helical ribbon and helical screw ribbon impellers in the laminar regime. They presented extensive comparisons between the predicted results and the data which was reported in the existing literature.

1.3. Aims and structure of the paper

This paper presents a Computational Fluid Dynamics (CFD) model able to reproduce the observations obtained from a laboratory investigation aimed at resembling a bitumen-rubber system during product development over a wide range of testing conditions (e.g. temperatures, particle contents, impeller speed). In order to allow visual inspections, the experimental programme was performed by using tyre rubber particles and transparent fluids having viscosities similar to the bitumen phase of rubberised binder at manufacturing and testing temperatures. The overall objective of the present study is to assess whether a CFD model would be able to simulate this complex scenario and to couple these outcomes with visual images to shed light on the results obtained in a previous study [19], where the DHI provided "more realistic" viscosity measurements when compared to the standard spindle. By doing this, we aim to highlight the benefits and limitations of using the DHI geometry to perform viscosity measurements of complex fluids, as well as using the model to validating the empirical calibration procedure (SMC and SRC).

Section 2 introduces a brief description of the experiments along with the numerical framework and governing equations for the CFD model. The results of the experimental and numerical modelling, along with a discussion thereof, are presented in Section 3, which ultimately aims to validate the numerical model. Finally, conclusions are presented in Section 4 with some thoughts about the next steps in this programme of work.

2. Methodology

2.1. Experimental campaign

As mentioned earlier, in a previous investigation experimental studies were carried out to calibrate the DHI and to evaluate the improved mixing when used in a Brookfield viscometer [19]. In order to allow visualisation of the movement of particles in the system, the viscometer was customised with a transparent outer cyclinder (e.g. Fig. 1). The experimental programme used multiphase fluids made up of a range of standard viscosity fluids and tyre rubber particles.

Thus, nine different complex fluids were made from the combination of different standard-viscosity fluids and different diameter tyre rubber particles (Table. 1)– all fluids being tested at 10, 100 and 200 rpm at ambient temperature (20 °C). The range of viscosity and particle diameters have been chosen in order to recreate systems similar in terms of viscosity and physical composition to tyre rubber-bitumen blends at temperatures between 100 and 200 °C. This is considered to be representative of the possible scenarios occurring during the low shear modification of bitumen with crumb rubber particles [18].

Due to the expected high torque, which would be close to the viscometer's limits, the tests with the f500 fluid were performed up to 100 rpm. Tests were conducted according to Subhy et al. [26], which are based on international standards on viscosity measurements of a rubberized bitumen (asphalt rubber) [1,2]. These were undertaken for durations of between 15 and 20 minutes, depending on how quickly the mixing was seen to reach a steady distribution. The particles were added to the fluid and the blend was shaken to produce an even distribution of the particles. In these conditions, the impellers were quickly submerged in the blend and the viscometer was turned on to carry out the test, during which torque and angular velocity were measured and the viscosity calculated from Eq. (3).

Results were compared against those obtained with a standard spindle, SC4-27, to establish which geometry produced the highest degree of homogenisation and hence the more realistic, repeatable and reliable viscosity measurements.

Table 1
Fluid and particle properties.

Name	Fluid		Particles	
	Density (kg m^{-3})	Viscosity (Pa s)	Diameter (μm)	Volume fraction
f10	940	0.01	200	1%
f100	960	0.1	400	3%
f500	970	0.5	1000	5%

2.2. CFD simulations

In parallel with these experiments, a CFD study was conducted with the aim of qualitatively comparing the two sets of results. Version 14 of ANSYS Fluent, the commercially available CFD software, was used in this work.

2.2.1. Governing equations

The modelling involves the solution of the Navier–Stokes equations, which are based on the assumptions of conservation of mass and momentum within a moving fluid. In order to simulate the behaviour of the complex, two phase fluids in the present application, the mixture model was used. Here, the momentum and continuity equations are solved for the mixture, the volume fraction equations for the secondary phases, while algebraic expressions are used for the relative velocities and inter-phase drag. The mixture model lends itself to particle-laden flows with relatively low volume loading, which is the situation in the present work.

First the mixture continuity equation

$$\frac{\partial \rho_m}{\partial t} + \nabla \cdot (\rho_m \mathbf{u}) = 0, \tag{8}$$

where $\mathbf{u}$ is the velocity, ρ is the density and the subscript m indicates a quantity defined for the mixture. The mixture velocity is a mass-weighted average of the n phases

$$\mathbf{u}_m = \frac{1}{\rho_m} \sum_{k=1}^{n} \alpha_k \rho_k \mathbf{u}_k, \tag{9}$$

where α is the volume fraction and k refers to the kth phase. The mixture density is

$$\rho_m = \sum_{k=1}^{n} \alpha_k \rho_k. \tag{10}$$

The momentum equation is

$$\frac{\partial}{\partial t}(\rho_m \mathbf{u}_m) + \nabla \cdot (\rho_m \mathbf{u}_m \mathbf{u}_m) = \nabla p + \nabla \cdot \left[\mu_m (\nabla \mathbf{u}_m + \nabla \mathbf{u}_m^T)\right] + \rho_m \mathbf{g} + \nabla \cdot \left(\sum_{k=2}^{n} \alpha_k \rho_k \mathbf{u}_{\mathrm{dr},k} \mathbf{u}_{\mathrm{dr},k} \right), \tag{11}$$

where $\mathbf{g}$ is the gravitational acceleration and $\mathbf{u}_{\mathrm{dr},k}$ is the drift velocity for the secondary phase k,

$$\mathbf{u}_{\mathrm{dr},k} = \mathbf{u}_k - \mathbf{u}_m. \tag{12}$$

The mixture model in ANSYS FLUENT uses an algebraic slip formulation, which is based on the work of Manninen et al. [21]. It uses the slip velocity, which is related on the drift velocity defined in Eq. (12). The velocity of the kth phase is calculated from algebraic expressions, rather than a separate momentum equation. So, the final term on the right hand side of Eq. (11) imparts a momentum source or sink to the mixture momemtum equation,

based on the relative motion of the primary and secondary phases. In the present work, the viscosity of the two phases are assumed to be equal to that of the primary, bituminous phase.

2.3. CFD model setup

It is accepted practice in stirred or mixing vessels to use the mixing Reynolds number, Re_m to characterise the flow

$$Re_m = \frac{\rho D^2 N'}{\mu} \quad (13)$$

where D is the diameter of the impeller and N' is the number of revolutions per second. For $Re_m > 10,000$, the flow is assumed to be fully turbulent. In the present application, with the least viscous fluid and the highest impeller speed, the mixing Reynolds number is approximately 100, which indicates all simulations are laminar.

For the spindle geometry, smooth, no slip wall boundary conditions were applied to the inner, outer and bottom walls. The upper boundary was set as a symmetry plane as the shear between air and bitumen is insignificant. A moving mesh approach was used, where the entire fluid domain was rotated about the vertical z axis at the appropriate angular velocity, while the outer wall was held stationary relative to the moving zone. The reason for doing this, rather than simply moving the outer wall relative to a stationary fluid domain was so that animations for the DHI impeller could be produced with the helices being seen in motion. There was no significant computational overhead associated with the approach used.

The geometry of the spindle was developed based on the Brookfield SC4-27 and realised with ANSYS DesignModeler. A mesh consisting of tetrahedra and triangular prisms (in the inflation layers adjacent to walls) was generated using ANSYS Meshing and the volume mesh associated with the surface mesh shown in Fig. 5 contains 155,000 cells.

The DHI geometry was designed to create a convective like flow within the sample, which allows the uniform distribution of suspended solids within a viscous fluid. The idea is that the outer helix pumps the fluid downwards while the inner helix pumps it upwards. Based on the prototype design, DesignModeler and Meshing were used to produce a mesh, which, due to the increased complexity of the design, contained approximately 1300,000 tetrahedral and triangular prism cells. The CAD model and associated surface mesh can be seen in Fig. 6. A mesh convergence study was conducted with the DHI geometry and key flow parameters at monitoring points were found not to change as the number of cells increased above the 1.3 million of the mesh shown in Fig. 6.

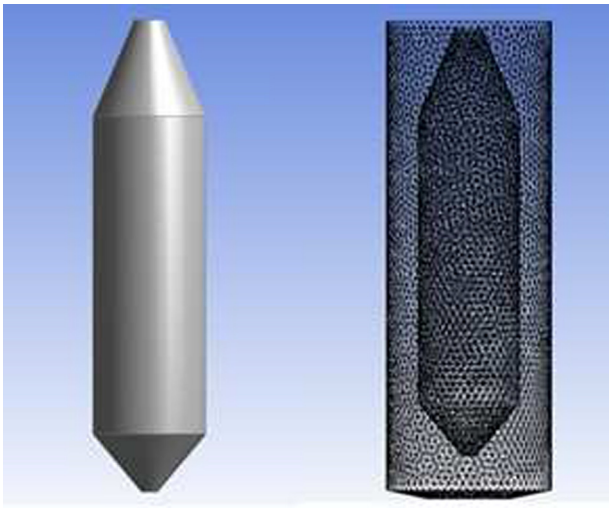

Fig. 5. On the left, a solid model of the Brookfield SC4-27 spindle; and on the right, the surface mesh on the spindle and outer wall.

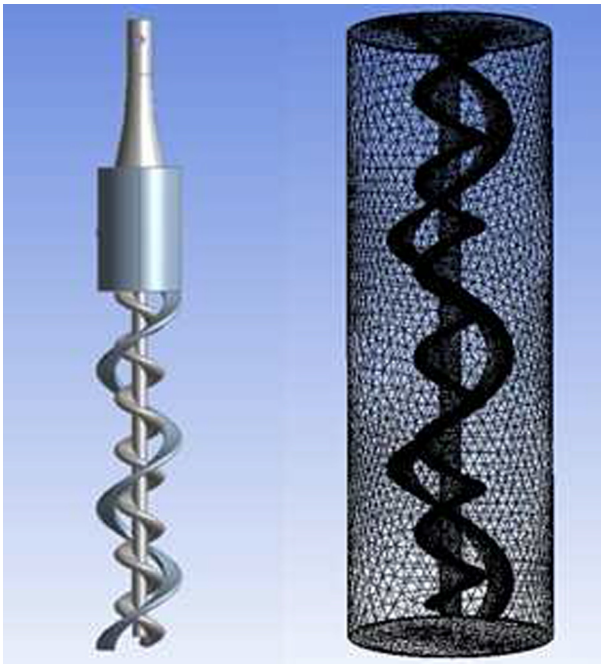

Fig. 6. On the left, a solid model of the DHI mixer; and on the right, the surface mesh on the mixer and outer wall.

Standard solver settings were used throughout: the SIMPLE algorithm was used for pressure–velocity coupling; the Least Squares Cell Based discretization for gradients and second order differencing for the momentum and volume fraction equations. Due to the use of a moving mesh, the solution was necessarily transient and it was found that the simulations had to be run for ~60 s of real time to achieve a stationary solution, where the mean velocity and volume fraction did not drift with time, as measured at a number of monitoring points. The exact run time varied depending on fluid properties and rotation rate.

3. Results

3.1. Experimental

In the manufacturing of rubberized bitumen, the process can take up to 2 h, at which point the particles have swollen to their maximum extent. However, in these experiments, in certain cases (i.e. for the f10 fluid with 400 μm particles) the particles were already settling after a few seconds. It was decided that a testing period of 10 minutes was sufficient to resolve the settling process without the swelling of the particles compromising the results.

Figs. 7 and 8 show images of the distribution of the particles within the blend at the start of the tests and after 10 minutes of rotation for the f100 and f500 fluids respectively. These figures show that using the lower viscosity fluid, f100, at 10 rpm both standard spindle and the DHI do not maintain particles in suspension. At 100 and 200 rpm it is interesting to note how, due its shape, the standard impeller creates two layers of crumb rubber particles on top and bottom. In this case, the particles are forced to migrate from the narrow gap into regions where the swirl is less intense.

However, at these higher rotation rates, the DHI creates a more even distribution of particles. Observations confirmed that this was

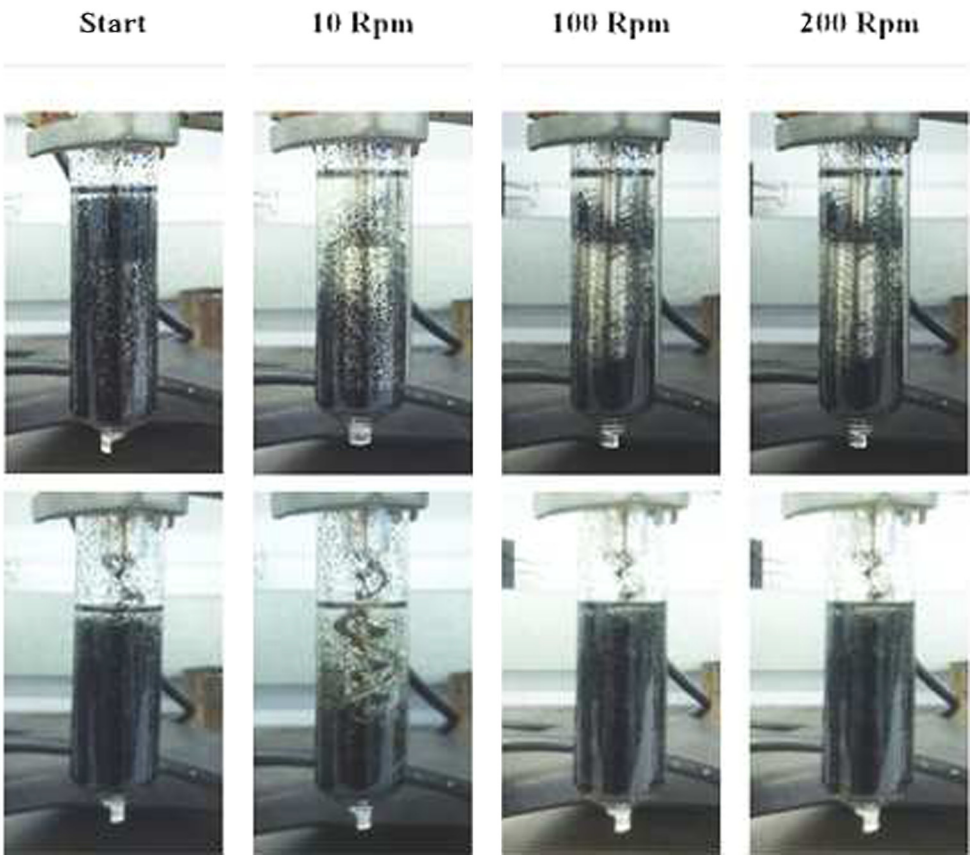

Fig. 7. Images of the distribution of particles in the viscometer using the f100 fluid for the SC4-27 spindle (top) and DHI (bottom) at the start of the test and after 10 minutes for various rotational speeds.

a result of a combination of effects consisting in the inner spiral transporting the particles upwards while the outer thread moves the particles back down – confirming that the design was working as intended. As a result, particles are circulated throughout the container and phase separation is avoided for the whole duration of the experiment.

These results show that the rotational speed is of fundamental importance when considering the extent to which the sample is homogenised and plays a crucial role in determining the efficacy of the impeller. This, of course, has significant consequences on the viscosity readings, which are a function of testing geometry, rotational speed and applied torque.

Fig. 9 shows that the apparent viscosity measurements are independent of the rotational speed for the DHI than the SC4-27 spindle (apart from at 10 rpm). The fact that the curves for 100 and 200 rpm are convergent for the DHI echoes the observations made about Fig. 7, where the higher rotational speeds produce a less heterogeneous blend. At 10 rpm, there is clearly some intermittency to the viscosity measurements as the particles do not reach a steady-state distribution. In any case, both viscosity values over time and shear dependency, play in favour of the DHI, which seems to provide more stable rheological information of this complex system – itself an indication of the better mixing efficiency over the timescale of the test.

For the higher viscosity fluid, f500, over the same timescale, these observations are not so clear (Fig. 10). In this test, all viscosity measurements are still increasing after 600 s, suggesting that the particles were still undergoing redistribution or possibly the swelling process is starting, especially at the higher rotational speed. Indeed, the absence of a 200 rpm result prevents the same conclusion being drawn for convergence of the viscosity results as the rotation speed is increased above 100 rpm. Indeed, after 20 minutes (1200 s) the viscosity had still not settled down to a consistent value. Unfortunately, running the tests for a longer period meant that the temperature of the mixture would begin to drop and viscosity measurements would then have a temperature component. Again, however, the viscosity trend with time still favours the DHI.

3.2. CFD simulations

3.2.1. Validation (Single Phase)

While not presented here, it should be noted that the CFD model of the SC4-27 spindle produced values of SRC and SMC that were very close (within 1%) as those quoted in the Brookfield literature for a range of rotational speeds and fluid viscosities.

Then, for the DHI geomerty, in an attempt to reproduce the single phase experimental testing of Lo Presti et al. [19], a number of single phase simulations were performed. The rotational speed of the impeller was again varied as too was the viscosity of the fluid. Values of both the rotational speed and dynamic viscosity were matched to those used by Lo Presti et al. [19] as closely as possible. The dynamic viscosity values used were 0.0094, 0.098, 0.488, 0.970 and 5.040 Pa s, while rotational speeds of 10, 50, 100 and 200 rpm were chosen. Thus, in total, 20 simulations were performed. In order to be able to compare across this range of viscosity and rotational speed, the mixing Reynolds number, Eq. (13), was used with an equivalent diameter of 11.7 mm. The choice of the diameter is somewhat arbitrary and corresponds in this case to the diameter of the SC4-27 spindle, although it is a value roughly halfway between the inner and outer helices of the DHI. The SMC values are calculated from a re-arrangement of Eq. (5), via a conversion

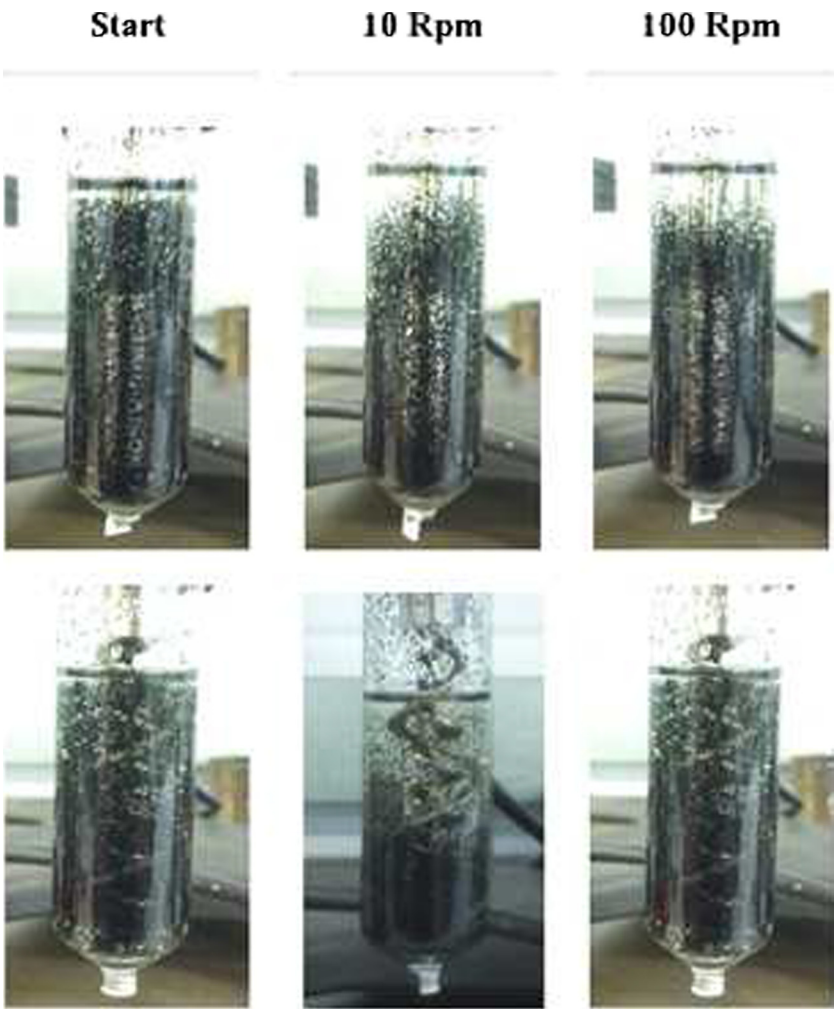

Fig. 8. Images of the distribution of particles in the viscometer using the f500 fluid for the SC4-27 spindle (top) and DHI (bottom) at the start of the test and after 10 minutes for various rotational speeds.

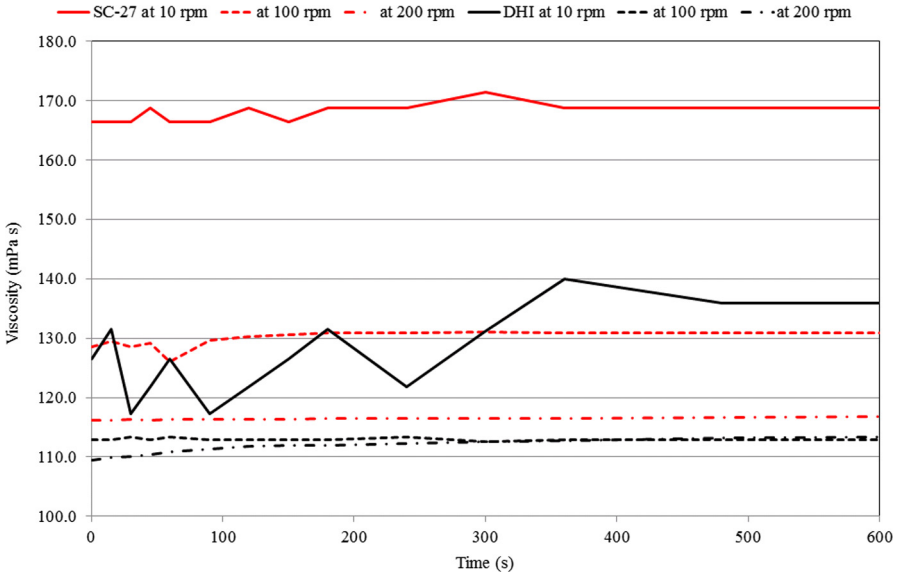

Fig. 9. The variation of viscosity with time during the tests for the SC4-27 spindle and DHI at 10, 100 and 200 rpm using the f100 fluid.

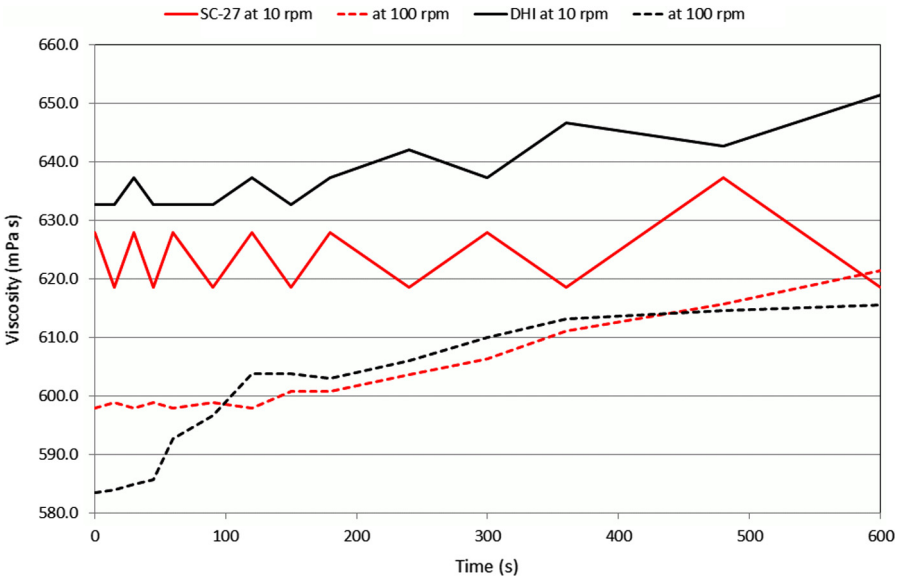

Fig. 10. The variation of viscosity with time during the tests for the SC4-27 spindle and DHI at 10 and 100 rpm using the f500 fluid.

of the torque that Fluent reported to an equivalent percentage torque, T%, reported by the Brookfield viscometer.

Fig. 11 shows a clustering of the SMC values around a value of 50, across a 5 decade range of Reynolds numbers. Note that the value of SMC that Lo Presti et al. [19] found for the DHI was 50 and so there is quantitative agreement between the experiment and simulations. What the numerical modelling reveals, however, is that at a fixed rotational speed, there is a dependency on the Reynolds number, the extent of which is reduced at the highest rotational speed of 200 rpm. Similarly, we see that for a fixed value of viscosity there is a marked increase in SMC as the rotational speed is increased. This can be seen in the clustering of results in lines comprised of the four symbols from left to right. There are several explanations for this functional dependence of SMC on Re_m. First since the same mesh was used for all simulations, the local cell Reynolds numbers would differ from simulation to simulation, which may result in a numerical errors being introduced.

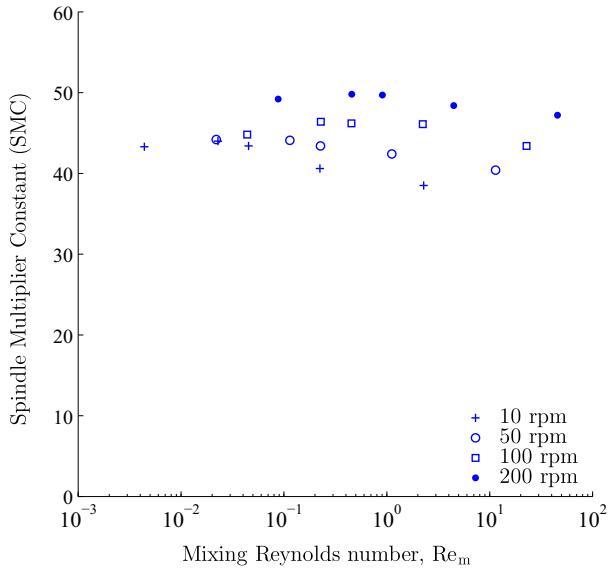

Fig. 11. Plot of the Spindle Multiplier Constant (SMC) against mixing Reynolds number for the DHI impellor.

Second, from the physical perspective, it is thought that the variations are down to the flow patterns changing across the range of Reynolds numbers. There is some experimental evidence to back this up. With reference back to Fig. 7, it can be seen that the DHI produces more consistent mixing at a rotational speed of greater than 100 rpm. This may be attributed to the impeller producing a different flow field, a more efficient flow field from the mixing perspective, that at 10 rpm. This difference may explain the function dependence of SMC on the mixing Reynolds number.

3.2.2. Understanding the DHI mixing process (multiphase)

When considering all the combinations of parameters in the experimental tests discussed in Section 3.1, it became apparent that there were two distinct sets of cases: those with stratification of the particulate phase and those where homogeneous mixing was observed. Thus, the numerical modelling focused on the cases where these extremes were exhibited. Table 2 shows the range of simulations that were run with a ♢ indicating those cases where phase stratification was expected and a • where a level of homogeneity in the secondary phase distribution was expected. The two gaps in the table are due to the high viscosity of the f500 preventing the viscometer from operating under those conditions. In all cases the volume fraction of the particulate phase was 3 % and the diameter of the particles was 400 μm.

Before considering the mixing efficiencies of the two designs, it is instructive to look at the velocity fields in both cases. Fig. 12(a) shows contours of the steady-state velocity magnitude for the SC4-27 spindle. The SC4-27 creates a Taylor–Couette flow between the rotating spindle and the stationary wall. There is a large circumferential or swirling component to the flow but not a vertical component. As such, particulates in the flow are not driven vertically through the gap (in either direction) but rather tend to sink to the bottom under the effects of gravity.

On the other hand, the instantaneous velocity field for the DHI, Fig. 12(b), presents a far more complex picture. Here the plot is showing a snapshot of the velocity magnitude and what cannot be gleaned from this plot that the outer helix is moving fluid downwards, while the inner one is moving fluid upwards. This becomes clear in Fig. 13, in which the vector length is constant but the colour represents the local velocity magnitude (blue is zero, red is 0.061 m s^{-1}). While the figure shows only the vectors on a vertical

Table 2
The CFD simulations (♢ indicates cases where experimentally there was phase stratification, • where there was a good level of mixing).

	SC4-27			DHI		
Fluid	10 rpm	100 rpm	200 rpm	10 rpm	100 rpm	200 rpm
f100	♢	♢	♢	♢	•	•
f500	♢	•		♢	•	

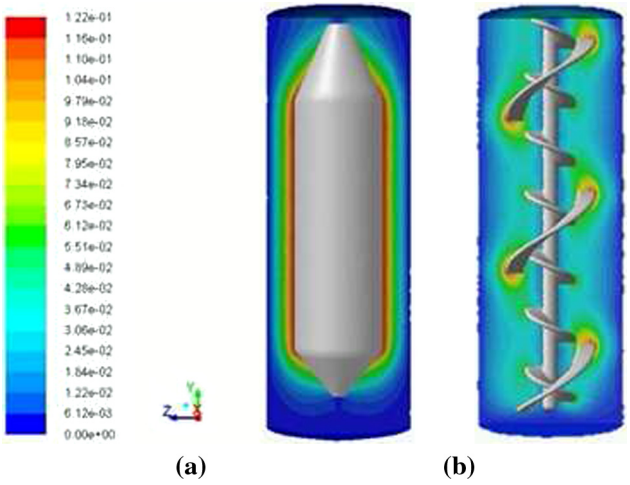

Fig. 12. Contours of velocity magnitude for the (a) SC4-27 spindle and (b) DHI (right) at 100 rpm.

plane and the view focusses on the mid-height region, the flow is now entirely 3D in nature and the simple observations and theory associated with Taylor-Couette flow are no longer possible.

To gain a better understanding of the degree of homogenisation, the volume fraction of the particulate phase was evaluated once the volume fraction for both types of spindle had reached a steady-state. For the DHI, while the velocity is not steady, the distribution of particles does reach something very close to a steady state because of the very low settling velocity of the particles in the highly viscous fluids under consideration. Qualitatively, the

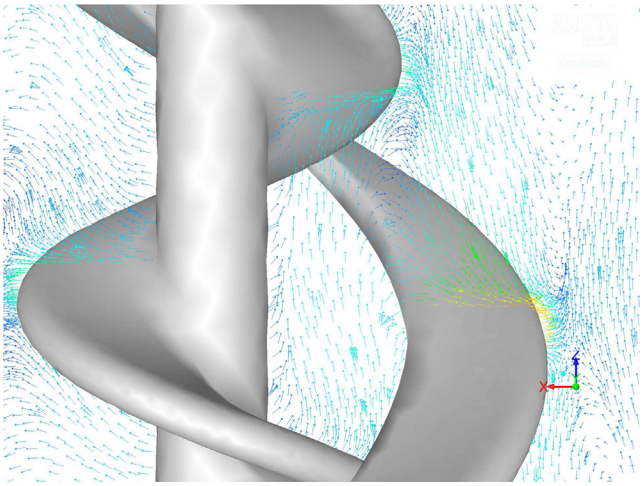

Fig. 13. A close-up of the inner and outer helices of the DHI impellor, showing the flow vectors on the plane $y = 0$. Vectors are the same length and the velocity magnitude is indicated by the color (blue is zero, red is 0.061 m s^{-1}). (For interpretation of the references to colour in this figure legend, the reader is referred to the web version of this article.)

results from the numerical simulations, compared very favourably with the experimental results.

Fig. 14 shows the results achieved using the f100 and f500 fluids at different rotational speeds for both the CFD model and the experimental tests. With reference to the figure, the contour plots of the volume fraction of the particulate phase do bear some similarity to the photographs from the experiments that are shown below them. The highly concentrated zone of particles near the bottom of the container (indicated by the red region, which corresponds to a volume fraction of 0.08) becomes less apparent when the angular velocity of the spindle and the viscosity of the fluids are increased. In fact, the contour range is clipped to a maximum of 0.08, so although the zone for the f100, 10 rpm case looks small, it is in fact a very small region of very high concentrations. In this case, the suspended particles are able to sink to the bottom and concentrate on the central region where fluid motion is minimal – see Fig. 12(a).

There is still some stratification of the secondary phase in all the plots in Fig. 14, which is also apparent in the experimental results. Two effects are not captured by the CFD model, however. First, the floating scum of particles on the surface of the liquid are not seen because the top boundary of the CFD domain is a symmetry boundary – these particles are held there by surface tension effects, which are not included in the numerical model. Second, the CFD model does not show the that some particles stay above the narrow Couette flow region, as well as falling below it. The gap between the spindle and the container wall seems to prevent the particles from settling out, at least on the time scales over which the experiments were run.

The CFD model confirms that the main issue of using the standard spindle is that it causes phase separation between the particles and bitumen leading to misleading viscosity measurements. This is due to the absence of vertical components of velocity in what is essentially a flow regime with cylindrical symmetry. Increasing the fluid viscosity (f500) can also lead to a more homogeneous distribution of particles in the liquid and reduces the phenomenon of particles concentration on the bottom. However, it is not clear that this enhanced mixing is not simply due to the lower terminal velocity of the particles in the more viscous fluid. A look at Fig. 10 would indicate that the apparent viscosity for the f500, 100 rpm case had not settled to a constant value and thus a longer test may have produced more stratification.

A very different picture generally emerges when considering the DHI impeller (Fig. 15). There is qualitative agreement between the CFD and experimental data in this case. However, at 10 rpm, the DHI still produces a noticeably stratified particulate phase. Again, due to the clipping of the volume fraction at 0.08, the fact that the red region (indicating volume fractions above 0.08) is larger than for the SC4-27 cases, then there is some agitation of the fluid in this region. This agitation is sufficient to keep the particles partially suspended above the base of the viscometer. Nonetheless, this level of mixing is not sufficient to render any apparent viscosity measurements reliable. At 100 rpm, a level of homogeneity is seen in the particulate phase, which indicates that the impeller is performing its intended task, which is to mix the particulate phase throughout the device.

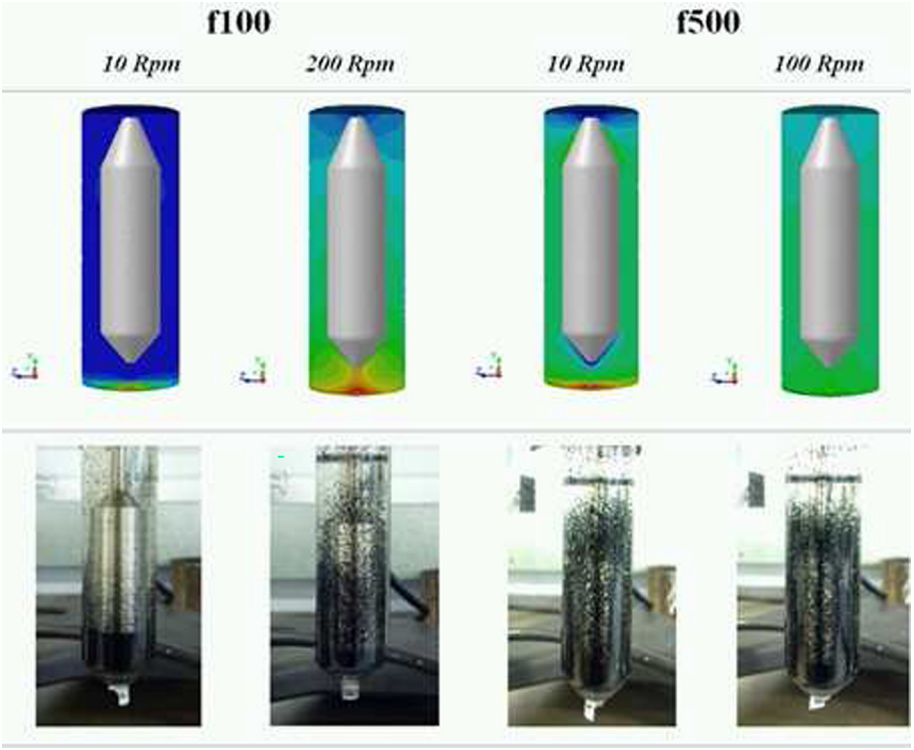

Fig. 14. Volume fractions from the CFD model (top) and experimental images (bottom) for the SC4-27 spindle. The volume fractions range from 0 (blue) to 0.08 (red). (For interpretation of the references to colour in this figure legend, the reader is referred to the web version of this article.)

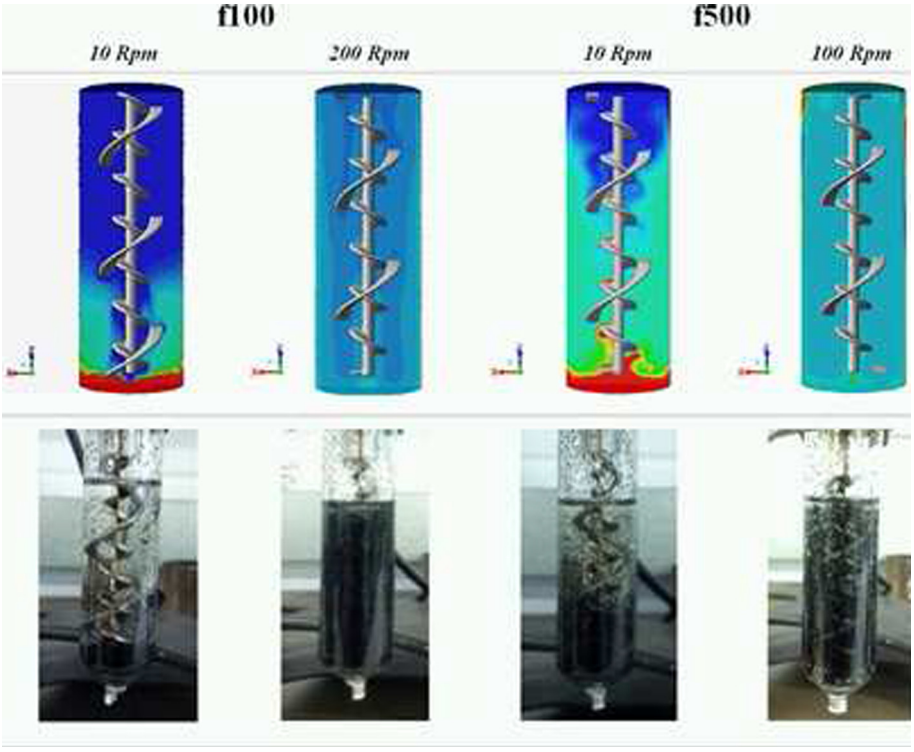

Fig. 15. Volume fractions from the CFD model (top) and experimental images (bottom) for the DHI. The volume fractions range from 0 (blue) to 0.08 (red). (For interpretation of the references to colour in this figure legend, the reader is referred to the web version of this article.)

4. Conclusions

In this study, the authors used customised laboratory testing and computer simulations to gain a deeper understanding of the fundamental mechanisms behind the improved viscosity measurements obtained when using the DHI with rubberised bitumen. Furthermore, this study look closely at the phase separation issues that can occur in a wide range of complex fluids. Overall, the following conclusions can be drawn:

- The experimental programme provided a clearer picture of the mixing enhancement provided by the DHI when measuring multiphase fluids composed of a liquid and a suspended particulate phase. Furthermore, the DHI geometry allows obtaining a steady apparent viscosity measurement and requires lower torques. This extends the range of measurable viscosity when compared to the standard spindle, SC4-27.
- CFD simulations clarified the mechanisms behind the previously assumed convective flow created by the DHI. In fact, the analysis of the velocity fields confirms that the central screw of the DHI drags up the complex system while the external screw transports the mixture downwards. Results also highlighted that with current design, the central screw of the DHI could be more effective at pumping the fluid vertically – this leads the way to enhancements in the design.
- The single phase CFD simulations produced values of SMC that were in close agreement with the experiments of Lo Presti et al. [19]. In summary, CFD helped to gain insights in the complex flow regimes and shows potential to be used as a platform to design new testing geometries for complex fluids as well as for virtual rheology measurements. In the next future, researchers should look with confidence in using CFD as platform for improving rheometry of complex fluids. The DHI showed to be a significant step forward from the testing geometries currently used for viscosity measurements of complex fluids, especially within product development. The author are looking at improving the current design as well as performing a campaign aimed at experimentally testing the viscometer for a variety of standard viscosity fluids with different particle loadings and diameters, as well as using complex systems with different rheological properties. This will allow to produce a library of results that will mean this rheometry can be used effectively in the bitumen and other industries for product development and quality control of these type of complex systems.

Acknowledgement

The authors wish to thank the University of Nottingham for the generous funding provided to support this research at two stages through the Bridging the Gaps feasibility award 2012 and the HERMES fellowship 2014. Furthermore, a special thanks goes to Mr. Clive Dixon who allowed customisation of the glass small sample containers. This work was supported by the Engineering and Physical Sciences Research Council (EPSRC) [grant number EP/M506588/1].

References

[1] ASTM. Standard test method for viscosity determination of asphalt at elevated temperatures using a rotational viscometer. American Society for Testing and Materials, a. D4402/D4402M.
[2] ASTM. Standard test method for measurement of apparent viscosity of asphalt-rubber or other asphalt binders by using a rotational hand held viscometer. American Society for Testing and Materials, b. D7741/D7741M.
[3] F. Barailler, M. Heniche, P.A. Tanguy, CFD analysis of a rotor-stator mixer with viscous fluids, Chem. Eng. Sci. 61 (9) (2006) 2888–2894, http://dx.doi.org/10.1016/j.ces.2005.10.064.
[4] F. Bertrand, P.A. Tanguy, E. Brito De La Fuente, P. Carreau, Numerical modeling of the mixing flow of second-order fluids with helical ribbon impellers, Comput. Methods Appl. Mech. Eng. 180 (3) (1999) 267–280, http://dx.doi.org/10.1016/S0045-7825(99)00169-3.
[5] Brookfield. More Solutions to Sticky Problems. Brookfield Engineering Labs., 2014.
[6] CALTRANS. Quality Control Manual for Hot Mix Asphalt. Department of Transportation, State of California, 2011.
[7] B. Celauro, C. Celauro, D. Lo Presti, A. Bevilacqua, Definition of a laboratory optimization protocol for road bitumen improved with recycled tire rubber, Constr. Build. Mater. 37 (2012) 562–572, http://dx.doi.org/10.1016/j.conbuildmat.2012.07.034.
[8] P.J. Cullen, C.P. O'Donnell, M. Houška, Rotational rheometry using complex geometries – a review, J. Texture Stud. 34 (1) (2003) 1–20, http://dx.doi.org/10.1111/j.1745-4603.2003.tb01052.x.
[9] G. Delaplace, J.C. Leuliet, V. Relandeau, Circulation and mixing times for helical ribbon impellers. Review and experiments, Exp. in Fluids 28 (2) (2000) 170–182, http://dx.doi.org/10.1007/s003480050022.
[10] G. Delaplace, R. Guerin, J.-C. Leuliet, R.P. Chhabra, An analytical model for the prediction of power consumption for shear-thinning fluids with helical ribbon and helical screw ribbon impellers, Chemical Engineering Science 61 (10) (2006) 3250–3259, http://dx.doi.org/10.1016/j.ces.2005.11.069.
[11] C. Devals, M. Heniche, K. Takenaka, P.A. Tanguy, CFD analysis of several design parameters affecting the performance of the Maxblend impeller, Computers & Chemical Engineering 32 (8) (2008) 1831–1841.
[12] R.B. Dow, The rheology of lubricants, Journal of Colloid Science 2 (1) (1947) 81–91.
[13] C. Gallegos, J.M. Franco, Rheology of food, cosmetics and pharmaceuticals, Current Opinion in Colloid & Interface Science 4 (4) (1999) 288–293, http://dx.doi.org/10.1016/S1359-0294(99)00003-5.
[14] G. Havas, J. Sawinsky, A. Deak, Investigation of the homogenization efficiency of the screw agitator, helical ribbon agitator, gate type anchor impeller and the multi-paddle agitator in the mixing of high-viscosity Newtonian liquids, Chemical Engineering 22 (4) (1978) 317–330.
[15] A. Iranshahi, M. Heniche, F. Bertrand, P.A. Tanguy, Numerical investigation of the mixing efficiency of the Ekato Paravisc impeller, Chem. Eng. Sci. 61 (8) (2006) 2609–2617, http://dx.doi.org/10.1016/j.ces.2005.11.032.
[16] A. Iranshahi, C. Devals, M. Heniche, L. Fradette, P.A. Tanguy, K. Takenaka, Hydrodynamics characterization of the Maxblend impeller, Chem. Eng. Sci. 62 (14) (2007) 3641–3653, http://dx.doi.org/10.1016/j.ces.2007.03.031.
[17] Shew-Fen Lin, Robert S. Brodkey, Rheological properties of slurry fuels (1978-present), J. Rheol. 29 (2) (1985) 147–175.
[18] D. Lo Presti, G. Airey, Tyre rubber-modified bitumens development: the effect of varying processing conditions, Road Mater. Pavement Des. 14 (4) (2013) 888–900, http://dx.doi.org/10.1080/14680629.2013.837837.
[19] D. Lo Presti, C. Fecarotti, A.T. Clare, G. Airey, Toward more realistic viscosity measurements of tyre rubber–bitumen blends, Constr. Build. Mater. 67 (2014) 270–278, http://dx.doi.org/10.1016/j.conbuildmat.2014.03.038.
[20] A.Y. Malkin, The state of the art in the rheology of polymers: achievements and challenges, Polym. Sci. Ser. A 51 (1) (2009) 80–102, http://dx.doi.org/10.1134/S0965545X09010076.
[21] Mikko Manninen, Veikko Taivassalo, Sirpa Kallio, et al. On the mixture model for multiphase flow, http://www.vtt.fi/inf/pdf/publications/1996/P288.pdf, 1996, VTT publications 288.
[22] W.I. Patterson, P.J. Carreau, C.Y. Yap, Mixing with helical ribbon agitators: Part II. Newtonian fluids, AIChE J. 25 (3) (1979) 508–516, http://dx.doi.org/10.1002/aic.690250317.
[23] E.L. Paul, V. Atiemo-Obeng, S.M. Kresta, Handbook of Industrial Mixing: Science and Practice, John Wiley & Sons, 2004.
[24] M. Robinson, P.W. Cleary, Flow and mixing performance in helical ribbon mixers, Chem. Eng. Sci. 84 (2012) 382–398, http://dx.doi.org/10.1016/j.ces.2012.08.044.
[25] M. Sommerfeld, S. Decker, State of the art and future trends in CFD simulation of stirred vessel hydrodynamics, Chem. Eng. Technol. 27 (3) (2004) 215–224, http://dx.doi.org/10.1002/ceat.200402007.
[26] A. Subhy, D. Lo Presti, G. Airey, Rubberised bitumen manufacturing assisted by rheological measurements, Road Mater. Pavement Des. 17 (2) (2015) 1–21, http://dx.doi.org/10.1080/14680629.2015.1079549.
[27] G. Tabilo-Munizaga, G.V. Barbosa-Cánovas, Rheology for the food industry, J. Food Eng. 67 (1) (2005) 147–156, http://dx.doi.org/10.1016/j.jfoodeng.2004.05.062.
[28] K. Takahashi, T. Yokota, H. Konno, Mixing of pseudoplastic liquid in a vessel equipped with a variety of helical ribbon impellers, J. Chem. Eng. Jpn. 21 (1) (1988) 63–68, http://dx.doi.org/10.1252/jcej.21.63.
[29] P.A. Tanguy, R. Lacroix, F. Bertrand, L. Choplin, E.B. De La Fuente, Finite element analysis of viscous mixing with a helical ribbon-screw impeller, AIChE Journal 38 (6) (1992) 939–944, http://dx.doi.org/10.1002/aic.690380614.
[30] Y.-Y. Tsui, Y.-C. Hu, Flow characteristics in mixers agitated by helical ribbon blade impeller, Eng. Appl. Comput. Fluid Mech. 5 (3) (2011) 416–429, http://dx.doi.org/10.1080/19942060.2011.11015383.
[31] B.-H. Um, T.R. Hanley, A CFD model for predicting the flow patterns of viscous fluids in a bioreactor under various operating conditions, Korean J. Chem. Eng. 25 (5) (2008) 1094–1102, http://dx.doi.org/10.1007/s11814-008-0179-y.
[32] W. Yao, M. Mishima, K. Takahashi, Numerical investigation on dispersive mixing characteristics of Maxblend and double helical ribbons, Chem. Eng. J. 84 (3) (2001) 565–571, http://dx.doi.org/10.1016/S1385-8947(01)00135-8.
[33] C.Y. Yap, W.I. Patterson, P.J. Carreau, Mixing with helical ribbon agitators: Part III. Non-Newtonian fluids, AIChE J. 25 (3) (1979) 516–521, http://dx.doi.org/10.1002/aic.690250318.

Road Materials and Pavement Design, 2020
https://doi.org/10.1080/14680629.2020.1724559

Taylor & Francis
Taylor & Francis Group

Check for updates

Are we correctly measuring the rotational viscosity of heterogeneous bituminous binders?

Gaspare Giancontieri[a], David Hargreaves[b] and Davide Lo Presti [a,b*]

[a]*Faculty of Civil Engineering, University of Palermo, Palermo, Italy;* [b]*Nottingham Transportation Engineering Centre, University of Nottingham, Nottingham, UK*

(*Received 18 February 2019; accepted 22 January 2020*)

Modified bituminous binders allow asphalt technologists to design asphalt mixtures with superior performance. However, several recent studies highlighted that due to the complexity of these material, their characterisation can be challenging since common procedures used to characterise neat bitumen might not be adequate. For instance, during high temperature rotational viscosity testing of recycled tyre rubber modified binders (RTR-MB), a number of changes may occur to the sample leading to the here-defined sample stability which in turn provides misleading results. In this study the authors want to first provide a deeper understanding of this phenomenon by a numerical analysis using a bespoke Computational Fluid Dynamics (CFD) model to simulate the laboratory tests and use innovative visual aids to monitor the sample stability of heterogeneous bituminous binders during the rotational test. The numerical analysis was complemented by a laboratory campaign aiming at proving the occurring of sample stability during viscosity measurement of heterogeneous bituminous binders with a standard testing setup (SC-27). Furthermore, a dual helical ribbon (DHR) is here introduced as a solution to overcome the issue. Hence, laboratory tests were undertaken also with DHR and differences in viscosity measurements of neat bitumen, SBS-MB and RTR-MB were recorded. Results of this combined numerical and empirical approach proved that the standard setup for rotational viscosity measurements seems not be adequate for RTR-MB and depending on the level of modification and test temperatures, might not be best suited for SBS-MB either. The DHR seems to solve the issue and authors strongly recommend the adoption of this testing geometry to obtain more realistic high-temperature viscosity measurement of heterogeneous bituminous binders.

Keywords: sample stability; dual helical ribbon; modified bitumen; CFD; recycled tyre rubber; rheology

1. Introduction

The experimental characterisation of bituminous material's rheological properties is of fundamental importance during their design as well as for predicting the asphalt mixtures performance. In order to assess whether adequate coating of aggregate occurs, as well as for ensuring pumpability and compactability of the mixtures, bitumen technologists are used to monitoring the high-temperature viscosity of bituminous binders (in the range 100–200°C) during product development and quality control (Caltrans, 2011). In a laboratory, usually rotational viscometers with coaxial cylinder configuration are used for this exercise. This testing setup consists of a tube into which the test fluid is poured, and a spindle is inserted and then rotated at a

*Corresponding author. Email: davide.lopresti@nottingham.ac.uk

© 2020 Informa UK Limited, trading as Taylor & Francis Group

selected rotational speed. The instrument will convert the value of torque applied into a viscosity reading. This setup was specifically designed for homogeneous systems (i.e. bitumen), however nowadays is used for any type of bituminous binders, no matters the complexity. In fact, the use of polymer modified bitumen is widely increased in pavement engineering. These binders are often able to improve the performance of asphalt mixtures (e.g. resistance to cracking, noise reduction etc.), (Huang, 2006; Peralta et al., 2010; Visser, Duhovny, & Sachkova, 2017; Zhang, Yu, Chen, & Jia, 2018) nevertheless, their rheological characterisation can be challenging due to complex structure of such materials. In fact, deviation from Newtonian behaviour, including shear rate dependent viscosity, elasticity and time-dependent rheological behaviour can provide misleading viscosity measurements (Celauro, Celauro, Presti, & Bevilacqua, 2012). The issue here is that some modified types of bitumen are multi-phase system that can present internal structure behaving differently from the bitumen matrix. This complexity sometime is highlighted by a lack of compatibility and in that case during hot storage the modifier could separate, either top or bottom of the container. This is a practical issue that bitumen technologists have to cope within asphalt plants, however if the difference between densities of modifier and bituminous matrix is significant, the same issue might be encountered also during laboratory measurements. This lack of sample stability may produce significantly inconsistent data.

These types of issues are encountered in other fields and for many other materials such as chocolate, plastic, rubber, ceramic, food, cosmetic, detergent, paints, glazing, lubricants, inks, adhesives, sealants, (Dow, 1946; Gallegos & Franco, 1999; Lin & Brodkey, 1985; Malkin, 2009; Tabilo-Munizaga, Barbosa-Cánovas, & Tonir, 2005). For these reasons the rotational viscometers are equipped with supplementary impellers designed to help rheologist for some of these scenarios. For instance, a vane spindle allows performing measurements with paste-like materials, gels, and fluids where suspended solids migrate away from the measurement surface of standard spindles. Furthermore, the Brookfield Helipath Stand is designed to slowly lower or raise a T-bar spindle so that it describes a helical path through the test sample. These accessories are all fit for purpose although they are not able to guarantee the sample stability of complex systems with high level of heterogeneity such as Recycled Tyre Rubber Modified Bitumen (RTR-MB) or other materials having the tendency to stratify during rotational tests due to phase density differences (Giancontieri, Hargreaves, & Lo Presti, 2018).

In a first attempt to address this issue, (Presti, Fecarotti, Clare, & Airey, 2014) successfully designed, manufactured and tested a prototype of a Dual Helical Impeller (DHI) for Brookfield Rotational Viscometers. Experimental studies were carried out to evaluate whether the DHI was able to improve the degree of homogenisation of high viscous fluids, in turns producing more realistic viscosity measurements. In comparison to the Brookfield standard cylindrical geometry (spindle SC-27), the DHI always predicted a different "apparent" viscosity. This result was explained by the capability of the DHI to create what have been likened to convective-like flows as opposed to the axisymmetric swirling flow induced by the standard SC-27 spindle. In a further study, (Presti, Giancontieri, & Hargreaves, 2017), the authors developed a bespoke numerical model able to reproduce the previous experimental campaign aimed to provide an insight into the flow field created by the DHI. Results proved that the modified impeller improved the overall grade of homogenisation within the sample, but also showed that a further optimisation of the DHI was possible. In fact, especially for the case of Recycled Tyre Rubber Modified Bitumen (RTR-MB), which can be considered as a heterogeneous blend of fluid and particles with different densities and size, testing the sample with an adequate thickness (gap size) is of primary importance to avoid misleading results. Rotational viscometers are equipped with spindles of different diameters and while this helps obtaining an adequate sample thickness, they still do not ensure sample stability. The DHI allowed a good mixing of the volume fractions but due to the

Figure 1. The DHR adapted to a Brookfield rotational viscometer.

tiny gap between the inner and outer helix, it can suffer of clogging especially when RTR-MB is used.

Considering the issues mentioned above, Giancontieri et al. (2018) carried out a shape optimisation of the DHI. Therefore, a testing configuration that improves the coaxial cylinders setup with a Dual Helical Ribbon (DHR) as impeller was developed. Figure 1 shows the DHR adapted for a rotational viscometer. The DHR was designed, manufactured and then validated using the Otto-Metzner method testing a wide range of non-Newtonian fluids. The optimised shape was designed to avoid issues of clogging as well as guaranteeing sample stability by creating an upward pumping within the inner region of the blades and allowing a downward stream on the peripheral side of the container. This leads to an effective convective flow of the fluid within the chamber with no risk of clogging and with improved dispersions of the particle.

To provide the reader with further information for the interpretation of the presented results and conclusions, the following sections will provide a background on measuring viscosity by means of non-standard equipment and a brief review on the use of CFD for modelling mixing of multi-phase fluids.

1.1. *Background – measuring viscosity using non-standard equipment*

For rheological measurements by means of rotational viscometer with coaxial cylinders, there is a theoretical basis for the calculation of the viscosity. Consider a cylinder of radius Rs, length, L, rotating at an angular velocity, ω, inside a stationary cylinder of radius, *Rc* (Mezger, 2006). The

shear rate at the surface of the spindle, $\dot{\gamma}$, is

$$\dot{\gamma} = \frac{2\omega R_c^2}{R_c^2 - R_s^2} \tag{1}$$

and the shear stress, τ, is

$$\tau = \frac{T}{2\tau R_s^2 L} \tag{2}$$

where T is the torque input by the machine. The viscosity, μ is

$$\mu = \frac{\tau}{\dot{\gamma}} = \frac{T(R_C^2 - R_S^2)}{4\pi\,\omega R_C^2 R_s^2 L} \tag{3}$$

So, since all the variables on the right-hand-side of Equation (3) are measurable, the viscosity can easily be determined. Now, when a non-cylindrical impeller is used in the viscometer, there are no tractable equations for the shear rate or shear stress akin to Equations (1) and (2). This presents a challenge since, while the impellers may be good at mixing, there is no simple way of deriving the viscosity of the mixture. The only quantities that can be measured directly are the torque, T, and the angular velocity, ω. In this case, the only way to proceed is to use the impeller design in a range of single and multi-phase fluids of known viscosity, which have been measured with the standard spindle viscometer. Then, the viscosity becomes a function of these two measurable variables

$$\mu = \mu(T, \omega) \tag{4}$$

There is no information about the shear rate or the shear stress that can be derived because the complex 3D nature of the flow precludes that. After testing a wide range of fluids of different viscosities, a surface fit could be made and then for a given T and ω, the viscosity of an unknown fluid could be calculated. The situation is further complicated in that the calibration procedure would then have to be done for each class of fluid (Newtonian, shear thinning, shear thickening, etc.) and a judgement would have to be made by the user as to which class of fluid they had in the viscometer.

A different approach is that promoted by Brookfield and utilised, for example, in (Celauro et al., 2012). Each different spindle geometry provided by Brookfield for use in their viscometers is ascribed a Spindle Multiplier (SMC) value. For example, the SC-27 has an SMC of 25. Further, each viscometer model, here we are using the LVDV-E, has a Torque Constant, *TK*, which allows the apparent viscosity to be found from

$$\mu = \frac{0.1}{N} \cdot TK \cdot SMC \cdot T\% \tag{5}$$

where N is the rotational speed (rpm) and $T\%$ is percentage of the maximum spring torque that the viscometer can deliver. In addition, the Shear Rate Constant (SRC) is defined as

$$\dot{\gamma} = SRC \cdot \dot{N} = SRC \cdot \left(\frac{60}{2\pi}\right)\omega \tag{6}$$

For a design such as a DHI, this is a simplification but one which can produce values of apparent viscosity that are of practical use. Presti et al. (2014) attempted, with some success, to match the behaviour of the DHI to the range of SC-XX spindles offered by Brookfield. The SC-XX range are of the cylindrical type and each has unique SRC and SMC values. The Brookfield viscometer

allows only the selection of a spindle code, which has associated SRC and SMC values, thus limiting fine adjustment to a discrete set of values. The authors were nevertheless able to find a spindle code that matched closely the DHI and did this by testing the DHI against a number of standard liquids of known viscosity. The SC4-28 spindle was found to most closely match the DHI with values of SRC of 0.28 and SMC of 50. The validity of this approach is open to question because of the radically differing spindle geometries of the SC4-28 and DHI.

Thus, computational fluid dynamics was seen as an alternative method of obtaining values of SRC and SMC for the DHI spindle. For those reasons, another approach was used by Giancontieri et al. (2018) to calibrate the DHR geometry. The calibration procedure involved the use of the Metzer-Otto method for non-Newtonian fluids (Metzner & Otto, 1957) that introduces the concept of apparent viscosity,η_{app}, which is linked to an effective shear rate $\dot{\gamma}_{\text{eff}}$. They suggested this effective shear rate to be proportional to the rotation frequency N:

$$\dot{\gamma}_{eff} = K_s N \tag{8}$$

where K_s is a function of the geometry and the flow index. The idea behind the calibration procedure was to find a correlation between the K_s and the flow index n.

Metzer-Otto also stated that:

$$\frac{\eta_{nN}}{\mu N} = \frac{M_{nN}}{M_N} \tag{9}$$

where $\eta_{nN}/\mu N$ is the ratio between the viscosity of a non-Newtonian and a Newtonian one calculated by means of dynamic shear rheometer. M_{nN}/M_N is the ratio between the torque of a non-Newtonian fluid and a Newtonian calculated by means of rotational viscometer. From Equation (9), it is easy to calculate the non-Newtonian viscosity:

$$\eta_{nN} = \mu N \left(\frac{M_{nN}}{M_N}\right) \tag{10}$$

From Equation (10), it was possible to calculate the apparent shear rate of the non-Newtonian fluid using the Ostwald–de Waele power law relationship:

$$\dot{\boldsymbol{\gamma}}_{\boldsymbol{eff}} = \left(\frac{\boldsymbol{\eta_{nN}}}{\boldsymbol{k}}\right)^{\frac{1}{n-1}} \tag{11}$$

where n and k are input parameters, k is a measure of the average viscosity of the fluid (the consistency index); n is a measure of the deviation of the fluid from Newtonian (the power-law index). The value of n determines the class of the fluid:

- $n = 1 \rightarrow$ Newtonian fluid
- $n > 1 \rightarrow$ shear-thickening (dilatant fluids)
- $n < 1 \rightarrow$ shear-thinning (pseudo-plastics)

For those reasons, firstly an experimental campaign using a parallel-plate system aimed to find out the n and the consistency index k was carried out. Then, the DHR was adapted to the rotational viscometer and for each material the torque as a function of the rotational speed (0–100 rpm at 25°C for approximately 45 min) was measured. Finally, coupling the results of the parallel-plate and the rotational viscometer, K_s was calculated for each material using Euqtion (8). Moreover, combining Equations (5) and (10) it was possible identify the unique constant for the DHR when used with the rotational viscometer.

1.2. *Background – mixing optimisation and using CFD simulation of mixing processes*

Before the development of numerical simulations, mixers were normally evaluated experimentally using various measures: power consumption (Cordobes, Brito de la fuente, & Gallegos, 1998; Takahashi, Sasaki, Arai, & Saito, 1982; Takahashi, Yokota, & Konno, 1979, 1984) mixing time and circulation time (Carreau, Patterson, & Yap, 1976; Smith 1970). However, none of these methods gives an understanding of the spatial variation of the phases or the nature of the transport processes, making the understanding and hence the efficient optimisation of the mixer designs difficult. Numerical simulations by means of Computational Fluid Dynamics (CFD) offer a greater flexibility in analysing and visualising the mixing. In both the previous (Presti et al., 2017) and the present work the authors performed several simulations producing basic scenario which provide a lower level of accuracy but guarantee conceptual information (flow fields and volume fractions) as well as performing long-lasting and more accurate simulations providing absolute values of torque, which in turns provided the computational viscosity values.

In recent years, the simulation of mixing vessels is widely used to optimise mixer geometries and get better insights of the complex flow patterns generated by the impeller-vessel wall interaction (Delaplace, Leuliet, & Relandeau, 2000; Paul, Atiemo-obeng, & Kresta, 2004). From the perspective of numerical analysis, one of the pioneering works focused on the mixing performance of helical ribbon impellers in cylindrical vessels is the contribution made by Tanguy (Tanguy, Lacroix, Bertrand, Choplin, & De La Fuente, 1992). They developed a three-dimensional model which was validated experimentally, based on the finite-element method for the analysis of a Helical Ribbon-screw impeller. The authors reported good liquid circulation at low impeller speeds (10 rpm) and showed evidence of poor pumping in the vessel bottom. They noticed that the segregation increased upon increasing the impeller speed. Subsequently, numerical works were developed for several helical ribbon geometries and fluids (Bertrand, Tanguy, Brito de la Fuente, & Carreau, 1999). The numerical modeling of mixing in a stirred tank has attracted a great deal of attention and a recent review of the state-of-the-art in CFD simulations of stirred vessels can be found in Giancontieri et al. (2018) and Sommerfeld and Decker (2004). The rapid development of numerical techniques and computational power has unleashed the possibilities of computational Fluids Dynamics (CFD) in this area. CFD is now an important tool for understanding the mixing in the stirred tanks (Um & Hanley, 2008). Presti et al. (2017) introduced the use of CFD model to reproducing an experimental campaign of viscosity measurements of complex bituminous binders. Results proved that CFD is a tool able to provide insights into the measuring chamber that otherwise it would be impossible to obtain. Modelling of the complex flow in the presence of a rotating impeller is a computational challenge because of the complex geometry of rotating impeller and the nature of the flow in stirred tanks. Nevertheless, the developed CFD model, regardless of the testing geometries, speed and type of material tested, was able to provide values of torque that practically matched those obtained from the laboratory investigation.

Although CFD codes have made remarkable steps towards the solution of several engineering problems over the last decade, it still remains a difficult task to use such codes to help the design and the analysis of multi-phase systems.

1.3. *Aim of the study*

This study aims to provide evidence that the standard coaxial cylinders setup for rotational viscosity measurements of bituminous binders might not be adequate for modified binders, particularly when dealing with high level of heterogeneity. In fact, when using standard rheological measurements for such complex systems, a number of changes, such as phase separation, sedimentation and agglomeration, may occur in the measuring chamber. These changes all contribute

to undermine the here-defined sample stability that if altered could provide significantly misleading results.

Instability of the modified bitumens at the usual temperature for rotational tests (135°C), can be minimal or none. However, this investigation wants to prove that if equilibrium times are considered, rather than high-level of heterogeneity of the sample, higher testing temperatures and high spindle speeds, the sample stability is compromised also in these conditions. This could lead to significant mistakes in further steps such as choosing wrong temperatures to guarantee appropriate aggregate coating during mixing and/or ensuring good workability during compaction of asphalt concrete. This issue is particularly relevant within design of rubberised binders by means of low-shear blending protocol that sees the adaptation of the rotational viscometer as a mixing device offering a continuous monitoring of the viscosity (Celauro et al., 2012; Subhy, Lo Presti, & Airey, 2015). In fact, in this scenario there is a contingency of high rotational speed and high-level of heterogeneity due to the high temperature where the bitumen viscosity is quite low (180°C) and rubber particles are not swollen yet and tend to agglomerate in layers, mainly at the bottom of the tube.

In order to avoid both the above-presented issues, this study also presents an innovative testing configuration that replaces the coaxial cylinders setup with a Dual Helical Ribbon (DHR) as impeller. The investigation will offer a comparison of experimental and numerical results to highlight whether the DHR helps ensuring sample stability during rotational test of complex bituminous binders.

2. Methodology

The experimental programme showed in Figure 2 was tailored to allow a comparison between the DHR and the SC-27 systems by means of a combined laboratory-based and computational approach. The laboratory work will provide results of rotational viscosity tests on neat bitumen, an SBS-MB and an RTR-MB. The numerical simulations will provide a qualitative insight into the measuring chamber, by means of velocity fields and distribution of volume fractions within the container. The results of this combined approach will be used to understand whether lack of sample stability occurs and will also allow clarifying whether using the DHR ensures it as well the improving of rheological measurements.

2.1. *Laboratory experimental campaign*

Three different binders were included in the experimental programme: a neat bitumen and two highly modified bitumen with different level and type of modifier (Table 1). The RTR-MB was produced by adding 15% of crumb rubber size 0,300 mm in 35/50 grade bitumen, while the PMB by adding 7.5 of SBS 30% rad in 180/240 grade bitumen. All fluids being tested at 5, 20 and 100 rpm in a range of temperature between 120–200°C. Due to the expected high torque for the lower range of temperatures, which would be close to the viscometer's limits, two Brookfield DV-II PRO Digital Viscometer were used: a low torque (LV model) and high torque (HA model). The two equipment differ mainly for the viscosity measurements range. The LV model is designed for low viscosity fluids (100% torque = 673.7 dyne cm), while the HA model is more appropriate for medium–high viscous fluid (100% torque = 14,374 dyne cm). Torque measurement accuracy specified by manufacturer is 1% of the full-scale range. Tests were conducted according to Subhy, Lo Presti, and Airey (2016), which are based on international standards on viscosity measurements of rubberised bitumens (ASTM D4402, ASTM D6114). The tests were undertaken for a total of about 45 min, where the first 15 min where allowed to reach the thermal equilibrium (0 rpm).

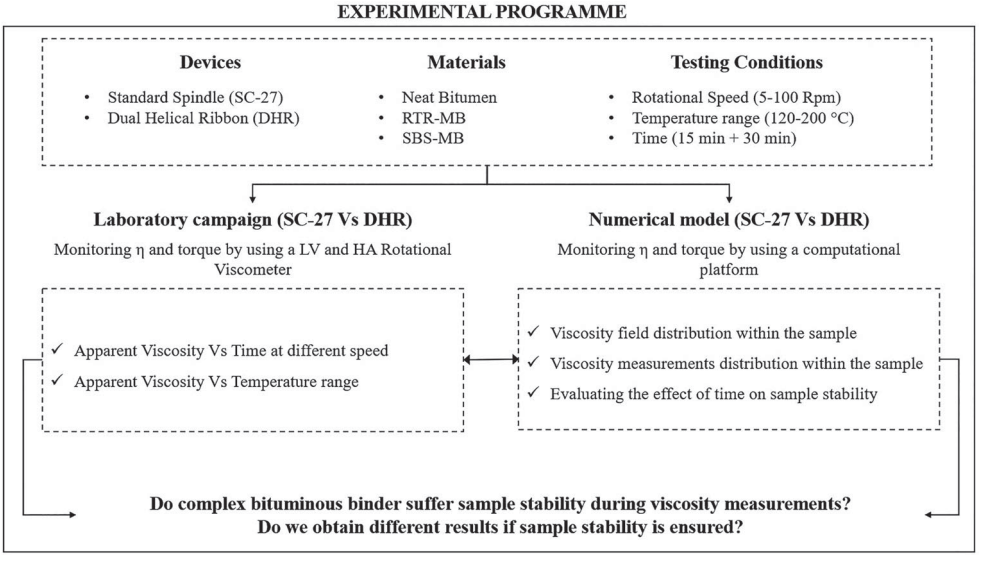

Figure 2. Methodology: combined laboratory-based and numerical approach.

Table 1. Characterisation of material's rheological properties.

No.	Material	Penetration	Rotational viscosity @150°C [mPa.s]	Softening point [°C]	n	$K_{s\ DHR}$	$K_{s\ Sc-27}$
1	Neat 35/50	40	170	51.4	–	–	–
2	RTR-MB	31	3000	63.2	0.8	0.055	0.34
3	PMB	76	2500	102.5	0.9	4.44	5.67

Then, impellers were quickly submerged in the blend and the viscometer was turned on to carry out the test, during which torque and angular velocity were measured and the viscosity calculated from Equation (5). Tests were performed in coaxial cylinder setup with both the standard spindle SC-27 and the DHR as impellers. Each of the reported results is obtained as average of at least two replicates.

2.2. *Numerical simulations by means of CFD*

In parallel with the laboratory experiments, a CFD study was conducted with the aim of offering a qualitative insight of the measuring chamber in order to assess whether lack of sample stability occurs and eventually assessing the reasons. Version 17 of ANSYS Fluent was used in this work.

2.2.1. *Governing equations*

The modelling involves the solution of the Navier–Stokes equations. In order to simulate the behaviour of the two-phase fluids in the present application, the mixture model was used. Here, the momentum and continuity equations are solved for the mixture, the volume fraction equations for the secondary phases, while algebraic expressions are used for the relative velocities and inter-phase drag.

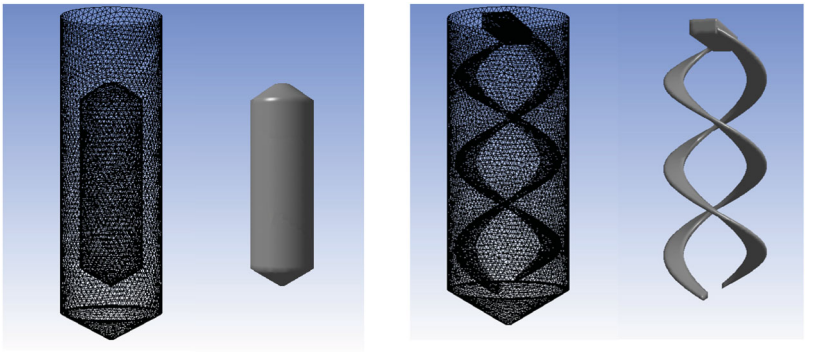

Figure 3. A solid model of the impellers and the surface mesh on the spindle and outer wall: Brookfield spindle SC-27 (left), DHR (right).

First the mixture continuity equation:

$$\frac{\partial \rho_m}{\partial t} + \nabla \cdot (\rho_m \mathbf{u}_m) = 0 \tag{12}$$

where $\mathbf{u}_m$ is the velocity, ρ is the density and the subscript m indicates a quantity defined for the mixture. The momentum equation is:

$$\frac{\partial}{\partial t}(\rho_m \mathbf{u}_m) + \nabla(\rho_m \mathbf{u}_m \mathbf{u}_m) = \nabla p + \nabla[\eta_m(\nabla \mathbf{u}_m + \nabla \mathbf{u}_m^T)] + \rho_m \mathbf{g} + \nabla \left(\sum_{k=2}^{n} \alpha_k \rho_k \mathbf{u}_{dr,k} \mathbf{u}_{dr,k} \right) \tag{13}$$

where $\mathbf{g}$ is the gravitational acceleration and $\mathbf{u}_{dr,k}$ is the drift velocity for the secondary phase k.

$$u_{dr,k} = \mathbf{u}_k - \mathbf{u}_m \tag{14}$$

The mixture model in ANSYS FLUENT uses an algebraic slip formulation, which is based on the work of Yap, Patterson, and Carreau (1979). It uses the slip velocity, which is related on the drift velocity defined in Equation (14). The velocity of the kth phase is calculated from algebraic expressions, rather than a separate momentum equation. So, the final term on the right-hand side of Equation (13) imparts a momentum source or sink to the mixture momentum equation, based on the relative motion of the primary and secondary phases.

2.3. *CFD model setup*

The geometry of the spindle (Figure 3) was developed based on the Brookfield Sc-27 and realised with ANSYS DesignModeler. A mesh consisting of tetrahedra and triangular prisms (in the inflation layers adjacent to walls) was generated using ANSYS Meshing and the volume mesh associated with the surface mesh shown in figure contains 110,000 elements.

The DHR geometry was designed according to Giancontieri et al. (2018). It allows creating a convective flow able to provide adequate mixing of complex blends also at low RPM. The idea is that the outer helix pumps the fluid downwards while the inner helix pumps it upwards. Based on the prototype design, DesignModeler and Meshing software were used to produce a mesh, which, due to the increased complexity, contained approximately 150,000 tetrahedral and triangular prism cells. The CAD model and associated surface mesh can be seen in Figure 4. The Viscous Model was selected in Fluent, it allows to set parameters for inviscid, laminar, and

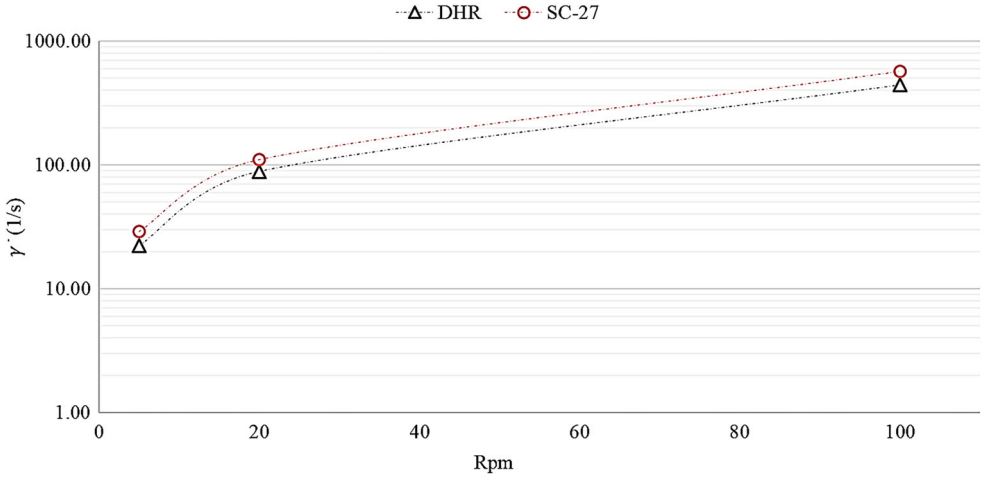

Figure 4. The effective shear rate vs the rotational for DHR and SC-27.

turbulent flow. It is accepted practice in stirred or mixing vessels to use the mixing Reynolds number, Re_m to characterise the flow:

$$Re_m = \frac{\rho D^2 N}{\mu} \tag{15}$$

where D is the diameter of the impeller and N is the number of revolutions per second. For $Re_m > 10000$, the flow is assumed to be fully turbulent. In the present application, with the least viscous fluid and the highest impeller speed, the mixing Reynolds number is approximately 100, which indicates all simulations are laminar. Fluent gives the option to select different viscosity model, in this work the non-Newtonian-power-law was selected, therefore, a non-Newtonian flow was modelled according to Equation (11).

Values n and of K_s(Table 1) have been calculated for each material by dynamic shear rheometer and used in Fluent. Then, the effective shear rate Vs the rotational speed for both SC-27 and DHR was calculated (Figure 4).

Furthermore, a "cut-off viscosity" was defined in the power-law model to run the simulation, this viscosity arbitrarily given will be the highest viscosity predicted by the software when simulating at very low shear rates. This is necessary because Ostwald-de Waele model gives an infinitive viscosity at shear rates close to zero. Finally, particles were added by defining the diameter (0.300 mm) and the concentration (15%). Therefore, non-Newtonian behaviour is applied to the continuous phase, and then crumb rubber particle particles were added to simulate their motion within continuous phase (bitumen). A moving mesh approach was used, where the entire fluid domain was rotated about the vertical z axis at the appropriate angular velocity, while the outer wall was held stationary relative to the moving zone. The reason for doing this, rather than simply moving the outer wall relative to a stationary fluid domain was so that animations for the DHR impeller could be produced with the helices being seen in motion. There was no significant computational overhead associated with the approach used. Then rotational speed was set from 0 to 100 rpm. For both the geometries; no slip wall boundary conditions were applied to the inner, outer and bottom walls. The upper boundary was set as a symmetry plane as the shear between air and bitumen is insignificant. Standard solver settings were used throughout: the SIMPLE algorithm was used for pressure–velocity coupling. Least Squares Cell Based discretisation for gradients and second order differencing for the momentum and volume fraction equations were

used. Due to the use of a moving mesh, the solution was necessarily transient, and it was found that the simulations had to be run up to 45 min of real time to achieve a stationary solution, where the mean velocity and volume fraction did not drift with time, as measured at a number of monitoring points. To simulate the movement of the DHR with accuracy, a maximum angular change of 2° was allowed per time-step. For example, at 100 rpm this means 1 revolution every 0.6 sec, 1 revolution is 360° therefore the DHR needs 180-time steps per revolution to complete a revolution, so it needs a time steep of $0.6/180 = 0.00333$ sec.

3. Results and discussion

3.1. *Laboratory campaign*

3.1.1. *Measurements on neat bitumen*

As mentioned above the whole experimental programme was carried out within a range of temperatures between 120°C and 200°C. Figure 5 and Table 2 shows viscosity measurements carried out on a 35/50 pen bitumen at 140°C and 180°C, by using both the SC-27 and the DHR impellers at different rotational speed. These two test temperatures were selected because close to the typically used to measure rotational viscosity at elevated temperatures of neat bitumen (ASTM D4402) and rubberised binders (ASTM D 6114-97). As a result, with a homogeneous material such as the neat bitumen DHR provides the same readings of the Sc-27.

3.1.2. *Measurements on modified bitumens: apparent viscosity vs time*

After the positive tests performed on neat bitumen, the SC-27 and the DHR have been used to measure the apparent viscosity of RTR-MB containing 15% (size 0.300 mm) and produced in high shear. Same tests were carried out for an SBS-MB produced by adding 7.5% of SBS 30% radial in 180/240 grade bitumen. Each test lasted 45 min, and in the first 15 mins the system was left reaching the thermal equilibrium (0 RPM). Considering the shear thinning nature of the modified bitumen, to evaluate the response of the two geometries tests were conducted respectively at 5, 20, 100 rpm. Figure 6 shows the apparent viscosity measurement of the modified binders performed at 180°C with a rotational speed of 20–100 rpm. The difference in terms of viscosity between the two geometries at the end of the thermal equilibrium is due to the higher initial momentum required by the SC-27. Figure 7 instead shows the differences in terms of percentage between the two testing geometries at 1, 5 and 30 min. Considering that for both the materials similar trends were recorded at low rpm (5 rpm) for simplicity only the graph at 20 and 100 rpm

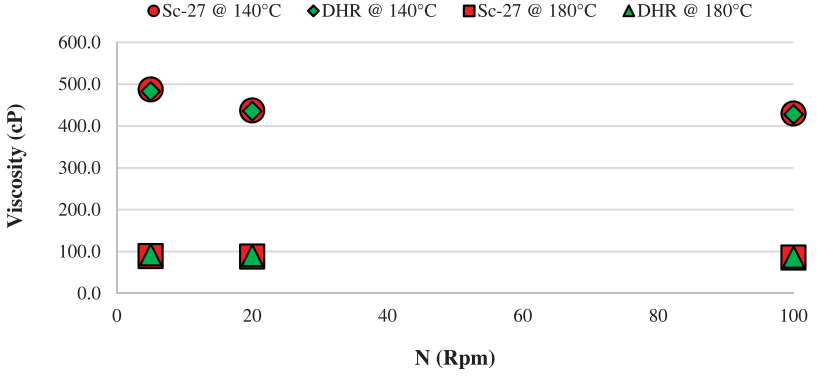

Figure 5. Viscosity measurements by using LV on a 35/50 bitumen at $T = 140$°C and 180°C.

Table 2. Apparent viscosity from 120°C to 200°C of RTR-MB and SBS-MB by using HA viscometer at 20 rpm.

Material	Temperature °C	SC-27 @ 20 rpm	DHR @ 20 rpm	Difference
Neat bitumen (pen 35/50)	120	1475	1564	– 6.03%
	140	437	436	0.23%
	160	179	182	– 1.68%
	180	88	90	– 2.27%
	200	50	54	– 8.00%
RTR-MB	120	–	–	–
	140	7000	9591	– 37.01%
	160	2625	3000	– 14.29%
	180	1325	2040	– 35.05%
	200	1000	1150	– 15.00%
SBS-MB	120	9425	10,833	– 14.94%
	140	3050	3243	– 6.33%
	160	1275	1414	– 10.90%
	180	750	770	– 2.67%
	200	375	396	– 5.60%

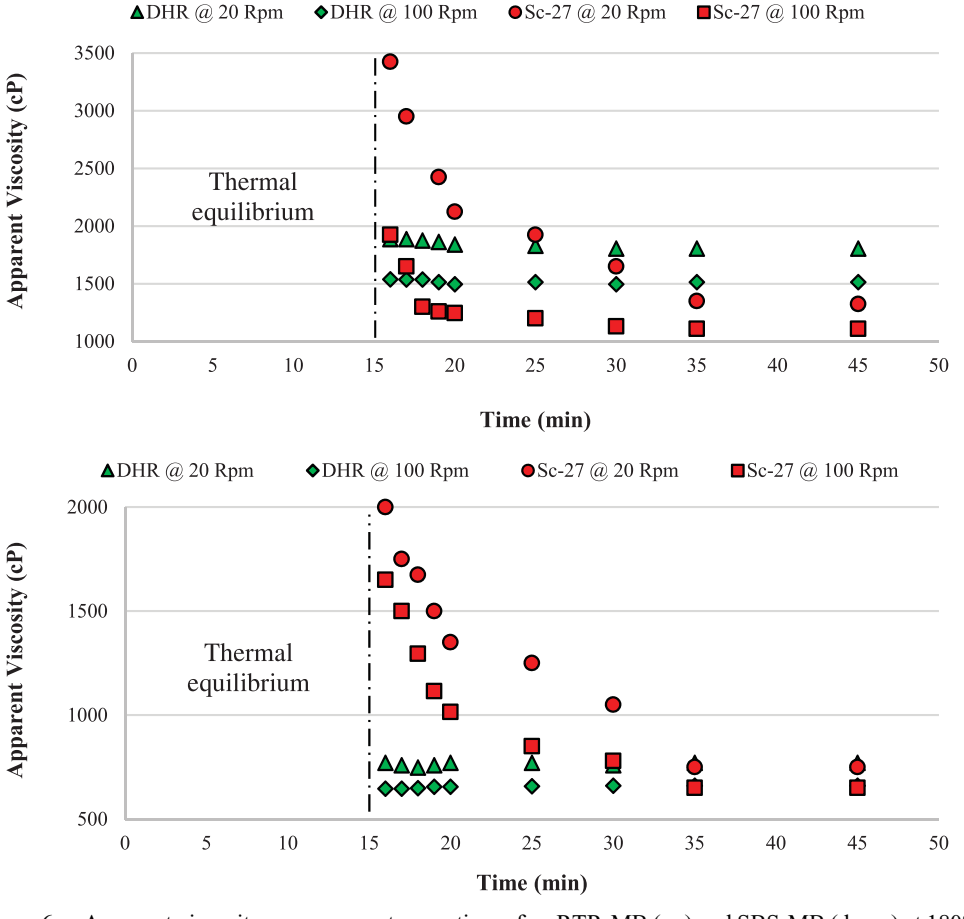

Figure 6. Apparent viscosity measurements over time of an RTR-MB (up) and SBS-MB (down) at 180°C at 20–100 rpm.

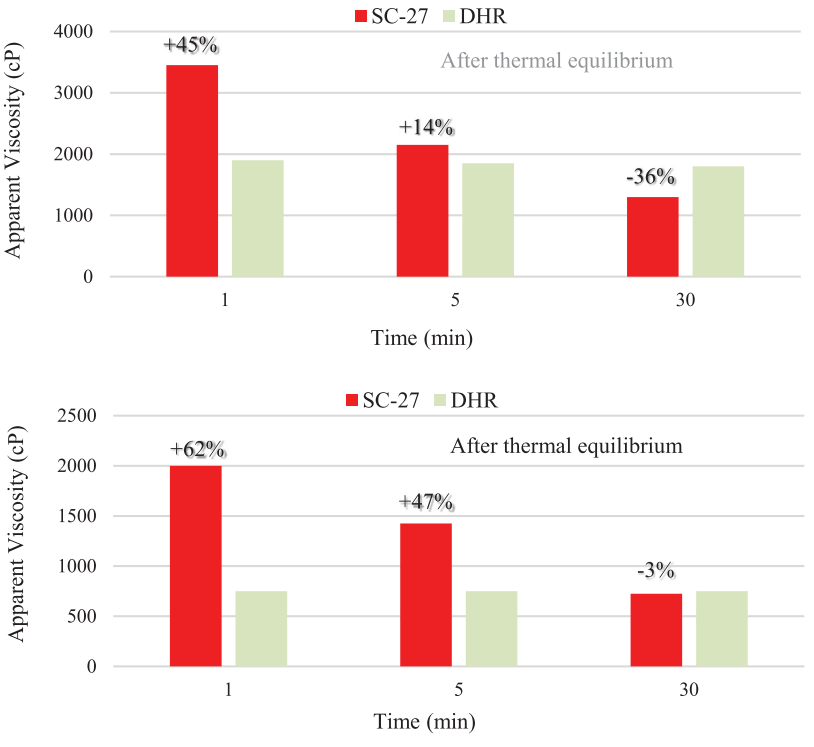

Figure 7. Apparent viscosity of RTR-MB (up) and SBS-MB (down) at 180°C by at 20 rpm. Percentages indicates the difference in terms of viscosity between the two geometries.

are reported. It can be observed that the SC-27 impeller provides measurements that pass through a wider transition period before achieving a stable measurement, while DHR allows obtaining measurements with a more stable trend. This is quite evident with both SBS-MB and RTR-MB, however higher speeds (100 rpm) seems diminishing the unstable trend showed from the SC-27. Moreover, during the whole campaign the SC-27 provided values of apparent viscosity (after 45 mins) that are always lower than the DHR. If compared with the measurements carried out on the neat bitumen, it seems that the modified bitumen is in some way affected during the measurements. Phenomena like phase separation and sedimentation may occur during the test leading to inconsistent results. Figure 6 highlights how the DHR instead provides a stable trend of results, which seems not be affected with time.

3.1.3. *Measurements on modified bitumens: apparent viscosity vs temperature*

Table 2 provides a numerical assessment of the differences recorded between the reading obtained with both SC-27 and DHR. It has to be underlined that differences between the two measurements increases with the increase in heterogeneity of the materials: neat bitumen > SBS-MB > RTR-MB.

In other words, using the SC-27 in standard conditions provides values of apparent viscosities that could be significantly different from those obtained with the DHR. Presti et al. (2014), arrived at this same conclusion, with this investigation we are coupling the laboratory campaign with a numerical approach that could provide us with an insight of the phenomena happening inside the measuring chamber with the ambition of arriving to figure out the reasons behind this.

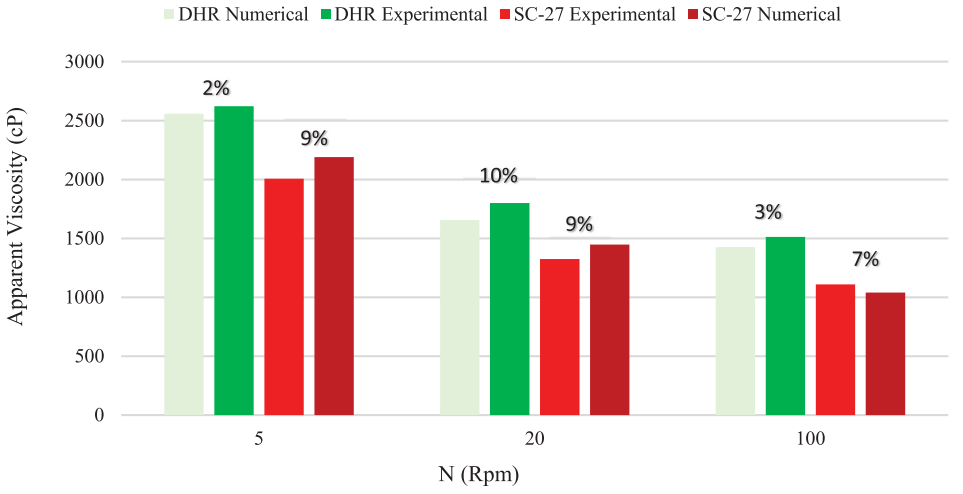

Figure 8. Apparent viscosity of RTR-MB Vs Rpm at 180°C obtained through laboratory campaign and numerical simulations.

Table 3. Comparison of results from laboratory campaign and numerical simulations for RTR-MB at 180°C at 5–100 rpm.

		Numerical			Experimental			
Device	*N* (rpm)	Torque (Nm)	Torque (%)	Viscosity (cP)	Torque (Nm)	Torque (%)	Viscosity (cP)	Error (%)
Sc-27	5	3.14E-05	46.7	2189.8	2.74E-05	40.7	2007.4	8.3
	20	8.32E-05	5.8	1447.1	7.62E-05	5.3	1325	8.4
	100	2.88E-04	20.1	1040.9	3.19E-04	22.2	1110	− 6.6
DHR	5	8.00E-05	5.6	2558.9	8.19E-05	5.7	2622	− 2.5
	20	2.37E-04	16.5	1805.3	2.58E-04	18.0	2040	− 8.7
	100	8.91E-04	62	1425.5	9.46E-04	65.8	1513.4	− 6.2

3.2. *Numerical simulations*

3.2.1. *Validation of the model*

The CFD was configured to reproduce the whole laboratory campaign, although since both binders shows similar trend this simulation focused only on the most severe instability of the RTR-MB scenario. The numerical simulations want to provide further insight of the sample instability phenomena by assessing the velocity fields, volume fraction and numerical measurements distribution within the measuring chamber. In order to use these simulations as a reliable source of information, at first a validation of the model was carried out. The validation consisted in comparing numerical measurements of the torque with those obtained from the laboratory test. Figure 8 and Table 3 show that the results obtained from the laboratory campaign and the numerical simulations, are in good agreement, therefore validating the reliability of the numerical model. Indeed, the software allows to compute the moments about a specified centre, and the coordinates of the centre of pressure for selected wall zones making possible the comparison with the experimental results. In support of this methodology, the reader should consider that rotational viscometers measure the viscosity by using a mechanical system to impose a controlled force or displacement onto a sample, hence the torque is the actual quantity directly measured during rotational tests. Once the model was considered able to reproduce the complex scenarios

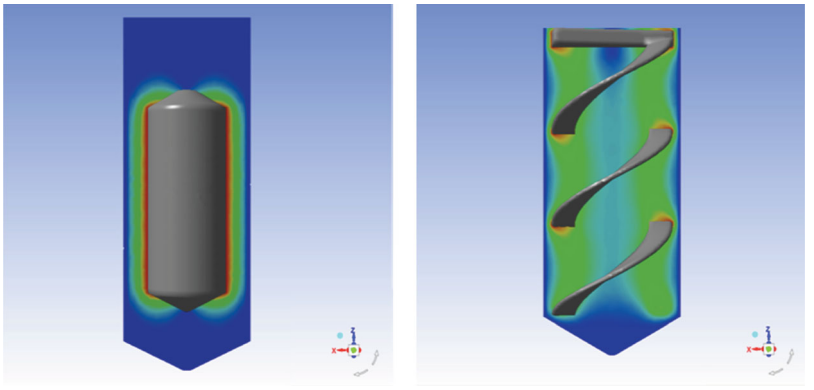

Figure 9. Numerical velocity field distribution of RTR-MB at 180°C at 20 rpm, Brookfield spindle SC-27 (left), DHR (right).

of rotational test even of complex binders, several investigations have been carried out. Each of them had the aim of providing a visual understanding of the phenomena happening within the measuring chamber while rotational measurements are performed. The next paragraphs offer the details of these simulations run only on the RTR-MB at 180°C at 20 rpm, the binder with the highest level of heterogeneity.

3.2.2. *Velocity field distribution within the chamber*

A study of the velocity field distribution within the sample (Figure 9) highlighted that the DHR shape allows a better distribution of the velocity flow field thanks to the pumping effect induced by the axial force. Indeed, the inner blades push the fluid upwards while the outer push the fluid downward allowing a continuous recirculation of the flow. Instead, the standard concentric spindle due to its geometry creates low velocity field at the top and the bottom of the tube, while all the stresses are distributed around the vertical walls of the spindle. This confirms that the vertical film of sample sandwiched along the container and the spindle is the only portion tested during the measurements. Also, there is no axial pumping but only tangential forces that do not allow creating a convective flow. Phenomena like phase separation, sedimentation and agglomeration may occur due to those issues.

3.2.3. *Apparent viscosity measurements distribution within the chamber*

Complementary to the previous simulations, this section presents an analysis of the viscosity measurements made directly using the numerical model at different height of the container: top, middle and bottom thirds (Figure 10). The figure also provides the comparison with the experimental data obtained within the laboratory campaign (last column). As a result, for the SC-27 high values have been found in the top and the bottom region, while in the middle region due to the tangential forces the values of viscosity reported are lower. This is in line to what was shown in the previous section showing that velocity fields are concentrated in the middle section; hence the measured torque will strongly depend from the tangential forces in this section. In other words, as shown in Figure 10 and Table 4, the values of viscosity reported by the instrument when the SC-27 is used, are related to the sample in the middle region. With the DHR the scenario is simplified. In fact, both Figures 9 and 10 show that DHR is able to offer a better mixing of the sample, which in turns provide a more homogeneous distribution of the velocity fields and viscosity readings over the entire length of the container.

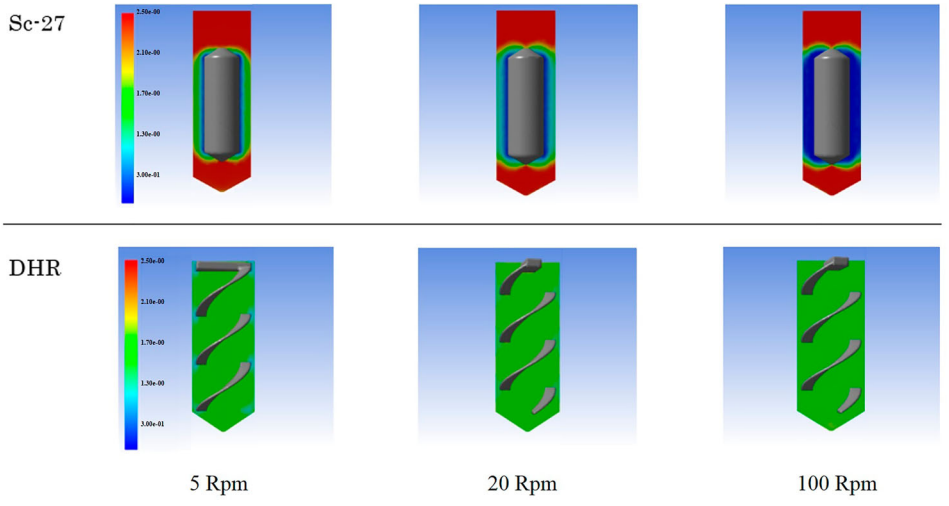

Figure 10. Numerical apparent viscosity distribution of RTR-MB at 180°C at 5–100 rpm.

Table 4. Numerical apparent viscosity distribution of RTR-MB at 180°C at 5–100 rpm.

Device	*N* (rpm)	Viscosity top (cP)	Viscosity centre (cP)	Viscosity bottom (cP)	Viscosity exp (cP)
Sc-27	5	2886	2046	3414	1907.4
	20	2737	1352	2836	1325
	100	1645	995	1666	1110
DHR	5	2537	2602	2649	2622
	20	1835	1803	1851	2040
	100	1419	1409	1437	1513.4

3.2.4. *Evaluating the effect of time on sample stability*

On the basis of the lesson learned in the previous section, the simulations in Figure 11 focused on understanding whether the viscosity measurements can be affected also by lack of sample stability over time. The idea was to reproduce the same methodology used for the experimental campaign, but with the additional feature of obtaining visual data by plotting the volume fractions distribution within the container and over time. As a result, in both scenarios, seems evident that within the thermal equilibrium (from 0 to 15 min), the particles tend to settle down to the bottom due to the gravity force. From 15 to 45, min the viscometer motor is turned on and the impellers start rotating at 20 rpm. In this phase, the SC-27 is not able to keep the particles evenly distributed within the tube leading to a high concentration of particles at the bottom. It is also important to observe that the fluid along the clearance between the wall and spindle - which as discussed seems to be the actual sample tested with the SC-27 - is heterogeneous for the entire length of the test. Instead, once the DHR starts rotating, it assures an evenly distribution of the particles within few minutes. For this reason, the value reported by the viscometer using a standard geometry cannot consider realistic. On the other hand, the DHR allows testing a well-distributed sample and this is surely contributing in guaranteeing a stable trend of results, as observed during the laboratory campaign.

At last, simulations were run to understand whether the sample stability can be connected also the nature of the sample itself. In other words, simulations were run without the geometry in the tube for 45 min (Figure 12). Results showed that there is a high level of instability within the

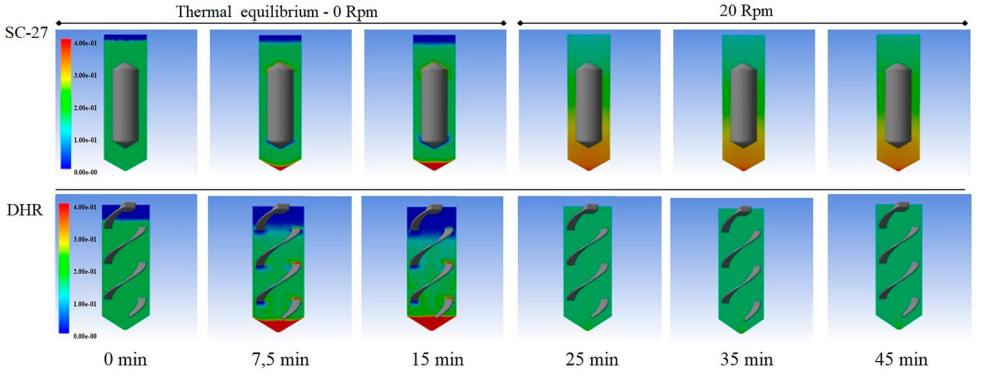

Figure 11. Effect of time on particles distribution of RTR-MB at 180°C by numerical model, rotational speed 20 rpm.

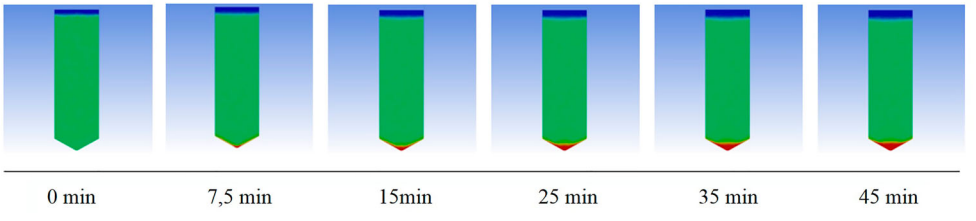

Figure 12. Sample stability of RTR-MB at 180°C over time, by numerical model and with no geometry within the sample.

sample due to the particles settling down for the gravity. As a result, sample of RTR-MB lack of sample stability over time, hence misleading results can be obtained if no agitation is provided during rotational tests.

4. Conclusions

This investigation offers an innovative approach consisting in a combined laboratory-based and computation approach aimed at understanding whether standard testing geometry for rotational tests are suitable for measuring high-temperature rotational viscosity of modified bituminous binders with high level of heterogeneity. The study also offers a solution to overcome some of the presented issues and this consists in changing the standard coaxial cylinder testing setup by substituting the standard spindle (SC-27) with a dual helical ribbon (DHR). In other words, the investigation aims at answering the following research questions:

Do heterogeneous modified bituminous binders undergo lack of sample stability during viscosity measurements at high-temperatures?

- The laboratory campaign provided evidence that highly heterogeneous modified bitumen do provide an un-stable trend of measurements during the testing with SC-27. The final values of apparent viscosities can be significantly different from those obtained with the DHR, which instead provided stable readings already after few minutes.
- The numerical simulations clarified that heterogeneous bituminous blends undergo sample instability already during thermal equilibrium, simply because they are stored at high temperatures in a vertical container. The lack of sample stability is not reversed when SC-27 is

used at 20 rpm. In this testing configuration, higher rotational speed (100 rpm) might help decreasing but not eliminating the issue.

Do we obtain different results if sample stability is ensured?

- The DHR instead is able to ensure sample stability even at low speed (5 rpm). This is due to an axial pumping induced by the rotating impeller within the sample.
- The laboratory campaign provided evidence that increasing the complexity of the bituminous blends is directly proportional to an increase in misleading readings of apparent viscosity of the blends, up to almost 40%. This trend is mainly governed by the material type as well as to differential values of densities and viscosities of the blend's components.
- The CFD analysis, provided the additional opportunity to have readings over three thirds of the vertical container. Results highlighted that SC-27 provides readings mainly governed by the middle region, while the viscosity results over the length of the tube are quite uniform when the DHR is used as impeller.

Hence, as general conclusion can be stated that bitumen technologist are invited to not underestimate sample stability arising while performing high-temperature viscosity measurements of heterogeneous modified bitumen with the standard coaxial cylinders setup. Sample stability certainly occurs when testing recycled tyre rubber modified bitumen, and it might be significant also for polymer modified bitumen such as SBS-MB. The DHR impeller offers a solution to ensure sample stability, hence asphalt technologists are strongly recommended to consider this solution within rheological characterisation of complex and heterogeneous bituminous binders at high-service temperatures.

This study was tailored for the rotational viscometer environment; however, the authors have already developed the same concept for Dynamic Shear Rheometers. Research is currently undergoing. Future recommendations can lie in using a similar approach to explore a wider range of modified binders and impellers. Also, this type of combined laboratory/computational approach is strongly recommended since provides new set of data and visual aids that could lead towards the definition of virtual laboratory testing protocols.

Acknowledgements

The authors confirm contribution to the paper as follows: study conception and design: Davide Lo Presti, Gaspare Giancontieri, Data collection: Gaspare Giancontieri; Davide Lo Presti Numerical simulations: Gaspare Giancontieri; David Hargreaves Analysis and interpretation of results: Gaspare Giancontieri, David Hargreaves, Davide Lo Presti; Draft manuscript preparation: Gaspare Giancontieri, Davide Lo Presti. All authors reviewed the results and approved the final version of the manuscript.

Funding

This investigation was initially supported by the Engineering and Physical Sciences Research Council (EPSRC) and it is now further developed within the SMARTI ETN project which has received funding from the European Union's Horizon 2020 Programme under the Marie Curie-Skłodowska actions for research, technological development and demonstration, under grant number 721493 (http://smartietn.eu); Italian Ministry of University and Research [grant number MIUR dm n.372 08/05/18].

ORCID

Davide Lo Presti http://orcid.org/0000-0002-5125-8074

References

Bertrand, F., Tanguy, P. A., Brito de la Fuente, E., & Carreau, P. (1999). Numerical modeling of the mixing flow of second-order fluids with helical ribbon impellers. *Computer Methods in Applied Mechanics and Engineering*, *180*(3–4), 267–280. doi:10.1016/S0045-7825(99)00169-3.

Caltrans. (2011, June). *Quality control manual for hot mix asphalt – State of California*. State of California, Department of Transportation, Division of Construction. Retrieved from http://www.dot.ca.gov/hq/construc/publications/qcqaman1.pdf

Carreau, P. J., Patterson, W. I., & Yap, C. Y. (1976). Mixing of viscoelastic fluids with helical-ribbon agitators I- mixing time and flow patterns. *Canadian Journal of Chemical Engineering*, *54*(3), 135–142.

Celauro, B., Celauro, C., Presti, D. L., & Bevilacqua, A. (2012). Definition of a laboratory optimization protocol fore road bitumen improved with recycled tire rubber. In *Construction and building materials* (Vol. *37*, pp. 562–572). Elsevier. doi:10.1016/j.conbuildmat.2012.07.034.

Cordobes, F., Brito de la fuente, E., & Gallegos, C. (1998). Effect of rheological properties on power input and effective shear rates when mixing with different impellers. *Anales de química*, *94*(4–5), 274–278. Springer. Retrieved from http://cat.inist.fr/?aModele = afficheN&cpsidt = 10064702

Delaplace, G., Leuliet, J. C., & Relandeau, V. (2000). Circulation and mixing times for helical ribbon impellers. Review and experiments. *Experiments in Fluids*, *28*(2), 170–182. doi:10.1007/s003480050022.

Dow, R. B. (1946). The rheology of lubricants. *Journal of Colloid Science*, *2*(1), 81–91.

Gallegos, C., & Franco, J. M. (1999). Rheology of food, cosmetics and pharmaceuticals. *Current Opinion in Colloid and Interface Science*, *4*(4), 288–293. doi:10.1016/S1359-0294(99)00003-5.

Giancontieri, G., Hargreaves, D., & Lo Presti, D. (2018). Are we correctly measuring the rotational viscosity of rubberized bituminous binder? In Jorge B. Sousa, George Way, & Alex Visser (Eds.), *Proceedings of the Rubberised Asphalt – Asphalt Rubber 2018 Conference* (7th). South Africa.

Huang, S. C. (2006). Rheological characteristics of crumb rubber-modified asphalts with long-term aging. *Road Materials and Pavement Design*, *7*(January 2015), 37–56. doi:10.1080/14680629.2006.9690057

Lin, S., & Brodkey, R. S. (1985). Rheological properties of Slurry Fuels. *Journal of Rheology*, *29*, 147. doi:10.1122/1.549814.

Malkin, A. Y. (2009). The state of the art in the rheology of polymers: Achievements and challenges. *Polymer Science Series A*, *51*(1), 80–102. doi:10.1134/S0965545X09010076.

Metzner, A. B., & Otto, R. E. (1957). Agitation of non-Newtonian fluids. *AIChE Journal*, *3*(1), 3–10. doi:10.1002/aic.690030103

Mezger, Thomas G. (2006). *The rheology handbook*. Hanover, Germany: Vincentz Network.

Paul, E. L., Atiemo-obeng, V., & Kresta, S. M. (2004). *Handbook of industrial mixing*. Hoboken: John Wiley & Sons, Inc.

Peralta, J., Silva, H. M., Machado, A. V., Pais, J., Pereira, P. A., & Sousa, J. B. (2010). Changes in rubber due to its interaction with bitumen when producing asphalt rubber. *Road Materials and Pavement Design*, *11*(4), 1009–1031. doi:10.1080/14680629.2010.9690317.

Presti, D. L., Fecarotti, C., Clare, A. T., & Airey, G. (2014). Toward more realistic viscosity measurements of tyre rubber–bitumen blends. *Construction and Building Materials*, *67*, 270–278. Elsevier Ltd. doi:10.1016/j.conbuildmat.2014.03.038.

Presti, D. L., Giancontieri, G., & Hargreaves, D. M. (2017). Improving the rheometry of rubberized bitumen: Experimental and computation fluid dynamics studies. *Construction and Building Materials*, *136*, 286–297. doi:10.1016/j.conbuildmat.2016.12.200

Smith, J. (1970). The mixing of Newtonian and non- Newtonian fluids. *Journal of the Society of Cosmetic Chemists*, *552*, 242. Retrieved from https://books.google.com/books/about/The_Mixing_of_Rubber.html?id = NV7L3Jb1URwC&pgis = 1

Sommerfeld, M., & Decker, S. (2004). State of the art and future trends in CFD simulation of stirred vessel hydrodynamics. *Chemical Engineering and Technology*, *27*(3), 215–224. doi:10.1002/ceat.200402007

Subhy, A., Lo Presti, D., & Airey, G. (2015). Rubberised bitumen manufacturing assisted by rheological measurements. *Road Materials and Pavement Design*, *16*(November), 1–21. doi:10.1080/14680629.2015.1079549

Subhy, A., Lo Presti, D., & Airey, G. (2016). Rubberised bitumen manufacturing assisted by rheological measurements. *Road Materials and Pavement Design*, *17*(2), 290–310. doi:10.1080/14680629.2015.1079549

Tabilo-Munizaga, G., Barbosa-Cánovas, G. V., & Tonir, S. (2005). Rheology for the food industry. *Journal of Food Engineering*, *67*(1–2), 147–156. doi:10.1016/j.jfoodeng.2004.05.062

Takahashi, K., Sasaki, M., Arai, K., & Saito, S. (1982). Effects of geometrical variables of helical ribbon impellers on mixing of highly viscous Newtonian liquids. *Journal of Chemical Engineering of Japan*, *15*(3), 217–224. doi:10.1252/jcej.15.217

Takahashi, K., Yokota, T., & Konno, H. (1979). Mixing of pseudoplastic liquid in a vessel equipped with a variety of helical ribbon impellers. *Journal of Chemical Engineering of Japan*, *45*(1978), 63–68.

Takahashi, K., Yokota, T., & Konno, H. (1984). Power consumption of helical ribbon agitators in highly viscous pseudoplastic liquids. *Journal of Chemical Engineering of Japan*, *17*(6), 657–659. doi:10.1252/jcej.17.657

Tanguy, P. A., Lacroix, R., Bertrand, F., Choplin, L., & De La Fuente, E. B. (1992). Finite element analysis of viscous mixing with a helical ribbon-screw impeller. *AICHE Journal*, *38*(6), 939–944. doi:10.1002/aic.690380614

Um, B., & Hanley, T. R. (2008). A CFD model for predicting the flow patterns of viscous fluids in a bioreactor under various operating conditions. *Korean Journal of Chemical Engineering*, *25*(5), 1094–1102.

Visser, A. T., Duhovny, G. S., & Sachkova, A. V. (2017). Comparison of bitumen–rubber use in extreme conditions in Russia and South Africa. *Road Materials and Pavement Design*, *18*(5), 1190–1199. doi:10.1080/14680629.2016.1201524

Yap, C. Y., Patterson, W., & Carreau, P. J. (1979). Mixing with helical ribbon agitators: Non- Newtonian fluids. *AIChE Journal*, *25*(3), 516–521.

Zhang, Y., Yu, X., Chen, L., & Jia, G. (2018). Comparison of the partitioning of evapotranspiration – numerical modeling with different isotopic models using various kinetic fractionation coefficients. *Plant and Soil*, *430*(1–2), 307–328. doi:10.1007/s11104-018-3737-z

Construction and Building Materials 233 (2020) 117351

Contents lists available at ScienceDirect

Construction and Building Materials

journal homepage: www.elsevier.com/locate/conbuildmat

Quality control of manufacturing and hot storage of crumb rubber modified binders

Juan Gallego Medina [a], Gaspare Giancontieri [b], Davide Lo Presti [b,c,*]

[a] Department of Transport Engineering, Urban and Regional Planning, Universidad Politécnica de Madrid, Spain
[b] Department of Engineering, Polytechnic School, University of Palermo, Palermo, Italy
[c] Nottingham Transportation Engineering Centre, University of Nottingham, Nottingham NG7 2RD, UK

HIGHLIGHTS

- The dual helical ribbon (DHR) guarantees sample stability while CRM binders are tested.
- Real-time monitoring provides control of CRM binders' rheological properties during manufacturing and hot storage.
- The procedure allows to provide recommendations for optimal hot storage.
- The procedure introduces parameters to establish targets for improved design and quality-control of CRM binders.

ARTICLE INFO

Article history:
Received 24 May 2019
Received in revised form 17 October 2019
Accepted 21 October 2019

Keywords:
Viscosity
Rubberised binder
Crumb rubber
Dual helical ribbon

ABSTRACT

The ultimate performance of crumb rubber modified (CRM) binders is linked to the accurate control of the properties during manufacturing and hot storage. However, due to their complexity, asphalt technologists find the characterisation of these materials still challenging. In this study, the adoption of a Dual Helical Ribbon (DHR), a novel mixing/measuring device for rotational viscometers, is proposed for the real-time monitoring of CRM binders during manufacturing and hot storage. According to the laboratory results, manufacturing periods of 45–60 min at 195°, as well as storage temperatures not exceeding 150 °C, are recommended for this type of modified binders.

© 2019 Elsevier Ltd. All rights reserved.

1. Introduction

The European countries have established management systems to organise the collection of used tyres and promote their valorisation in several applications [1]. However, tyre rubber is engineered to be chemically very stable, durable and suffers biodegradation slowly. For the same reason, reclaiming natural rubber from waste tyres thorugh devulcanization is not that easy, hence the natural application of reusing tyre rubber for new tyre is not a straightforward option. The necessity of re-using tyre rubber as secondary material in other application has therefore arisen and a very succesfull application has been incorporating the crumb rubber modifier (CRM) into asphalt mixtures. In fact, the use of CRM in asphalt applications provides a solution to improve pavements performance [2] including the reduction of the tyre/road noise when applied in wearing course [3]. The use of the ground rubber in asphalt paving materials can play a notable role in reducing the landfill of used tyres.

The enhanced engineering properties obtained by using these modified binders in different asphalt applications are well documented. The rutting resistance of rubber-binders is superior to that of the pure bitumen before being modified with crumb rubber [4]. At intermediate temperatures, the CRM binders display a reduced stiffness [5] and even at low temperatures, as is the cases of Russia, this family of materials have shown good performance [6].

Nevertheless, the properties of CRM binders depend on a number of variables, including not only the proportions and nature of the components (bitumen and rubber) but also the parameters of the manufacturing procedure (temperature, mixer type and mixing time), with significant influence on the viscosity and the rheology of the final product [7,8]. In this regards, the increasing of the CRM content usually turns into more modified binders and higher viscosities, as reported by Lee et al. [9]. The same authors report that the CRM produced by ambient grinding generally increases the

* Corresponding author at: Department of Transport Engineering, Urban and Regional Planning, Universidad Politécnica de Madrid, Spain.
E-mail addresses: davide.lopresti@unipa.it, davide.lopresti@nottingham.ac.uk (D. Lo Presti).

https://doi.org/10.1016/j.conbuildmat.2019.117351
0950-0618/© 2019 Elsevier Ltd. All rights reserved.

viscosity more than the same content of cryogenically ground CRM, because of the shape of the rubber particles and their larger specific area. Thodesen et al. [10] conclude that cryogenic crumb rubber yield lower level of bitumen modification and proves it via scanning electron microscope (SEM) images of bitumen modified with both cryogenically and ambient ground CRM particles. On the other hand, the high temperatures and prolonged mixing times foster rubber-bitumen interaction but, excessive temperatures, above 200 °C, can degrade the quality of the CRM binder [11].

To understand better the influence of these variables on the CRM binder it is necessary to consider the rubber-bitumen interaction mechanisms, as they explain how the components and the parameters of the manufacturing procedure can determine the ultimate properties of the modified binder. The rubber is affected in two ways: swelling of the rubber particles and a progressive degradation by depolymerisation and devulcanization [12]. The swelling of the rubber particles can reach a ratio of 250% as a result of the interaction until saturation with the oily fractions of the bitumen [13]. Lopez-Moro et al. [14] investigated the interchange of aromatic oils between the rubber particles and the bitumen and determined a high concentration of this asphalt fraction around the rubber particles via fluorescent microscopy. In the same way, they concluded that some portions of the rubber particles, including black carbon in their composition, were delivered to the bitumen. At low manufacturing temperatures (below 160 °C) the primary mechanism is the absorption of oily fractions by the rubber particles [15] as shown by the results of the thermogravimetric analysis.

Moreover, according to the results of the viscoelastic study, the increased interaction parameters results in the delivery of portions of rubber into the bitumen, modifying its rheology. The importance of the processing conditions has also been insightfully described by Lo Presti et al. [16] making clear that CRM binder overcomes an evolution of properties that, in terms of viscosity, can be summarised as follows. Phase I starts with a predominant role of the swelling of the rubber particles due to the absorption of the oily fractions of the bitumen, producing a progressive increase of the viscosity. During phase II, although the swelling phenomena slow down, the maximum value for the viscosity is achieved because the oily fractions continue diminishing until the saturation of the potential of the rubber particles to capture light components of the bitumen. And finally, during phase III, if the temperature is high enough, the viscosity starts decreasing along time because of the depolymerisation of the rubber. Obviously, in technical terms, phase III should be as minimised as possible to prevent the loss of quality of the modified binder.

The objective of limiting the degradation of the CRM binder should be easy to achieve by controlling the storage time and temperature. Nevertheless, at this point, a new concern arises, the poor storage stability of these modified binders. After the manufacturing of the CRM binders, it is necessary to store them in tanks at high temperatures, until the modified binder is used in the production of asphalt mixtures. As the rubber particles are prone to settlement as a solid in suspension in the liquid phase (bitumen), the tank has to be provided with a stirrer to keep the rubber particles in suspension. Several attempts have been carried out to provide the CRM binders with enhanced storage stability by diminishing the size of the CRM particles [17], by adding sulfur [18] or reactive polymers [19]. But the problem has not been satisfactorily solved, and the stirring of the stored rubber binders continues being necessary at industrial scale.

Nevertheless, the stirrer in the tank during prolonged storage periods, beyond preventing decantation, could promote the third phase of the rubber-binder interaction, this is, the depolymerisation of the rubber an so the loss of quality of the stored CRM binders. The increase of the viscosity by increasing the temperature and the mixing time, as proposed by Hosseinnezhad [20], is a stringent rule only in some ranges of temperature and processing time. In experiments prolonged during 8 h, the increase of viscosity reaches a sort of horizontal asymptote over time [21]. This lack of progression in the evolution of the viscosity could be referred to the depolymerisation of the rubber that counteracts the hardening due to the capture of oily fractions and the ageing of the binder because of the high mixing temperature. In line with this result, a study by Ragab and Abdelrahman [22] showed that the separation index during resting periods of 8 h decreases as the mixer speed goes from 10 to 50 Hz in the manufacturing procedure. The authors interpreted this observation as the evidence of the extensive depolymerisation and degradation of the rubber particles along time when the interaction parameters increase. The depolymerisation destroys the rubber particles and makes them less prone to suffer settlement.

Because of the above reasons, it should be necessary to estimate the conditions for the storage period to prevent or minimise the loss of viscosity of the CRM binders during prolonged storage times. Since the tank stirrer is conceived to avoid the settlement of the rubber particles, the foremost parameters to be defined are the storage time and temperature.

Pais et al. [23] carried out a study of the evolution of the viscosity and the rheological parameters of CRM binders during processing times of 0.5, 8, 24, 30 and 40 h. The study included several percentages of ambient and cryogenically ground crumb rubber. The authors concluded that the viscosity slowly decreases during prolonged period times for the binders modified with ambient crumb rubber. Nevertheless, the cryogenic rubber achieves lower viscosity values although no decreasing was observed during the 40 h. Probably the first limitation of this investigation could be referred to the fact that the samples were collected at proper times and prepared for testing, instead of continuously monitoring the properties of the CRM binder.

Some attempts have been performed to achieve a procedure for the monitoring of the viscosity of the binders in real-time in the laboratory. Celauro et al. [24] tried to do it with a standard Brookfield spindle #27. The device was conceptualised as a low shear mixer. The manufacturing of the CRM binder as well as the continuous monitoring of the viscosity was carried out by the Brookfield equipment. Nevertheless, the authors observed that the procedure was affected by the settlement of the rubber particles. To overcome this inconvenience, Lo Presti et al. [25] developed and calibrated a dual helical impeller to substitute the conventional spindle. The new device was able to keep the rubber particle continuously in suspension measuring the viscosity of the CRM binder at the same time. The new tool and the procedure has been checked and improved with a Computational Fluid Dynamics model [26].

The present study aims to introduce an improved quality control procedure for CRM binders aiming at assessing their viscosity development during a laboratory simulation of their manufacturing and stirred hot storage. The procedure developed in this work consists in adapting a rotational viscometer to act as a low shear mixer/storage tank with a modified dual helical ribbon impeller (DHR) previously designed and calibrated [27]. With this setup, several processing variables are investigated (types, contents, sizes of CRM and different storage times and temperatures) to withdraw practical recommendations.

2. Materials and methods

The experimental programme showed in Fig. 1 was tailored to evaluate the effect of the processing variables affecting the CRM binders rheology during the product manufacturing and the hot storage. Eight different binders were included in the experimental

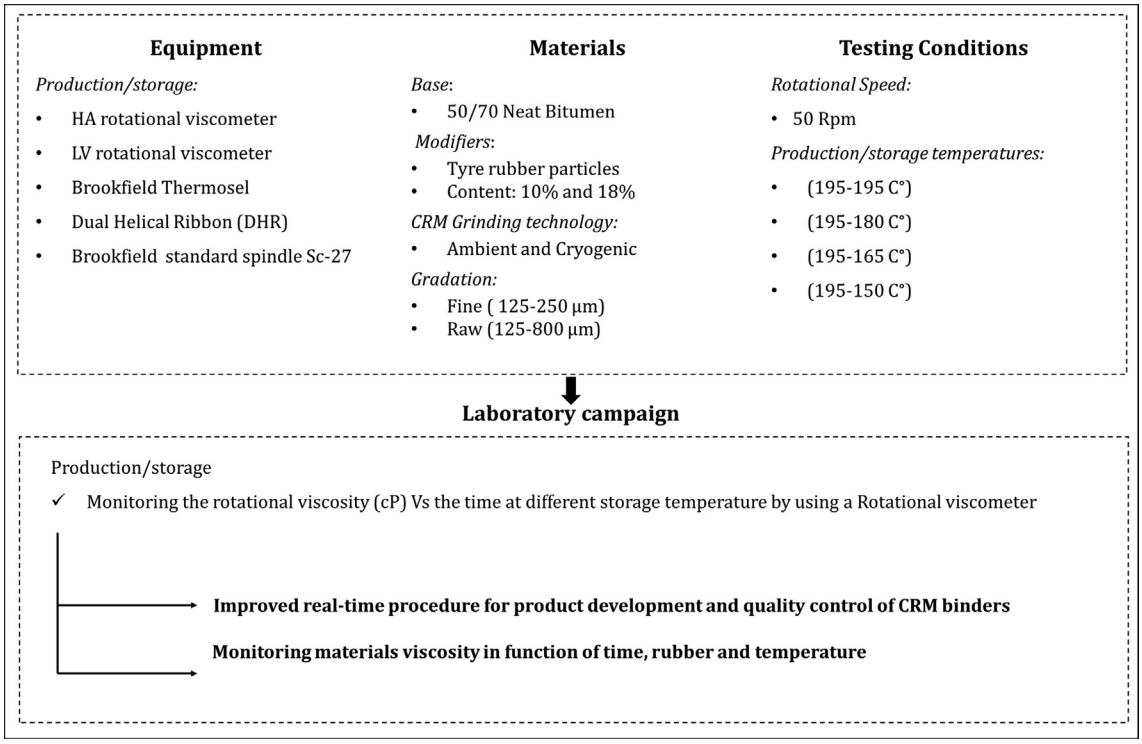

Fig. 1. Experimental programme.

programme: four modified binders were produced by adding 10% and 18% by bitumen weight of fine CRM size (125-250μ) in 50/70 grade bitumen and four by adding 10 and 18% of raw crumb rubber size (125-800μ). This programme was undertaken by using both ambient and cryogenic CRM. The proposed laboratory simulation for the manufacturing and agitated storage of CRM binders was performed by manufacturing the above-mentioned blends at 195 °C and simulating the storage at different temperature (195 °C, 180 °C, 165 °C, 150 °C). Each of the reported results was obtained as the average of at least two replicates. It has to be noted that, in this investigation, two Brookfield DV-II PRO Digital Viscometer were used: a low torque (LV model) and high torque (HA model). The two equipment differ mainly for the viscosity measurements range and as a consequence, they offer different accuracy of the measurement. In fact, torque measurement accuracy specified by the manufacturer is 1% of the full-scale range, with the LV model designed for low viscosity fluids (100% torque = 673.7 dyne cm), while the HA model is more appropriate for medium–high viscous fluids (100% torque = 14,374 dyne cm). An overview of the experimental programme is provided in Fig. 2.

2.1. Laboratory simulation of manufacturing and hot storage

According to Caltrans [28], rheologists have used the high-temperature viscosity of rubberised binders in the range 100–200 °C to ensuring the proper pumpability and compactability of the mixtures but also to guarantee adequate coating of the aggregates. Usually, this exercise is carried out in the field with hand-held viscometers or more typically in the laboratory by using a rotational viscometer with coaxial cylinders testing geometries. The dynamic/rotational viscosity is, therefore, a key engineering parameter that asphalt technologists need to control and target the CRM binder during product development. Hence, real-time monitoring of the viscosity of rubberised binders as a function of processing time and temperature provides asphalt technologists with a better understanding of the actual physical change throughout the processing of the material and overall allows higher confidence during product development and quality control. Furthermore, adapting a rotational viscometer as rheo-mixer offers the chance to study the change in material rheology with different base bitumens, or different crumb rubber content, by drastically reducing the material and time consumption.

On this regard, recent studies [24,25,27] have successfully demonstrated the concept of adapting a rotational viscometer as a low shear mixer for CRM binders. In all these studies, viscosity measurements were carried out according to international standards on viscosity measurements of rubberised binders (ASTM D4402 [29], ASTM D7741M [30]), but they all presented specific peculiarities: Celauro [24] proposed a procedure where the real-time monitoring was undertaken by using conventional spindles, Lo Presti [25] introduced the use of improved testing geometry (Dual Helical Impeller), while Subhy [11] suggested the use of specific parameters such as the swelling extent and swelling rate to monitor the viscosity change over time.

2.1.1. The dual helical ribbon

The adaptation of a Brookfield viscometer with standard impellers is not trivial. In fact, the conventional testing geometry of rotational viscometer (coaxial cylinders with spindle geometry as impellers) seems not being well suited for complex materials such as CRM binders. Recent studies [26,27] highlighted that such setup is not designed for heterogonous bituminous binders. Indeed, it is common incurring in phenomena like phase separation, sedimentation or agglomeration, which could lead to having not representative samples. To overcome these issues, this work introduces a novel geometry, the DHR (Fig. 3), where, c (1.25 mm) is the clearance between blades and the container wall and d (35 mm), s (17 mm) and w (3 mm) are respectively the diameter, the pitch and width of the impeller. The DHR was specifically designed and calibrated to guarantee the sample stability minimising the above-mentioned phenomena [27]. In fact, during viscosity measurements at high operational temperature, CRM binders seem to

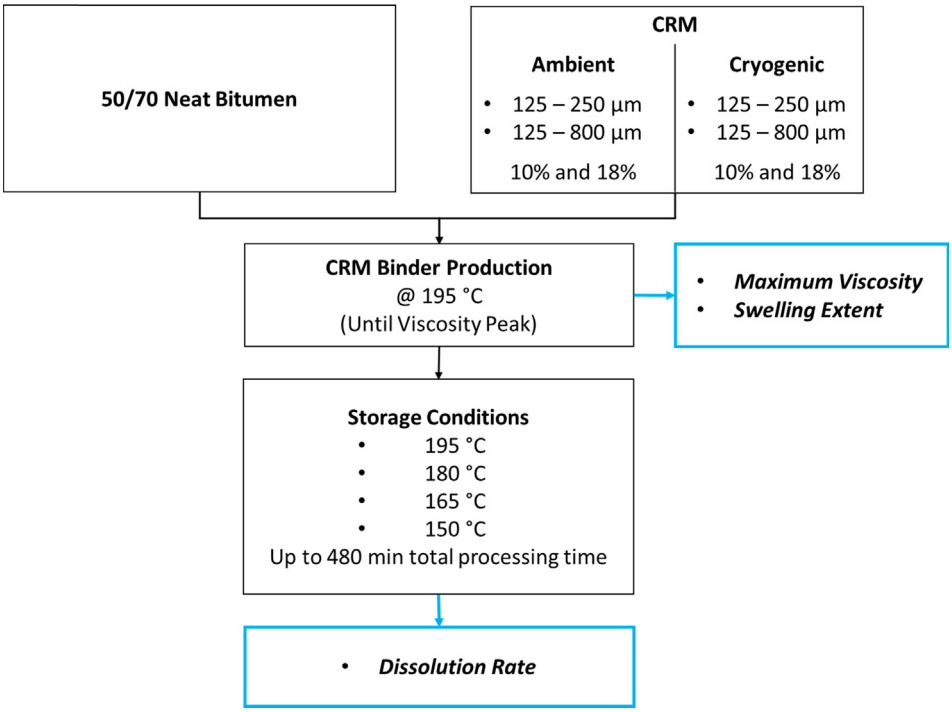

Fig. 2. Flow chart of experimental design procedures for evaluating the interaction effects on the production of CRM binders.

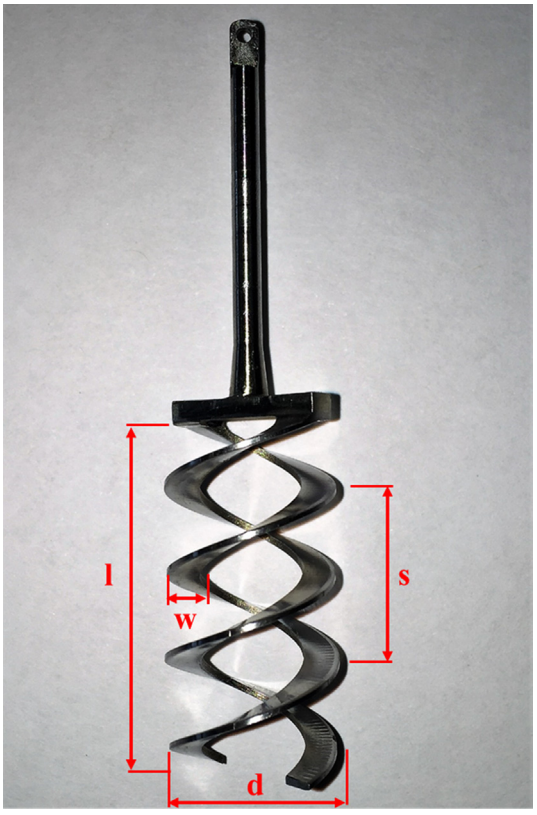

Fig. 3. The DHR impeller for use in a Brookfield Viscometer.

suffer significantly of sample instability, and this does not allow having a homogenous distribution of rubber particles within the binder, hence moving the spindle up and down during the mixing is necessary to help distribution of the rubber particles. Of course, this doesn't guarantee the homogeneity of the sample, it doesn't provide reliable measurements, and it could even lead to damaging the equipment [25,26]. The DHR, was designed to reduce the level of heterogeneity of complex binders and to guarantee the sample stability during the high temperature rotational test. This configuration allows the investigation of the variables associated with the manufacturing and storage of CRM binders (e.g. swelling extent and dissolution rate) while measuring viscosity in real time without incurring in common issues related to standard equipment such as phase separation and sedimentation. Overall, the Brookfield viscometer with DHR has several benefits including the precise control of mixing and testing temperatures, continuous monitoring of viscosity measurements, the ability to keep the rubber uniformly distributed within the blend, and all of this by using small quantities (10–15 g) of material. The DHR presented in this work is an upgrade of a dual helical impeller (DHI) designed and developed by Lo Presti [25]. The previous investigation showed the benefit of using the DHI to reduce the heterogeneity of complex systems such as the case of crumb rubber modified binders and, in turn, to provide more stable and realist viscosity measurements. Fig. 4 shows the homogeneity of the sample being proceeded with the DHR device. To take this pictures, a transparent container was used along with a transparent liquid, a standard visco-fluid of known viscosity (50 cp) + CRM. It can be seen the positive evolution of the homogeneity of the sample thanks to the mixing action of the DHR device. In the beginning, the settlement of the rubber particles is obvious (a). After the DHR starts rotating the rubber follows an ascendent flow along the axel of the container (b), and after some seconds the distribution of the rubber particles gets homogeneous (c).

2.1.2. Real-time monitoring of CRM binder's properties during manufacturing and hot storage

In this study, the real-time monitoring of the properties' development of CRM binders is extended to perform quality control also during the stirred storage phase. As widely described above, maintaining sample stability allows achieving the target viscosity for

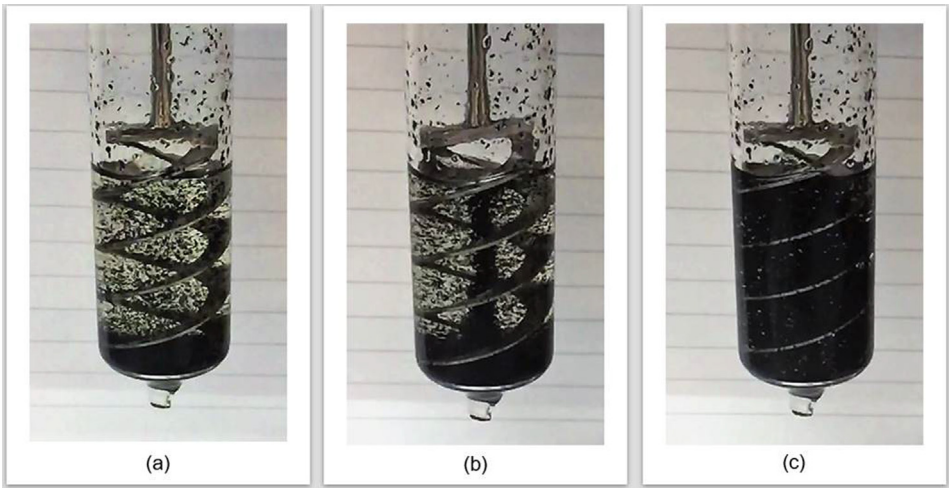

Fig. 4. Photographs of the DHR impeller showing the axial pumping force with a mixture of a visco-fluid (η = 50 cP) and rubber particles at the start (a), after few seconds (b) and at the end (c).

the CRM binders after both manufacturing and storage. Hence, a laboratory procedure enabling to predict the viscosity changes during storage would allow assessing the right conditions during hot storage. Here is the laboratory procedure used in this investigation:

- The low shear manufacturing process is simulated by using a rotational viscometer with a small cylindrical container testing geometry and a coaxial Dual Helical Ribbon (DHR) (Fig. 3) in place of more conventional spindles (I.e. SC-27).
- Manufacturing of materials is carried out at 50 rpm. This value is not simulative of field production, and it was chosen since it is high enough to guarantee sample stability. The value is kept constant to avoid possible complications due to the shear-thinning nature of CRM binders as well as to keep consistent the shear rate and obtain homogeneous data from the tests.
- After the viscosity peak is reached, the simulation of the hot storage is undertaken by simply changing the temperature of the thermal chamber, when needed. This is done under the assumption of storing the binder in an agitated tank with a rotational speed of 50 rpm
- The monitoring of the hot storage phase is undertaken for at least 8 h. The experiment could be prolonged to simulate longer storing time (i.e. 24 h, 48 h), but for practical reasons, 8 h can be considered long enough.
- The effect of different storage temperatures can be investigated by changing the temperature setting of the thermal chamber and keeping monitoring the change in viscosity.
- This procedure can be adapted to any rotational viscometer equipped with a DHR; however, asphalt technologists are recommended to compare a-priori the expected high torque for the lower range of temperatures and the viscometer's limits.
- The real-time monitoring produces five parameters that can serve asphalt technologists to optimise manufacturing and storage conditions (more details in the next section). These five parameters are:
  - 1) the swelling extent, which is the time to reach the maximum viscosity at the production temperature;
  - 2) the swelling rate, a ratio given by the maximum viscosity at production temperature over the time elapsed from the start of the production;
  - 3) the maximum viscosity, which is the peak viscosity recorded at the end of the manufacturing stage and/or at the beginning of the storage period, after the storage temperature has been reached;
  - 4) the dissolution rate, given by the ratio of the final storage viscosity over the initial storage viscosity, which provides information about the percentage of viscosity loss during the storage period;
  - 5) final viscosity, which provides information about the viscosity value at the end of the storage period

A qualitative evaluation of the mixing capabilities of the DHR was preliminarily undertaken in this investigation and reported below. The experiment was carried out to provide an example of the results obtainable with real-time monitoring of CRM binder manufacturing and storage, as well as to highlight the importance of using a DHR for the suggested procedure.

2.1.3. Qualitative assessment of the proposed procedure

Fig. 5 shows the curve of a laboratory simulation of the manufacturing of CRM binder made of a 50/70 pen base bitumen mixed with 18% of crumbs (Raw size). For this example, the whole process was monitored for a total time of 360 mins. At first, manufacturing at 177.5 °C was performed by using both SC-27 and DHR and ended once the peak viscosity was reached. Immediately after, a simulation of hot storage at the same temperature was carried out, and viscosity values monitored up to the end of the 5 h.

The rubber is gradually added within 5 min after which, only for the SC-27, a drastic increase in viscosity is followed by a severe decrease up to more realistic viscosity measurements. This phenomenon is due to the necessity of the operator to move up and down the impeller to ensure proper distribution of rubber particles within the bituminous matrix. After this phase, the SC-27 records a build-up of viscosity values typical of a swelling process. This increment is due to the rubber particles swelling which results in a reduction in the inter-particle distance as well as stiffening of the binder by reducing the oily fractions of the bitumen (adsorbed by the rubber particles). As the swelling ends, the rubber particles start devulcanizing/depolymerising which leads to a decrease in viscosity. On the other hand, using the DHR guarantees appropriate mixing of the material, allows having a smooth curve of viscosity build-up and does not need the intervention of the operator. Also, the swelling process seems to act faster and to a higher peak value that is a symptom of a more intimate interaction between bitumen and CRM. On this regard, Table 1 provides a quantitative estimation of the parameters used to compare the simulation carried out by using both SC-27 and DHR and displayed in Fig. 5.

At last, to have a confirmation of the different interaction achieved by using the SC-27 and the DHR, at the end of the tests

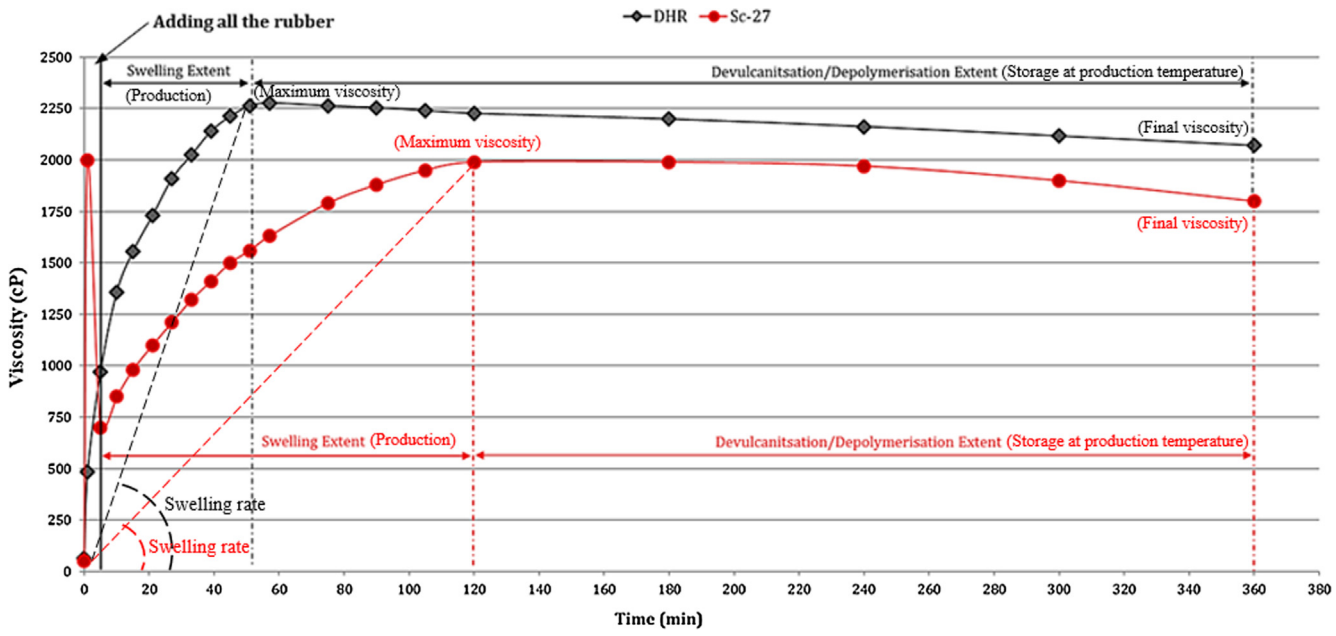

Fig. 5. Real-time monitoring of the manufacturing stage (177.5 °C, 50 rpm 18% ambient 125–800 μm CRM).

Table 1
Quantitative parameters associated with the interaction process.

	DHR	SC-27
Swelling Extent (min)	51	120
Swelling Rate (cP/min)	46.9	18.5
Maximum Viscosity (cP)	2263	1990
Dissolution rate (cP/min)	0.8	1.1
Final Viscosity (cP)	2070	1800

the samples were poured to allow a visual evaluation (Fig. 6). Results show a clear difference in terms of system heterogeneity: the material manufactured using the SC-27 presents particles agglomeration that inevitably affects the viscometer readings while the DHR provides a final blend where the rubber is clearly better integrated, showing an aspect similar to that of industrial scale CRM binders. Fig. 7 shows SEM images (x50) of the aspect of the surface for both samples. The sample processed with the DHR displays a surface smoother than that of the sample produced with SC-27, meaning that the DHR device promotes advanced the rubber-bitumen interaction.

3. Results

The idea behind the experimental programme tests was to reproduce the binder manufacturing as well as the storage periods under different temperatures, aiming at investigating the impact of different processing conditions on the viscosity evolution. As listed in Fig. 1 eight different materials were analysed as a result of blending CRM binders having different rubber content (10 and 18%) size (raw 125–800 μm and fine 125–250 μm) and grinding technology (ambient and cryogenic) for a total duration (production + storage) of 480 min. Real-time monitoring procedure was used for both manufacturing and storage stage as described in section 2.1. CRM binders were produced at 195 °C with the DHR device. Once peak viscosity was reached, the temperature of the

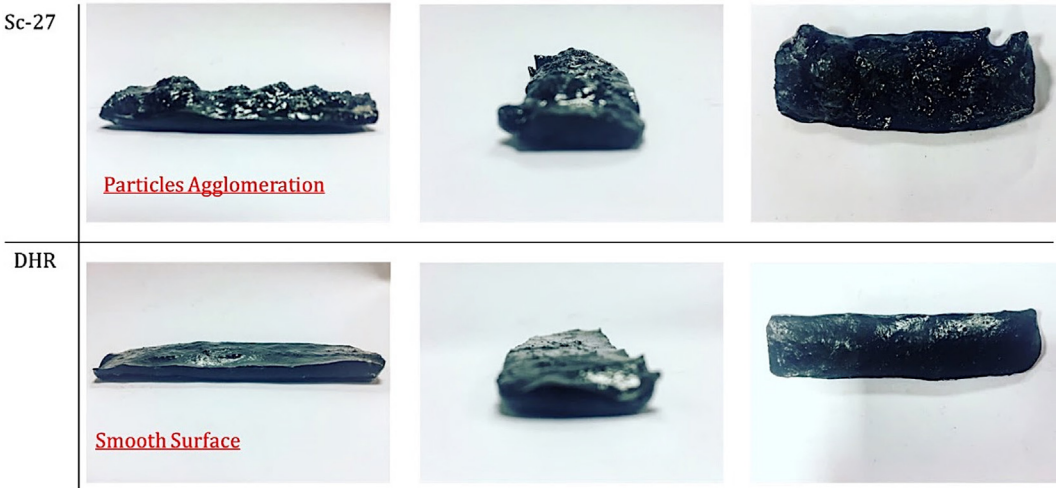

Fig. 6. Qualitative assessment of the improved bitumen-rubber interaction obtained using DHR instead of SC-27.

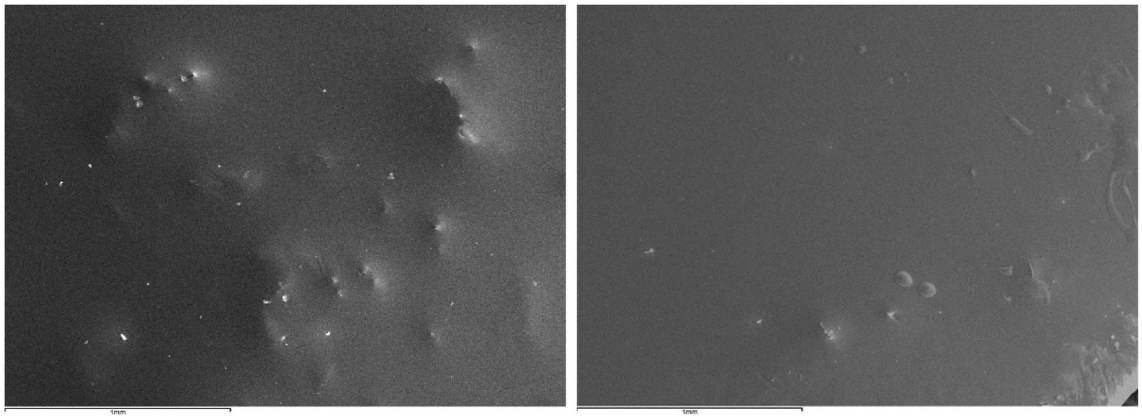

Fig. 7. SEM images (×50) of the samples processed with SC-27 and DHR, respectively.

Table 2
Quantitative assessment of the real-time monitoring exercise.

Particle Content	(%) Grinding Tech	Particles size	Production Temp (°C)	Swelling Extent (minutes)	Storage Temp (°C)	Initial Storage Viscosity (cP)	Dissolution Rate (%)	Final Storage Viscosity (cP)
10%	Ambient	Raw	195	45	195	276	33	184
					180	418	28	276
					165	662	13	602
					150	1002	9	910
		Fine	195	39	195	211	33	137
					180	349	25	262
					165	616	10	552
					150	818	10	740
	Cryogenic	Raw	195	39	195	179	13	156
					180	326	7	312
					165	547	4	529
					150	938	2	915
		Fine	195	33	195	151	12	133
					180	234	6	220
					165	427	5	404
					150	763	3	745
18%	Ambient	Raw	195	63	195	1159	36	740
					180	1734	35	1140
					165	2258	26	1665
					150	3215	11	2944
		Fine	195	60	195	1209	49	611
					180	1656	23	1274
					165	2208	24	1633
					150	2994	10	2668
	Cryogenic	Raw	195	51	195	1030	21	851
					180	1527	10	1370
					165	2231	7	2070
					150	2792	5	2645
		Fine	195	45	195	1071	18	878
					180	1527	8	1412
					165	1932	7	1826
					150	2589	8	2484

thermal chamber was reduced and the simulation of the hot storage phase at different storage temperatures undertaken.

In order to facilitate a comparative analysis of the real-time monitoring exercise of the blend's viscosity evolution with storage time and temperature, the results are summarized in Table 2, then to better analyse the trends observed, results are plotted in Figs. 8–15 and discussed in the following paragraphs

As a first result, from the real-time monitoring of the manufacturing phase (Fig. 8), it can be highlighted that it is evident that higher CRM content requires more time to reach the maximum viscosity at production temperature of 195 °C. These results agree with the general rule at the industrial scale that the minimal time to reach a proper rubber-bitumen interaction is 45 min and 60 min for low and high rubber content modified binders, respectively. The higher the content of rubber, the larger the time needed to reach the maximum viscosity.

3.1. Investigating the relation between storage temperatures and initial storage viscosity

With regards to the influence of the CRM type on the initial storage viscosity, Fig. 9 confirms that ambient rubber produces CRM binders with slightly higher viscosities. This result can be referred to the larger specific surface of the ambient rubber that allows the rubber particles absorbing more oil and swell more. Of course, CRM binders with 18% of CRM display higher viscosity values that when incorporating 10% of rubber, however all the

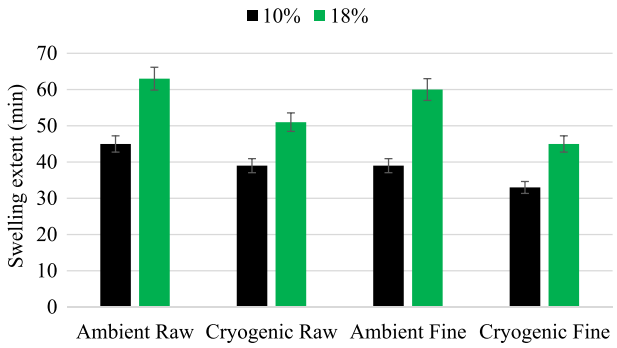

Fig. 8. Swelling extent for ambient and cryogenic CRM.

blends show having a similar trend of initial storage viscosity by changing the storage temperature.

3.2. Investigating the relation between storage temperatures and CRM size

For this analysis, four storage temperatures have been considered (195 °C, 180 °C, 165 °C and 150 °C). To make the discussion of results easier, here only results of blends with 18% ambient CRM are reported, while a complete quantitative assessment of these simulations is reported in Table 2.

Figs. 10 and 11 show the viscosity trend over the time at different storage temperatures; the first shows the details of a blend manufactured by using 18% ambient raw CRM (125–800 μm), while the latter refers to the blend with the ambient fine CRM (125–250 μm). In both graphs, the eventual bump in viscosity values at approx. Fifty minutes are due to the transition from the production temperature (195 °C) to the different storage temperatures. Results show a similar trend for both cases in terms of swelling extent and viscosity peak during the production period. Regarding the storage period, while it is clear that CRM particles are easier to be digested/dissolute at 195 °C, as was shown by the highest dissolution rates, only slight differences between raw and fine CRM binders were recorded. This partial conclusion is thoroughly analysed in section 3.4 by considering all the dissolution rates obtained in this investigation.

3.3. Investigating the relation between storage temperatures and CRM content and type

Fig. 12 provides a comparison of the viscosity evolution of the blends obtained with different rubber content, respectively 10% and 18%. As expected, using higher rubber content allows reaching a higher viscosity peak at the end of the production period (approx. 50 min). In addition to that, it can also be observed for both cases that the viscosity dissolution is affected by the storage temperature: while the dissolution rates at 150 °C are 9 and 11% for the modified binders with 10 and 18% CRM respectively, at 180 °C storage temperature these rates reach values of 28 and 35% respectively, around three times higher. These results mean that for both modified binders, with 10 and 18% CRM, the increase in the storage temperature brings about higher dissolution rates.

Fig. 13 shows that using cryogenic rubber the interaction mechanism between rubber and bitumen is reduced. For example, with a storage temperature of 180 °C and 18% content of raw rubber using the cryogenic technology a dissolution rate of 10% is obtained, lower than the 35% value obtained in Fig. 12 with CRM by the ambient technology. A similar trend is also recorded at 150 °C storage temperature (5% and 11% dissolution rates, for cryogenic and ambient CRM respectively), indicating once again that the cryogenic CRM reacts more slowly with the bitumen. In other words, cryogenic CRM produces modified binders with lower dissolution rates during the storage period.

For the sake of brevity, this section presents only a few detailed comparison examples to show the capabilities and the method to analyse the results from the DHR device. Beyond these examples, all the values for dissolution rates obtained in this investigation are plotted together in the following section to withdraw and support general conclusions and recommendations aimed to maintain the quality of CRM binders during the storage period.

3.4. Investigating the relation between storage temperatures and dissolution rates

Due to the high temperature during the storage period, the CRM binders loses part of their initial storage viscosity. This phenomenon has been quantified in this study as the dissolution rate, which represents the percentage of viscosity that has been lost from the beginning to the end of the storage period. By looking at data in Table 2 and trends in Figs. 14 and 15, as a general comment, it can

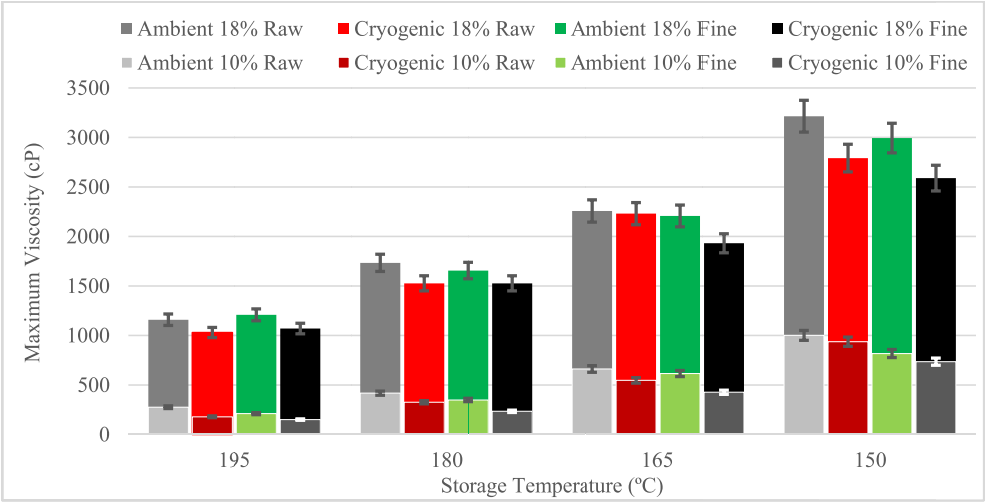

Fig. 9. Initial storage Viscosity vs storage temperature, 10% and 18% CRM.

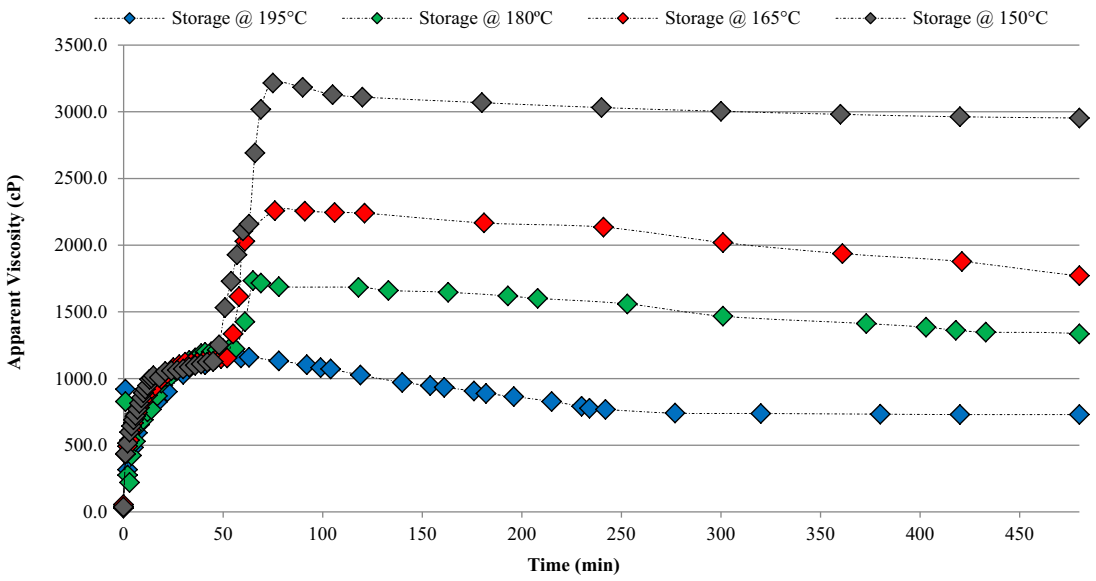

Particle Content (%)	Grinding Tech	Particles size	Production Temp (°C)	Swelling Extent (min)	Storage Temp (°C)	Initial Storage Viscosity (cP)	Dissolution Rate (%)	Final Storage Viscosity (cP)
18	Ambient	Raw	195	63	195	1159	36	740
					180	1734	35	1140
					165	2258	26	1665
					150	3215	11	2944

Fig. 10. Viscosity evolution at different storage temperatures. 18% ambient CRM 125–800 μm.

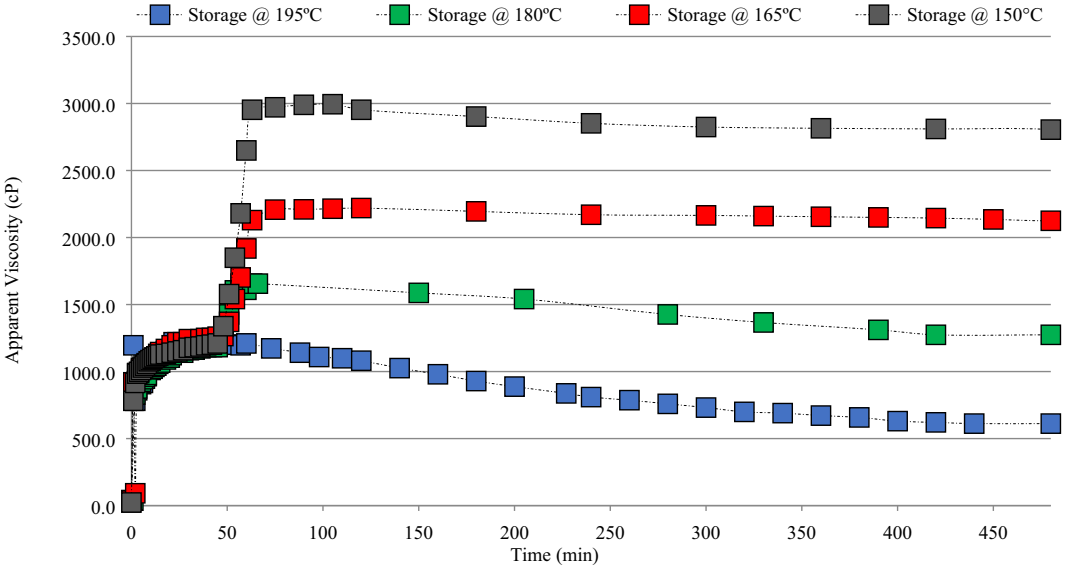

Particle Content (%)	Grinding Tech	Particles size	Production Temp (°C)	Swelling Extent (min)	Storage Temp (°C)	Initial Storage Viscosity (cP)	Dissolution Rate (%)	Final Storage Viscosity (cP)
18	Ambient	Fine	195	60	195	1209	49	611
					180	1656	23	1274
					165	2208	24	1633
					150	2994	10	2668

Fig. 11. Viscosity evolution at different storage temperatures. 18% ambient CRM 125–250 μm.

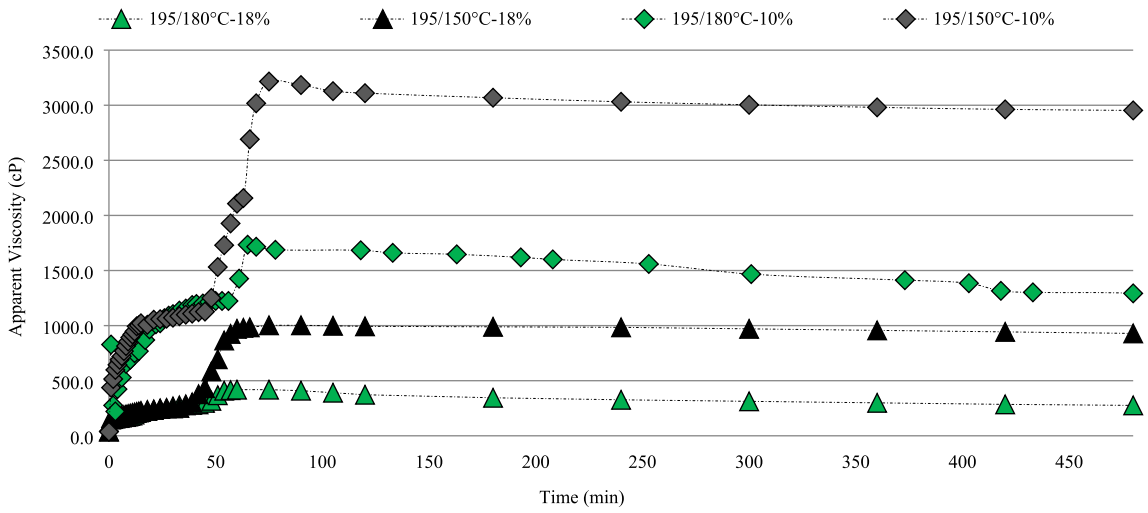

Grinding Tech	Particles size	Production Temp (°C)	Particle Content (%)	Swelling Extent (min)	Storage Temp (°C)	Initial Storage Viscosity (cP)	Dissolution Rate (%)	Final Storage Viscosity (cP)
Ambient	Raw	195	10	45	180	418	28	276
					150	1002	9	910
			18	63	180	1734	35	1140
					150	3215	11	2944

Fig. 12. Evolution of viscosity at different concentration of ambient CRM 125–800 μm.

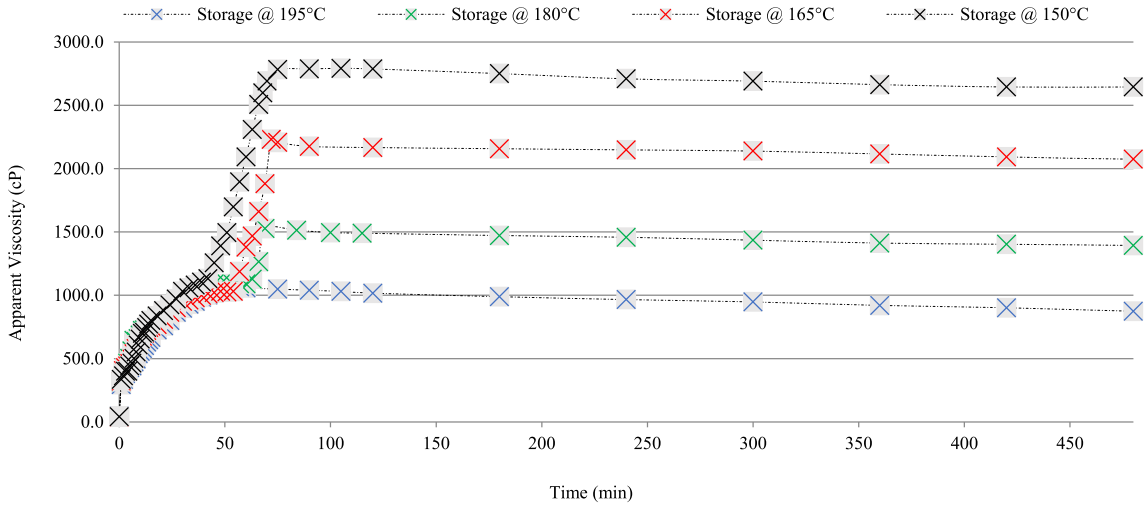

Particle Content (%)	Grinding Tech	Particles size	Production Temp (°C)	Swelling Extent (minutes)	Storage Temp (°C)	Initial Storage Viscosity (cP)	Dissolution Rate (%)	Final Storage Viscosity (cP)
18	Cryogenic	Raw	195	51	195	1030	21	851
					180	1527	10	1370
					165	2231	7	2070
					150	2792	5	2645

Fig. 13. Evolution of viscosity at different storage temperature using cryogenic CRM 125–800 μm.

be stated that ambient CRM always presents the highest dissolution rates. This fact could be related to the lower specific surface of the cryogenic rubber particles that slow the depolymerisation of the rubber. On the contrary, the ambient CRM, due to its higher specific surface, is more vulnerable to the effect of temperature during stirred storage, resulting in higher dissolution rates.

The size of the rubber appears not to have an essential influence on the dissolution rate. From these results, it seems that cryogenic rubber should be recommended to minimize the loss of viscosity during the storage of the CRM binder at the asphalt plant. Anyway, by reducing the storage temperature to 150 °C, the dissolution rate diminishes considerably for both ambient and cryogenic rubber.

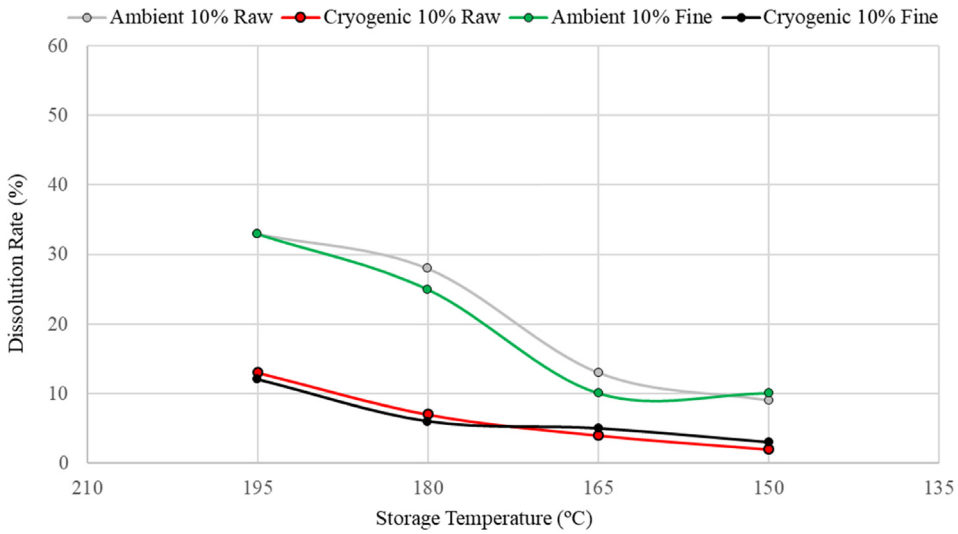

Fig. 14. Dissolution rates vs storage temperature, 10% CRM.

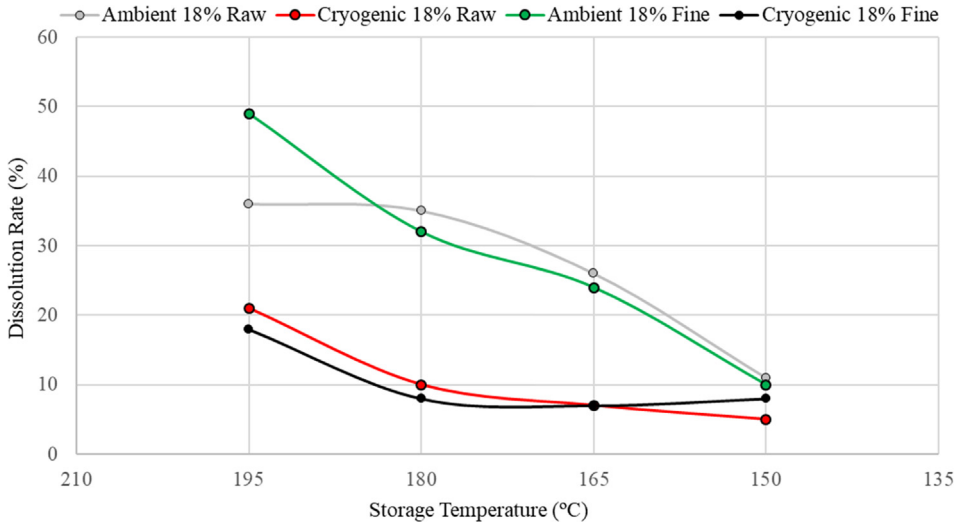

Fig. 15. Dissolution rates vs storage temperature, 18% CRM.

4. Conclusions and recommendations

In this investigation, the conventional Brookfield spindle SC-27 has been substituted by a novel Dual Helical Ribbon (DHR) In fact, the DHR not only allows to continuously measure the viscosity of the sample but also provides improved mixing performance which guarantees the stability of the sample during measurements. Previous studies have shown the possibility of using rotational viscometers to emulate the manufacturing of CRM binders. This research extends the possibility of governing the modification process also to the hot storage phase.

Several CRM binders with different CRM type and content have been manufactured and tested at different storage temperatures to show the capabilities of the procedure. Blends were manufactured at 195 °C, and after the peak viscosity was reached, the chamber temperature was reduced at different levels to reproduce different storage temperatures. The impeller was always kept at 50 rpm to avoid settlement problems during manufacturing and keep constant the shear rate to achieve a fair comparison among all the data obtained in the testing program. Real-time monitoring of each blend can be translated into five parameters that allow performing a comparative analysis of the modification process during manufacturing and hot storage. The percentage of viscosity lost during the simulation of the storage period has been defined as the dissolution rate. High dissolution rates indicate a loss of properties of the binder during the storage period. As a result of the work done, this study helped to produce evidence to support the following conclusions:

- It has been observed that the dissolution rate of the blends is strongly influenced by the storage temperature and the grinding technology of the rubber.
- In terms of industrial production, it seems that the use of cryogenic rubber will result in slightly lower viscosities during the production phase of the CRM binders. However, cryogenic CRM is less affected during hot storage, leading to lower dissolution rates.
- In any case, reducing the temperature of the storage tanks at the asphalt plant to 150 °C will minimise the dissolution rates, this is, will better keep the quality of the CRM binders in the tanks.

In future investigations, the relation between the shear rate of DHR at several speeds and the shear rate of full-scale mixers and stirrers should be investigated. This knowledge could help to adapt the speed of the DHR to the specific industrial equipment to be used for the production of the CRM binder in a determined construction project and obtain more accurate predictions, adapted to each study case. Further studies should also look at evaluating the procedure with an extended experimental programme which includes longer storage time. In fact, the dissolution rate seems to be a promising parameter to engineer the optimal storage conditions of modified binders, even beyond CRM binders.

Declaration of Competing Interest

The authors declare that they have no known competing financial interests or personal relationships that could have appeared to influence the work reported in this paper.

Acknowledgements

The collaboration for this investigation between the University of Nottingham and the Technical University of Madrid was possible thanks to Grant n. PRX17/00675 by the Spanish Ministry of Education, Program Salvador de Madariaga for Investigation Stays of Senior Researchers in Foreign Universities. Furthermore, this study is supported by European Commission within the SMARTI ETN project which has received funding from the European Union's Horizon 2020 Programme under the Marie Curie-Skłodowska actions for research, technological development and demonstration, under grant n.721493 (http://smartietn.eu). Finally, this work was partially supported by the Italian Ministry of University and Research (MIUR dm n.372 08/05/18).

Authors' contribution

The authors confirm contribution to the paper as follows: Study conception and design: Juan Gallego Medina, Davide Lo Presti; Data collection: Gaspare Giancontieri, Juan Gallego Medina; Analysis and interpretation of results: Juan Gallego Medina, Gaspare Giancontieri, Davide Lo Presti; Draft manuscript preparation: Davide Lo Presti, Gaspare Giancontieri, Juan Gallego Medina,. All authors reviewed the results and approved the final version of the manuscript.

References

[1] M. Sienkiewicz, J. Kucinska-Lipka, H. Janik, A. Balas, Progress in used tyres management in the European Union: a review, Waste Manag. 32 (10) (2012) 1742–1751.
[2] D. Lo Presti, Recycled tyre rubber modified bitumens for road asphalt mixtures: a literature review, Constr. Build. Mater. 49 (2013) 863–881.
[3] M. Bueno, J. Luong, F. Terán, U. Viñuela, V.F. Vázquez, S.E. Paje, Noise reduction properties of an experimental bituminous slurry with crumb rubber incorporated by the dry process, Coatings 4 (2014) 602–613.
[4] P. Hajikarimi, M. Rahi, F. Moghadas Nejad, Comparing different rutting specification parameters using high temperature characteristics of rubber-modified asphalt binders, Road Mater. Pavement Des., Oct. 16 (4) (2015) 751–766.
[5] A. Behnood, J. Olek, Rheological properties of asphalt binders modified with styrene-butadiene-styrene (SBS), ground tire rubber (GTR), or polyphosphoric acid (PPA), Constr. Build. Mater. 151 (Oct. 2017) 464–478.
[6] A.T. Visser, G.S. Duhovny, A.V. Sachkova, Comparison of bitumen–rubber use in extreme conditions in Russia and South Africa, Road Mater. Pavement Des. 18 (5) (Sep. 2017) 1190–1199.
[7] J.G. Chehovits, R.L. Dunning, G.R. Morris, Characteristics of asphalt-rubber by the sliding plate microviscometer, in: Asphalt Paving Technology: Association of Asphalt Paving Technologists-Proceedings of the Technical Sessions, 1982, pp. 240–261.
[8] D. Lo Presti, G. Airey, Tyre rubber-modified bitumens development: the effect of varying processing conditions, Road Mater. Pavement Des. 14 (4) (2013) 888–900.
[9] S.J. Lee, C.K. Akisetty, S.N. Amirkhanian, The effect of crumb rubber modifier (CRM) on the performance properties of rubberized binders in HMA pavements, Constr. Build. Mater. 22 (7) (Jul. 2008) 1368–1376.
[10] C. Thodesen, K. Shatanawi, S. Amirkhanian, Effect of crumb rubber characteristics on crumb rubber modified (CRM) binder viscosity, Constr. Build. Mater. 23 (1) (2009) 295–303.
[11] A. Subhy, D. Lo Presti, G. Airey, Rubberised bitumen manufacturing assisted by rheological measurements, Road Mater. Pavement Des 17 (2) (2016) 290–310.
[12] M.A. Abdelrahman, S.H. Carpenter, Mechanism of interaction of asphalt cement with crumb rubber modifier, Transp. Res. Rec. 1661 (1999) 106–113.
[13] P. Taylor et al., "Changes in Rubber Due to its Interaction with Bitumen when Producing Asphalt Rubber Changes in Rubber Due to its Interaction with Bitumen when Producing Asphalt Rubber," Road Mater. Pavement Des., no. October 2014, pp. 37–41, 2010.
[14] F.J. López-Moro, M.C. Moro, F. Hernández-Olivares, B. Witoszek-Schultz, M. Alonso-Fernández, Microscopic analysis of the interaction between crumb rubber and bitumen in asphalt mixtures using the dry process, Constr. Build. Mater. 48 (2013) 691–699.
[15] A. Ghavibazoo, M. Abdelrahman, Composition analysis of crumb rubber during interaction with asphalt and effect on properties of binder, Int. J. Pavement Eng. 14 (5) (Jul. 2013) 517–530.
[16] D. Lo Presti, G. Airey, P. Partal, Manufacturing terminal and field bitumen-tyre rubber blends: the importance of processing conditions, Procedia – Soc. Behav. Sci., Oct. 53 (2012) 485–494.
[17] F.J. Navarro, P. Partal, F. Martínez-Boza, C. Gallegos, Thermo-rheological behaviour and storage stability of ground tire rubber-modified bitumens, Fuel 83 (14-15) (2004) 2041–2049, https://doi.org/10.1016/j.fuel.2004.04.003.
[18] N.F. Ghaly, Effect of sulfur on the storage stability of tire rubber modified asphalt, World J. Chem. 3 (2) (2008) 42–50.
[19] A. Pérez-Lepe, F.J. Martínez-Boza, C. Gallegos, High temperature stability of different polymer-modified bitumens: a rheological evaluation, J. Appl. Polym. Sci. 103 (2) (2007) 1166–1174.
[20] S. Hosseinnezhad, D. Holmes, E.H. Fini, "Decoupling the Physical Filler Effect and the Time Dependent Dissolution Effect of Crumb Rubber on Asphalt Matrix Rheology," in Transportation Research Board 93rd Annual Meeting. January 12-16, Washington, D.C., 2014, pp. 1–20.
[21] K.D. Jeong, S.J. Lee, S.N. Amirkhanian, K.W. Kim, Interaction effects of crumb rubber modified asphalt binders, Constr. Build. Mater. 24 (5) (May 2010) 824–831.
[22] M. Ragab, M. Abdelrahman, Enhancing the crumb rubber modified asphalt's storage stability through the control of its internal network structure, Int. J. Pavement Res. Technol. 11 (1) (2018) 13–27.
[23] J. Pais, D. Lo Presti, C. Santos, L. Thives, P. Pereira, The effect of prolonged storage time on asphalt rubber binder properties, Constr. Build. Mater., Jun. 210 (2019) 242–255.
[24] B. Celauro, C. Celauro, D. Lo Presti, A. Bevilacqua, Definition of a laboratory optimization protocol for road bitumen improved with recycled tire rubber, Constr. Build. Mater., Dec. 37 (2012) 562–572.
[25] Davide Lo Presti, Claudia Fecarotti, Adam T. Clare, Gordon Airey, Toward more realistic viscosity measurements of tyre rubber–bitumen blends, Constr. Build. Mater. 67 (2014) 270–278, https://doi.org/10.1016/j.conbuildmat.2014.03.038.
[26] D. Lo Presti, G. Giancontieri, D.M. Hargreaves, Improving the rheometry of rubberized bitumen: experimental and computation fluid dynamics studies, Constr. Build. Mater., Apr. 136 (2017) 286–297.
[27] G. Giancontieri, D. Hargreaves, D. Lo Presti, Are we correctly measuring the rotational viscosity of heterogeneous bituminous binder?, Road Mater. Pavement Des. (2019) (In press).
[28] Caltrans, Quality Control Manual for Hot Mix Asphalt – State of California, State California, Dep. Transp. Div. Constr. (2011). http://www.dot.ca.gov/hq/construc/publications/qcqaman1.pdf.
[29] ASTM a. D4402/D4402M, Standard test method for viscosity determination of asphalt at elevated temperatures using a rotational viscometer., ASTM Int. (2015). http://dx.doi.org/10.1520/D4402_D4402M-15.
[30] ASTM b. D7741/D7741M, Standard test method for measurement of apparent viscosity of asphalt-rubber or other asphalt binders by using a rotational handheld viscometer., ASTM Int. (2018). http://dx.doi.org/10.1520/D7741_D7741M-18.